Development and Application of Free-Fall Fast Pyrolysis Technology to Produce Valorized Bioproducts from Lignocellulosic Materials

A Dissertation
Presented in Partial Fulfillment of the Requirements for the
Degree of Doctor of Philosophy
with a
Major in Mechanical Engineering
in the
College of Graduate Studies
University of Idaho
by
Ethan R. Struhs

Approved by:

Major Professor: Amin Mirkouei, Ph.D.

Committee Members: Armando McDonald, Ph.D.; Michael McKellar, Ph.D.; Haiyan Zhao, Ph.D.

Department Administrator: Eric Wolbrecht, Ph.D.

December 2023

Abstract

Lignocellulosic biomass has several advantages that set it apart as a convenient source for renewable energy. Among the conversion technologies, thermochemical decomposition of biomass by fast pyrolysis has shown to be a simple, cost-efficient route for producing valorized liquid (bio-oil) and solid (biochar) products. Bio-oil has potential for heat, biofuels, and pharmaceutical applications, while biochar can be used as a soil amendment and remedy water eutrophication. This dissertation focuses on assessing free-fall fast pyrolysis reactor design through the implementation of experiments that assess several biomass-to-bioproduct pathways. To do so, a review on thermochemical biomass conversion technologies and pathways geared towards increasing fuel properties of liquid bio-oil was performed. Both critical and systematic reviews made evident the need for a single-step, intensified pathway for lignocellulosic-based fuel blendstocks production. Next, the potential of a mixed fast and slow pyrolysis process for the conversion of several feedstocks into bio-oil and biochar was evaluated. The effects of feedstock type on the physical and chemical properties of bio-oil and biochar attributes were assessed with the help of various characterization techniques. The desirable characteristics of pine-derived bio-oil led to it being selected for further upgrading experiments. A comparison of γ-alumina as a catalyst for in-situ and ex-situ catalytic fast pyrolysis in a free-fall reactor configuration was examined using pinewood flour. Efficiency and the effect of methanol as a direct quenching fluid for fractionation were also examined. γ-Alumina was shown to successfully decrease acidic compounds and increase esters in the bio-oil. Bio-oil produced from ex-situ catalytic pyrolysis presents a promising oil with the highest average yield, high phenolic content, and thermally stable properties. Fractions condensed in methanol exhibited the highest thermal stability and esterification potential; however, they still possessed relatively high amounts of acidic compounds. It was concluded that the use of γ-alumina with methanol impingers for fractionation could potentially produce an oil high in small chain esters and low in acids. Also, the use of γ-alumina as a catalyst support for hydrodeoxygenating metal catalysts could result in an inexpensive route for biomass-to-hydrocarbon fuels production. Also, a sustainability study on the market opportunity and environmental benefits of converting cattle manure to nutrient-rich biochar on-site, using a portable refinery unit, was conducted. Techno-economic and life cycle assessments were performed to assess the feasibility. Converting cattle manure, using the presented strategy and process near the collection sites could address upstream and midstream sustainability challenges and stimulate the biochar industry.

Acknowledgments

I would like to convey my deepest appreciation to Dr. Amin Mirkouei, my Ph.D. advisor, and for his guidance and encouragement during my time as a graduate student. His passion for research and the sciences has been inspirational. I am grateful for his mentoring and the can-do attitude he instilled in me. He helped me stay focused and gave me confidence as a researcher.

I would also like to express my gratitude to Drs. Armando McDonald, Haiyan Zhao, and Michael McKellar for serving on my committee and for their invaluable help and feedback throughout the duration of my program.

I would like to state my appreciation to Dr. Amin Mirkouei, Dr. Armando McDonald, Dr. Maria Magdalena Ramirez-Corredores, Dr. Martha Chacon, Dr. Farid Sotoudehnia, Dr. Yaqi You, Dr. Amir Mohajeri, and Harrison Appiah for their contributions as co-authors, resulting in several publications.

I would like to thank Alice Allen for helping me with registration and for answering all the random questions that I had.

I would also like to thank Meladi Lanier for her help and patience in ordering all the materials needed for our research.

Dedication

I would like to dedicate my work to my wife, Brittany, and three sons, Reilly, Caelum, and Ezra for their unending patience and support for me. They bring joy to my life, and I would not have gotten this far without them.

Table of Contents

List of Tables

List of Figures

Statement of Contribution

Several chapters included in this dissertation were co-authored and submitted for publication. Co-authors and their contributions are provided below:

Chapter 2

Contributors: Ethan Struhs wrote the manuscript with support from Amin Mirkouei, Maria Magdalena Ramirez-Corredores, Armando G. McDonald, and Martha L Chacon.

Chapter 3

Contributors: Ethan Struhs and Amin Mirkouei contributed to the conceptualization. Ethan Struhs pyrolyzed biomass to produce samples. Farid Sotoudehnia and Armando G. McDonald performed sample characterization. Ethan Struhs wrote the manuscript with support from Farid Sotoudehnia, Amin Mirkouei, Armando G. McDonald, and M. M. Ramirez-Corredores.

Chapter 4

Contributors: Ethan Struhs, Amin Mirkouei and Armando G. McDonald contributed to the conceptualization. Ethan Struhs pyrolyzed biomass to produce samples. Ethan Struhs and Armando G. McDonald performed bio-oil sample characterization. Harrison Appiah determined bio-oil higher heating values and performed proximate analysis on biochar. Ethan Struhs wrote the manuscript with support from Harrison Appiah, Amin Mirkouei, and Armando G. McDonald.

Chapter 5

Contributors: Ethan Struhs and Amin Mirkouei contributed to the conceptualization. Ethan Struhs performed LCA and simulation modeling. Ethan Struhs and Amin Mirkouei performed TEA and analysis. Ethan Struhs wrote the manuscript with support from Amin Mirkouei, Yaqi You, and Amir Mohajeri.

Chapter 1: Introduction

1.1 Research Motivation

On a global scale, the demand for transportation fuels is projected to grow by 40% by 2035 [1]. Currently, the transportation sector is responsible for 28% of total US energy consumption where 90% is derived from crude oil [2]. The majority of total energy consumed by the US comes from nonrenewable sources, which contribute significantly to greenhouse gas emissions (Figure 1.1) [3]. Therefore, bioenergy produced from renewable resources is key for mitigating the rise in greenhouse gas emissions. Among all renewable sources of energy consumed, biomass is the greatest contributor as a source of heat and electricity [2]. Currently, bioenergy production from various biomass feedstocks comprises the largest portion of renewable energy sources in the U.S. [4].

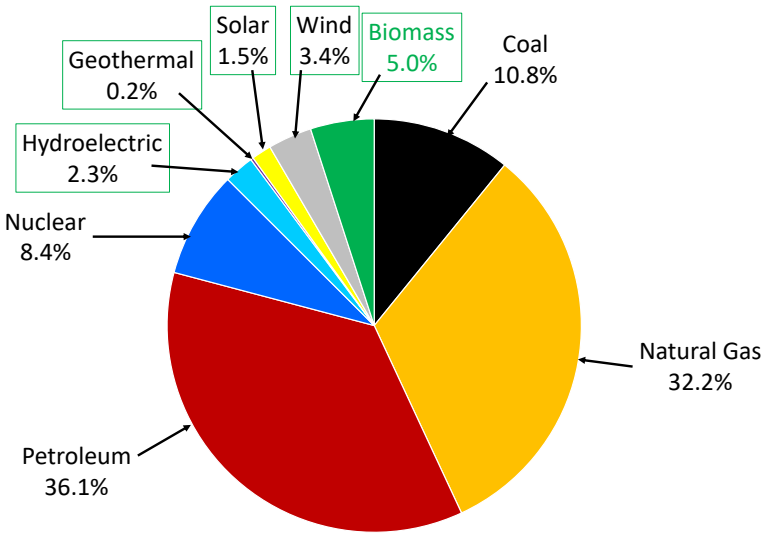

Figure 1.1. USA energy consumption for 2021.

Biomass is an abundant raw material that can be used for the production of biofuel blendstocks, pharmaceutical chemicals, and soil amendments [5]. It has the potential to address challenges faced by energy security, environmental impacts, and developmental concerns faced in rural regions [6]. Through various conversion technologies, renewable biomass can be converted into energy products that help offset nonrenewable source dependence and subsequent greenhouse gas emissions [7]. However, over 45% of raw biomass is underutilized due to a lack of commercial technologies [8]. As such, attention needs to be placed on biomass-to-energy conversion pathways and strategies.

1.2 Background

Lignocellulosic biomass is seen as a promising source for renewable energy products due to desired characteristics (e.g., natural abundance and conversion potential) [9]. Feedstocks such as agricultural waste and forest residue have the added benefit of not being competitors in food and land markets. However, the current cost of technologies for biomass conversion pathways makes biofuel production economically unfeasible [10].

Thermochemical technologies can be feedstock flexible, efficiently converting a variety of biomass feedstocks to fuel, heat, and power [11]. The resulting product can vary greatly in yield and quality, depending on operating conditions, unit configuration, and feedstock type. Pyrolysis stands out as a promising pathway for bio-oil production due to its high product quality [12]. Pyrolysis processes can be categorized according to operating conditions, namely, slow and fast pyrolysis. Slow pyrolysis describes a process that favors higher yields of carbonaceous solids with conditions of low heating rates (0.1-1°C/s), moderate temperature (300-500°C), and long residence times (<10 min) [13]. Fast pyrolysis favors higher liquid oil yields and is defined by high temperatures (400-650°C), fast heating rates (10-200°C/s), and short residence times (<2 s) [14].

The quality of the obtained bio-oil varies with biomass composition, process conditions, and type of catalyst employed. Bio-oil is a complex mixture of a variety of chemical compounds and functional groups that tend to react with each other, giving way to volatile unstable composition [15]. Because of this, the interactions among bio-oil compounds create problems, resulting in low heating value, thermal instability, high viscosity, and corrosion. Factors such as water content, abundance of oxygenated compounds, ash content, chemical instability, and high viscosity make bio-oil incompatible with conventional fuels [16].

Fast pyrolysis process in the presence of a catalyst is capable of producing bio-oil with the improved quality through key reactions such as cracking, hydrocracking, hydrogenation, decarbonylation, decarboxylation, and hydrodeoxygenation [17,18]. One of the major challenges faced by catalytic fast pyrolysis is the identifying stable, highly active, selective, and inexpensive catalysts that maximize the quality and yield of bio-oil for further processing [19]. The two main pathways for catalytic upgrading (i.e., hydrodeoxygenation and zeolite cracking) have received great attention, but further research into single-stage and multi-stage upgraded is needed to identify a commercially viable route [20].

An additional promising method to increase yield, quality, and stability of bio-oil is by direct quenching [21]. Direct quenching involves the pyrolysis vapors and gases making direct contact with

a liquid coolant. This method of condensation is able to capture lighter weight molecules entrained in the incondensable gases and mitigate undesirable secondary reactions [22]. Generally, immiscible hydrocarbon solvents, alcohols, and recirculated bio-oil are chosen as the cooling media [23,24]. The advantages of using these kinds of condensers include high heat transfer rates and physicochemical interactions between liquid and vapor. Properties of the liquid coolant may even result in stabilization of condensed bio-oils [25,26].

Another valuable product of pyrolysis is biochar, with applications as a fuel, fertilizer, and eutrophication reduction material [27,28]. When applied to soil, biochar significantly improves nutrient supply to crops and soil physical and biological properties while reducing greenhouse gas emissions [29]. Biochar is also seen as a solution for environmental carbon capture and storage as it is biologically stable, giving it the ability to slowly release carbon back into the soil [30]. Though many studies outline the advantages of biochar for environmental purposes, lack of established large-scale management practices creates limitations for biochar market assessment [31,32].

Suitable pyrolysis pathways for high-value products can be identified through assessments of techno-economic feasibility and environmental impact. The goal should be to create a technology that is not only cost-competitive, but one that decreases greenhouse gas emissions and sustains a competitive biomass-based energy market [29]. Due to the nascency and lack of an established market for pyrolysis products, future prices of biofuel and biochar are met with a high degree of uncertainty [33].

1.3 Research Objectives

The aim of this research is to identify and develop a thermochemical technology pathway for the conversion of biomass to valorized liquid (bio-oil) and solid (biochar) products with desirable chemical and physical properties by examining pyrolysis unit configuration and product recovery techniques. The goal is to distinguish cost-effective techniques to produce nutrient-rich biochar, thermally stable bio-oil and propose future work to progress the field of pyrolysis unit development for marketable bioproducts. Research objectives to achieve this goal are:

1. Exploring feedstock thermochemical conversion pathways and bio-oil upgrading and recovery processes.
2. Investigating the characteristics of bio-oil and biochar produced from different feedstocks in a continuous free-fall fast pyrolysis reactor.
3. Examining catalytic fast pyrolysis configurations and the effect on liquid product chemical and thermal properties.

4. Exploring the recovery and fractionation of bio-oil using direct quenching methods.
5. Assessing the feasibility of a pyrolysis unit to produce nutrient-rich biochar through techno-economic and life cycle impact analyses.
6. Characterization and comparison of resulting products to assess state pyrolysis unit effectiveness.

1.4 Dissertation Outline

This dissertation is presented in a manuscript format and consists of six chapters and an appendix. Chapter 1 covers the research motivation, background, research objectives, and tasks.

Chapter 2 is a review on thermochemical biomass conversion technologies and pathways geared to increase the fuel properties of liquid bio-oil. Challenges in production, commercialization gaps, and potential solutions to address market needs are also identified. This chapter is an article published in *Journal of Environmental Chemical Engineering*.

Chapter 3 assesses the bio-oil and biochar attributes produced using a custom free-fall pyrolysis reactor and several feedstocks. Bio-oil and biochar sample physical and chemical properties are assessed through multiple characterization techniques. This chapter is an article published in *Journal of Analytical and Applied Pyrolysis.*

Chapter 4 attempts to address stable bio-oil production from biomass and improve applicability. A comparison of ex-situ and in-situ catalytic pyrolysis using γ-alumina as a catalyst is performed, while the potential of methanol for direct quenching fractionation is investigated. This chapter is an article that has been submitted to *Journal of Analytical and Applied Pyrolysis.*

Chapter 5 provides techno-economic and environmental impact assessments with stochastic optimization modelling to calculate the total cost and emissions of biochar production and distribution, highlighting the practical use of portable pyrolysis units to convert cattle manure to biochar on-site and reduce the carbon footprint of conventional cattle manure management practices. This chapter is an article published in *Applied Energy.*

Chapter 6 provides the summary, overall conclusions, research contributions, and recommends routes for future work.

Chapter 2: Overview and technology opportunities for thermochemically-produced bio-blendstocks

This chapter was published in *Journal of Environmental Chemical Engineering*, under the title "*Overview and Technology Opportunities for Thermochemically-Produced Bio-Blendstocks*," by Ethan Struhs, Amin Mirkouei, Maria Magdalena Ramirez-Corredores, Armando G. McDonald, and Martha L Chacon.

https://doi.org/10.1016/j.jece.2021.106255.

2.1 Abstract

Global demand for transportation fuels is projected to increase 40% by 2040, and biomass-derived fuels (biofuels) play a crucial role in substituting fossil fuels and mitigating greenhouse gas emissions. Currently, biofuels are mainly consumed as blendstocks combined with petroleum-based fuels, and effective conversion technologies can address the quality challenges for offering standalone biofuels. Thermochemical conversion process is one of the most promising pathways among existing technologies for biofuel production. However, the major barriers are unwanted characteristics (e.g., thermal instability) of intermediate products, such as bio-oil, and required upgrading treatments for producing compatible fuels. This study highlights the merits and critical challenges of thermochemical conversion and physicochemical upgrading technologies for bio-blendstock production from lignocellulosic biomass. The novelty of this study lies in potential directions for future research through both critical and systematic literature reviews, and the proposed intensified process for lignocellulosic-based fuel blendstocks production. It is concluded that recovery and fractionation strategies (e.g., quenching and stripping) can maximize process yields and add values in the efficient conversion pathways. Effective quenching can stop secondary free radical reactions and improve liquid yields over gas and solid yields. Stripping process can improve process yield, catalyst lifespan, and thermal stability. It is further concluded that physicochemical treatments are not as effective as thermochemical treatments, but have advantages of mild operating conditions and potential for integrated solutions in conjunction with other treatments.

2.2 Introduction

Fossil fuels (predominantly diesel, jet fuel, and gasoline) are used extensively in different sectors (e.g., transportation, agriculture, commercial, domestic, and industrial) for various purposes, such as manufacturing operations, process heating, and electricity generation. On a global scale, the transportation sector is almost entirely dependent on petroleum-based fuels and is responsible for over

60% of the world's crude oil consumption [34]. According to the International Energy Agency and the US Energy Information Administration, the energy produced from fossil fuels significantly contributes to greenhouse gas (GHG) emissions, which are responsible for global warming and climate change [3]. Therefore, renewable fuels (e.g., biofuels) from renewable resources (e.g., agricultural and forestry resources, algae, and municipal solid waste) are valid substitutes to petroleum-based transportation fuels key for mitigating GHG emissions.

Biofuels can address several sustainability challenges and national priorities, such as energy security, foreign exchange savings, environmental impacts, and socio-economic concerns related to rural regions. Advantageously, lignocellulosic-based biofuels significantly solve environmental issues and simultaneously circumvent ethical dilemmas between energy production and food supply chains [6]. The growing interest in widespread use and application of biofuels stems from the need to overcome two of the world's greatest and urgent needs to (i) veer away from the unsustainable dependence on fossil fuels and (ii) mitigate humankind's impacts on global climate change [35].

Biomass-to-biofuel supply chains suffer from the upstream (e.g., biomass supply and pretreatment) and midstream (e.g., process efficiency and product quality) challenges that increase the total production cost and reduce commercial viability [36]. In fact, the costs of current technologies for biomass pretreatment (e.g., size reduction and dewatering), conversion (e.g., pyrolysis or gasification), and upgrading make biofuel production, economically unfeasible [10]. The present operating costs of conversion and upgrading are the major cost-driver for biofuel production, consisting of over 60% of the total cost [37]. A significant research effort is being put into transforming biomass to biofuels by focusing on conversion processes, resulting in various developed technologies, including biochemical and thermochemical pathways [38]. Thus far, each technology offers unique advantages and disadvantages, however, none of them has overcome the economic barriers to become viable and sustainable.

Lignocellulosic biomass (i.e., dry plant matter, consisting mainly of lignin, hemicellulose, and cellulose) has several advantages that set it apart as a convenient source for renewable energy, such as natural abundance, inedible raw materials that do not compete within the food markets, and avoidance of land-use competition [9]. The large abundance of lignocellulosic resources provides great potential for fuels and green chemicals production (Figure 2.1). Studies on supply chain and integrated biorefineries recommend performing pretreatments and conversion processes near collection sites, for biomass, volume, and energy densification. In this way, transporting highly compacted and high-energy density materials will reduce upstream issues and costs, instead of moving high moisture content and low-energy, large volume biomass resources.

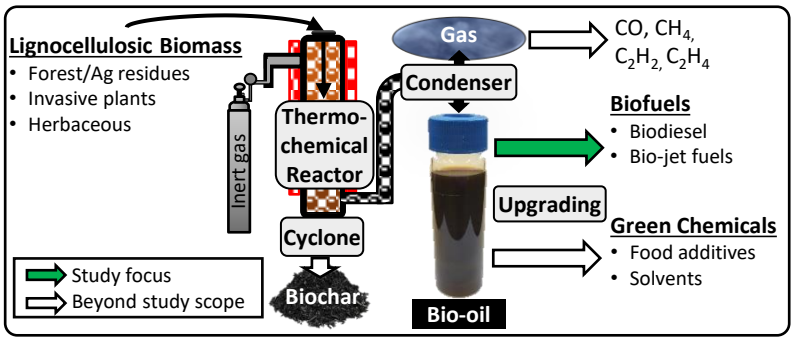

Figure 2.1. Biomass thermochemical conversion pathway to biofuels and green chemicals

Among the conversion technologies, thermochemical processes (e.g., gasification, hydrothermal liquefaction (HTL), and pyrolysis) have proven to be an appealing way to produce biofuel blendstocks from the valorization of intermediate products (e.g., bio-oil) [39]. A specific feedstock may be suitable for a particular process over another process, therefore, feedstock composition is essential in determining the optimal process. Additionally, pyrolysis, especially catalytic fast pyrolysis (CFP), stands out as a promising pathway for bio-oil production due to its high product quality [12]. Rapid condensation of pyrolysis vapors is essential for inhibiting undesired over-cracking. Therefore, various techniques have been considered to maximize bio-oil recovery operations, such as quenching, stripping, aerosol condensing, and fractionation [21]. These techniques attempt to avoid liquid yield losses and improve its quality by increasing the recovery rate and decreasing coking, biochar entrainment, and entrapment by the non-condensable gases.

Compared to crude oil, bio-oil exhibits a greater O/C ratio and a lower H/C ratio, determined by the presence of oxygenated organic compounds and water that, in turn, confer on a poor energy value. Productive use of bio-oil has proven challenging due to the need for enhancements before consumption. Using current combustion engines and boilers is deterred by bio-oil deficient fuel characteristics, instability, and complex chemical compounds [40]. Bio-oil can also suffer from many adverse effects regarding its quality, including incompatibility with traditional fuels due to high water and oxygen content, high solids (or ash) content, chemical instability, and high viscosity [16]. Several optional pathways (e.g., fluid catalytic cracking, hydrotreating, and electrochemical) have been considered to upgrade bio-oil to transportation fuels [17]. Upgrading objectives include (i) reducing oxygen (deoxygenation) and water content and (ii) increasing the hydrogen content (hydrogenation) to become compatible with fossil fuel components, existing

combustion engines, and fuel distribution infrastructure. Figure 2.2 presents several key chemical reactions occurring during bio-oil upgrading processes.

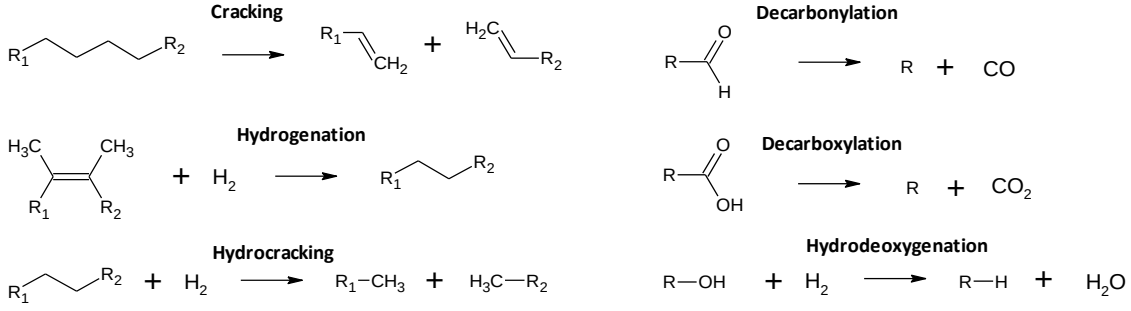

Figure 2.2. Chemical reactions for upgrading bio-oil to biofuels

Objective. *This study* applies both critical and systematic review techniques to explore thermochemical approaches and advancements of biomass conversion and bio-oil upgrading processes, as well as to identify production challenges, unsolved problems and issues, commercialization gaps, and potential solutions to address market needs. Special attention is given to the insights of current technologies to further visualize potential promises or capabilities that may address known inadequacies. Additionally, this study proposes an intensified process, including thermochemical conversion and physicochemical upgrading technologies for lignocellulosic-based fuel blendstock production.

2.3 Systematic Review

Systematic reviews can help in identifying and integrating previous relevant studies to ascertain the scope of existing research, and the followed trends, as well as to potentially identify gaps and contradictions, and forecast directions for future studies. The conducted search strategy herein assesses keywords, publication records, citations, and research methodologies on published studies surrounding lignocellulosic-based fuel production. Furthermore, the presented analysis covers relevant technologies related to the conversion and upgrading approaches used for functionally equivalent biofuel production. To conduct the systematic review, two databases were generated for this study, using the following keyword sets and Web of Science, searching the titles, abstracts, and keywords of published peer-reviewed articles (TS, advanced search field tag) between January 2010 and December 2020. The search results show 5,478 and 5,792 records for keyword sets 1 and 2, respectively. A comparison of the two databases found 1,064 articles in common.

- Keyword Set 1: TS = (Biomass OR Lignocellulosic) AND (Bio-oil OR Thermochemical) AND (Biofuel OR Fuel OR Upgrading)

- Keyword Set 2: TS = (Biomass OR Bio-oil OR Thermochemical OR Pyrolysis) AND (Fuel OR Biofuel OR Upgrading) AND (Electrochemical OR Hydrotreatment OR Hydrogenation OR Cracking OR Ultrasound OR Ultrasonic)

Figure 2.3 presents that the interest in this field is accelerating over the last ten years. From the systematic review results for the keyword searches, bio-oil production and upgrading research is rising, with the most advancement occurring over the last three years. Bio-oil recovery methods mentioned in the keyword set 1 saw increased publications in general. Keyword set 2 shows the growing interest in catalytic upgrading, electrochemical, and ultrasonic upgrading technologies reflected by the continual increase in publications during the past ten years.

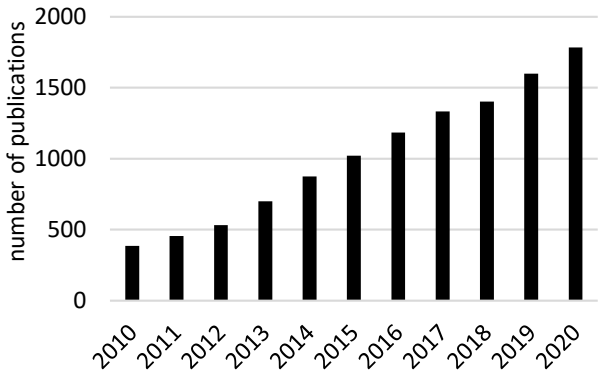

Figure 2.3. Increase in number of publications by year for both keyword sets during the last ten years

Figure 2.4 depicts subsets of the retrieved, combined publications, providing insight into subjects of interest within the keyword sets. Using keyword sets 1 and 2, the most studied technology is pyrolysis, which catalytic pyrolysis is major. During these ten years, the number of gasification and HTL publications are almost marginal. The most discussed issues were yield and quality of the products, followed by deactivation and recovery. Published studies focused more on upgrading and product slate, with much less focus on feedstock type and technology development.

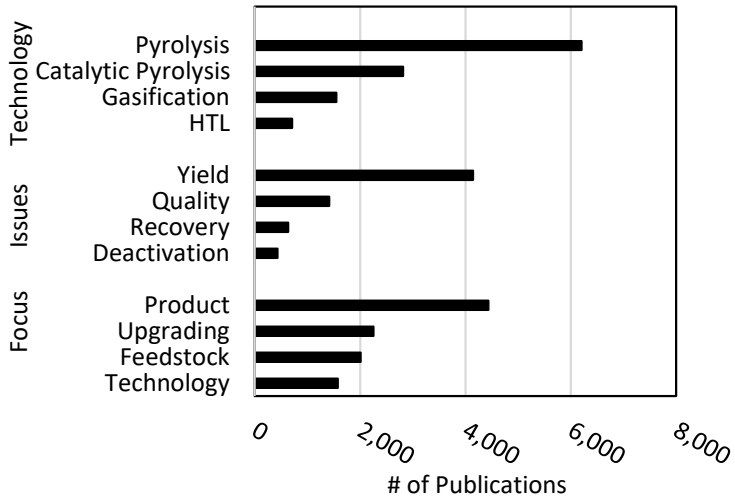

Figure 2.4. Classification of keyword subsets

Looking into the most cited articles of each keyword set can provide insight into popular data and topics in the current scientific community. Carpenter et al. (2014) is the most cited article in the keyword set 1 and reviews feedstock and pretreatment impact on bio-oil yield and product distribution [41]. It was found that little is known about the effects of pretreatment and feedstock, and current studies were summarized. Chen et al. (2015) appeared as the second most cited article in the same keyword search, performing a review on the thermochemical conversion (e.g., torrefaction, liquefaction, pyrolysis, and gasification) of microalgal biomass into biofuels [42]. The conversion processes and subsequent products were described. The third most cited, Lehto (2014), reviewed combustion and quality of fast pyrolysis bio-oil from lignocellulosic biomass, focusing on bio-oil burning applications [43]. They recommend that bio-oil grades should be standardized to create reliable bio-oil combustion systems, and attention should be placed on quality control from feedstock harvesting to end-use. Zhang et al. (2013) is the fourth most cited article and reviewed fast pyrolysis bio-oil upgrading techniques (e.g., hydrogenation, hydrodeoxygenation, catalytic pyrolysis, catalytic cracking, steam reforming, molecular distillation, supercritical fluids, esterification, and emulsification) [44]. Current problems and future development directions are summarized.

Gilkey et al. (2016) is the most cited article in the keyword set 2, and it presents the current progress of upgrading biomass through heterogeneous catalytic transfer hydrogenation, focusing on hydrogenation mechanisms and cleavage [45]. Challenges and future research direction to turn catalytic transfer hydrogenation into a competitive process. Luo et al. (2014) ranks as the second most cited paper, which assessed advancements for using sonication for biomass pretreatment and conversion to fuels and chemicals [46]. Ultrasound was shown to provide positive process benefits,

depending on frequency and intensity. Bussemaker et al. (2013) appears as the third most cited article from keyword set 2, studying the effects of ultrasound as a pretreatment method for biorefinery applications [47]. They conclude that a mix of high-frequency ultrasound, oxidizing solutions, and the use of combined alternative augmentation techniques have the potential for reducing energy requirements and provide synergistic ultrasonic enhancement. Hu et al. (2014) is the fourth most cited article and systematically summarizes selective hydrogenation of hydroxymethylfurfural to dimethylfuran [48]. Several hydrogen donors (e.g., molecular hydrogen, formic acid, alcohols, and water) were discussed, and the reaction mechanisms of dimethylfuran, combustion performance, and safety issues of dimethylfuran.

Ultimately, the citation trend indicates a clear move towards green chemicals that represent higher value-added products compared to biofuels or bio-blendstocks, which might be an attempt to leverage the deficient economics of upgrading. Based on the systematic review results, thermochemical treatment methods (e.g., fractionation, hydrotreatment, and fluid catalytic cracking) have been extensively studied and reviewed compared to other physicochemical methods, such as ultrasonic cavitation (UC) treatment. There are 112 studies that applied UC treatment method during the past ten years, showing a growing interest and UC's potentiality. However, thermochemical methods can be considered as the leading and mature methodology compared to other methods.

2.4 Critical Review

A critical review was conducted to identify recent advancements and breakthroughs to elucidate the current state of biomass-to-biofuel production pathways. Particularly, the critical review focuses on bio-oil production, recovery, and upgrading to explore existing challenges and potential solutions for future research and development.

2.4.1 Bio-oil Production

Thermochemical pathways have dominated the conversion of biomass into bioproducts (e.g., chemicals and fuels). Many of these approaches, however, utilize high temperatures and pressures and are very indiscriminate in product yield and quality, leading to the production of fuels exhibiting hydrogen deficiency and oxygen enrichment as opposed to that of conventional fossil fuels [49]. Thermochemical conversion processes (e.g., fast pyrolysis, catalytic pyrolysis, and hydrothermal liquefaction) produce varying bio-oil qualities, each with unique advantages and deficiencies.

2.4.1.1 Pyrolysis

Fast and slow pyrolysis. Pyrolysis can be categorized into two broad groups: slow pyrolysis (SP) and fast pyrolysis (FP). SP operates at moderate temperatures (300-500°C), low heating rates, and long residence times (0.2-60 min) and is more favorable for biochar production [50]. Biomass pyrolysis is the thermochemical decomposition of solid materials that can be highly affected by mass and heat transfer phenomena. Thus, parameters, such as temperature and heating rate (thermal component), as well as composition, particle size, and shape, and residence time (the chemical component), will affect thermochemical reactions and material reactivity. FP is a promising technology, using high temperatures (400-650°C), rapid heating rates (up to 1000°C/s), short residence times (below 2s), and rapid quenching of the produced vapors to achieve high liquid yield [14]. In the vein of FP, there are several different reactor designs and configurations (e.g., fluidized bed, microwave, ablative, auger, and free-fall) to convert biomass feedstocks into the liquid product (bio-oil) [51], each of these offering a range of advantages and disadvantages. Figure 2.5 depicts a pyrolysis scheme incorporating mixed fast and slow pyrolysis to optimize the yield and quality of products. Fan et al. (2017) reviewed the effects of process parameters, including temperature, reactor types, residence time, feed rate, and lignin characteristics, to determine the optimal parameter conditions for improving process yield and bio-oil quality [52]. However, the optimal conditions for improved yields and quality remain unknown. The understanding of the pathways and mechanisms underpins the development of more robust processes. A comprehensive review of proposed pathways and mechanisms for pyrolysis and catalytic pyrolysis of biomass components and the whole biomass was published in 2013 [53]. For hemicellulose, more recently, Zhou et al. developed a mechanistic pyrolysis model to detail its decomposition pathways during pyrolysis to improve the understanding of occurring chemistry and kinetics [54]. Suriapparao et al. (2018) analyzed the effects of biomass particle size, shape, composition, heating rate, and residence time on the kinetics of devolatilization during slow pyrolysis, and bio-oil composition in fast pyrolysis to find ideal parameters for plant scale-up [55].

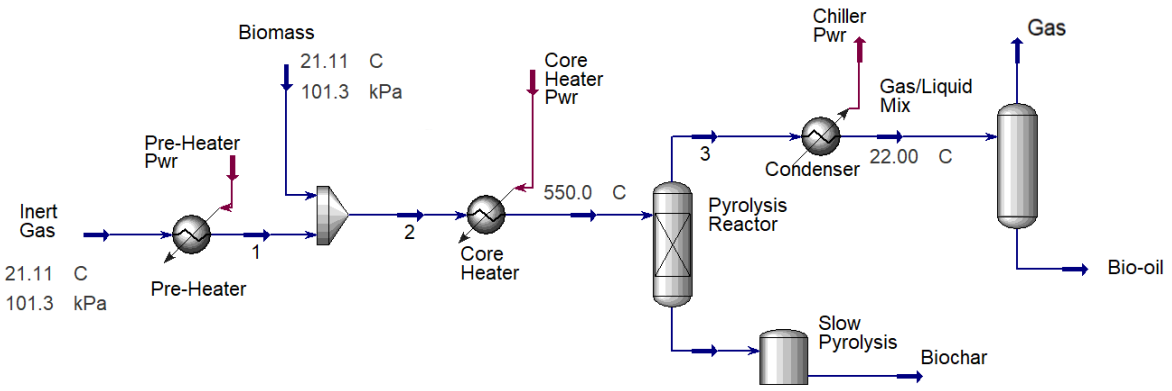

Figure 2.5. Aspen HYSYS scheme of mixed fast and slow pyrolysis unit **[56]**

Further research into pyrolysis oil characterization and analysis, upgrading methods, and reactor design optimization is required for viability. Extensive reviews of FP have been done by Bridgwater (2011), Mostafazadeh et al. (2018), and Sharifzadeh et al. (2019) [16,57,58]. As the conversion step in biofuels production, FP has not reached a commercial scale, which indicates the existence of unresolved issues and challenges. Bio-oil from FP suffers from many detrimental physical and chemical properties, including undesirable O/C and H/C ratios, high water and ash content, and low higher heating value that necessitates further chemical upgrading and prevents it from being competitive with fossil fuels [17].

Catalytic fast pyrolysis (CFP). CFP integrates catalytic transformations with FP to produce smaller molecules and improve the O/C and H/C ratios, which is more suitable for biofuels and green chemical production. CFP improves selectivity and enables the occurrence of new chemical reactions during pyrolysis (e.g., decarbonylation, decarboxylation, dehydroxylation, and hydrogen transfer), enhancing bio-oil properties through reduction of the oxygen content and of molecular weight, and changing molecular structures to be closer to that of transportation fuels [59]. Techno-economic analysis of the CFP technology estimates minimum selling fuel price as about $3.3/G for ex-situ CFP, and $2.5/G for in-situ CFP [60], positioning CFP as a viable thermochemical alternative for producing more compatible products in comparison to other conversion pathways. However, the most competitive minimum selling fuel price was assessed, using KIOR's configuration and public information, but the bankruptcy and shut down of this plant is clear evidence that economic sustainability and such competitive prices are unrealistic. Technical feasibility and bio-oil quality improvements are supported by published data, an example is provided by Zhang et al., who performed a comparison of CFP and FP, using HZSM-5 as a catalyst and corncob as a feedstock in a fluidized bed reactor, demonstrating that the presence of catalysts reduced the oxygen content of bio-

oil by 25% [61]. Ciesielski et al. reported on the role of integrated multi-scale modeling and experimentation in supporting strategies for technology development and its eventual commercialization. They emphasize the fact that isolated solutions to individual problems might not lead to holistic solutions. The improvements needed for the CFP pathway require additional clarification of physical and chemical interconnected multi-scale phenomena, as well as a multidisciplinary and multifaceted approach. The entire visualization of the challenges and their interplay for the whole process technology was suggested [62]. Catalyst screening for selective deoxygenation to improve bio-oil quality, avoiding detrimental effects on yield, was reported for many catalysts, including Al_2O_3, CaO, MgO, CuO, Fe_2O_3, NiO, ZnO, ZrO_2, TiO_2, HZSM-5, and MCM-41. The balance between yield and deoxygenation could be provided by increases in decarboxylation combined with a decrease in dehydration [63].

Notwithstanding research advancements, government funding, and predicted economic feasibility, CFP has not yet realized widespread industrial implementation [64]. One of the CFP challenges is the design of highly active, selective, and stable catalysts that could maximize the bio-oil yield of suitable quality for further processing [19]. The other and probably most relevant challenge is the development of feedstock-flexible processes, particularly processes that could cope with biomass feedstock variability [65]. Finally, process development requires an integrated view of all the unit operations involved from feeding throughout to product recovery, together with a holistic visualization for upstream (supply of conversion-ready feedstocks meeting process specifications) and downstream operations (providing a bio-oil product suitable for upgrading).

2.4.1.2 Hydrothermal Liquefaction (HTL)

HTL is a thermochemical liquefaction process used to convert biomass into bio-oil at high temperature (200-400°C), pressurized conditions (3,500-6,000 psi), i.e., water sub-/super-critical conditions, which provides means for treating high moisture biomass feedstocks (e.g., algae) without the need for drying or dewatering [66]. Since pretreatment (e.g., dewatering and size reduction) of feedstock is one of the energy-intensive steps in converting biomass to value-added products (e.g., fuel, cosmetics/perfumes, food additives, nutritional supplements, detergents, and plastics), HTL can take advantage of low dewatering requirement, for reducing the pretreatment costs [67]. Additionally, catalysts are not required for the HTL process, however, there has been a significant change in gears towards using catalytic approaches to improve the quality of the products obtained by HTL technology [68].

Recent studies have investigated the effect of process conditions on bio-oil quality and yield for the HTL conversion pathway, using algae as feedstock to liquid fuels and varying temperature, residence time, and catalyst. Zou et al. achieved a maximum bio-oil yield of 26% for the HTL of microalgae *Dunaliella tertiolecta* at 360°C, and 50 min of reaction time, using 5% Na_2CO_3 as catalyst [69]. Biller et al. found that bio-oil yields were 25% higher than the lipids content of various microalgae with different biochemical compositions, using 1 M Na_2CO_3 and 1 M formic acid during HTL operation, indicating conversion products from the proteins and carbohydrates also present in the feedstocks [70]. Bio-oil yield could be increased by increasing temperature, biomass loading amount, and residence times, while water density had negligible effects [71]. Catalyst screening (Pd/C, Pt/C, Ru/C, Ni/SiO_2−Al_2O_3, CoMo/γ-Al_2O_3 (sulfided), and zeolite) under HTL processing of microalgae *Nannochloropsis* sp., and in the presence and absence of hydrogen has been reported. The only effect of hydrogen was to decrease the gas yield, and only the Ni catalyst exhibited catalytic (desulfurization) activity [72].

Although HTL initially focused on the highest moisture feedstocks, i.e., algae, it showed promising results for good quality diesel production. The net economy derived from the higher pressure (5-25 MPa) and longer residence time has hindered the commercialization of this application [66]. Further research is needed to better understand the interplay complexity of critical parameters (e.g., temperature, pressure, catalyst effect, and residence time) and broaden the application from wet biomass towards dry feedstocks. More information on HTL of biomass has been provided by Toor et al. (2011), Gollakota et al. (2018), and Ponnusamy et al. (2020) [73–75]. Nevertheless, commercialization of the HTL process technology has followed a different course of action, and currently, four companies have based their production on this technology, namely ARA ReadyFuels, Licella-Canfor, Renmatix, and Steeper Energy. This new course of action concerns the production of higher value-added products and, in few instances, is accompanied by biofuels.

2.4.1.3 Gasification and Synthesis

Gasification is another thermochemical process in which biomass reacts with a gasification agent (e.g., air, oxygen, CO_2, steam, or supercritical water) to produce synthesis gas (syngas) [76]. Operating conditions are very high temperatures (750-1,000°C or higher) and approximately atmospheric pressure. Syngas is a mixture composed of CO and H_2, with minor amounts of other compounds depending on the feedstock and process technology employed. The Fischer-Tropsch (FT) process can be used for the synthesis of hydrocarbons from syngas. In addition to hydrocarbons, methanol (and ethanol) can also be synthesized, and attractive chemicals and fuels can be derived from tandem reactions, e.g., methanol-to-olefins (MTO), methanol-to-gasoline (MTG), and ethanol-

to-jet (ETJ) [77]. The produced liquid hydrocarbons from syngas are identical to those present in fossil fuels and products, requiring only mild finishing treatments [78]. Regardless of the hydrogen-depleted nature of biomass, most of the efforts have been targeting a high H_2/CO ratio of the product. For instance, Fe in Fe/CaO catalysts improved the H_2 concentration and yield for a fluidized bed gasifier [79]. Catalytic gasification has been proven a valid approach for enhancing the selectivity toward H_2 formation in the gasifier [80]. Biofuel production through the gasification pathway was only economically feasible at very high oil prices [81].

While gasification and FT synthesis are mature technologies when applied to fossil resources, but that is not the case for renewable resources. The production of hydrocarbons has also reached maturity through this pathway from carbonaceous (fossil) viscous and solid materials, such as bitumen and coal (coal to liquid, CTL processes), which biomass (biomass to liquid-type of processes) do not appear to be competitive [82]. Further information on gasification and synthesis has been provided by Molino et al. and Santos and Alencar [82,83]. At this point, it is worth mentioning that while this pathway is economically hindered for the case of biomass, it has become the preferred technology for the processing of municipal solid wastes, and several companies have centered their business model on it, such as Enerken and Red Rock.

2.4.2 Bio-oil Recovery

Currently, the considered conversion processes operate at a smaller scale than the processes considered for bio-oil upgrading. Therefore, bio-oil must be produced, recovered, and accumulated from a few conversion units before being fed to the upgrading unit. More than one operating unit needs to be integrated into a recovery train or system. Some of these operating units for bio-oil recovery have been proven, and their objective is to maximize yield recovery of produced bio-oil, minimizing any organic losses through the system.

2.4.2.1 Quenching

Quenching in chemical processes refers to the rapid cooling of the reacting media to temperatures below which the undesired reactions will not occur. It is a widely practiced heat exchanging process where liquid coolant comes into direct contact with gases and vapors (Figure 2.6). Pyrolysis units commonly utilize quenching columns to condense pyrolysis vapors to form liquid bio-oil [16]. Standard coolants comprise immiscible hydrocarbon solvents or even recirculated liquid bio-oil. Rapid condensation of pyrolysis vapors is essential in mitigating bio-oil yield losses by preventing secondary reactions of the most reactive species (e.g., free radicals) present in the vapor phase [84]. High heat transfer rates between the vapor and coolant liquid are the main requirement when

implementing quenching in pyrolysis, while one of the main advantages is the significant amounts of gas scrubbing.

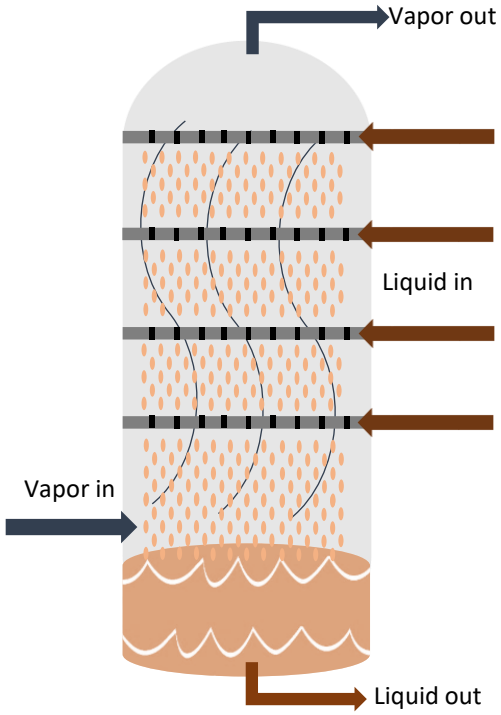

Figure 2.6. Quenching spray tower schematic

Spray towers/columns are commonly used for quenching. Incorporating a quenching spray tower in the FP process and using previously produced bio-oil as a quenching liquid, Shemfe et al. (2015) increased the total condensable vapor recovery factor by over 17%, with a bio-oil collection efficiency of 84%, indicating the suitability of bio-oil as quenching liquid [85]. This method was also effective at preventing tar buildup on the walls of the condenser. Using a Venturi scrubber/condenser to perform quenching with bio-oil during pyrolysis has also been shown to improve the collecting rate to 95-98% of total bio-oil produced [86]. Daugaard et al. (2015) accomplished quenching and fractionation, using various inert gases (e.g., nitrogen, helium, argon, and other noble gases) and liquids (e.g., liquid nitrogen, bio-oil aqueous phase, and other small hydrocarbons) as quenching coolants while also manipulating quenching temperature. The various recovered bio-oil fractions exhibited higher quality [87]. Isopar, an ExxonMobil refined isoparaffin product, has also been used as a quenching coolant in pyrolysis units. Isopar is lighter than bio-oil, causing isopar to accumulate at the top of storage vessels while the bio-oil sinks to the bottom, facilitating (anti)solvent recovery and recycling [88].

Regardless of the criticality of quenching in FP, publications are not as prolific as they are in other aspects of operating units of the process [89]. Quenching columns may face problems regarding flooding and heat transfer efficiency if not appropriately designed. Flooding occurs when the flow of liquid becomes restricted because of high gas velocity, which leads to the liquid getting entrained in the vapor, pulling the fluid with vapor through the column [90]. To eliminate the phenomena of flooding, a study performed by Palla et al. (2015) examined several quenching column designs to test gas flow, liquid flow distribution, and heat transfer [21]. Park et al. (2016) studied condensation characteristics by varying heat transfer conditions in quenching, such as the ratio of vapor flow rate to liquid flow rate, as well as quenching temperatures to maximize [91]. They also developed an empirical relationship for measuring the volumetric heat transfer coefficient for direct contact heat exchangers. A recent study performed by Dalluge et al. (2019) investigated the effects of cooling rates on pyrolysis vapors had on the resulting bio-oil composition [92]. A decrease in unwanted secondary decomposition reactions was noted, as well as a significant increase in bio-oil product yield. Further information on pyrolysis condensing systems has been provided by Papari et al. (2018) [23].

2.4.2.2 Electrostatic Precipitation

ESP could be effectively used, in conjunction with quenching [93] for capturing aerosols entrained in the fluid [88]. These aerosols are fine bio-oil particles generated in condensers and exiting with the non-condensable gases [94]. Bio-oil aerosols size range from sub-micron to micron-scale [95], resulting in nearly impossible to entirely remove, using cyclones and quenching columns [96], remaining entrained in the non-condensable gas pyrolysis product. The ESP uses an electric field to generate a corona discharge, which ionizes the gas stream particles. These particles are attracted to grounded walls where they build up and are collected [97]. The liquids captured by the precipitator, along with those removed by quenching, can then either be drained to storage or recycled to the quenching unit.

Huang et al. investigated the filtration characteristics of ESP by examining several parameters, such as particle size, flow rate, voltage, and discharge polarity [98]. A train of ESPs connected in series will improve bio-oil recovery and minimize yield losses, as shown by Bedmutha et al. (2009), comparing the recovery efficiency of single and double-stage electrostatic precipitators, which were 92.4 and 93.2 wt%, respectively [99]. ESP can also be combined with condensers in the fractionation train of bio-oil. Gooty et al. (2014) used the ESP with a condenser on either side to produce bio-oil with low water content [100]. The optimized series of condensers were able to obtain an almost water-free (below 1 wt%) bio-oil in the first condenser and ESP, and a high-water content product in

the third condenser. Challenges faced by ESP usage include energy conservation and ozone generation [101]. Higher collection efficiency can be achieved using a negative polarity ESP as opposed to one of positive polarity, but the increase in ozone production makes these ESP unusable indoors. Positive polarity ES, though less economical, is more widely used. More detailed information on ESP technologies and applications can be found in earlier studies by Mizuno (2000) and Jaworek et al. (2007) [102,103].

2.4.2.3 Stripping

Stripping is the physical reverse of quenching and involves using a vapor or gas stream to remove (transfer) components from a liquid stream or from a porous solid, which is generally performed in packed columns or trayed towers. The application of stripping in pyrolysis aids in increasing catalyst life span, decreasing coking, and removing bio-oil compounds entrained within the solids (e.g., heat carrier, catalyst, biochar, and ash) that leave the pyrolysis reactor [104].

Steam stripping is commonly used in petroleum refineries for catalytic cracking to reduce coking and can have a similar application for pyrolysis. Although the needs for stripping in pyrolysis are low since most heat carriers are non-porous, they can be considerably greater for catalytic pyrolysis. Thus, stripping is a common operating unit in catalytic pyrolysis [105], though a systematic study for operating conditions, design, and configurations is still pending. An earlier study on pyrolysis shows the effect of stripping on the gas product yield and the characteristics of the produced biochar [106]. The effects of stripping in catalytic pyrolysis are multiple, including product recovery, coke formation, heat balance for units with continuous regeneration, and product distribution and quality [107].

2.4.2.4 Separation and Fractionation

Fractionation is a separation process, which involves dividing and collecting bio-oils or bio-vapors under different conditions to obtain products with varying compositions. Several fractionation concepts have been proven, including distillation, extraction, and separation by solubility properties [108]. Within these concepts, several methods are practiced, focused on producing value-added chemicals and fuels while overcoming the challenges created from the complexity of bio-oil composition and properties. Pinheiro et al. (2019) extensively reviewed the methods and strategies for bio-oil fractionation [109].

Figure 2.8a presents the fractionation of pinewood-based oil by differential precipitation. The oil is dissolved in toluene and sequentially mixed with a solvent of increased dipolar moment (e.g.,

dichloromethane – DCM, methanol). The process yields two fractions: a soluble material and a precipitate. The solid precipitate is redissolved again and mixed with a solvent mixture of increased polarity. The method enables the stepwise extraction of soluble fractions with the increased dipolar moment. Molecular-level analysis, performed via atmospheric pressure photoionization coupled to FT-ICR MS, enables access to molecular properties, such as H/C (hydrogen deficiency) and O/C (polarity) ratios for tens of thousands of compounds detected for each sample. Figure 2.7b presents the molecular composition of pine oil and its solubility cuts, represented in van Krevelen diagrams, in which the *y*-axis represents the H/C ratios, whereas the *x*-axis features the O/C ratios. Each pixel corresponds to a unique molecular formula, and the color scale indicates the relative abundance, i.e., from gray (low) to red (high) [110]. Bio-oils are ultracomplex mixtures, which chemical separation could be challenging. Regardless of its complexity, Figure 2.7b indicates a slight O/C increase as a function of increasing fraction polarity. Future and ongoing efforts are focused on liquid chromatography fractionation with online FT-ICR MS detection to capture compositional trends not easily accessible by direct infusion MS [111].

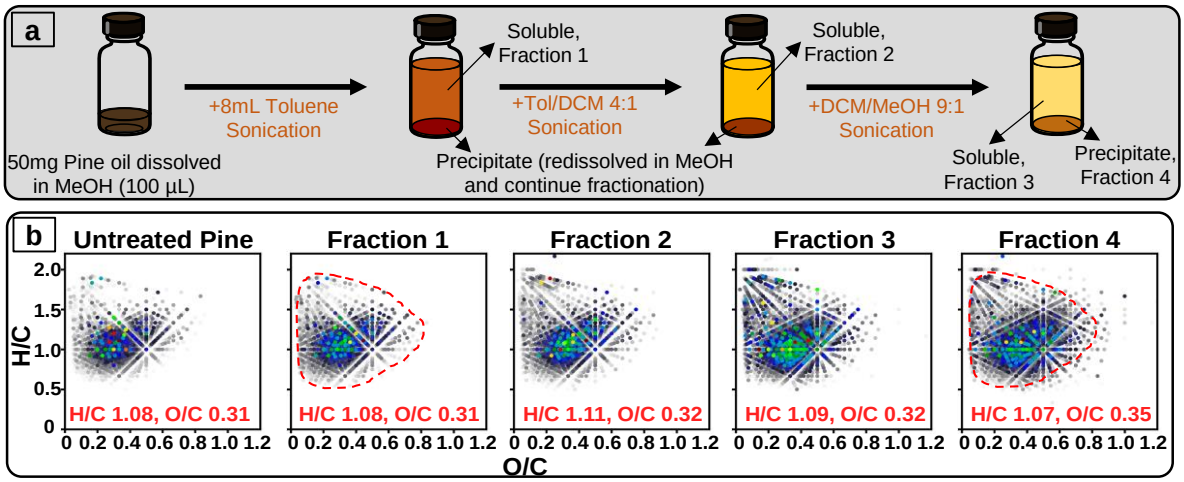

Figure 2.7. (a) Prior fractionation attempts on pinewood-based oil and (b) characterization results in Van Krevelen diagrams by MagLab's APPI 9.4 Tesla FT-ICR MS (H/C and O/C ratios included in Red)

Pollard et al. (2012) [112], Schulzke et al. (2016) [113], and Gooty et al. (2014) [100] conducted fractionation studies and developed bio-oil recovery systems, using stage fractions consisting of pairs of condensers and electrostatic precipitators in series, with each condenser operating at different temperatures. With this setup, water and acidic compounds were mostly condensed in the last stage, producing higher quality oil in the front stages. Persson et al. performed stepwise thermal treatment of the lignocellulosic biomass feedstocks rather than fractionating bio-oils. Biomass was first treated at

200-300°C and then 550°C, with the study revealing the pyrolytic liquid to have higher phenolics content and lower acid number than the liquid product from a single-step process [114]. The comparison of two different fractionation concepts (i) performing fractionation during liquid recovery and (ii) carrying it out after liquid recovery through phase separation resulted in oil with lower moisture content from the first concept, while the second proved to be more useful in dividing bio-oil into different compound groups [115]. While one stage condensing maximizes yield, other fractionation approaches are typically better for producing higher quality bio-oil [115]. Several fractionation approaches have been reported from different types of thermochemically produced bio-oils [116], however, there is a lack of literature focused on the optimization of fractionation conditions (i.e., number of stages, temperature gradients, and relative product composition comparisons), and also on comparison on the different fractionation approaches. Further information has been provided in published studies [109,117].

2.4.3 Upgrading Treatments

2.4.3.1 Catalytic Conversion

Two commonly used methods of deoxygenating bio-oil are catalytic cracking and hydrodeoxygenation. The specific catalytic conversion methods discussed in this article are fluid catalytic cracking and hydrotreating.

Fluid catalytic cracking (FCC). FCC is seen as a convenient way of using bio-oil for biofuels production without the need for significant capital-intensive investments, particularly for cases of co-processing with fossil feedstocks, in installed facilities (Figure 2.8) [118]. In FCC, bio-oil or bio-oil blend is heated to a high temperature under moderate pressure and brought into contact with a hot, powdered catalyst (acidic zeolites-based), breaking bonds of the large molecules in the absence of hydrogen. FCC is expected to show enhanced prospects for bio-oil upgrading because of its capabilities for processing heavy, complex feeds [119]. The current trend considers FCC for co-processing bio-oil with the typical petroleum feed (i.e., vacuum gas oil) in existing refinery units, resulting in a liquid hydrocarbon product that contains a small proportion of oxygenates from bio-oil [120].

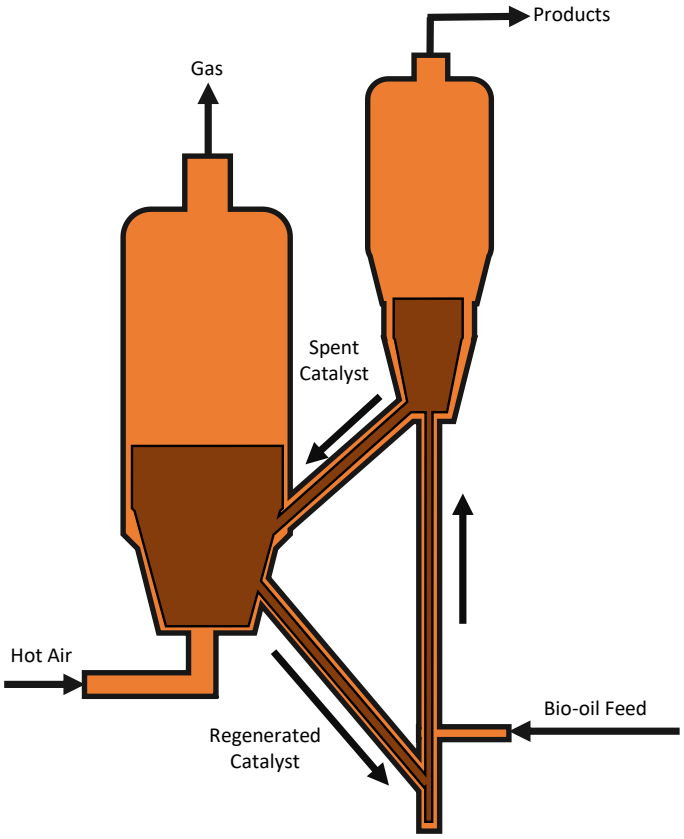

Figure 2.8. Schematic of a fluid catalytic cracking unit for bio-oil refining

Lappas et al. (2002) designed one of the first pilot plants for catalytic pyrolysis, producing bio-oil with reduced oxygen content and decreased molecular weight of the heavier fractions, finding significant synergies between the thermal and catalytic cracking of biomass [121]. Ma et al. (2018) used FCC to co-process bio-oil with kitchen waste oil with HZSM-5 as the catalyst, showing an improvement in bio-oil yield, inhibition of coke formation, and a significant decrease in oxygen content [122]. Studies that support the feasibility of co-processing bio-oil with vacuum gas oil are discussed and presented in a recent study [120], including some of the drawbacks of using FCC in co-processing. For instance, the buildup of coke, tar, and char leads to reactor plugging that causes major operational problems and decreases biofuel yield. These problems are greater when processing bio-oil and are diminished by co-processing with petroleum feeds due to the synergistic effect on the cracking of bio-oil, promoting the conversion of the oxygenates to liquid hydrocarbons [120]. Overall, FCC methods for treating bio-oils have proven to improve physicochemical properties. A review of FCC co-processing of bio-oil can be found in an earlier study by Stefanidis et al. (2018) [118].

Hydrotreatment (HDT). HDT of bio-oil is expected to eliminate the reactive functionalities by either deoxygenating, cracking, or hydrogenating the molecules [123]. Generally, achieving these HDT objectives requires higher pressures (above 125 bar) and temperatures (above 380 °C) compared with the conditions commonly used in crude oil refining due to the chemical nature of the oxygenated compounds present. However, in typical HDT operations, the feed is preheated to reaction temperatures, but this step is precluded for bio-oil due to its thermal instability. Hydrogenation has been suggested to stabilize the bio-oil, and noble metals have been tested for this purpose to avoid extreme heating stress of bio-oil [124]. Thus, two-step processes involving a first stabilizing step (hydrogenation), followed by hydrodeoxygenation, have been suggested and widely tested. In the first step, the most reactive functional groups, i.e., carbonyl and carboxyl functional groups, might be transformed into alcohols or decarboxylated, respectively. Formed alcohols are easier to deoxygenate and stabilize media that might allow heating at HDT required temperatures for cracking and hydrodeoxygenation [125]. Product properties, distribution, and relative yields depend on temperature, pressure, catalyst, and space velocity. HDT catalysts play a major part in determining product properties [126].

HDT reactions are advantageous when treating bio-oil. The massive presence of oxygenated compounds in pyrolysis oil has made HDT an effective processing option for the required deoxygenation when producing drop-in fuels or improving compatibility with commercial fuels [63]. Upgraded bio-oils proved to be more soluble in biodiesel, blends containing up to 38-48 wt% bio-oil, could be prepared upon HDT for augmenting solubility. HDT has been successfully used with Ru/C catalyst and temperatures of 200-325°C [127]. Fundamental studies mainly focus on catalyst activity but do not address the troublesome issues found in HDT. For instance, a comparison of Ni and Ru nanospring based catalysts for the HDT of phenol (as model compound) showed better activity and conversion for Ru than Ni [128].

Catalyst deactivation in bio-oil HDT is fast enough to shorten the catalyst life cycle to hours and has precluded long-term runs, even at a pilot scale. Efforts for understanding the deactivation of HDT catalysts include both noble metal hydrogenation catalysts and common HDT formulations (e.g., CoMo and NiMo). An example is the study of sulfided Ru/C and CoMo/C using various analytical techniques, which concluded that fouling caused by condensation reactions of aldehydes and ketones and loss of the catalyst active sites by the transport of inorganic elements from the bio-oil and the reactor construction material onto the catalyst surface are causes of deactivation [129]. Fouling consequences were confirmed by investigating temperature effects on the hydrotreatment of pyrolysis oil from mallee wood, on sulphided NiMo catalyst, at 375-450°C at 70 bar. Coke deposition was

favored at higher temperatures that accelerated polymerization reactions, leading to blockage and decreased product yield [130].

The reactions responsible for catalyst deactivation, reactor plugging, and coke formation are aggravated with increasing scale due to their exothermicity [131] and are exacerbated at the industrial scale at which HDT is operated adiabatically. Bio-oil instability is probably the main responsible for these issues [109], and for this reason, one approach has been the two-step processes that includes a stabilization step [15]. In summary, the required process severity (e.g., pressure, temperatures, and heat) of existing HDT technologies, together with the operational burdens derived from the bio-oil thermal instability, have made these processes cost-intensive and precluded their commercial application. New and improved processes are needed for decreasing these high energy requirements and high operational costs, therefore, enabling the commercial production of lignocellulosic bio-blendstocks. Future work on HDT should focus on the separation of bio-oil fractions and upgrading them further to value-added products. An in-depth review of bio-oil HDT has been provided by Han et al. [132].

2.4.3.2 Electrochemical Upgrading

The main use of electrochemical processes for upgrading bio-oil is electrochemical hydrogenation (Figure 2.9). Electrochemical upgrading of bio-oil benefits from mild operating temperatures and pressures, control over product selectivity, and water use as a source of protons for hydrogenation [133]. The electrochemical hydrogenation treatment of rice husk whole bio-oil, using platinum electrodes to investigate the evolution of aromatic structures was facilitated by producing radicals from cellulose and hemicellulose-derived species [134]. Elangovan et al. (2015) accomplished a noticeably decreased oxygen content after the electrochemical deoxygenation of pine oil in the aqueous phase in an oxygen ion conducting ceramic membrane-based cell [135]. Lister et al. (2018) designed a three-compartment electrochemical cell, for upgrading and stabilizing bio-oils prior to HDT. The upgraded pine bio-oil showed a lower total acid number, higher pH, and a reduction in carbonyl groups content, which were considered insufficient for HDT purposes [136]. Most electrochemical studies have taken an applied approach to demonstrate the feasibility of upgrading different molecules, giving a little perspective into optimized electrochemical biofuel production. To efficiently upgrade bio-oil into biofuel, it would require plotting out all possible complex compound reaction pathways involved in the conversion process [137]. A further expansion of the basic understanding of controlling selectivity throughout more competitive pathways, which might involve a contribution to deoxygenation, would be required to make this treatment option viable.

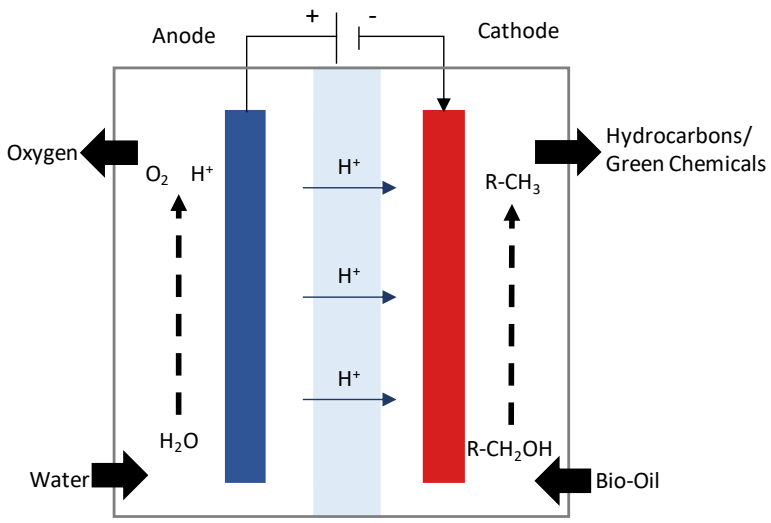

Figure 2.9. Electrochemical cell for bio-oil upgrading

2.4.3.3 Ultrasonic Cavitation

Though showing promise, few studies have been performed using UC to increase the quality of bio-oil. The application of UC proved to be an efficient and economically functional technique to increase biodiesel production [138]. UC facilitates mass transfer by increasing the formation of smaller particles and disaggregation of cluster and large agglomerated particles, with far superiority from other mixing methods [139]. Cavitation created by ultrasound might split heavy bio-oil molecules. The range of temperature and pressure in the cavitation bubbles might be high enough to cause the breaking of C-O bonds and the evaporation of water or emulsification with the bio-oil [140]. In this case, the treated oil would have lower oxygen content and viscosity. If the UC treatment is carried out in the presence of catalysts and hydrogen donors, the number of C-H bonds would increase, resulting in more stable oil. Once the bonds of the larger molecules are broken sufficiently, generation of free radicals will be favored, leading to reactions with other groups to form stable compounds, as shown in Equations (1)-(4) [141]:

$$H_2O \rightarrow \cdot OH + \cdot H \quad (1)$$

$$\cdot OH + RH \rightarrow R \cdot + H_2O \quad (2)$$

$$RR'CH - OOH \rightarrow RR'CHO \cdot + \cdot OH \quad (3)$$

$$RR'CHO \cdot + RH \rightarrow RR'CHOH + R \cdot \quad (4)$$

A UC-upgraded bio-oil exhibited a higher heating value, and no long-term stratification was observed upon storage for 112 days [141]. Qin et al. performed the UC-assisted upgrading of pyrolyzed pine-

nut bio-oil using a methanol/n-octanol mixture as a solvent. Additionally, to the increased heating value, results also a decrease in viscosity and moisture content. It was also noted that the time and power of the ultrasonic processor had a noticeable effect on the bio-oils' physicochemical properties and stability [141]. Similar experiments using pine-nut bio-oil tested the effects of using various solvents (e.g., ethyl acetate, acetone, n-octanol, and polyethylene glycol). Out of all the solvents, n-octanol proved to be the best performing solvent, increasing heating value, and decreasing viscosity with no signs of stratification 60 days after the experiments [142]. Nevertheless, the stabilizing effect of alcohols and their energy value are well-known facts [143]. Yang and Duan used HTL bio-oil from microalgae to test the effects of frequency, power, time, and temperature to analyze viscosity and elemental composition [144]. While enhanced production of bio-oil by UC has been proved [46], UC treatments have not been directly and conclusively applied to bio-oil upgrading. All these results seem to indicate promise from UC treatments in improving bio-oil physical and chemical properties, and subsequently, overall quality. Regardless of the promise shown, the lack of systematic and systemic studies limits a valid assessment of process efficiency or feasibility. Further details about UC treatments of vegetable oils or the upgrading of heavy oil are given in earlier studies by Kumar (2017) and Xie et al. (2015) [145,146].

2.5 Discussion

The current state of the transportation sector, its impact on undesirable emissions, and the imminent implementation of decarbonizing strategies bring about the use of biomass feedstocks and low-emissions energy sources in the game for more efficient production and valorization of conversion products in various forms to low-carbon and carbon-neutral fuels. The conducted critical and systematic reviews in this study offer an overview of existing lignocellulosic biomass-to-biofuel technologies, emphasizing each of the operating units that still exhibit problems and represent challenges for bringing technology to the market plate. The challenges associated with producing a stable bio-oil and the design and development of new innovative upgrading methods open the door for potential research approaches and prospects for future work. The critical review examines the leading conversion processes for bio-oil production, recovery, and valorization based on efficiency and complexity. Even with recent advancements, the development of biofuel technologies entails further investigation and advancements to overcome conversion yield inefficiencies, product compatibility, and quality inadequacies to become commercially feasible. Bio-oil primarily suffers from high water and oxygen content, high ash content, chemical instability, and high viscosity. Without integration, current pathways are insufficient, unsustainable, energy intensive, and overall ineffective.

Prior studies have conducted techno-economic assessments to identify the key parameters and cost drivers of biomass to bio-oil production pathways. Table 2.1 presents a comparison of these studies over the last decade. These costs only represent the costs to produce the bio-oil and do not consider further costs of upgrading. The average Brent crude oil price of 2020 was $1.43 per gallon. Even though the cost to produce bio-oil is slightly less than that to obtain crude oil, fuels produced from bio-oil are still not produced at an economically competitive price.

Table 2.1. Comparison of bio-oil production costs

Study	Cost ($/gal)	Feedstock	Technology	Year
Rogers and Brammer [147]	1.00	Miscanthus	Fast pyrolysis	2012
Jones and Male [148]	0.59	-	Fast pyrolysis	2012
Brown et al. [149]	1.76	Forest Residue	Fast pyrolysis	2013
Mirkouei et al. [11]	1.15	Forest residue	Fast pyrolysis	2015
Wang and Jan [150]	2.08	Rice husk	Fluidized bed fast pyrolysis	2018
Schalkwyk et al. [151]	1.09	Forest residue	Fast Catalytic pyrolysis	2020

Although some companies have currently announced their technology licensing availability, no commercial-scale bio-oil to biofuel pathway technology has been implemented. KiOR in 2013 started construction and implementation of its CFP followed by HDT pathway technology, and by the end of 2014, the production of nearly a million gallons of fuels demonstrated the technical feasibility of such technology. However, the bankruptcy filing a few months later was a clear indication of the lack of economic feasibility [152]. Therefore, further research into improving and developing various integrated technologies is deemed necessary. Several pathways for bio-oil upgrading have been reviewed by Hansen et al. [4]. So far, both CFP and HTL have been shown to be capable of producing reasonable quality bio-oils, which can be upgraded. Integration of these technologies with other hydrodeoxygenation processes could be an effective way of converting bio-oil into intermediate products compatible with existing refinery infrastructure and end-user vehicles. A fully deoxygenated bio-oil can be fractionated into drop-in biofuels or alternative hydrocarbon fuels that can meet these criteria [154]. Nevertheless, cost-effective upgrading technologies need to be developed up to a commercial scale. Clearly and regardless of the promising technical aspects of the CFP followed by

HDT pathway, its economic feasibility still needs to be demonstrated. New physicochemical approaches are being studied to intensify and compliment CFP, such as electrochemical hydrogenation [136], electrocatalytic hydrogenation [155], catalytic transfer hydrogenation [156], and UC [144]. Further details about the CFP, upgrading, the advantage of multifunctional catalysts, and end products are given in earlier studies by Elliot et al. [157], Patel and Kumar [158], and Rover et al. [159].

The promise of UC could be enhanced further by integrating UC with catalytic transfer hydrogenation, leading to an increased efficiency process. Earlier studies explored the application of ultrasound in the preparation of catalysts (e.g., titanium, palladium, and Ni–Mo–B amorphous), and their effect on the performance of these various catalysts for deoxygenation hydrogenation and hydrodeoxygenation [160,161]. Preliminary results have indicated the incorporation of hydrogen from the hydrogen donor (ammonium formate) into the organic phase, however, the details of this incorporation remain unknown. Additional efforts are also needed to improve deoxygenation under the treatment conditions [162].

Aside from the need for integrated technologies, further investigation should be placed into recovery and treatment approaches that deal with the complexities of bio-oil compounds and their interactions. Understanding the physics and physicochemistry involved in the quenching and stripping processes, as well as miscibility studies, can be very useful for the design of an effective and efficient conversion pathway. Although there is no consensus on the pyrolysis reaction mechanisms, it is well accepted that it occurs via free radicals [53]. Most of the quality issues and thermal instability have their root causes in those mechanisms. Quenching is typically carried out under normal pyrolysis operations to stop free radicals' reactions. Quenching with water has been examined in the literature and practiced commercially [163]. Separating the gas, vapor, and liquid products entrained into the solid product is part of the recovery operation. If the quenching solvent is selected to dissolve all these organic entrained products, then stripping and the first stage quenching can be integrated into a single unit. However, it might be convenient to keep the product as gas and vapor and avoid condensation into liquid form for effective stripping. Figure 2.10 presents a schematic of a novel refinery unit that integrates discussed recovery and treatment methods. Such integrated refinery units can be beneficial for developing and modeling feasible biofuel production pathways. For the proposed multi-step pathway, each step can be studied and optimized for improving integration means and paving the way towards intensification.

Feedstock type, while not reviewed in this article, is another crucial facet to consider when optimizing product quality and yield. Particularly, lignin, hemicellulose, and cellulose are the three main

components of lignocellulosic biomass, of which lignin stands out for having higher energy content. Additionally, lignin's chemical structure is suited for producing high quality chemicals and fuels with less intensive post-conversion upgrading compared to other lignocellulose components [164]. However, prior studies have reported that lignin is relatively challenging to decompose (over the range of 160-900°C) while its conversion also produces high amounts of solid byproduct [165].

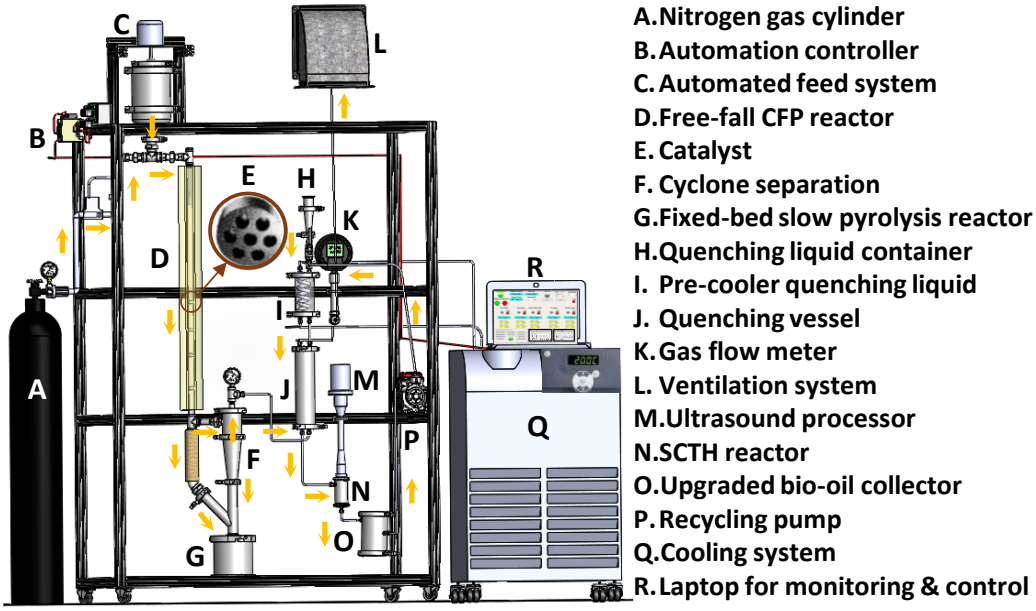

Figure 2.10. Proposed integrated multi-step process for lignocellulosic-based fuel blendstocks production

Prior studies have defined various chemical decomposition and fractionation techniques, which set the basis for a simple classification of isolable chemical compounds of commercial importance [166]. These techniques (e.g., high-resolution mass spectrometry and multi-dimensional hyphenated chromatographic and spectrometric techniques) are able to obtain a detailed chemical profile of compounds in each isolated chemical family. A better understanding of the composition might reveal insights into these physical, physicochemical, and chemical events. The complexity of the interplay among compounds and their root causes can interfere with catalysts, extraction, fractionation, transport, and refining or upgrading processes. The simplification attained through a multi-level chemical characterization could enable the application of advanced techniques for in-depth knowledge of obtained fractions. Particular attention should be placed on current and future generations of recovery and post-treatment technologies to enhance quality and commercial competitiveness.

2.6 Conclusion

This study has determined that recovery and fractionation strategies can be beneficial for maximizing pyrolysis yields and add values in the efficient conversion pathways. Effective quenching of pyrolysis vapors can stop secondary free radical reactions and improve liquid yields over gas and solid yields. Electrostatic precipitators are a simple and efficient means to recover fine bio-oil particles entrained in the gas stream. The stripping process can improve the overall pyrolysis process by decreasing coking, increasing bio-oil yield, and lengthening catalyst lifespan. Proper fractionation improves bio-oil quality, however, avoiding yield losses requires further research and optimization. The gaps in bio-oil treatment methods have been highlighted in this study. Thermochemical treatments, such as FCC and HDT, are effective, but intense process conditions are economically unsustainable. The mild operating conditions and product selectivity of the electrochemical processes are beneficial; however, the complexity of the present compounds makes it difficult to efficiently achieve desired properties in the product. The physicochemical treatments are not as effective as thermochemical treatments but have the advantages of mild operating conditions and the potential for integrated solutions in conjunction with other treatments.

Both critical and systematic reviews conducted in this study make evident that there is a need for a single-step, intensified pathway for lignocellulosic-based fuel blendstocks production. Integrated biomass-to-biofuels pathways can provide solutions to global issues (e.g., reducing GHG emissions, natural resource utilization, energy security, and economic growth in rural areas). Therefore, attention should be placed on research and development to solve the shortcomings of conventional biofuel production methods.

Chapter 3: Effect of Feedstocks and Free-Fall Pyrolysis on Bio-oil and Biochar Attributes

This chapter was published in *Journal of Analytical and Applied Pyrolysis*, under the title "Effect of Feedstocks and Free-Fall Pyrolysis on Bio-Oil and Biochar Attributes," by Ethan Struhs, Farid Sotoudehnia, Amin Mirkouei, Armando G. McDonald, and M. M. Ramirez-Corredores.

https://doi.org/10.1016/j.jece.2021.106255

3.1 Abstract

This study evaluates the potential of a mixed fast and slow pyrolysis process for the conversion of four feedstocks (i.e., hybrid poplar, maple, pine, and sugarcane bagasse) into bio-oil and biochar. The novelty of this study lies within the integration of a free-fall reactor with a batch reactor to take advantage of both fast and slow pyrolysis, and adapt conversion parameters (e.g., carrier gas pressure, feedstock particle size, bulk density, reactor height, and path tortuosity) to maximize the desired product quality and yields. Thermogravimetric analysis was used to provide insight into the thermal degradation of the specified feedstock. Biomass samples were pyrolyzed at 500-550°C, and the conversion products were evaluated. Biochar properties were characterized using proximate and ultimate analyses and surface area. Bio-oil characterization was obtained by gas chromatography-mass spectrometry (GC-MS), electrospray ionization-mass spectrometry (ESI-MS), Fourier transform infrared (FTIR) spectroscopy, and thermal stability testing. GC-MS identified dominant bio-oil compounds, such as levoglucosan, furfural, and acetic acid. ESI detected molecular weights that are higher than average, necessitating further in-situ cracking (e.g., thermal or catalytic). FTIR showed similar peak patterns and functional groups across the feedstock. The results show that maple produced the greatest biochar yield at 56%, while hybrid poplar had the greatest bio-oil yield at 38%. Among the feedstocks, bio-oil produced from hybrid poplar presents a promising oil with the lowest moisture content (<20%), high phenol content, and the most thermally stable properties, while bio-oil from pine had the next best thermal stability, but with the highest content of levoglucosan (a favorable platform molecule). Analytical results are compared to prior studies to identify the advantages and disadvantages of the free-fall fast pyrolysis reactor. Shortcomings of the current reactor configuration are identified, along with the direction for future studies.

3.2 Introduction

Currently, the main sectors of the economy (e.g., manufacturing, transportation, and agriculture) rely on fossil fuels to provide power and heat for a variety of operations [167]. Renewable energy

produced through repurposing available renewable resources (e.g., biomass feedstocks) is seen as a compelling alternative source to conventional petroleum-based energy. Because of the diminutive influence on the greenhouse effect, biomass is worth noting when investigation can meet the demands for renewable energy [168]. Biomass is an abundant raw material that is used in the production of biofuels [5]. Great interest is being placed in the widespread development and consumption of biofuels in an attempt to overcome the world's reliance on fossil fuels and alleviate humankind's effect on global warming [35].

Thermochemical processes (e.g., pyrolysis and gasification) are suitable pathways for converting a wide variety of feedstocks to heat, fuels, and power in terms of process yield and cost efficiency, as well as simplicity for an on-site, mobile biorefinery to reduce the overall cost [11]. Pyrolysis can be classified into two broad generalized groups dependent on operating conditions: slow and fast pyrolysis. Slow pyrolysis is defined by the process parameters of moderate temperatures (300-500°C) with low heating rates (0.1-1°C/s) and long residence time (10-100 min) [13]. Slow pyrolysis favors an increased production of carbonaceous solid char due to the protracted reaction time of the vapors. On the other hand, fast pyrolysis (FP) is operated at high temperatures (400-650°C), rapid heating rates (10-200°C/s), and short residence times (<2 s) [14]. FP is generally favored for bio-oil production over the other products (e.g., pyrolysis char and gas products), with yields of 30-70 wt% of liquid bio-oil, 15-25 wt% of solid char, and 10-20 wt% of non-condensable gases. The yield is dependent on several parameters, such as operating conditions, feedstock type, and particle size [169]. FP reactor technologies are varied in design and configuration (e.g., fluidized bed, microwave, auger type, and free-fall), and each reactor has a range of advantages and disadvantages [51].

This study focuses on a free-fall reactor due to its simple design and control of variables, minimal sweep gas use, and high process yield. Free-fall reactors are also advantageous because they allow convenient examination of kinetic parameters, residence time, and mass balance [170–172]. Bio-oil, as the main product of free-fall FP, has proven challenging to be used as transportation fuels due to incompatible characteristics, thermal instability, and chemical complexities [40]. Bio-oil is a complex mixture of various chemical compounds that tends to self-react and continuously alter overall composition [15], resulting in bio-oil being highly thermally unstable. Storage conditions can affect bio-oil properties, particularly at elevated temperatures or over extended periods [173,174]. The thermal degradation of bio-oil can result in partial decomposition of compounds, which leads to loss of volatiles and an increase in viscosity [175]. Analyzing conversion technology design and converted products is vital to understanding and creating the optimal production and upgrading pathway for high-quality, stable bio-oil. To make bio-oil more stable and processable, upgrading is required and

may involve various physical or chemical techniques (e.g., fluid catalytic cracking, hydrotreating, distillation, and electrochemical) [17]. To determine which technique is the most viable upgrading pathway, bio-oil produced from a conversion process should undergo various analyses to illuminate the specific deficiencies, such as feedstock type, moisture content, oxygenated compounds, and thermal stability. Table 3.1 presents a summary of research works related to free-fall FP.

Table 3.1. Recent free-fall pyrolysis studies

Study	Temperature (°C)	Feedstocks	Main Products	Ref.
Zanzi et al. (1996)	850	Birch, White quebracho, Straw pellets, Bagasse, Sugar cane residue	Biochar	[176]
Yu et al. (1997)	700-900	Birch wood	Bio-oil	[177]
Li et al. (2004)	500-800	Legume straw, apricot stone	Gas	[178]
Wei et al. (2006)	500-800	Legume straw, Tobacco stalk, Pine, Apricot stone	Gas	[179]
Onay and Koçkar (2006)	400-700	Rapeseed	Bio-oil	[180]
L. Zhang et al. (2007)	500-700	Legume straw/coal mix	Bio-oil, biochar, and gas	[181]
Pattiya et al. (2012)	350-550	Sugarcane, Casava residue	Bio-oil, biochar, and gas	[182]
Ellens and Brown (2012)	450-650	Red oak	Bio-oil	[171]
Pidtasang et al. (2013)	400-550	Eucalyptus bark	Bio-oil	[183]
Chen et al. (2013)	800-1,000	Beech	Gas	[184]
Zhao et al. (2013)	100-750	Macroalgae	Bio-oil	[185]

Table 3.1. continued

Hu et al. (2013)	400-600	Pine	Bio-oil	[186]
Quan et al. (2014)	600	White pine/coal mix	Bio-oil, biochar, and gas	[187]
Ngo and Kim (2014)	550-750	Pine	Bio-oil and gas	[188]
Zhang et al. (2015)	700	Pine/coal mix	Bio-oil and tar	[189]
Gable and Brown (2016)	550	Red oak	Bio-oil	[190]
Rueangsan et al. (2019)	500	*Dipterocarpus alatus Roxb* and rubber wood	Bio-oil	[191]
Struhs et al. (2020)	550	Cattle Manure	Biochar	[56]
Rueangsan et al. (2021)	500	Cassava Rhizomes	Bio-oil and biochar	[192]
This study	500-550	Pine, Maple, Hybrid Poplar, Sugarcane Bagasse	Bio-oil and biochar	

The goal of this study is to determine the characteristics of bio-oil and biochar produced from four different feedstocks in a free-fall FP reactor under constant operating conditions. The relative effects on bio-oil and biochar production were assessed, along with the composition and thermal stability of bio-oil samples.

3.3 Materials and Methods

3.3.1 Materials

Four different samples of biomass feedstocks were used in this study, including sugarcane bagasse, hybrid poplar, maple, and pine that can be categorized into hardwood (i.e., hybrid poplar and maple), softwood (i.e., pine), and herbaceous (i.e., sugarcane bagasse). Detailed information on the biomass feedstocks obtained by INL can be found in their Bioenergy Feedstock Library [193]. Biomass was dried to a moisture content <10% and a particle size <2 mm. The particle size of the feedstock was measured using a sieve column, and moisture content of the feedstock was accounted for by mass

difference before and after drying in the oven at 95-105°C for 12-16 hours. Table 3.2 presents proximate analysis, including fixed carbon (FC), volatile matter (VM), and ash provided by the supplier of the feedstock [193], as well as the particle size distribution of the raw feedstocks measured in lab. Moisture content was measured gravimetrically and was consistently between 7-8% for all feedstock samples. Additionally, the value observed on the VM can be taken as the maximum theoretical yield of the gas and liquid products, attainable under ideal FP conditions, while the solid yield would be in the range of the FC value.

Table 3.2. Proximate analysis of raw feedstock **[193]**.

Feedstock	**VM (%)**	**Ash (%)**	**FC (%)**	**Particle Size (wt%)**			
				2000-500 µm	**500-250 µm**	**250-125 µm**	**125-63 µm**
Pine	84.50	1.08	14.41	0	23	64	13
Maple	72.70	5.60	13.40	0	19	59	23
Hybrid poplar	86.48	0.87	12.65	55	34	10	2
Sugarcane bagasse	76.02	10.56	13.41	6	49	35	10

3.3.2 Experimental Setup

Biomass was thermochemically converted to bio-oil and biochar, using a customized, built in-house free-fall FP process, followed by the slow pyrolysis process (Figure 3.1). The free-fall reactor utilized for the experiments is a gas-solid co-current downflow cylindrical reactor (inner diameter of 2.09 cm and length of 107 cm) with an integrated batch slow pyrolysis reactor below the solid's separator under a nitrogen purge (15-20 L/min), and no intermediate stripping step is included. The integrated slow pyrolysis reactor served to increase biochar quality and decrease the amount of bio-oil entrained in the biochar. Biomass was continuously fed into the reactor using a motorized auger feed system, located at the top of the reactor at 15 g/min. Upon entering the reactor, pyrolysis was performed at a pressure of 34-69 kPag (5-10 psig) and at a temperature of 500-550°C with a vapor residence time of approximately 1.5 s. The reactors were heated using external tape heaters which were controlled using programmable logic controllers. Thermocouples were attached to the walls of the reactor to monitor temperature. Residence time was estimated using inert gas flow through the reactor. The FP

unit was run for ten minutes continuously. The produced pyrolysis vapors and solids from the free-fall reactor were entrained into a cyclone, where the solid biochar was separated and moved into the slow pyrolysis reactor (350°C for 30 minutes). Vapors (or gases) were rapidly cooled and condensed through a condenser column (tube heat exchanger) kept at around 5°C, by using an external chiller. The bio-oil was collected in a vessel following the condenser while incondensable gases exited the system. The bio-oil yield was measured as the weight percentage of liquid produced compared to the total mass of fed biomass (before bio-oil water content analysis). Bio-oil samples were immediately stored in a refrigerator at 5°C to mitigate the change in composition due to potential bio-oil instability. Experiments for each feedstock were performed in triplicate.

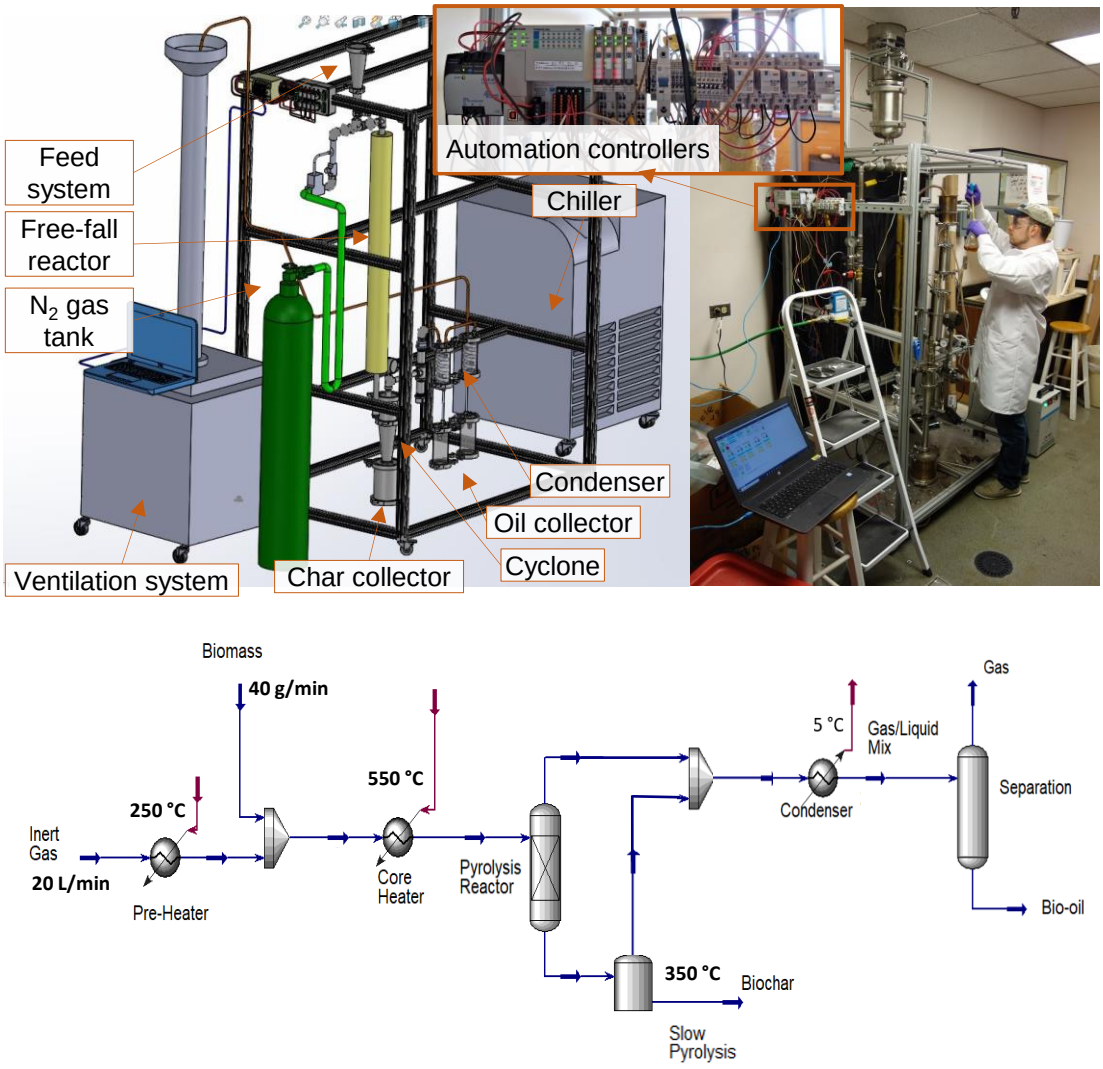

Figure 3.1. SolidWorks sketch (top left), built in-house free-fall FP (top right), and Aspen HYSYS model (down)

3.3.3 Thermogravimetric Analysis (TGA)

The thermal decomposition of biomass samples (7-8 mg) was determined by TGA using a PerkinElmer TGA-7 instrument from 30 to 1000°C at heating rates (β) of 5, 15, 25, 35, and 50°C/min under nitrogen (30 mL/min). The TGA and differential thermogravimetric (DTG) data were analyzed using Pyris v11 software. The activation energy (Ea) of the decomposition reactions was derived from the thermogram. A model-free Flynn-Wall-Ozawa's (FWO) method that relied on TGA data was used to determine apparent E to eliminate the need for a reaction model [194,195]. Flynn has proposed a correction for Doyle's approximation method that uses the results of a series of TGA experiments with varying heating rates to calculate the Ea [196]. During the TGA experiments with heating rates β1, β2, … βi, a temperature Tj,i was recorded at a conversion ratio αj and heating rate βi. A plot of log β against Ti,j-1 for each of j conversion ratios α1, α2, …, αj provided j iso-conversion lines for which the slopes (-Ea/R) were calculated [197].

3.3.4 Product Characterization

Bio-oil samples were characterized using ultimate and proximate analyses, along with gas chromatography-mass spectrometry (GC-MS), electrospray ionization-mass spectrometry (ESI-MS), Fourier transform infrared (FTIR), and thermal stability testing. The semi-volatile composition was determined by GC-MS analyses, carried out in duplicate on bio-oil samples (1 mg in 1 mL CH_2Cl_2), with trichlorobenzene (100 µg/mL) as an internal standard (Trace 1300-ISQ, ThermoScientific). A ZB-5 capillary column (30 m 0.25 mm, Phenomenex) was used to separate product compounds using a temperature program of 40°C (1 min) to 320°C (10 min) at 5°C/min and injector temperature of 325°C. Compounds were identified with authentic standards from the literature, and NIST 2017 MS library [198–200].

A Finnigan LCQ-Deca equipment was used to assess the molar mass of bio-oil samples (ThermoQuest) [201]. The bio-oil samples (1 mg/mL) were dissolved in a 50% dichloromethane, 49% methanol, and 1% acetic acid solution before being exposed to negative ion ESI–MS (m/z 100–2,000) at a flow rate of 10 L/min. At 275°C, the capillary and ion source voltages were 4.5 kV and 50 V, respectively. The spectral mass distribution was used to evaluate both the number average molar mass (M_n) and the weight-average molar mass (M_w), respectively, using Equations (1) and (2), where N_i is the intensity of ions and M_i is the ion mass [197,201].

$$M_n = \sum N_i M_i / \sum N_i \quad (1)$$

$$M_w = \sum N_i M_i^2 / \sum N_i M_i \quad (2)$$

The FTIR spectra of bio-oil samples were acquired in quadruplicate using a ZnSe attenuated total reflection (iD5 ATR) accessory of a Thermo-Nicolet iS5 spectrometer. The (Thermo-Nicolet) Omnic v9 software was used for baseline correction and for averaging the FTIR spectra.

The thermal stability test performed in this study involved measuring the change in viscosity of bio-oil caused by aging the bio-oil at a moderate temperature. The accelerated aging method was performed by placing three sealed bio-oil samples in an oven set to approximately 90°C. The samples were exposed to this heat treatment for 8, 24, and 48 hours, as indicated in Figure 3.2. Before treatment, bio-oil sample viscosity was measured (t_0) as a baseline reference, which occurred between 48-72 hours after production. Each of the samples was removed from the oven at the corresponding time point and allowed cooling back to room temperature 23°C before removing the caps. Viscosity was measured at room temperature using a digital rotary viscometer (KUNHEWUHUA NDJ-9S, No. 2 spindle at 60 rpm). The viscosity (μ) was determined following equipment protocols for viscosity measurements.

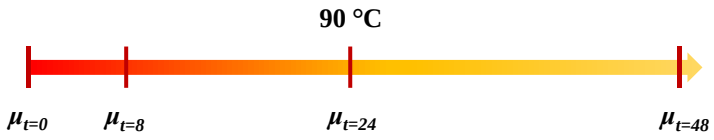

Figure 3.2. The timeline for accelerated aging studies of bio-oil

For most bio-oil samples, the observed changes in viscosity (measured in centipoise, cp) with time (in h) generally fit a straight line. Therefore, as a first approach, the slope of that line would be considered as a stability parameter (SP), using Equation (3). By this definition, the higher the thermal stability of the bio-oil, the lower the SP values.

$$SP = \frac{\partial(Viscosity)}{\partial(time)}\ cp/h \tag{3}$$

On a Micromeritics FlowSorb 2300 instrument, the specific surface areas of all degassed (105°C for 16 h) biochar samples (0.25 g in duplicate) were evaluated using 30% N_2 in He to obtain an N_2 adsorption-desorption isotherm at 196°C according to ASTM D6556-10.

3.4 Results and Discussion

3.4.1 Thermogravimetric Results

The thermal decomposition and kinetic behavior of all biomass samples were determined using TGA. TGA helps in the understanding of the biomass thermal characteristics and calculation of the

activation energy for its decomposition. This understanding and the decomposition kinetics are vital for designing and operating the pyrolysis reactor [202]. Figure 3.3 shows the TGA and DTG thermograms of hybrid poplar, maple, pine, and sugarcane bagasse. A peak shift observed in the DTG curves and occurring at high temperatures would most likely be due to a change in reaction kinetics [203]. The peaks also increased in intensity for higher temperatures.

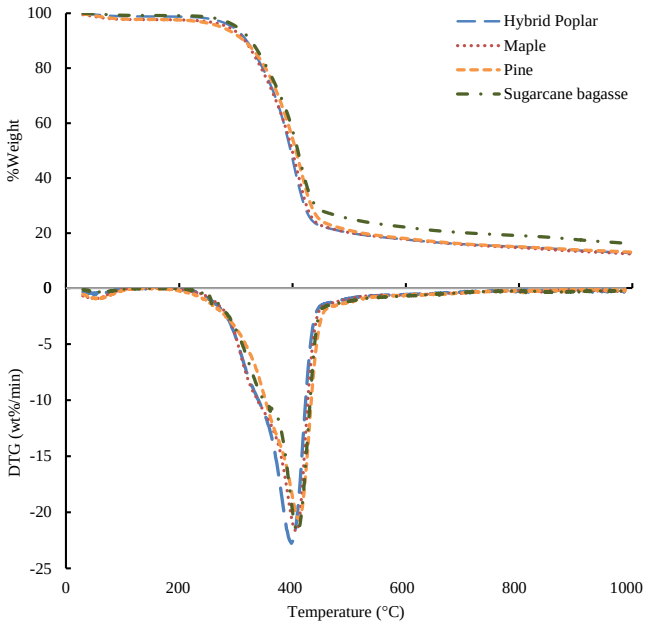

Figure 3.3. TGA (top) and DTG (down) thermograms at β 25°C/min heating rates

Previous research has discovered that cellulose, hemicellulose, and lignin are found in decreasing order of abundance in lignocellulosic materials from various sources [204,205]. According to Raveendran et al. (1996), pyrolysis of biomass typically involves three stages: (a) dehydration, (b) devolatilization (results in the creation of biochar), and (c) gradual transformation of biochar [206]. The step originally identified as a devolatilization process was the decomposition process itself, from which the formed volatile compounds scaped the solid phase. In the samples used in this study, the decomposition stage started at temperatures <290°C and was characterized by small mass loss due to water evaporation and the formation of light volatiles [207].

The primary weight loss took place between 300 and 500°C, with one distinct DTG peak detected at around 400°C [208]. In the end, more than 90% of the material had decomposed. Trans-glucosidation is the main reaction in cellulose decomposition to produce levoglucosan and oligomers [209]. Although lignin decomposition starts at temperatures above 250°C [53] and is maximized at 470°C in

our samples. Above 500°C, a gradual weight loss was noticed, which could be attributed to biochar slow transition [210]. The remaining residue in the samples ranged from 12.5% (maple) to 16.6% (sugarcane bagasse), which is consistent with the proximate analysis results, since this latter analysis is basically a thermal analysis (ASTM D3172 or ASTM D7582) developed for coal analysis and now also applied to biomass, at different conditions than the TGA carried out in this study. The proximate analysis determines moisture content (by heating to 105°C), volatile content (when heated to 950°C), and the fixed carbon remaining at that point. The mineral ash in the sample and the HHV are based on the complete combustion of the sample to carbon dioxide and liquid water.

Based on a linear regression model, the apparent E_a was estimated using the iso-conversional technique, as described above. Figure 3.4 shows a linear regression of the FWO method in the conversion (α) range of 10% to 85%. Two groups of parallel iso-conversional lines are seen, one corresponding to 10-70%, and the other to 80%. This parallelism might indicate that the two groups have comparable kinetic characteristics, implying different reaction mechanisms [211].

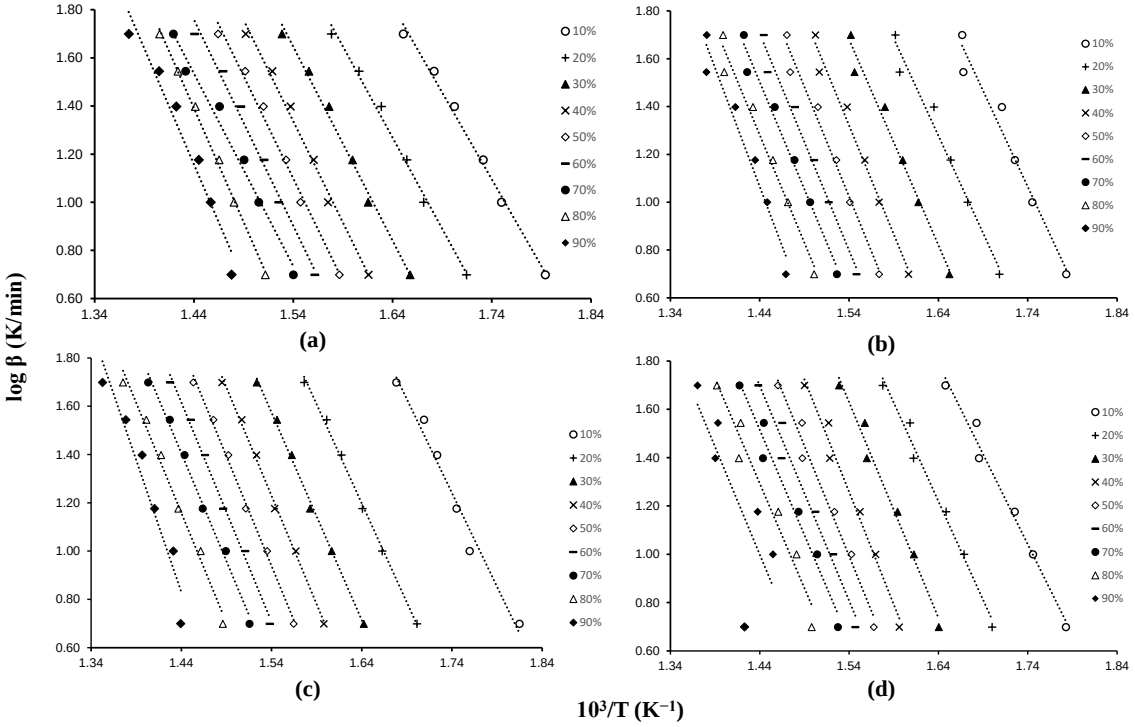

Figure 3.4. Determination of apparent activation energy (Ea) according to the FWO method at heating rates (β) of 5, 15, 25, 35, and 50°C/min for (a) hybrid poplar, (b) maple, (c) pine, and (d) sugarcane bagasse

As presented in Table 3.3, E_a values for $\alpha \geq 80\%$ are larger than those calculated for $10\% \leq \alpha \leq 70\%$. The E_a values found for the latter group are in the range reported for lignocellulosic materials

[212,213]. Ding et al. (2017) used the FWO method to calculate average E_a values as 183-188 kJ/mol for softwood (e.g., pine) and 160-173 kJ/mol for hardwood (e.g., maple and poplar) for conversion of 5-85% [214]. Zanatta et al. (2016) reported an average E_a value for sugarcane bagasse as 134.6 kJ/mol for conversion from 20-80% [215].

Table 3.3. Activation energy values (Ea) at various conversion factors (α) for hybrid poplar, maple, pine, sugarcane bagasse determined by TGA

Conversion	**Hybrid Poplar**		**Maple**		**Pine**		**Sugarcane bagasse**	
α	**E_a (J/mol)**	**R^2**	**E_a (J/mol)**	**R^2**	**E_a (J/mol)**	**R^2**	**E_a (J/mol)**	**R^2**
10%	131	0.994	146	0.966	141	0.9777	136	0.985
20%	138	0.993	148	0.978	149	0.997	150	0.986
30%	147	0.992	156	0.981	157	0.997	162	0.983
40%	153	0.991	166	0.983	163	0.997	170	0.982
50%	155	0.99	167	0.982	166	0.996	166	0.979
60%	156	0.989	165	0.983	166	0.995	162	0.976
70%	146	0.983	163	0.982	163	0.993	158	0.973
80%	172	0.998	164	0.977	166	0.989	158	0.956
85%	175	0.959	181	0.958	199	0.938	162	0.603
Average	**153**	**0.988**	**162**	**0.977**	**163**	**0.987**	**158**	**0.936**

3.4.2 Product Yield Results

The estimated average bio-oil yield was based on the average yield after 3-5 experiments, each experiment included ten minutes of running biomass through FP, in the free fall reactor, followed by an additional 30 minutes of slow pyrolysis after FP was complete. Table 3.4 shows the yields of bio-oil and biochar collected. Feedstock particle size was given previously in Table 3.2.

Table 3.4. The yield of free-fall FP products from different feedstocks

Feedstock	Biochar (%)	Bio-oil (%)
Pine	53.6 ± 2.7	23.3 ± 1.2
Maple	56.4 ± 2.8	19.4 ± 1.0
Hybrid Poplar	32.0 ± 5.0	38.4 ± 6.0
Sugarcane Bagasse	53.3 ± 7.9	23.5 ± 2.4

As the setup was optimized for high-quality biochar production, the biochar yield is much greater than bio-oil, except for hybrid poplar. Maple has the highest biochar yield, while hybrid poplar was most favorable for bio-oil production in the current conversion configuration. The general trend is to observe decreasing biochar yields with decreasing particle size [176,179]. However, the biochar yield is higher for smaller particle size may be due to the customized free-fall process, increasing heat transfer and tortuosity. Wei et al. (2006) noted that the conversion process for large particle size biomass (>200 μm) is controlled by heat and mass transfer within the particle, while small particle size (<200 μm) is mainly controlled by kinetics [179]. Additionally, an increase in secondary vapor cracking can result in lower liquid yields and higher char/tar formation [216]. Although the interplay between tortuosity and particle size is unknown, the high bio-oil yield from hybrid poplar could be due to its particle size causing fewer secondary reactions. With residence times being estimated by inert gas flow rate, it is also possible that the smaller particle sized biomass (e.g., pine and maple) had shorter residence times due to high gas flow rates. Prior studies utilizing free-fall FP reveal yields of 35-45% for bio-oil, with decreasing yields seen at temperatures of ≥500 °C [178,182,188]. Incorporation of stripping could remove bio-oil vapors entrained in the char leading to a noticeable effect on bio-oil and biochar yield ratio. Ash content is another factor to consider when analyzing yield as the composition (alkali and alkaline earth metal) can have a big impact [217,218]. K, Na, Mg, and Ca influence thermal decomposition to favor higher char and gas yield even at low concentrations. Ash content was not analyzed in this study but might have provided further insight.

3.4.3 Product Characterization Results

The first feature to notice from the proximate analysis results (Table 3.5) is the low inorganics concentration in the bio-oil since biochar retains most of the mineral ash originally present in the

feedstock. High heating values (HHV) were largely affected by the moisture content [216] since water does not add energy value. HHV findings fall well within those reported by Sadaka et al. (2009) of values between 16-26 MJ/kg for bio-oils with moisture content between 15-30% [219]. In this study, HHV can increase with decreasing water content, as expected. The proximate analysis shows similar values to those provided in the literature, with water content between 15-30%, ash below 0.3%, and higher heating values between 16-19 MJ/kg. Tsai et al. (2006) reported biochar HHV between 24.8-26.5 MJ/kg for sugarcane bagasse, while Kim et al. (2011) produced poplar biochar with an HHV of 29 MJ/kg using FP at 500°C [220,221]. Kim et al. (2013) stated softwood biochar HHV between 30-32 MJ/kg [222]. The surface area of the biochars was also somewhat low compared with literature values, from slightly less than 1 m^2/g to >400 m^2/g for woody biochar produced at 500°C [223]. Additionally, these values are well below the detection accuracy of the employed method. However, both the low HHV and low surface area values may result from low biomass conversion due to low residence time (below 2 sec) and lack of stripping. These results on the heating value of the main products demonstrate the advantages of a simple process rendering at least 70% of energy densified products.

Table 3.5. Proximate analysis of bio-oil and biochar as received.

Feedstock	Water by KF	Avg Surface Area (m^2/g)	Ash (%)	FC (%)	VM (%)	HHV (MJ/kg)
Pine						
Bio-oil	16.1 ± 2.70	-	0.09 ± 0.04	13.68 ± 0.26	70.12 ± 2.37	19.11 ± 0.81
Biochar	-	0.63	1.29 ± 0.01	27.97 ± 0.34	70.74 ± 0.86	21.64 ± 0.26
Maple						
Bio-oil	27.1 ± 3.98	-	0.32 ± 0.17	11.50 ± 0.98	61.06 ± 3.18	15.81 ± 1.21
Biochar	-	0.37	0.77 ± 0.07	20.95 ± 1.12	78.28 ± 1.86	19.29 ± 0.26
Hybrid Poplar						
Bio-oil	22.2 ± 4.32	-	0.20 ± 0.02	10.58 ± 3.33	67.05 ± 0.96	16.61 ± 1.91
Biochar	-	0.46	2.59 ± 0.64	36.69 ± 2.95	60.72 ± 2.49	23.03 ± 0.88

Table 3.5. continued

Sugarcane Bagasse						
Bio-oil	27.3 ± 4.96	-	0.29 ± 0.05	11.58 ± 1.58	60.81 ± 3.43	15.69 ± 0.82
Biochar	-	0.9	17.7 ± 0.62	22.15 ± 1.18	60.16 ± 1.21	17.29 ± 0.46

The results from the ultimate or elemental analysis of bio-oils are collected in Table 3.6. The elemental analysis of the bio-oils shows that the values in the literature for carbon (54-58%), hydrogen (5.5-7.0%), nitrogen (0-0.2%), and oxygen (35-40%) agree with the values produced in this study [17,224].

Table 3.6. Ultimate analysis of bio-oil and biochar as received.

Feedstock	C (%)	H (%)	N (%)	O (%)	H/C	O/C
Pine						
Bio-oil	58.07 ± 1.46	6.37 ± 0.17	0.10 ± 0.01	35.94 ± 1.53	1.31 ± 0.07	0.46 ± 0.02
Biochar	56.54 ± 0.68	5.54 ± 0.07	0.11 ± 0.01	36.5 ± 0.63	1.17 ± 0.06	0.48 ± 0.02
Maple						
Bio-oil	54.77 ± 2.48	6.21 ± 0.09	0.19 ± 0.03	31.71 ± 1.99	1.35 ± 0.07	0.43 ± 0.02
Biochar	51.84 ± 0.76	5.80 ± 0.09	0.08 ± 0.01	41.50 ± 0.72	1.33 ± 0.07	0.60 ± 0.03
Hybrid Poplar						
Bio-oil	55.15 ± 4.12	6.40 ± 0.37	0.13 ± 0.03	34.79 ± 1.46	1.38 ± 0.07	0.47 ± 0.02

Table 3.6. continued

Biochar	60.42 ± 2.46	5.04 ± 0.24	0.16 ± 0.10	31.77 ± 1.85	0.99 ± 0.05	0.39 ± 0.02
Sugarcane Bagasse						
Bio-oil	55.49 ± 3.15	6.03 ± 0.26	0.40 ± 0.02	36.14 ± 2.92	1.29 ± 0.06	0.49 ± 0.02
Biochar	45.90 ± 1.20	4.60 ± 0.11	0.33 ± 0.02	31.44 ± 1.05	1.19 ± 0.06	0.51 ± 0.03

Biochar elemental composition also proved comparable to literature values. Igalavithana et al. (2017) analyzed 40 biochar samples from various feedstocks, providing biochar elemental compositional ranges of carbon (60-91%), hydrogen (1.8-4.9%), and oxygen (8.5-32%) [225]. All samples in Table 5 have slightly lower carbon content and higher hydrogen and oxygen content comparatively. These results also show that H/C and O/C ratios are relatively the same for bio-oil in the range of 1.1-1.5 for H/C and 0.4-0.6 for O/C [224]. Maple produces bio-oil with the best O/C ratio compared with other oils, however, the ratios are far from petroleum H/C and O/C around 1.5-2.0 and 0.06, respectively [224]. As expected, the produced bio-oil requires further treatment and upgrading (e.g., catalytic cracking and hydrodeoxygenation) before being considered as a compatible transportation fuel for existing combustion engines.

3.4.4 Bio-oil Thermal Stability Results

The initial viscosity (35-194 cP) of the samples matches decently with prior reports (25-100 cP) with the exception of bio-oil from sugarcane bagasse [17,219]. Viscosities of bio-oil are largely dependent on the pyrolysis process (e.g., reactor type, temperature, and residence time) and feedstock, and are shown to vary widely. Values obtained from the accelerated stability test experiments were analyzed and correlated to determine the SP. Table 3.7 provides the viscosity changes and SP (cP/hr) values of bio-oil samples. The calculated changes have a linear fit, simplifying the determination of SP. Other stability studies show the SP from 0.5-11, allowing the results of this study to be acceptable [174,226]. Thermally aging bio-oil increases the average molecular weight while decreasing the number of molecules, alluding to condensation reactions, forming water, and higher molecular weight compounds [226,227]. While higher water content could attribute to a lower viscosity, bio-oil

produced from hybrid poplar has 22.2% water content but the lowest SP, while sugarcane bagasse has the highest water content (27.3%) and the highest SP (6.7 cP/h). The more viscous samples see a larger change over time, resulting in a high SP value or low thermal stability. Chemical composition analysis and testing more feedstock types could shed more light on SP trends. The SP results show that the proposed free-fall reactor can produce high-quality bio-oil with a high yield compared to other reactors. Particularly, hybrid poplar and pine have the first and second highest stability and yield, respectively.

Table 3.7. Viscosity and SP values for bio-oil samples over time.

Time (hrs)	**Viscosity (cP)**			
	Pine	**Maple**	**Hybrid Poplar**	**Sugarcane Bagasse**
0	52	104	35	194
8	64	147	36	272
24	86	231	42	397
48	116	340	48	520
SP (cP/h)	**1.33**	**1.44**	**0.28**	**6.71**

3.4.5 Gas Chromatography-Mass Spectrometry Results

GC-MS was used to examine the volatile components in bio-oil produced at 550°C (Figure 3.5) [228,229].

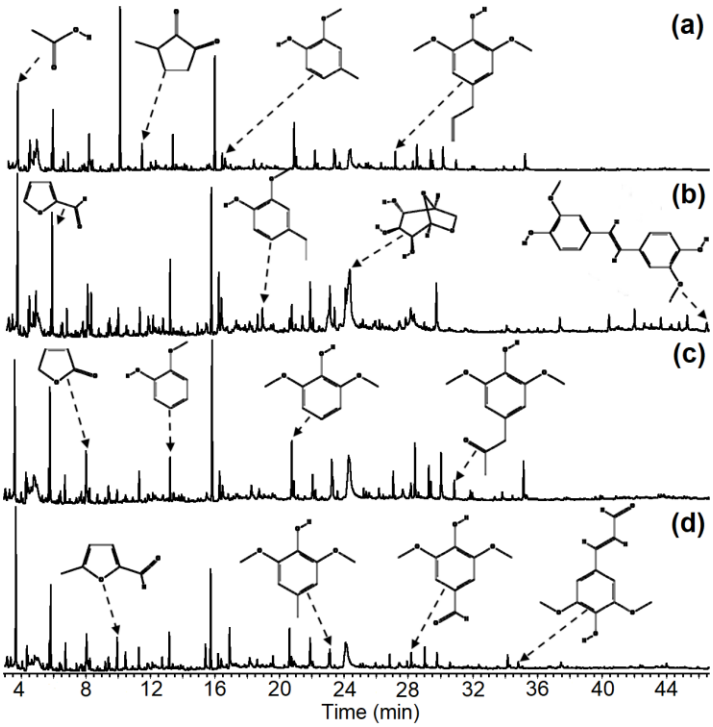

Figure 3.5. GC-MS Chromatograms of bio-oil produced at 550°C from (a) hybrid poplar, (b) pine, (c) maple, and (d) sugarcane bagasse

Identified compounds in bio-oil are listed in the Supplementary Materials (Appendix A). The chromatograms of four bio-oil samples revealed a diverse combination of chemical compounds with carbon atoms ranging from C3 to C18, levoglucosan, and some other pyrans, which are the main products of the thermal pyrolysis of polysaccharides. The detected compounds in bio-oil samples also included lignin-derived phenolic compounds with methoxy-substitutes and benzenediols phenols, which confirm the high population of G (guaiacyl) and S (syringyl) units in the lignin composition of maple, pine, and hybrid poplar [230]. The complexity of some of these phenolic compounds indicates that they were generated from the recombination reactions among primary intermediates, mainly from lignin but also from the other cellulosic components. Simpler phenols with methyl replacements were also found, although their overall chromatogram area was lower. Furans (5-methyl furfural and furfural) and smaller linear hydrocarbons, aldehyde/ketones, and acids have been also found by many other studies and associated with pyrolysis results of cellulosic materials (e.g., acetaldehyde, acetic acid, and propanoic acid) [17,231,232]. A common noticeable trend is that many compound concentrations (e.g., benzaldehyde and guaiacol) change at 400°C [233].

Bio-oils tend to convert to liquid fractions of phenolic compounds, anhydro-sugars, furans, ketones, and acids [234]. Levogluclosan is the principal compound in the pine (13.2 µg/mg), maple (6.61

µg/mg), and sugarcane bagasse (7.17 µg/mg) bio-oil samples while also appearing dominantly in hybrid poplar (6.26 µg/mg), according to the GC-MS results. Lyu et al. (2015) produced bio-oil with levoglucosan content between 4-42 µg/mg through FP of several feedstocks at 480-580°C [234]. The content for bagasse was between 3-9 µg/mg, while pine could reach up to µg/mg under optimal conditions. Hybrid poplar differs from the others with the primary compound being phenol (11.5 µg/g), appearing to support phenolic liquid production from the lignin fraction of the biomass [235]. Acetic acid and furfural are all highly present in each sample and are consistently mentioned in the literature as dominant compounds [232,235,236]. Furfural content can be comparable across all bio-oil samples. Other notable compounds are 3-methylbutanal, trans-isoeugenol, and dihydro-4,4-dimethyl-2(3H)-furanone.

3.4.6 Electrospray Ionization Mass Spectrometry Results

The molar mass distribution of bio-oil was determined using ESI-MS analysis (Figure 3.6) [197,201]. Most of the peaks spanned over the m/z range of 100−1,200 [237–239]. The predominant $[M-H]^-$ ions at m/z 161 and m/z 111 in the negative ion ESI-MS were ascribed to levoglucosan and $C_6H_8O_2$, respectively (or $C_5H_4O_3$). Other minor ions $[M-H]^-$ also verified by GC/MS were attributed to guaiacol, hydroxymethylfurfural, ethyl guaiacol, eugenol/isoeugenol, coniferyl aldehyde, and cellobiosan at m/z 123, 137, 151, 163, 177, and 323, respectively. These results mirror those produced using GC-MS. Many of the peaks produced through ESI-MS identify compounds with much higher molecular weight than what is found using GC-MS. Several taller peaks are located between the m/z range of 300-350, suggesting an abundance of subfractions of lignin-derived compounds [237,238,240]. Additionally, accurate mass analysis and equivalent homologue series would be required to identify the possible elemental compositions of these compounds.

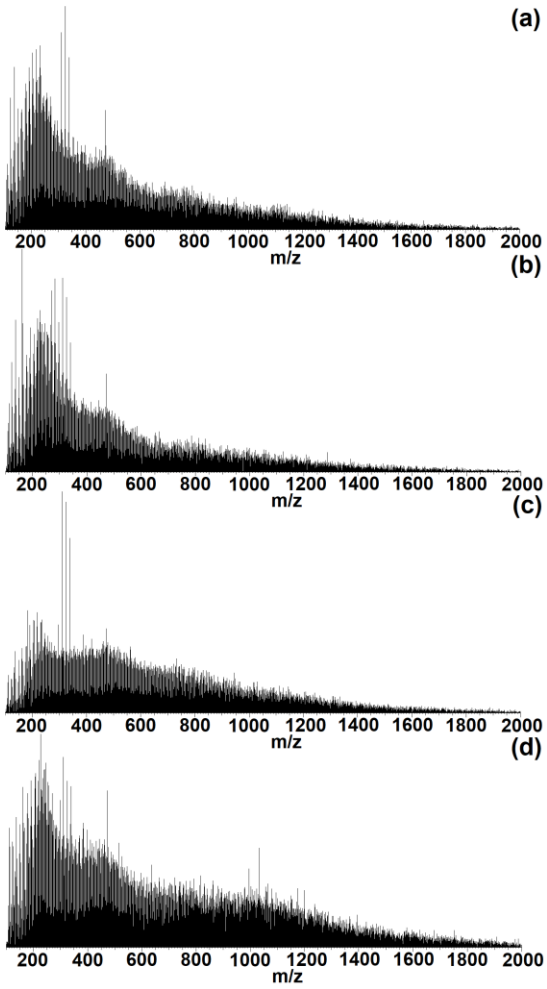

Figure 3.6. Negative-ion ESI-MS spectra of products via pyrolysis of (a) hybrid poplar, (b) pine, (c) maple, and (d) sugar cane bagasse

Negative ion ESI-MS studies were used to determine the molar mass (M_w and M_n) of bio-oils (Table 3.8). The MS revealed a bimodal distribution centered on m/z 250 (monomers) and 450 (oligomers). For bio-oils, ion intensities m/z 100-300 / m/z 301-2000 were used to assess the monomer to oligomer ratio. The highest monomer/oligomer ratio belonged to pine and the lowest to the maple sample, indicating more thermal breaking of smaller molecular fragments. However, bio-oils are not stable, and oligomerization occurs during storage resulting in certain levels of aging taking place between pyrolysis and ESI-MS measurements. Past studies have reported average molecular weights of bio-oils between 300-800 using various methods of analysis [240,241], putting these results at the higher end of the reported ranges. These results are also consistent with the nature of biomass samples and the stability of the produced bio-oils. The most stable bio-oil was obtained with hybrid poplar, followed by pine, maple, and sugarcane bagasse, with the latter two feedstocks having very similar SP values, and Monomer/Oligomer ratios, indicating similar levels of aging. Although hybrid poplar

bio-oil was the most stable, it had the largest particle size and may have undergone the fastest pyrolysis based on the relative bio-oil and biochar yields. Additionally, hybrid poplar had the lower dihydroxylation/dehydration reactions compared to pine yielding lower anhydro-sugars (e.g., levoglucosan) and lower water content in the bio-oil, with higher yield and heavier bio-oil than pine. Increased thermal treatment during FP or catalytic cracking could remedy the high average molecular weight and molar mass. Other influencing factors affecting the molecular weight of bio-oil could also include reactor configuration and the method of heat transfer as ablative processes produce bio-oils of lower molecular weights [216,242].

Table 3.8. Weight (Mw) and number average molar mass (Mn) of bio-oil samples determined from negative ion ESI-MS data

Sample Name	M_n	M_w	Monomer/Oligomer
Hybrid Poplar	590	843	0.39
Pine	564	816	0.45
Maple	674	892	0.2
Sugarcane Bagasse	717	970	0.25

3.4.7 Fourier Transform InfraRed (FTIR) Spectroscopy Results

The chemical groups of bio-oil samples were determined using FTIR analysis (Figure 3.7) [243].

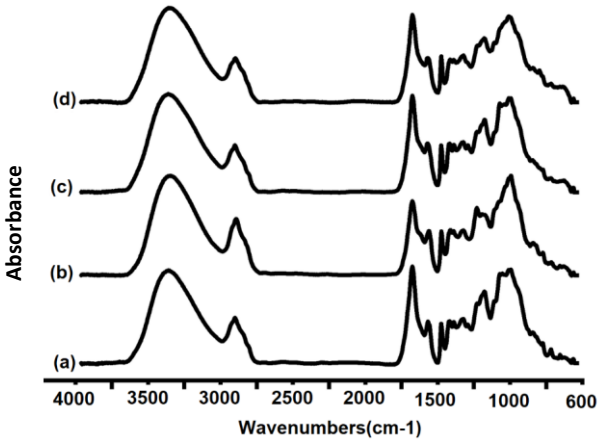

Figure 3.7. FTIR spectra of pyrolysis bio-oil produced at 550°C from (a) hybrid poplar, (b) pine, (c) maple, and (d) sugarcane bagasse

The band assignments for all bio-oil samples are shown in Table 3.9 and are based on prior studies [244,245]. Previous FTIR analyses of poplar, pine, and sugarcane bagasse support the resulting peak pattern similarities across the feedstock despite differences in biomass types (e.g., woody or herbaceous), revealing that the corresponding functional groups should also be comparable [220,246–248]. Strong O-H stretching and C-H stretching absorptions were seen in the IR spectra of all samples and their constituents at 3,391 and 2,913 cm^{-1}, respectively. O-H stretching vibrations indicate the presence of water, phenols, acids, and alcohols in the mixture from biomass decomposition [249]. C=O stretching caused the absorption at 1,715 cm^{-1} suggestive of ketones, carboxylic acids, or aldehydes [220]. The asymmetric stretching band of the carboxyl group of glucuronic acid in hemicellulose and C=O stretching in conjugated carbonyl of lignin were represented by the absorption at 1,606 cm^{-1}, indicating accompanying alkenes and aromatic moieties. Because of the C-H deformation of methyl and methylene in lignin, a band at 1,456 cm^{-1} was identified. At 1,515 cm^{-1}, the C=C-C stretching vibrations signify benzenes found in both phenols and aromatics [250]. At 1,364 cm^{-1}, cellulose, hemicellulose, and lignin C-H bending were found (aliphatic C-H stretching in methyl and phenolic alcohol). 1,331 cm^{-1} was given to CH_2 wagging in cellulose and hemicellulose, and the C-O stretching of C_5 substituted aromatic units, such as syringyl and condensed guaiacyl units. In lignin, the C-O stretching of the guaiacyl unit was determined to be 1,215 cm^{-1}. Aromatic C-H was related to the absorption at 1,034 cm^{-1}. At 1,032 cm^{-1}, the C-O stretching of cellulose and primary alcohols, as well as the C-H in-plane deformation for the guaiacyl unit, were visible. At 814 cm^{-1}, aromatic C-H out of plane bending in lignin was demonstrated to identify the characteristics of aldehydes [247]. Despite the overlap of numerous FTIR bands of different biomass components, the IR spectra of samples nevertheless provide essential hints, such as changes in chemical composition, functionalization, and other biomass transformations for understanding the applied biomass processing.

Table 3.9. FTIR analysis results for hybrid poplar, pine, maple, and sugarcane bagasse bio-oil samples

Assignment / Components	**Hybrid Poplar**	**Pine**	**Maple**	**Sugarcane Bagasse**
C-H out of plane bending (Pyridine)	694	-	-	-
C-H bending out of plane peaks (Furfural)	757	-	-	-

Table 3.9. continued

Aromatic C-H out of plane bending (Lignin)	814	-	-	-
C-O stretching, aromatic C-H in plane deformation	1,034	1,033	1,047	1,048
C-O stretching of guaiacyl unit (Lignin)	1,216		1,215	1,217
H-C-H Stretching methylene	-	1,272	-	-
C-H deformation of secondary alcohol (Glycerol)			1,331	
C-H bending, C-H stretching in CH3 (Cellulose, Hemicellulose, Lignin)	1,364	1,364	1,364	1,364
Symmetric CH2 bending vibration, symmetric stretching band of carboxyl group, C-H deformation (Cellulose, Hemicellulose, Lignin)	1,428	-	1,427	-
C-H deformation (in methyl and methylene) (Lignin)	1,456	1,451	1,456	1,453
C=C-C aromatic ring stretching and vibration (Lignin)	1,515	1,513	1,515	1,515
Aromatic skeletal vibration, C=O stretching, adsorbed O-H (Hemicellulose, Lignin)	1,606	1,600	1,609	1,608
C=O stretching (Hemicellulose, Lignin)	1,715	1,714	1,714	1,714
C-H stretching (Cellulose, Hemicellulose, Lignin)	2,339	2,931	2,939	2,937
O-H stretching (Cellulose, Hemicellulose, Lignin)	3,391	3,393	3,401	3,391

3.5 Conclusion

The primary goal of this study was to determine the characteristics of bio-oil and biochar produced from four different feedstocks (i.e., hybrid poplar, maple, pine, and sugarcane bagasse) using a customized, mixed conversion process (free-fall FP and batch slow pyrolysis) under constant operating conditions. The relative effects of feedstock type and conversion configuration on bio-oil and biochar attributes were examined, using various analyses (e.g., proximate, ultimate, GC-MS, ESI-MS, and FTIR), along with the composition and thermal stability (change of bio-oil viscosity over the treatment time) of bio-oil samples. Particularly, this study compared the quality and stability of bio-oil and biochar composition, provided insight into what feedstocks may be ideal, and identified the key conversion parameters to improve the product yield and quality. GC-MS was used to detect prevalent bio-oil compounds (e.g., levoglucosan, furfural, and acetic acid). The results indicate that pine bio-oil has the most levoglucosan and hybrid poplar has the most phenol, and all samples had similar furfural content. ESI-MS results show higher than average molecular weights that may justify low thermal treatment in the pyrolysis reactor, which can be remedied through increased thermal or added catalytic cracking. FTIR peak patterns show small differences for all samples, suggesting a slight disparity of functional groups.

It is found that biomass particle size correlates directly with biochar yield and inversely with bio-oil yield. Thermal stability of bio-oil improves with lower moisture content. Hybrid poplar stability is slightly better than pine, even though they shared similar energy values and pine had a smaller particle size. It is also found that the higher biochar yield for smaller particle sizes may be a result of the free-fall process design, leading to longer residence time and an increase in undesirable secondary reactions for smaller particle sizes. Though bio-oil produced from sugarcane bagasse comparatively had the least desirable characteristics, it shows promise with biochar quality (e.g., yield and surface area). It can be concluded that pine at smaller particle sizes produced bio-oil with the best physical qualities (e.g., HHV and moisture content of <20%) and composition (e.g., highest levoglucosan content). However, hybrid poplar bio-oil has the highest thermal stability. Both pine and hybrid poplar feedstocks show promising results for future bio-oil production studies using the free-fall fast pyrolysis process. It is further concluded that bio-oil from different feedstocks requires further upgrading to be comparable with existing fuels (e.g., diesel, gasoline, biodiesel) due to a large amount of oxygenated compounds and incomparable elemental properties. Further development of the pyrolysis conversion process or post-treatment upgrading to improve quality and stability is required to create a truly valorized product from biomass. In addition, process configuration focusing on high-quality biochar production may also have significantly impacted bio-oil characteristics. Reactor

reconfiguration to increase thermal treatment and increase ablative heat transfer and the addition of catalytic conversion may also help in more effective cracking, resulting in a product of lower molecular weight and an increased discrepancy between bio-oil and biochar characterizations.

Chapter 4: Examination of in-situ and ex-situ catalytic fast pyrolysis and liquid fractionation utilizing a free-fall reactor

This chapter was submitted to *Journal of Analytical and Applied Pyrolysis*, under the title "Chapter 4: Examination of in-situ and ex-situ catalytic fast pyrolysis and liquid fractionation utilizing a free-fall reactor" by Ethan Struhs, Harrison Appiah, Amin Mirkouei, and Armando G. McDonald

4.1 Abstract

This study evaluates the potential of in-situ and ex-situ catalytic fast pyrolysis, using a free-fall reactor and γ-alumina as a catalyst, along with direct quenching for fractionation, using methanol. The novelty of this study lies within the conversion reaction pathways and the free-fall pyrolysis reactor design with catalyst bed integration. In this study, pinewood feedstocks were pyrolyzed at 550°C, and the resulting products were pyrolysis oil and char (bio-oil and biochar). Characterization of bio-oil was completed through gas chromatography-mass spectrometry (GC-MS), electrospray ionization-mass spectrometry (ESI-MS), Fourier transform infrared (FTIR) spectroscopy, and thermal aging. GC-MS detected the volatile fraction of bio-oil compounds, such as levoglucosan, furfural, hydroxyacetone, methyl acetate, and catechol. ESI-MS was used to determine the average molar mass, revealing improved cracking, thermal treatment, and fraction stabilization. FTIR spectroscopy provided insight into the change in functional groups in relation to experimental parameters. The results show that γ-Alumina successfully decreased acidic compounds and increased esters in the bio-oil. Also, bio-oil produced from ex-situ catalytic pyrolysis showed the highest process yield (~41%), high phenolic content, and thermally stable properties. In-situ catalytic pyrolysis exhibited lower yields and favored high ketone formation. Fractions condensed in methanol exhibited the highest thermal stability and esterification potential, however, they still possessed relatively high amounts of acidic compounds. It is concluded that ex-situ catalytic pyrolysis, using γ-alumina catalyst, and fractionation with methanol can improve conversion reactions, particularly bio-oil quality, process, yield, and thermal stability. Decoration of γ-alumina with non-noble hydrodeoxygenating metals could lead to an effective and inexpensive biofuel production pathway.

4.2 Introduction

Among renewable energy sources in the United States (U.S.), biomass contributed the largest portion (38%) to bioenergy production in 2022 [251]. Producing renewable energy using available renewable resources (e.g., biomass feedstocks) is a promising alternative to offset reliance on non-renewable resources (e.g., fossil fuels) [168]. Many conversion processes can provide potential routes for converting raw biomass to chemicals, heat, fuels, and power [5]. However, the costs of current

technologies for biomass pretreatment, conversion, and upgrading make biofuel production economically impractical [10]. Evaluating biomass conversion pathway technologies is critical to identifying optimal processes and producing valorized energy products [252]. Of these processes, thermochemical decomposition of biomass by fast pyrolysis (FP) has shown to be simple and comparatively cost-effective in producing a liquid product with higher energy content than the raw materials [11]. Pyrolysis-oil (often called "bio-oil") is the liquid product from pyrolysis of lignocellulosic materials that can be used as a heating source in its raw form [253]. Conversely, some of bio-oil's quality attributes, such as low heating value, corrosivity, and thermal instability, make it inequivalent to existing petroleum-based transportation fuels (e.g., gasoline and diesel). The lower heating value of bio-oil is associated with the high oxygen and water content, as well as the low hydrogen-to-carbon (H/C) ratio and high oxygen-to-carbon (O/C) ratio [254]. Some other unwanted bio-oil characteristics (e.g., viscosity and acidity) preclude many other potential applications, as well [255]. Biofuels and bio-blendstocks produced from bio-oils have been considered as a potential source of renewable transportation fuels [256]. However, the corrosivity of an acidic fuel ruins boiler, turbines, and engine components [257], while storage and thermal instability limit processing and prevent long-term storage necessary for distribution at the commercial level [258]. Therefore, upgrading treatments (before storage and distribution) attempt to address bio-oil quality issues and improve usability and applicability.

Addition of catalysts to the pyrolysis process improves key chemical reactions, such as cracking, hydrocracking, hydrogenation, decarbonylation, decarboxylation, and hydrodeoxygenation [17]. The goal of catalysis is to produce a bio-oil with fewer oxygenated compounds and increased hydrocarbon and short chain molecule content. Solid acid catalysts (e.g., zeolite) have been shown to possess superior cracking and dehydration activity, making them preferable for catalytic pyrolysis [20]. Though, due to the microporous structure and acidity of zeolite, pore blockage from polymerization and polycondensation reactions results in a low bio-oil yield and rapid catalyst deactivation from coke formation [59]. While not as effective as zeolites, other catalysts have merit in being used for catalytic pyrolysis, such as γ-alumina, due to lower costs and desirable characteristics (i.e., surface area, pore volume, and pore-size distribution) [259]. γ-Alumina is a solid acid catalyst and exhibits high activity due to a large number of Lewis acid sites on its surface [260]. The effectiveness of γ-alumina can also be increased by using it as a catalyst support. Depending on the results of the bio-oil composition, undesirable functional groups for fuel product may be identified and targeted in further experiments by decorating the γ-alumina with metals (e.g., Ni, Mo, Co, and Fe), increasing active sites for cracking and reforming reactions [261]. Gupta and Mondal (2021) performed pyrolysis on pine needles using γ-alumina and nickel-doped γ-alumina [262]. The results showed that the catalyst

caused a considerable reduction in activation energy and improved reaction rate. The catalyst also increased the hydrocarbon and phenolic content in the bio-oil and reduced oxygen content. Other studies have shown that using reactive distillation with an alcohol and an acid catalyst resulted in bio-oil esterification and improved fuel qualities [263,264].

Another technique that can be integrated into a pyrolysis unit to increase bio-oil yield and quality is the utilization of direct quenching columns (e.g., spray towers and impingers). Pyrolysis units commonly utilize these columns due to the physical and chemical condensation interactions between the quenching fluid and pyrolysis vapors. Condensation achieved in this way can capture lighter weight molecules and mitigate undesirable reactions [22]. Earlier studies investigated various quenching fluids, such as water [163], paraffin oil [91], liquid nitrogen [92], reused bio-oil [265], immiscible hydrocarbon solvents [23], alcohols [24], and dichloromethane [266]. Methanol is particularly interesting since it is relatively inexpensive and very effective at decreasing the aging rate of bio-oil [25,26,267]. Suggested reactions that occur between bio-oil compounds and methanol include esterification and acetalization, resulting in a simple, economically feasible upgrading approach [224].

This research utilizes a free-fall reactor configuration for the fast pyrolysis of pinewood particles. The rationales behind the free-fall pyrolysis reactor lie in the simple conversion pathway design, efficient control, high process yield, and minimal use of sweep gas, as well as convenient control of the kinetic parameters, mass balance, and residence time [170,172,268]. The focus of this research is on evaluating the effect of in-situ and ex-situ free-fall catalytic fast pyrolysis (CFP). While CFP is commonly practiced, to the best of our knowledge, there is no study on a free-fall CFP reactor. This study also integrates a direct quenching column in the form of a methanol impinger to both increase bio-oil yield capture and assess the quenching fluid's effects on condensed products. Comparisons of liquid fractions will be made to a previous study utilizing the same reactor [269]. Table 4.1 presents an overview of earlier similar studies.

Table 4.1. Recent pyrolysis studies utilizing γ-alumina and/or direct quenching methods.

Study	**Catalyst**	**Placement**	**Condensing Method**	**Reactor**	**Feedstock**	**Focus**
[270]	γ-Al_2O_3	In-situ	Cold trap	Fluidized bed	Oak Sawdust	Water-gas shift reaction
[24]	-	-	Methanol Impinger, SPA tubes	Semi batch	Spruce Chips	Condensing method effect on product

Table 4.1. continued

[271]	$(SnO)_2(Al_2O_3)_8$, $(SnO)_1(ZnO)_1(Al_2O_3)$, $(ZnO)_2(Al_2O_3)_8$	In-situ	Glass condenser	Semi batch	Soybean oil	Effects of catalyst on products' composition
[272]	Al_2O_3	In-situ	Ice bath	Semi batch	Corncob	Liquid composition, yields
[273]	ZSM-5, Al_2O_3–SiO_2	In-situ	Methanol impinger	Spouted bed reactor	Miscanthus	Operating conditions, product distribution
[274]	ZSM-5, γ-Al_2O_3	In-situ	Impinger	Semi batch	Castor meal	Effects of catalyst on products' composition
[275]	H-ZSM-5 and derivative	In-situ	Cold trap, Propanol N_2 impinger	Micro-fluidized bed reactor	Oak sawdust	Effect of different zeolite catalysts on products
[276]	Na_2CO_3/γ-Al_2O_3, HZSM-5	Ex-situ	-	Tandem micro reactor	Sugarcane bagasse/PET	Effects of catalyst on products' composition
[262]	γ-Al_2O_3, Ni/γ-Al_2O_3	In-situ	Water/ice baths	Semi batch	Pine needles	Thermal degradation, kinetics
This Study	γ-Al_2O_3	In-situ, ex-situ	Shell and tube/Methanol Impinger	Continuous Free-fall	Pinewood particles	Effects of catalyst on product composition, process configuration

This study compares the advantages and deficiencies of the proposed conversion pathways with prior studies, along with the potential of γ-alumina in CFP, and the efficiency and effect of methanol as a direct quenching fluid. This study attempts to address stable bio-oil production from biomass and improve usability and applicability. To do so, the effectiveness of ex-situ and in-situ CFP are examined and compared. The physicochemical properties of methanol as a quenching fluid and stabilizing agent are also assessed. The key research impacts of this study are: (a) assisting in defining the basic principles that guide the production of stable bio-oil and (b) explaining the resulting phenomena occurring in the catalysis and direct quenching of pyrolysis vapors.

4.3 Materials and Methods

4.3.1 Materials

Biomass. Pinewood flour (PWF) was used as the sole biomass feedstock in this study, sourced from American Wood Fibers (Table 4.2). PWF was dried to a moisture content of below 10% and screened (between 60 and 120 standard mesh) to a particle size between 125-250 µm. The moisture content of the feedstock was accounted for by mass difference before and after drying in the oven at 105°C for 12 h.

Table 4.2. Characterization of raw PWS [193].

Feedstock	Volatile Matter (%)	Ash (%)	Fixed Carbon (%)	Moisture Content (%)	Particle Size (µm)
Pine	84.50 ± 4.23	1.08 ± 0.05	14.41 ± 0.72	7.3 ± 0.37	125-250

Catalyst. The catalyst used in this study has a hollow cylinder (Raschig ring) structure and is composed of γ-alumina (GH New Material). This structure was chosen to eliminate char blockage when performing in-situ catalysis. The γ-alumina possessed a BET surface area of 231m2/g and pore volume of 0.66 ml/g.

Experimental setup. The thermochemical conversion of the pinewood was achieved using a free-fall fast pyrolysis reactor (Figure 4.1). The free-fall reactor is a gas-solid co-current downflow cylindrical reactor (inner diameter of 2.09 cm and length of 107 cm). Biomass was continuously fed into the reactor using a motorized auger feed system, located at the top of the reactor at 10 g/min over the span of 5 min. The system pressure was monitored and varied between 0-48 kPa_g. Temperature was set at 550°C with an approximated biomass residence time of 0.7-1 s. The reactor was heated using external tape

heaters and an internal heating cartridge, which were controlled using programmable logic controllers. Thermocouples were attached to the reactor wall and the heating cartridge to monitor temperature at multiple points along the unit. For in-situ catalytic fast pyrolysis (I-CFP), a catalyst bed was placed in the bottom of the free-fall reactor, giving the biomass sufficient time to pyrolyze before the vapors and char passed through the catalyst. A catalyst bed was placed directly after the cyclone for ex-situ catalytic fast pyrolysis (E-CFP). Our previous experiments performed on PWF, using the free-fall reactor, without incorporating catalysts or direct quenching [269].

The solid biochar was separated from the pyrolysis vapors via a cyclone. A custom impinger-type direct quencher was fabricated and placed in series with a shell and tube condenser directly after the cyclone. For the catalytic experiments, the impinger was placed after the shell and tube condenser. Additional experiments were performed where the impinger was placed first in series (FPQ) to examine the effect on bio-oil fractions, however, no catalyst was used in these experiments. The indirect condenser was cooled using a chiller filled with a mix of water and ethylene glycol at 0°C. Pyrolysis vapors were rapidly cooled and condensed by the impinger using a known amount of methanol (100 mL) kept at 0°C by internal coils connected to the chiller. Bio-oil fractions were condensed inside both columns and analyzed separately. Post experiment, the bio-oil and methanol were collected and stored in a refrigerator at 5°C to mitigate the change in composition due to potential bio-oil instability. Bio-oil and char yield were determined gravimetrically, and gas was calculated by difference. Experiments under different conditions were performed in triplicate.

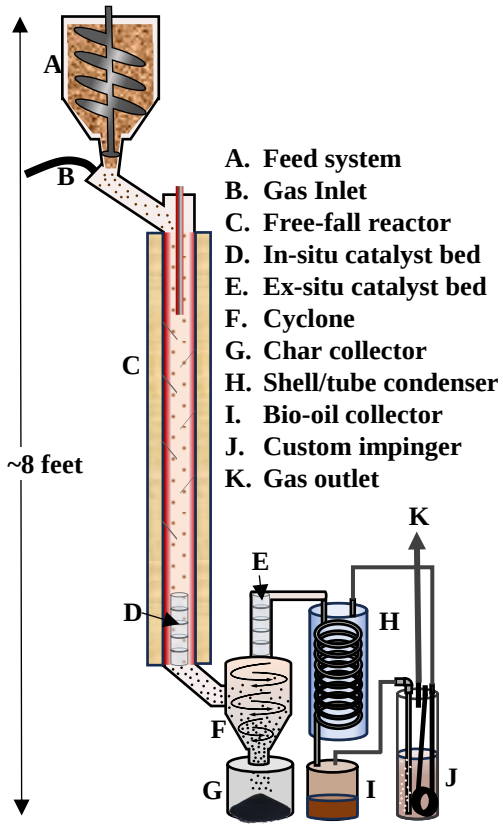

Figure 4.1. Diagram of CFP reactor unit used for pyrolysis experiments.

4.3.2 Product Characterization

Bio-oil samples were characterized using bomb calorimetry, gas chromatography-mass spectrometry (GC-MS), electrospray ionization-mass spectrometry (ESI-MS), Fourier transform infrared (FTIR), and thermal stability aging, as well as proximate analysis for biochar characterization.

Proximate analysis. Higher heating values (HHV) of the biochar and bio-oil (dried over anhydrous sodium sulfate prior to analysis) samples were obtained by bomb calorimetry (Parr Instruments model 1261) according to ASTM D5865-04 and calibrated with benzoic acid.

GC-MS. Semi-volatile composition of the bio-oil was determined by GC-MS analyses and carried out in duplicate (Trace 1300-ISQ, ThermoScientific). GC-MS samples were prepared by mixing 1 mg bio-oil with 1 mL CH_2Cl_2 containing trichlorobenzene (100 µg/mL) as an internal standard. A ZB-5 capillary column (30 m 0.25 mm, Phenomenex) was used to separate bio-oil compounds using a temperature program of 40°C (1 min) to 250°C (10 min) at 5°C/min and injector temperature of 255°C. Peaks on the chromatogram were identified using authentic standards from the literature and the NIST 2017 MS library [198–200].

ESI-MS. Molar mass, monomer/oligomer ratios, and predominant compounds of the bio-oil samples were determined using spectral mass distribution obtained from a Finnigan LCQ-Deca mass spectrometer (ThermoQuest) [201]. ESI-MS samples were made by dissolving bio-oil (1 mg/mL) in a 99% methanol/1% acetic acid solution before being injected and exposed to negative ion ESI–MS (m/z 100–2,000) at a flow rate of 10 μL/min. Temperature was set to 275°C with capillary and ion source voltages set to 4.5 kV and 50 V, respectively. Equations (1) and (2) were used to calculate molar masses as the number-average (M_n) and weight-average (M_w), where N_i is the intensity of ions and M_i is the ion mass [197,201].

$$M_n = \sum N_i M_i / \sum N_i \quad (1)$$

$$M_w = \sum N_i M_i^2 / \sum N_i M_i \quad (2)$$

FTIR. Major functional groups and compounds were identified by FTIR spectra of bio-oil samples. Spectra was obtained in duplicate using a ZnSe attenuated total reflection (iD5 ATR) accessory of a Thermo-Nicolet iS5 spectrometer. The (Thermo-Nicolet) Omnic v9 software was used for baseline correction, averaging the FTIR spectra, and for identifying functional group frequencies.

Thermal stability. The thermal stability test was performed by rapidly aging the bio-oil at a moderate temperature and measuring the change in viscosity (NDJ-9S viscometer, spindle 2 at 60 rpm) over time. When undergoing accelerated aging, bio-oil shows a decrease in total molecules but an increase in molecular weight, indicating condensation reactions and water formation [226,227]. Methods for the thermal stability test and obtaining the stability parameter (SP) can be found in our previous published study [269]. Equation (3) was used to calculate the SP values:

$$SP = \frac{\partial(Viscosity)}{\partial(time)}\ cp/h \quad (3)$$

4.4 Results and Discussion

4.4.1 Product Yield Results

Bio-oil yield is represented by the average and standard deviation of the sum of oil collected from the condenser and impinger over three experiments. Table 4.3 shows the yields of products collected.

Table 4.3. The yield of free-fall FP products (liquid, solid and gas) from different reactor configurations.

Experiment	Liquid (%)	Char (%)	Gas (%)
FP	23.3 ± 1.2	53.6 ± 2.7	23.1 ± 3.1
E-CFP	41.1 ± 4.3	27.6 ± 2.7	31.3 ± 2.6
I-CFP	31.9 ± 1.5	36.7 ± 3.8	31.4 ± 2.7
FPQ	38.5 ± 3.2	33.2 ± 1.1	32.9 ± 4.3

FP: fast pyrolysis; E-CFP: ex-situ catalytic pyrolysis, I-CFP: in-situ catalytic pyrolysis, FPQ: fast pyrolysis with direct quenching.

I-CFP resulted in higher solids (char and coke) and gas yields than E-CFP, while ex-situ had higher liquid yields. Through a t-test, it is found that only the difference in the means of char yields is statistically significant ($p = 0.02$) while the difference in the means of liquid yield barely fails to reject the null hypothesis ($p = 0.05$). Prior comparison studies of in-situ and ex-situ pyrolysis generally find higher yields from ex-situ pyrolysis [277,278]. Earlier published studies examining free-fall FP reveal yields of 35-45% for bio-oil, though none incorporate catalyst [178,182,188]. Liquid yields were higher and solid yields were lower in comparison to data produced for pyrolysis of PWF with no catalyst, which may be attributed to an increase in heat transfer efficiency inside the reactor and the incorporation of the impinger. The impinger was responsible for capturing 6-14% of total bio-oil yield during catalytic pyrolysis experiments.

4.4.2 Biochar Analysis Results

The results showed the extremely high ash content present in the catalytic samples, especially on E-CFP process. Ash content and fixed carbon of biochar generally increase with increasing treatment temperature while volatile matter decreases (Table 4.4) [279]. Increased thermal treatment could explain slight increases in ash, however, ash concentration has been shown to be influenced less by pyrolysis temperature and mainly by feedstock [280]. The high ash content seen in these char samples was probably due to the presence of inorganic foreign material, such as dirt, or contamination of char sample before analysis. HHV also significantly decreased for the catalytic samples, confirming that HHV can be correlated to fixed carbon and ash concentrations [281]. Further screening of initial biomass samples would be required to comprehensively identify factors for proximate analysis results.

Table 4.4. Proximate analysis of biochar samples.

	FP	E-CFP	I-CFP
Fixed C%	27.97 ± 0.34	11.95 ± 1.98	43.76 ± 1.22
Ash %	1.29 ± 0.01	54.80 ± 0.36	20.57 ± 0.98
Volatile Matter %	70.74 ± 0.86	33.38 ± 1.05	35.67 ± 2.19
Moisture Content %	-	2.58 ± 0.17	0.84 ± 0.06
HHV (kJ/g)	21.64 ± 0.26	8.04 ± 1.22	15.29 ± 1.08

4.4.3 Bio-oil Heating Value Results

HHV values fall within 16-23 MJ/kg found for other bio-oil samples in prior studies with the exception of I-CFP [282,283]. Figure 4.2 compares HHV of commercial fuels or solvents with liquid samples collected in this study. FPQ produced bio-oils with the highest HHV, close to that of methanol. Physicochemical interactions during the condensation of vapors may contribute to this result. Traces of methanol may also have evaporated and recondensed in the second condenser. I-CFP samples performed the worst, indicating undesirable cracking reactions when considering product fuel quality. Addition of 10 wt% methanol increased the HHV for E-CFP samples by an average of 17% while showing a slight change in FPQ samples. Insufficient I-CFP sample led to inconclusive results when adding methanol. Still, the HHV of the samples falls well short of conventional fuels by 40-50%. While Heating value alone would not be enough to determine fuel blending potential, further treatment of bio-oil samples (e.g., fluid catalytic cracking, hydrotreating, distillation, and electrochemical) would be required if a pathway for fuel production was desired [17].

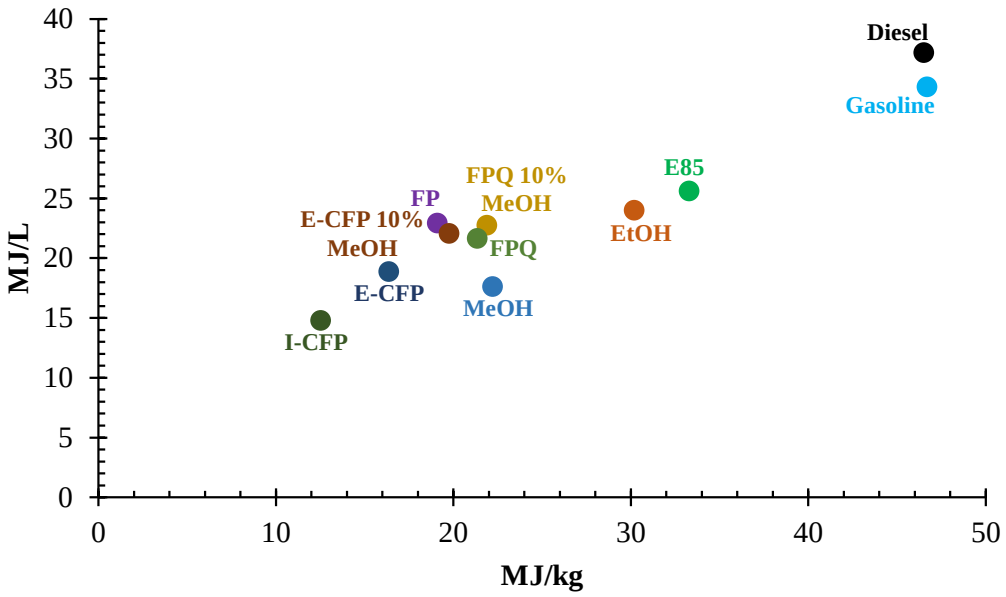

Figure 4.2. Energy densities of samples compared with commercial fuels.

4.4.4 Bio-oil Thermal Stability Results

The results of bio-oil viscosity show a relative linear correlation, given by R2 values close to 1 (Figure 4.3).

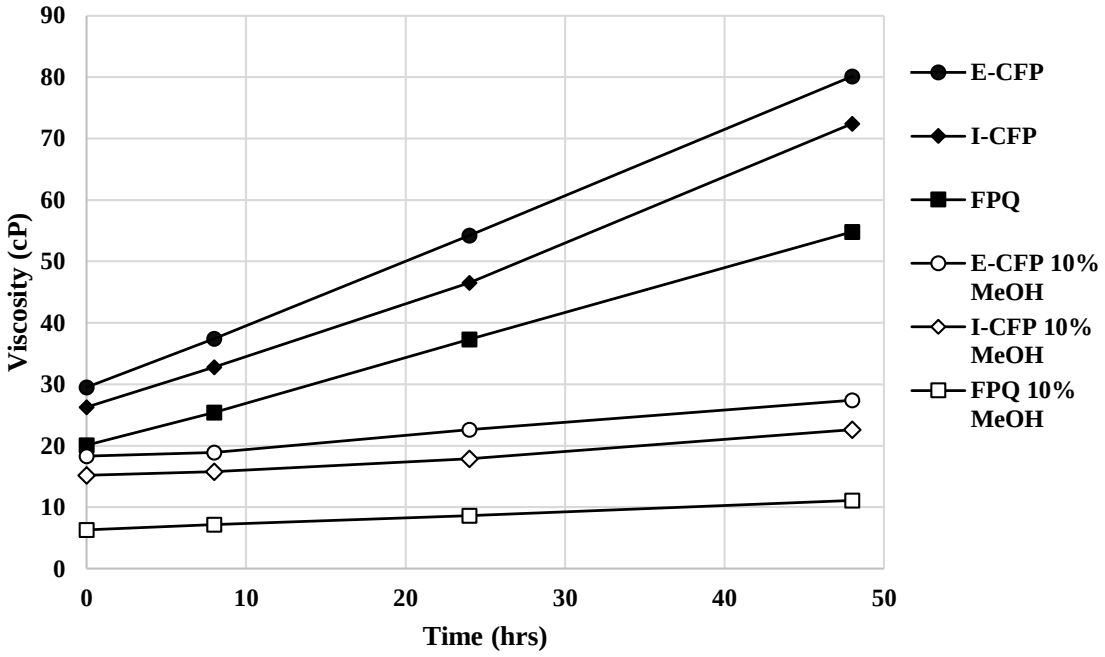

Figure 4.3. Bio-oil viscosity changes over time.

The initial viscosities before the addition of alcohol ranged between 20-30 cP. SP values were determined using data obtained from the thermal aging experiments and ranged between 0.1 and 0.2 cP/h for methanol added bio-oils and between 0.7 and 1.3 cP/h for the bio-oils (Table 4.5). Other stability studies covering the addition of methanol give SP values from 0.5-11 cP/h, backing the results of this study [174,226]. Methanol addition decreased the viscosity and reduced the rate of increasing viscosity of bio-oils. Bio-oils produced during E-CFP had slightly higher initial viscosities and SP values, while those produced from FPQ had both the lowest initial viscosities and SP values. The low viscosity values for the FPQ samples could be attributed to a decrease in acidic compounds due to the catalytic effects of γ-alumina [259]. The FPQ liquid samples were collected in the second condenser following the impinger, resulting in a bio-oil that shows the least change in viscosity over time. This could be the result of some interaction with the vapor initially passing through the methanol or trace amounts of methanol vaporizing and condensing in the second condenser, increasing the stability of the fraction [267]. Further characterization analysis during each step of the aging process would be beneficial in determining the specific stabilizing reactions and the impact on functional groups. The SP results show that the use of γ-alumina as a catalyst for fast pyrolysis has a significant positive effect on bio-oil stability.

Table 4.5. SP values for bio-oil samples.

	FP	**E-CFP**	**I-CFP**	**FPQ**	**E-CFP 10% MeOH**	**I-CFP 10% MeOH**	**FPQ 10% MeOH**
SP (cP/h)	1.33	1.06	0.96	0.73	0.20	0.16	0.10
R^2	0.98	0.99	0.99	0.99	0.99	0.98	0.99

4.4.5 Gas Chromatography-Mass Spectrometry Results

GC-MS was used to examine the volatile compounds in the bio-oil produced by the different pyrolysis unit configurations (Figure 4.4) [228,229].

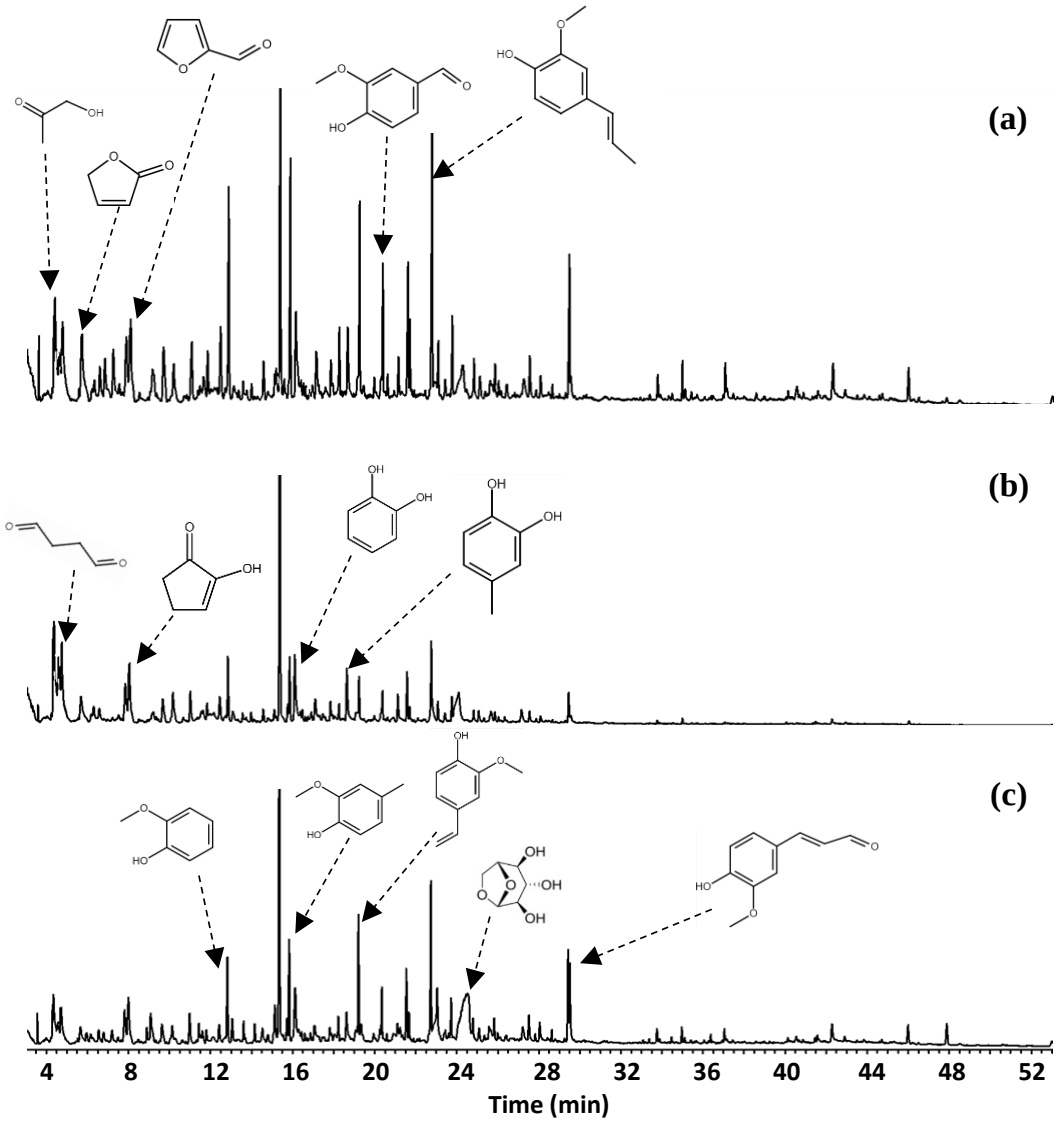

Figure 4.4. GC-MS Chromatograms of bio-oil collected from (a) E-CFP, (b) I-CFP, (c) and FPQ experiments.

Chemical compounds identified in the chromatograms were diverse in structure (e.g., phenolics, sugar derivatives, furans, ketones, alcohols, aldehydes, and acids) with carbon atoms ranging from C_3 to C_{20} [234]. The results show a high amount of phenolic compounds with methoxy-substitutes and benzenediols phenols, which are attributed to high amounts of guaiacyl and syringyl units in the lignin fraction of PWF [230]. The presence of syringyl units is likely from hardwood species present in the PWF. The complexity and variety of phenolics indicate recombination reactions occurred among intermediates after primary decomposition reactions.

Levoglucosan is the primary compound in the E-CFP and FPQ bio-oil samples while also being predominant in I-CFP samples (Table 4.6). I-CFP seemed to favor the production of ketones, namely

hydroxyacetone. This results from cracking of anhydro-sugars by dehydration and decarbonylation reactions favored in the I-CFP configuration [284]. It is also speculated that a longer residence time caused by integration of a catalyst bed in the reactor, and a low feed/gas flow rate contributed to ketonization of the carboxylic acids, producing ketones, water, and carbon dioxide [236,285]. The additional water formation could explain the decrease in HHV for the I-CFP samples examined earlier.

Table 4.6. High-concentration compounds identified by GC-MS in bio-oil samples.

Compound	**M+**	**Formula**	**Apex RT**	**FP**	**E-CFP**	**I-CFP**	**FPQ**
				µg/mg			
Acetic acid	60	$C_2H_4O_2$	3.67	4.44	-	-	-
Hydroxyacetone	74	$C_3H_6O_2$	4.33	0.35	5.13	9.36	6.37
Succindialdehyde	86	C_4H6O_2	4.56	0.76	2.53	4.43	1.48
dihydro-4-hydroxy-2(3H)-Furanone	102	C_4H6O_3	4.71	-	3.40	4.03	-
3-methyl-butanal,	86	$C_5H_{10}O$	4.83	1.06	-	-	-
Furfural	96	$C_5H_4O_2$	5.65	3.62	2.62	1.52	1.32
tetrahydro-2,5-dimethoxy-Furan	132	$C_6H_{12}O_3$	7.19	0.32	2.45	0.98	2.50
2(5H)-Furanone	84	$C_4H_4O_2$	7.81	2.43	2.56	2.14	2.17
2-hydroxy-2-Cyclopenten-1-one	98	$C_5H_6O_2$	8.00	1.81	3.82	2.74	3.78
2-methyl-1,2-Hexanediol	132	$C_7H_{16}O_2$	9.08	-	-	2.17	-
Phenol	94	C_6H_6O	9.63	1.36	1.85	1.01	1.57
3-methyl-1,2-Cyclopentanedione	112	$C_6H_8O_2$	10.99	1.3	1.49	1.10	1.60

Table 4.6. continued

Guaiacol	124	$C_7H_8O_2$	12.81	2.78	3.34	1.81	3.77
1,2-Cyclopentanediol	102	$C_5H_{10}O_2$	13.03	-	-	0.86	1.08
Creosol	138	$C_8H_{10}O_2$	15.82	2.6	3.20	1.62	4.15
Catechol	110	$C_6H_6O_2$	16.07	1.94	3.49	2.38	4.69
1,4:3,6-Dianhydro-α-d-glucopyranose	144	$C_6H_8O_4$	16.37	-	0.32	0.83	-
5-Hydroxymethylfurfural	126	$C_6H_6O_3$	17.10	0.53	1.07	0.76	1.54
4-Methylcatechol	124	$C_7H_8O_2$	18.60	1.62	2.79	1.57	2.73
Vinyl guaiacol	150	$C_9H_{10}O_2$	19.20	0.34	2.61	1.31	0.45
Eugenol	164	$C_{10}H_{12}O_2$	20.34	1.05	1.64	1.76	2.12
Geraniol	154	$C_{10}H_{18}O$	21.18	-	-	0.62	0.56
Vanillin	152	$C_8H_8O_3$	21.53	2.43	2.51	1.16	2.77
Isoeugenol	164	$C_{10}H_{12}O_2$	22.73	4.48	6.25	2.25	6.49
propyl-guaiacol	166	$C_{10}H_{14}O_2$	23.04	0.36	0.84	0.25	4.17
Methyl syringol	168	$C_9H_{12}O_3$	23.06	2.8	-	-	-
Apocynin	166	$C_9H_{10}O_3$	23.71	-	1.29	1.44	-
Levoglucosan	162	$C_6H_{10}O_5$	24.31	13.2	8.57	5.05	15.99
Syringaldehyde	182	$C_9H_{10}O_4$	28.17	1.15	-	-	-
Coniferyl aldehyde	178	$C_{10}H_{10}O_3$	29.41	-	2.28	0.70	8.19
Acetosyringone	196	$C_{10}H_{12}O_4$	29.77	2.93	-	-	-
5-Hydroxy-7-methoxyflavanone	270	$C_{16}H_{14}O_4$	42.11	1.17	-	-	-

Figure 4.5 reveals the relative abundance of functional groups among the volatile compounds identified through GC-MS. I-CFP and E-CFP samples show a slightly decreased content of sugar-derived compounds caused by the catalyst via decarbonylation, decarboxylation, dehydration, and cracking reactions, leading to the formation of alcohols, furans, and ketones. These compounds then can also undergo further conversion, resulting in phenols [286]. There is only a small change in alcohol, aldehyde, furan, and ketone content after catalytic reactions in E-CFP due to the secondary reactions. E-CFP samples have the highest phenolic content. This can be attributed to the cracking and deoxygenation properties of the catalyst transforming lignin-derived compounds into phenols through cleavage of C-O and C-C bonds [286]. Lewis acid sites on the surface of the catalyst also allow for rehydroxylation reactions, permitting water to be converted into hydroxy groups [259]. FPQ samples also exhibited high amounts of phenolic content. With no catalyst used, it is assumed that the methanol reacted with the pyrolysis vapors, increasing alkylated phenols and aromatics [287]. Methanol also shows a stabilizing effect on the second fraction, resulting in fewer condensation reactions, leading to a higher content of lighter molecules. The phenolic content in bio-oil has industrial significance for resin, adhesive, dye, pharmaceutical, and food additive production [288]. Appropriate analysis and extraction techniques (e.g., solvent extraction, column chromatography, and distillation) should be examined to pursue this application pathway [289]. Both E-CFP and I-CFP showed a noticeable decrease in acidic compounds, leading to reduced corrosivity and improved thermal stability, as shown previously. All configurations resulted in a certain amount of ester formation, particularly FPQ, where the interaction between organic acids and alcohols produces esters [290]. It has been reported that the ester reactions during pyrolysis of biomass are promoted by acidic catalysts, such as γ-alumina [291]. These catalysts convert acidic compounds into esters through catalytic esterification. FPQ samples had the highest amount of ester content. This can be attributed to esterification that occurs when the vapors interact with the methanol in the impinger [224]. FPQ still has relatively the same acid content as noncatalytic pyrolysis, emphasizing the effect γ-alumina has on acid conversion.

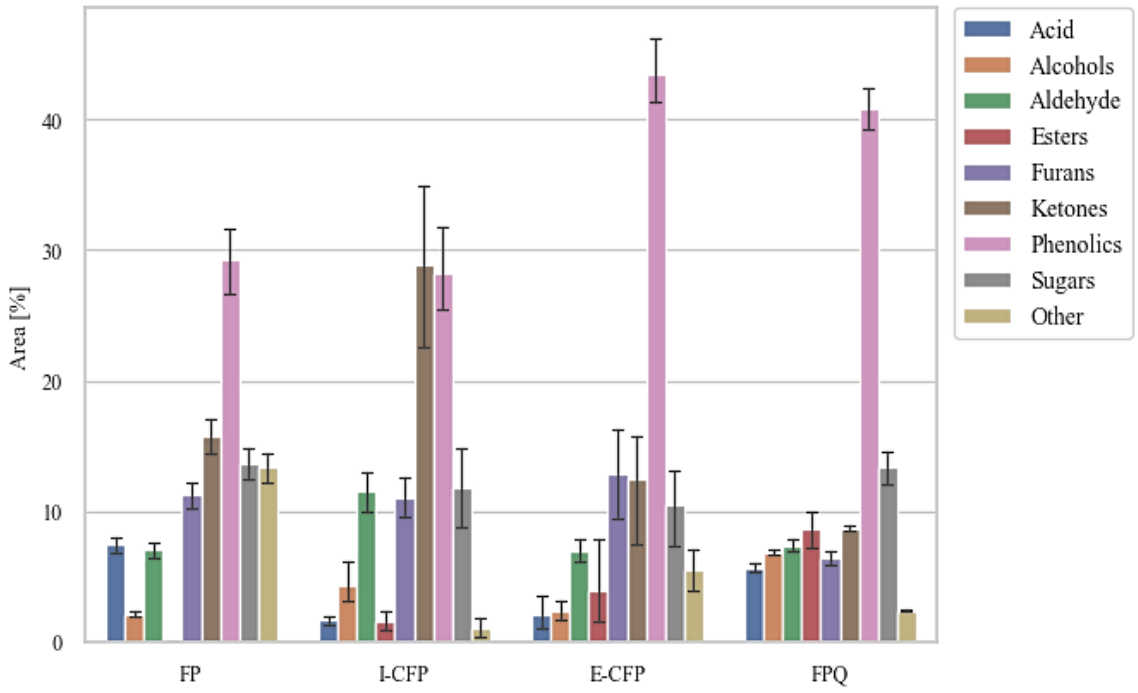

Figure 4.5. Abundance of functional groups identified in volatiles analyzed in bio-oil samples.

Fewer samples were captured in the methanol impingers during catalytic pyrolysis. Prominent compounds included oleic acid, methyl palmitate, glyceraldehyde, dodecyl acrylate, and other methyl esters. As the impinger was used as the primary condenser during FPQ, the compounds are more diverse, but similar to the first fractions condensed during the catalytic experiments. Esterification of acids is recognized by the high presence of methyl acetate and isobutyl propionate [292]. Though, the carboxylic acid content was still high with the presence of pyruvic acid and higher molecular weight acids (e.g., homovanillic acid, 2-undecenoic acid, 9-hexadecenoic acid, and oleic acid) mostly found in the second bio-oil fraction.

4.4.6 Electrospray Ionization Mass Spectrometry Results

ESI-MS analysis was used to determine the molar mass distribution of bio-oil (Figure 4.6) [197,201]. Peaks generally spanned over the m/z range of 100−1,200 [237–239]. The more noticeable $[M-H]^-$ ions were credited at m/z 161 to levoglucosan, m/z 109 to catechol, m/z 123 to guaiacol, and m/z 123 to coniferyl aldehyde. Subfractions of lignin-derived compounds, such as anhydro-sugars and phenolics appear as peaks between m/z 300-350 [237,238,240]. GC-MS results verify the volatile compounds identified. Further mass analysis and equivalent homologue series are required to thoroughly identify compounds, peaks produced through ESI-MS reveal higher molecular weight compounds than the volatiles identified by GC-MS, allowing for mass calculations.

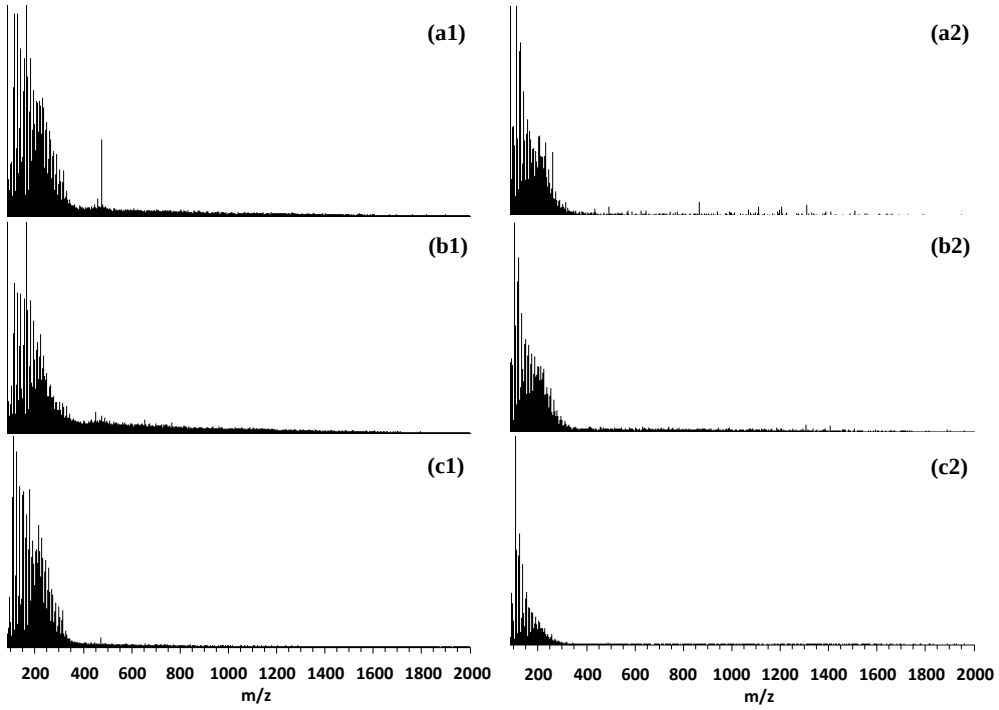

Figure 4.6. Negative-ion ESI-MS spectra of bio-oil produced from (a1) E-CFP condenser, (a2) E-CFP impinger, (b1) I-CFP condenser, (b2) I-CFP impinger, (c1) FPQ condenser, and (c2) FPQ impinger.

Molar masses (M_w and M_n) of bio-oil samples were determined using prior studies on negative ion ESI-MS (Table 4.7). The spectra revealed bimodal distribution seen mostly in the condenser samples centered on m/z 250 and 450, indicating monomers and oligomers, respectively. Due to the bimodal distribution, the ion intensity ratio of m/z 100-300 / m/z 301-2000 was used to calculate the ratio of monomers to oligomers. The highest monomer/oligomer ratio belonged to fractions produced during FPQ, being significantly higher than any other sample, and all methods being higher than FP, which indicates improved thermal breaking caused by both catalysis and direct quenching. Generally, because of thermal instability, bio-oil undergoes oligomerization during storage, resulting in the average molecular mass increasing between the time of pyrolysis and ESI-MS measurements. FPQ proved to have the best results because of methanol's stabilizing effects decreasing oligomerization. Earlier studies reported average molecular weights around 300-800, complementing the results of this study [240,241]. These results are also consistent with the thermal stability of samples analyzed earlier. The most stable bio-oils in descending order were obtained during FPQ, I-CFP, E-CFP, and FP. I-CFP samples have the widest variance in molecular mass, but ultimately seem very comparable in molecular weight to E-CFP. Samples collected in the second fraction tend to have molecular weights lower, proving the successful capture of some of the more volatile compounds that are

entrained in the incondensable gas. Compared to FP, the effect of catalytic cracking seems to remedy the high average molecular weight and molar mass from previous experiments.

Table 4.7. Weight (M_w) and number average molar mass (M_n) of bio-oil samples determined from negative ion ESI-MS data.

Config.	Fraction	Mn	Mw	Monomer/Oligomer
FP	Condenser	564 ± 28	816 ± 41	0.45 ± 0.17
E-CFP	Condenser	387 ± 11	697 ± 20	1.66 ± 0.20
	Impinger	321 ± 117	603 ± 229	1.55 ±0.94
I-CFP	Condenser	410 ± 61	726 ± 83	1.49 ± 0.92
	Impinger	514 ± 234	776 ± 292	0.56 ± 0.37
FPQ	Condenser	261 ± 10	453 ± 18	5.11 ± 0.89
	Impinger	264 ± 119	461 ± 199	5.06 ± 4.31

4.4.7 Fourier Transform Infrared Spectroscopy Results

FTIR analysis was used to verify functional groups in the bio-oil samples (Figure 4.7) [85].

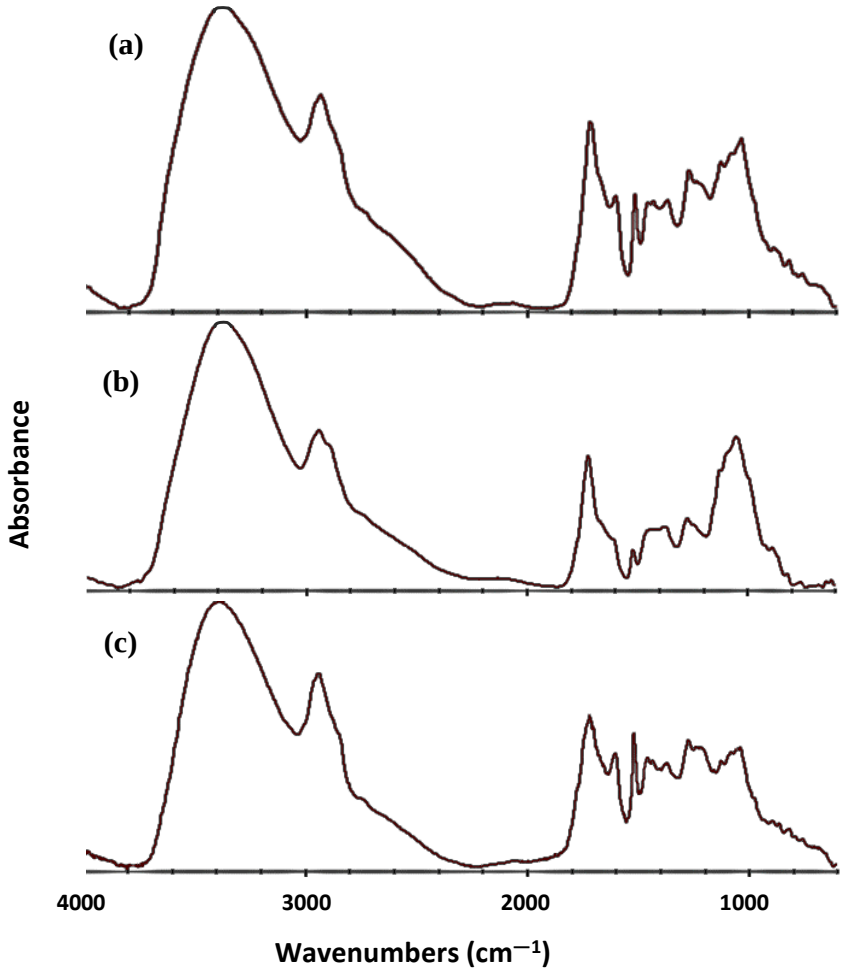

Figure 4.7. FTIR spectra of pyrolysis liquid collected from the condenser after (a) E-CFP, (b) I-CFP, (c) and FPQ.

Spectra were averaged taken for each experiment configuration and averaged before analysis. Band assignments for the bio-oils were acquired from the earlier published studies and labeled appropriately (Table 4.8) [244,245]. In the IR spectra, strong O-H stretching vibrations in all the samples around 3,365 cm^{-1} were indicative of phenols, acids, alcohols, and water [249]. C-H stretching absorptions were seen around 2,935 cm^{-1}, revealing the presence of possible aliphatic hydrocarbons [293]. C=O stretching seen by absorption at 1,715 cm^{-1} suggests the presence of open chain ketones and aryl aldehydes, but was generally more suggestive of aliphatic and fatty acids [220]. At 1,515 cm^{-1}, the C=C-C stretching vibrations signify aromatics with various substitutions [250]. Aromatic C-H and C-O stretching were related to the absorption at 1,032 cm^{-1}, revealing primary alcohols and guaiacyl compounds. At 813 cm^{-1}, aldehydes were identified by the aromatic C-H out of plane bending in lignin [247]. I-CFP seemed to have a prominent band around 1,035 cm^{-1} relating to C-O and C-C-O of lignin and cellulose constituents [294]. Though, bands between 1,035-

1,716 cm^{-1} were significantly lower than other samples, showing lower C=C-C aromatic ring stretching, and C-H bending and stretching. E-CFP has a noticeably large band at 1,716 cm^{-1}, which confirms the large number of phenolics/aromatics seen in the other analyses. The overview of sample functionalization FTIR band and IR spectra provide quick insight into chemical shifts that occur when changing experiment methodologies.

Table 4.8. FTIR analysis results for E-CFP, I-CFP, and FPQ bio-oil samples.

Assignment/Components	**E-CFP**	**I-CFP**	**DQ**
O-H stretching (Cellulose, Hemicellulose, Lignin)	3,359	3,367	3,374
C-H stretching (Cellulose, Hemicellulose, Lignin)	2,930	2,935	2,936
C=O stretching (Hemicellulose, Lignin)	1,715	1,715	1,715
Aromatic skeletal vibration, C=O stretching, adsorbed O-H (Hemicellulose, Lignin)	1,597	1,604	1,597
C=C-C aromatic ring stretching and vibration (Lignin)	1,514	1,515	1,514
C-H deformation (in methyl and methylene) (Lignin)	1,454	1,429	1,454
C-H bending, C-H stretching in CH3 (Cellulose, Hemicellulose, Lignin)	1,362	1,362	1,362
H-C-H Stretching methylene	1,268	1,268	1,270
C-O stretching of guaiacyl unit (Lignin)	1,128	1,125	1,120
C-O stretching, aromatic C-H in plane deformation	1,032	1,035	1,032
–C–H bending vibration; aldehydes	883	878	888
Aromatic C-H out of plane bending (Lignin)	813	813	813
C-H bending out of plane peaks (Furfural)	755	753	755

In order to better understand and improve the free-fall CFP conversion process, especially bio-oil quality and thermal stability, future studies can focus on the following directions:

- Exploration of several inexpensive hydrodeoxygenation catalysts in the ex-situ CFP configuration.

- Examination of the effects of catalytic loading ratio and physical parameters on pyrolysis liquid product composition and yield.
- Exploration of direct quenching with varying solvents and their physicochemical effects on the liquid product.
- Investigation of solvent promoting fractionation and reactive distillation integrated with CFP.

4.5 Conclusion

The effects of γ-alumina as a catalyst for in-situ and ex-situ catalytic fast pyrolysis of pinewood in a customized free-fall reactor were successfully studied. The physicochemical effects of methanol as a direct quenching agent were also examined. All three pyrolysis process configurations had higher liquid and gas yields, and greater thermal stability than the prior FP experiments. γ-Alumina had a significant positive effect on bio-oil thermal stability. The addition of 10 wt% methanol to samples improved HHV by a visible amount. GC-MS was used to detect the volatile fraction of bio-oil compounds (e.g., levoglucosan, furfural, hydroxyacetone, methyl acetate, and catechol). E-CFP favored the production of phenolic compounds due to the cracking and deoxygenating effects of the catalyst on lignin compounds. I-CFP supported higher ketone formation (mostly hydroxyacetone) through dehydration and decarbonylation, possibly due to ketonization by longer residence times caused by the in-situ catalyst bed. The γ-alumina was effective in both configurations for decreasing acidic content in the bio-oil. FPQ also exhibited higher phenol content and had the highest ester content because of the esterification effect of methanol. However, FPQ also had the highest acidic compound content. ESI-MS results show low to average bio-oil molecular weights and a noticeable increase in monomer/oligomer ratios compared to FP bio-oil. FPQ samples had the lowest molecular weights and ratios, alluding to thermal stabilization from methanol between production and analysis of samples. FTIR peak patterns showed slight differences among the samples, particularly for I-CFP, which exhibited differences in lignin-derived functional group formation. Both the addition of catalyst and methanol impinger give favorable results for future free-fall fast pyrolysis bio-oil production studies. The γ-Alumina as an inexpensive catalyst support for hydrodeoxygenating catalysts (e.g., Ni, Mo, Fe, and Co) could remedy the insufficiencies of γ-alumina as a catalyst. Methanol was successful as a direct quenching agent for the first liquid fraction, converting much of the carboxylic acid content into fatty acid methyl esters, producing high phenolic content, and thermally stabilizing the fraction upon collection, resulting in a low molecular weight bio-oil fraction. The fraction did, however, still possess a visible amount of acidic compounds. The use of γ-alumina with methanol impingers for fractionation could potentially produce an oil high in small chain esters and low in acids.

Chapter 5: Techno-economic and environmental assessments for nutrient-rich biochar production from cattle manure: A case study in Idaho, USA

This chapter was published in *Applied Energy*, under the title "Techno-Economic and Environmental Assessments for Nutrient-Rich Biochar Production from Cattle Manure: A Case Study in Idaho, USA," by Ethan Struhs, Amin Mirkouei, Yaqi You, and Amir Mohajeri

https://doi.org/10.1016/j.apenergy.2020.115782

5.1 Abstract

Bioproducts from biomass feedstocks and organic wastes have shown great potential to address challenges across food-energy-water systems. However, bioproducts production is at an early, nascent stage that requires new inventions and cost-reducing approaches to meet market needs. Biochar, a byproduct of the pyrolysis process, derived from nutrient-rich biomass feedstocks (e.g., cattle manure and poultry litter) is one of these bioproducts that has numerous applications, such as improving soil fertility and crop productivity. This study investigates the market opportunity and sustainability benefits of converting manure to biochar on-site, using a portable refinery unit. Techno-economic and environmental impact assessments are conducted on a real case study in Twin Falls, Idaho, USA. The techno-economic analysis includes a stochastic optimization model to calculate the total cost of biochar production and distribution. The environmental study employs a life cycle assessment method to evaluate the global warming potential of manure-to-biochar production and distribution network. The total cost of biochar production from cattle manure near the feedlots is approximately $237 per metric ton, and total emission is 951 kg CO_2 eq. per metric ton. The on-site operation and manure moisture content are two key parameters that can reduce biochar unit price and carbon footprint of manure management. It is concluded that converting cattle manure, using the presented strategy and process near the collection sites can address upstream and midstream sustainability challenges and stimulate the biochar industry.

5.2 Introduction

Challenges and Motivation. Based on the U.S. National Oceanic and Atmospheric Administration (NOAA), atmospheric CO_2 concentration increases every year and it reached 414.7 parts per million (ppm) in 2019, which is 3.5 and 14.7 ppm higher than the 2018 and 2014 recorded level, respectively [295]. Carbon sequestration should be deployed to stabilize the concentration of CO_2 in the atmosphere. Biochar-based carbon sequestration is considered a negative emission strategy for reliable carbon management because of its ability to lock black carbon in the soil, which will remain

there for multiple centuries [296]. Biochar produced from nutrient-rich agricultural leftovers and waste streams has multiple environmental benefits and can be used as a soil amendment explicitly for organic crop production [297,298]. It can significantly enhance soil fertility and crop yield while reducing greenhouse gas (GHG) emissions and leaching of nutrients, heavy metals, and pesticides to surface and groundwater [299]. Specifically, slow pyrolysis (SP) condition is more favorable than fast pyrolysis for the production of biochar and generates biochar with higher stability that allows long-term carbon sequestration in soils [50,300,301].

Biochar can retain nutrients in the soil and release macronutrients, e.g., nitrogen, phosphorus, and potassium (NPK), for plant growth [302]. Biochar can, thus, reduce the need for soil fertilization and work as a slow-release fertilizer [303]. Moreover, the enhanced water-holding capacity in biochar-amended soils will increase crop yield per drop of water applied [304]. Its porous nature enables biochar to adsorb heavy metals and thus reduce their uptake by plants and subsequent ingestion by humans and animals [305]. Apart from agronomic applications, unblended biochar and biochar blended with other compositions have broad applications, such as nutrient recovery and reuse [306], livestock farming [307], and pharmaceutical [308]. Biochar also has large potential in the treatment of water [309], a quintessential resource for the future of the population and the standard of living [310]. Despite considerable empirical evidence of agronomic and environmental benefits of biochar from laboratory and field studies [311], systems-level assessment of biochar effects is still limited, impeding translation into large-scale management practices [31,32].

Background. The future of resources (e.g., food, water, and energy) sustainability is an ever-increasing global concern due to the rapidly growing population and the doubling of global demands in the next 25 years [4,312,313]. Particularly, a global increase in the demand for food requires substantial land, energy, and water resources while mitigating negative environmental impacts of food systems. Reusing or recycling resources is one promising approach to reduce the negative impacts of the food system on agro-ecosystems. Delaney (2015) reported that the U.S. national market potential of biochar is projected to reach over $5 billion across various sectors (e.g., aquaculture, agriculture, and horticulture) [314]. Existing biochar on the market is mainly from wood-based feedstocks that can increase forest restoration and employment [315]. Wrobel-Tobiszewska et al. (2015) developed an economic analysis for on-site biochar production in Tasmania, using eucalypt plantations residue wood as feedstock [316]. They used the biochar within the system or sold it as a product, and their cost model revealed an annual income of $179,000, with benefit depending mainly on biochar unit price and distribution.

A comprehensive classification of research related to this study based on the characteristics of biochar problems is provided in Table 5.1. This classification is based on the following distinguishing factors:

- *Production strategies.* Several studies have conducted cost analysis for biochar and bio-oil production from different feedstocks (e.g., rice husk, pinewood, wheat straw, maize straw, poplar wood, and rice straw) in various regions (e.g., USA, China, Vietnam, and Australia), using various thermochemical conversion technologies [10,11,317]. Among thermochemical technologies, SP technology can produce biochar with higher stability and carbon content. SP is expected to grow rapidly due to high process yield (around 35%) and end-product quality (over 55% carbon content) in comparison to other conversion pathways (e.g., fast pyrolysis and gasification) [319]. A comprehensive overview of biochar production and utilization has been given by Panwar et al. (2019) [320].

- *Techno-economic analysis (TEA).* Recent studies reported varying biochar selling prices, such as $231-$283 per ton using pyrolysis and gasification processes as modeled with ECLIPSE software [321], $474-$704 per ton using pyrolysis with a case study developed around the Upper Klamath Basin [315], and $220-$280 per ton, using SP [322]. TEA shows that capital and operating costs of a pyrolysis unit have the lowest sensitivity impact, while the biochar selling price and biomass management cost have the highest impact [323]. Similar studies also show that capital investment, feedstock costs, and labor costs are the greatest influencing factors of biochar and bio-oil minimum selling price [32,324,325].

- *Environmental impact assessment.* Biochar has greater agronomic benefits and is generally more environmentally beneficial than mineral fertilizers in terms of global warming potential (GWP), acidification potential (AP), and eutrophication potential (EP) [326]. Several studies used life cycle assessment (LCA) for evaluating biochar and bio-oil production by pyrolysis technology in different countries (e.g., Spain, Brazil, and USA) [317,327]. A Monte Carlo simulation of biochar climate impact on harmful emissions in Stockholm, Sweden showed a near-linear correlation between the concentration of biochar used and its effects [328]. LCA suggested biochar made from the main crop for biodiesel in the EU, winter oilseed rape, may decrease GHG emissions by 73% and 83% [329].

- *Multi-objective studies.* Belmonte et al. (2018) developed an optimization model with both economic (profit) and environmental (carbon sequestration) objectives and conducted a Philippine case study to explore the trade-off between these two objectives. Li et al. (2019) performed regional TEA and LCA of biochar production for an integrated pyrolysis-bioenergy-

biochar platform in three U.S. states, considering different feedstocks (wood, straw, grass) in each state [330]. Their TEA concluded that farmer's willingness-to-pay ranged from $75 to $1,272 per metric ton of biochar, LCA proved that higher ash content of the feedstocks led to higher biochar yield, resulting in a larger reduction of GHG emissions. Case studies performed in Belgium attempted to monetize the environmental impacts of biochar production from willow and pig manure. Wood-based biochar outperformed manure in all categories of environmental impact and cost due to the high energy demand for pretreatment, especially dewatering manure [331].

- *Uncertainties incorporation.* Campbell et al. (2018) conducted a comparative TEA for biofuel and biochar production, using two different conversion pathways [33]. They also incorporated the effects of uncertainty and volatility often critical variables. A study involving four scenarios, using different pyrolysis technologies and end-use of products, was performed to calculate carbon emission abatement [332]. Monte Carlo analysis was used to model 16 uncertainty parameters. In another study, techno-economic uncertainties of two pathways for catalytic pyrolysis were assessed [256]. Uncertainty of variables, such as internal rate of return, feedstock price, total project investment, electricity price, biochar yield, and bio-oil yield was evaluated.

- *Biochar from nutrient-rich sources.* Animal manure and poultry litter are sources, containing phosphorus and nitrogen, which are mainly used as a fertilizer and soil conditioner [333,334]. Biochar-based products derived from nutrient-rich organic resources (e.g., manure) have been suggested as sustainable materials for addressing environmental issues, such as nutrient leaching and chemical fertilizer runoff, which lead to eutrophication (oversupply nutrients) in surface waters. It is essential to supply enough nutrients for healthy crop growth and yields, while not polluting the environment. Earlier studies estimated that eutrophication could cause approximately $2 billion per year in the U.S. [335]. These environmental challenges require new solutions and biochar products derived from nutrient-rich organic biomass hold the promise of replacing synthetic fertilizers. Raw manure has high levels of pollutants and pathogens, however, it is a valuable resource given high content of NPK for farming and cropping [333]. In the U.S., manure transportation costs vary and depend on the state. For example, the average management cost is $1.05 per cow per month ($12.6 per cow per year) in California [333], which is over $50,000 annually for a dairy with around 4,000 cows. This amount of manure management cost can be used for building a portable refinery unit that can convert manure to value-added products on-site, subsequently reducing the carbon footprint of manure management operation and livestock GHG emissions (roughly 80 MMT CO_2 eq.) [333].

Table 5.1. A summary of recent biochar studies, focusing on economic and environmental aspects

References	Objectives		Pyrolysis	Uncertainties	Sources	Solution Method	Case Study
	Economic	Environmental					
[296]	✓	✓	✓	×	Coconut	ε-Constraint	✓
[317]	✓	×	✓	×	Rice	LCA	✓
[319]	×	✓	✓	×	Vines	LCA	✓
[321]	✓	×	✓	×	Poultry Litter	TEA	✓
[322]	✓	×	✓	×	Pine	TEA	×
[323]	✓	×	✓	×	Biosolid	TEA	✓
[324]	✓	×	✓	×	Forest	TEA	×
[326]	×	✓	✓	×	Oak residue	LCA	✓
[328]	×	✓	✓	×	Woodchip	LCA	✓
[329]	×	✓	✓	×	Oilseed	LCA	✓
[330]	✓	✓	✓	×	Rice; corn; peanut	TEA, LCA	✓
[331]	×	✓	✓	×	Willow; pig manure	LCA	✓
[33]	✓	×	✓	✓	Forest	TEA, Monte Carlo	✓
[332]	×	✓	✓	✓	Olive husk	LCA, Monte Carlo	✓
[256]	✓	×	✓	✓	Pine pulpwood	TEA, Monte Carlo	×
This study	✓	✓	✓	✓	Cattle manure	TEA, LCA, GA	✓

LCA: life cycle assessment; TEA: techno-economic assessment; GA: genetic algorithm.

The novelty of this study lies in (i) the proposed multi-criteria decision making, including TEA and LCA for sustainable nutrient-rich biochar production from cattle manure, (ii) the proposed stochastic optimization model to incorporate the effects of uncertainty parameters and explore the commercial feasibility of biochar production, and (iii) the presented case study in Twin Falls, Idaho, USA for verifying the proposed methods and models. Additionally, this study contributes to techno-economic and environmental dimensions of biochar production, highlighting the feasible use of portable refinery units to convert cattle manure to biochar near the collection sites and reduce the environmental footprint of dairy manure management. The TEA investigates a mixed conversion pathway for producing nutrient-rich biochar and high yield bio-oil, and a stochastic optimization model to minimize the total cost of biochar production and distribution (i.e., collection, grinding,

drying, conversion, storage, and transportation). The stochastic model has two constraints that investigate the uncertainty of manure moisture and biochar nutrients on the total cost and biochar quality. The environmental assessment evaluates GWP of manure-to-biochar production systems and distribution networks, using the LCA method, including four phases (i.e., goal and scope definition, life cycle inventory, life cycle impact assessment, and interpretation). Finally, a case study in Twin Falls, Idaho, USA investigates the sustainability benefits of the proposed conversion process in regions with a high density of dairy feedlots and demonstrates the applicability of the optimization model in energy and agricultural areas.

5.3 Methods and Materials

The portable refinery unit in this study employs mixed fast and slow pyrolysis reactors to produce nutrient-rich biochar and high-yield bio-oil (Figure 5.1). Pyrolysis oil and gas are fed for heat and electricity production for pretreatment purposes, such as dewatering manure and particle size reduction. Fresh cattle manure generally has a moisture content between 80-90% and is ideally reduced to 50% by composting processes [336,337]. Typically, biomass moisture content should range below 5% in order to produce quality products [338]. Moisture content in the composted manure was assumed to be 50% and was decreased to around 5%, utilizing a Roto-Louvre rotary dryer along with produced bio-oil and syngas as sources of heat. Grinding cost was simulated for a Peterson 5710C horizontal grinder. The required storage facilities and equipment are 0.5 tons (over 1,000 lbs) bulk bags for biochar and a tanker with 50 gallons capacity for bio-oil storage, connected to the refinery unit. Besides, a double-trailer truck is considered for transferring biochar from the production site to storage facilities. The capital and variable costs are estimated using an approach reported in the earlier study [339] and adjusted for inflation to 2019, using the Producer Price Index [340].

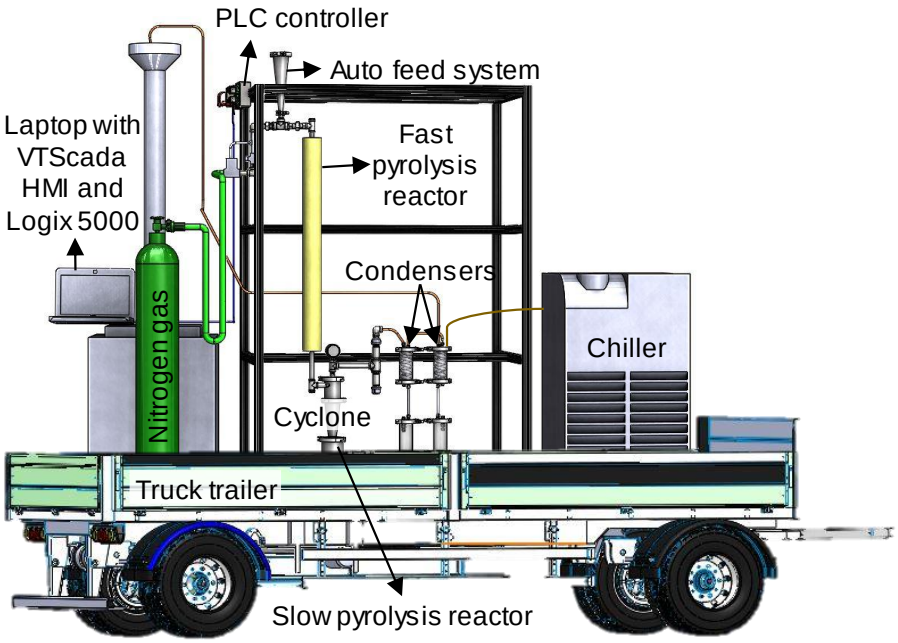

Figure 5.1. Schematic of mixed fast and slow pyrolysis portable refinery unit

The portable refinery unit in this study is a simulated, scaled-up model of our design and built in-house portable refinery, which was used to perform manure pyrolysis experiments to determine relative yield, generate products for physicochemical analysis, and provide a basis for simulation. Pretreatment for the experimental smaller unit was carried out by drying the manure in a laboratory oven, running at a setpoint of 100°C for several hours. Grinding of the dried manure was performed, using an electric coffee grinder. Products produced by the unit were stored in storage vessels connected directly to the setup. The produced biochar samples were analyzed in two analytical laboratories (i.e., Environmental Analytical Laboratory at Brigham Young University, UT and Huffman Hazen Laboratories, CO). For simulation purposes, the pyrolysis reactor was modeled in Aspen HYSYS (a chemical process modeling simulator), using a continuously stirred-tank reactor (CSTR) because of their ability to model kinetic reactions (Figure 5.2). The CSTR was used to simulate the primary decomposition reactions of pyrolysis as well as some of the secondary reactions. Nitrogen was used as an inert gas to control reactor residence time and promote the decomposition of biomass within the reactor. Nitrogen and biomass enter the unit at ambient temperature, and the pyrolysis unit operates between 0-15 psi [16]. The refinery capacity is approximately 50 metric tons of biomass per day. Nitrogen mixes with biomass and pushes it through the pipeline. Mixed inlet streams enter the primary pyrolysis reactor and are heated by the core heater, making sure that biomass reaches 550°C while in the primary reactor [16,20]. Upon entering the primary reactor, biomass decomposes and solid carbonaceous residue (biochar) exits through the bottom stream. The

biochar stream then enters a fixed-bed reactor where it undergoes slow pyrolysis to produce nutrient-rich biochar. The reactor is heated to 350°C, and biochar has a residence time of one hour [341]. The vapor phase exits through the top stream, which enters the secondary reactor. Secondary pyrolysis reactions take place to further break down the products of the primary reactor. From the secondary reactor, products exit to a condenser, bringing down the stream temperature to 21°C and proceeding to be separated into syngas and bio-oil streams. The simulation was used to estimate biochar yield and emissions released as syngas, as well as energy required to heat and cool the material streams. Details on process flow parameters simulated in Aspen HYSYS are provided in Supplementary Materials, Appendix E. The HYSYS simulation was used to simulate a scaled-up version of the small portable refinery unit designed and built in-house, allowing for predictions of biochar yield, unit emissions, and power requirement.

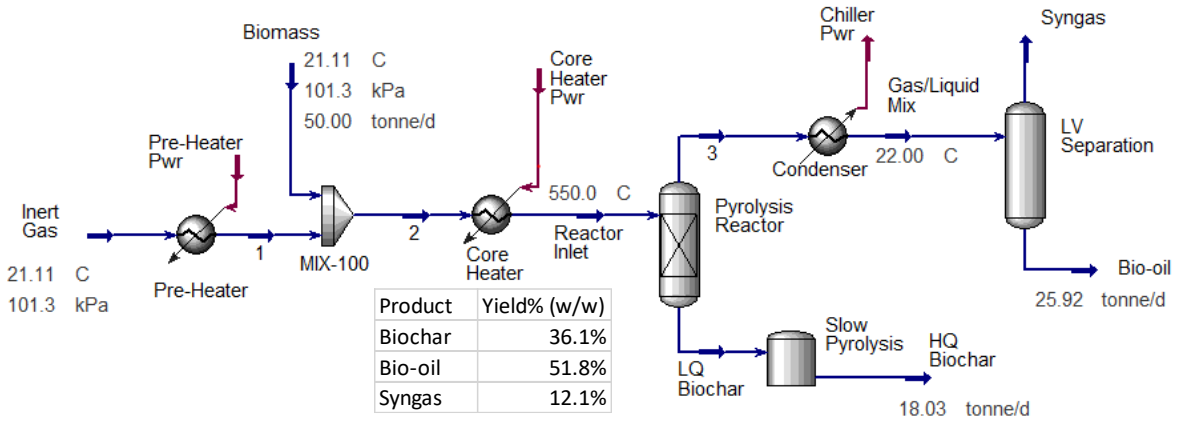

Figure 5.2. Aspen HYSYS simulation of biochar production

The developed evaluation procedure for multi-criteria decision making encompasses two main steps (i.e., techno-economic modeling and environmental impact assessment) to explore manure-based biochar production (Figure 5.3).

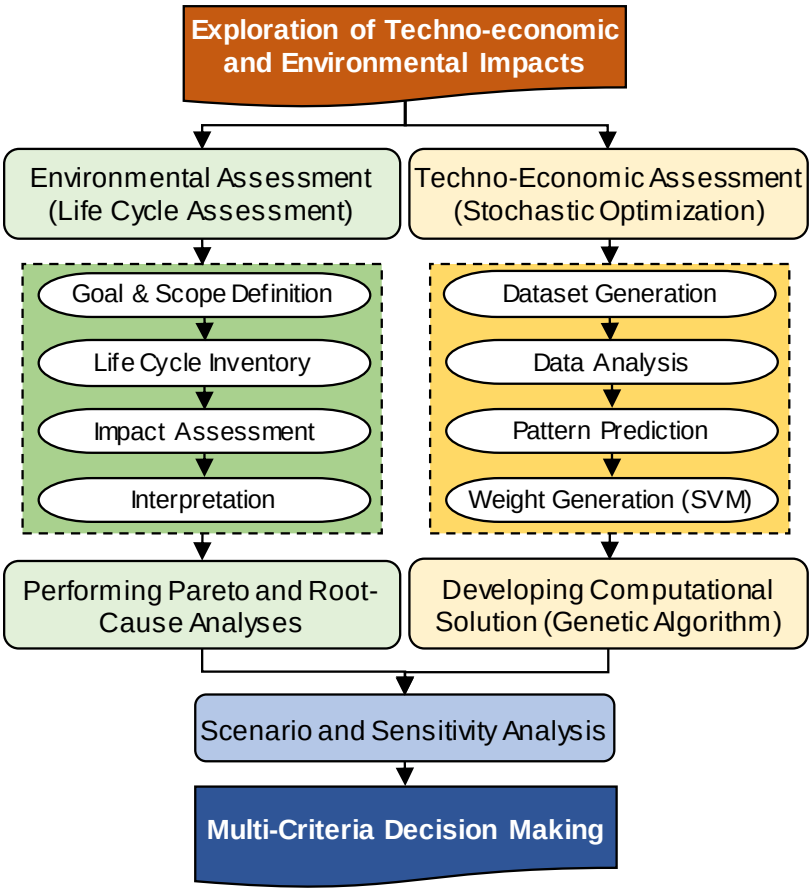

Figure 5.3. Evaluation procedure for multi-criteria decision making.

5.3.1 Techno-Economic Assessment

A stochastic optimization model is formulated to explore the potential for biochar commercialization, using the proposed portable refinery unit. The main operational and capital cost elements of the mathematical model include collection, pretreatment (i.e., grinding and dewatering), refinery or conversion, storage, and distribution costs. The presented model has two stochastic constraints to incorporate the uncertainties and investigate the economic feasibility of nutrient-rich biochar production, using the mixed conversion pathway. The support vector machine (SVM) method is utilized to predict the pattern of uncertainty variables (i.e., biomass and biochar quality), which are highly influential in terms of biochar commercialization and sustainability performance. Based on the data collected using methods detailed below, the stochastic constraints manage uncertainties by considering probability distributions of the defined parameters.

Particularly, biomass quality in this study is determined by manure water content and carbon content (wt%). Manure with high water (H_2O) content is considered as low-quality biomass because it requires more energy for dewatering that subsequently increases the pretreatment cost. Cattle manure

typically has a high water content of around 70-80% and a carbon content around 7-9%. Additionally, biochar quality is determined through pH and nutrient (NPK) content (wt%). In this study, the manure water content before and after drying procedure is measured, using a moisture meter. For produced biochar, carbon content, nutrient content, and pH are measured with standard methods at analytical chemical laboratories. Due to the lack of large datasets for the SVM approach, we randomly generated a dataset, using a uniform distribution within the defined ranges reported in the literature (Table 5.2) for each parameter [342–345].

Table 5.2. Cattle manure and biochar property values **[342–345]**.

Parameters	**Cattle Manure (min-max wt%)**	**Manure-based Biochar (min-max wt%)**
Water content	70-80	< 10
pH	7.4-8.9	8.3-9.5
C	11.2-19.7	61.5-75.2
N	0.8-1.5	1.3-1.8
P	0.003-0.007	0.000-0.002
K	0.008-0.011	0.004-0.013

The developed dataset forms the training and testing datasets (provided in Supplementary Materials, Appendix F) used by the SVM model, including input and output data. The inputs are raw manure water ,carbon content, biochar pH, and carbon and nutrient (N, P, and K) content. The outputs are manure and biochar quality in terms of percentages. Training and testing datasets have 30 and 10 sample values, respectively. These datasets are used to recognize the pattern of uncertainty variables (manure and biochar quality) through the SVM supervised learning algorithm. SVM learning algorithms (i) analyze and classify the data, (ii) predict the pattern of parameters and variables, using regression analysis, and (iii) generate the weight for uncertainty parameters, using the training dataset.

The stochastic optimization model used herein targets the commercial feasibility of biochar production. The objective function (Eq. (1)) aims to minimize the total manure-to-biochar cost over a

specific time horizon. Total cost includes both capital (fixed) and operational (variable and labor) costs. Notations of model parameters and variables are provided in the Nomenclature section.

$$\boldsymbol{Min\ Z} = C_1 + C_2 + C_3 + C_4 + C_5 + C_6 \quad (1)$$

Each of the terms (C_1-C_6) in Eq. (1) is defined in the sequence below. The collection cost (C_1) is calculated (Eq. (1-a)) as follows:

$$C_1 = \sum_a \sum_b \sum_t C_{C-co} \times Z_{abt} + (C_{V-co}) \times \frac{MN_{abt}}{CO_u} \quad (1\text{-a})$$

The grinding cost (C_2) is calculated (Eq. (1-b)) as follows:

$$C_2 = \sum_a \sum_b \sum_t (C_{C-gr} + C_{V-gr}) \times \frac{MN_{abt}}{GR_u} \quad (1\text{-b})$$

The drying cost (C_3) is calculated (Eq. (1-c)) as follows:

$$C_3 = \sum_a \sum_b \sum_t (C_{C-dr} + C_{V-dr}) \times \frac{MN_{abt}}{DR_u} \quad (1\text{-c})$$

The conversion cost (C_4) is calculated (Eq. (1-d)) as follows:

$$C_4 = \sum_a \sum_b \sum_t \left(C_{C-py} + C_{V-py}\right) \times \frac{MN_{abt}}{PY_u} \quad (1\text{-d})$$

The storage cost (C_5) is calculated (Eq. (1-e)) as follows:

$$C_5 = \sum_b \sum_c \sum_t (C_{C-cs} + C_{V-cs}) \times \frac{Char_{bct}}{CS_u} + \sum_b \sum_d \sum_t (C_{C-os} + C_{V-os}) \times \frac{Oil_{bdt}}{OS_u} \quad (1\text{-e})$$

The distribution cost (C_6) is calculated (Eq. (1-f)) as follows:

$$C_6 = \sum_c \sum_e \sum_t (C_{C-tr} + C_{V-tr}) \times \frac{Char_{cet}}{TR_u} \quad (1\text{-f})$$

The model includes several constraints that include capacity, linking-shipping, structure, flow conservation, balance, and uncertainty, as well as non-negativity, binary, and integer constraints. Capacity constraint (Eqs. (2)) ensures that the sum of the flow exiting from all collection sites to each conversion site does not exceed the annual capacity of a conversion refinery unit. Equation 3 presents the annual available amount of processed cattle manure (*AMN*) in each collection area, and the sum of the manure flow in the whole system does not exceed the total amount available annually in the region.

$$\sum_{a\in A} MN_{abt} \le CAP_b \qquad \forall_b \in B, \forall_t \in T \qquad (2)$$

$$\sum_{a\in A}\sum_{b\in B} MN_{abt} \ge AMN_t \qquad \forall_t \in T \qquad (3)$$

Linking-shipping constraint (Eq. (4)) ensures that there are no links between any collection site and conversion site without actual shipments, and there is no shipping between any non-linked collection site and conversion site.

$$MN_{abt} \ge 1 - M(1 - Z_{abt}) \qquad \forall_a \in A, \forall_b \in B, \forall_t \in T \qquad (4)$$

Structure constraint (Eq. (5)) ensures that the sum of the connection links from collection sites to each conversion site does not exceed the maximum limit of selected collection sites.

$$\sum_{a\in A} Z_{abt} \le NCS_t \qquad \forall_b \in B, \forall_t \in T \qquad (5)$$

Flow conservation constraints (Eqs. (6) and (7)) ensure that the sum of the exiting biochar flow from each conversion site to biochar storage sites does not exceed the conversion rate of manure-to-biochar at each conversion site, and the sum of the exiting biochar and bio-oil flow from each conversion site to storage sites does not exceed the flow of manure mass entering each conservation site from all collection sites, respectively. Conversion yield (*CY*) that can be obtained multiplying the average manure quality rate (*MQ*) by the calculated weight, using SVM method.

$$\sum_{c\in C} Char_{bct} \le CY_{char} \times \sum_{a\in A} MN_{abt} \qquad \forall_b \in B, \forall_t \in T \qquad (6)$$

$$\sum_{c\in C} Char_{bct} + \sum_{d\in D} Oil_{bdt} \le \sum_{a\in A} MN_{abt} \qquad \forall_b \in B, \forall_t \in T \qquad (7)$$

Balance constraint (Eq. (8)) ensures that the flow of biochar entering each storage site from all conversion sites is equal to the sum of the exiting biochar flow from this storage site to distribution centers.

$$\sum_{b\in B} Char_{bct} - \sum_{e\in E} Char_{cet} = 0 \qquad \forall_c \in C, \forall_t \in T \qquad (8)$$

Uncertainty constraints (Eqs. (9) and (10)) ensure that quality rate of manure flow entering each conversion site from all collection sites at least meet the average manure quality rate, and quality rate of manure-based biochar at each conversion site at least meet the average biochar quality rate, respectively.

$$\sum_{a\in A}\mu_{abt}\times Z_{abt}+\sqrt[2]{\left(\sum_{a\in A}\sigma_{abt}^{2}\times Z_{abt}\right)}\times\frac{(1-PR)}{\varphi}\leq MQ_t \qquad \forall_b\in B,\ \forall_t\in T\ \ PR\in[0,1] \quad (9)$$

$$\sum_{a\in A}\mu_{abt}\times Z_{abt}+\sqrt[2]{\left(\sum_{a\in A}\sigma_{abt}^{2}\times Z_{abt}\right)}\times\frac{(1-NR)}{\varphi}\leq BQ_t \qquad \forall_b\in B,\forall_t\in T\ \ NR\in[0,1] \quad (10)$$

Other constraints (Eq. (11)-(13)) are non-negative, integer, and binary variables, respectively.

$$MN_{abt}\geq 0 \qquad \forall_a\in A,\forall_b\in B,\forall_t\in T \quad (11)$$

$$Char_{bct}\,, Char_{cet}, and\ Oil_{bdt}\ are\ integers \qquad \forall_b\in B,\forall_c\in C,\forall_d\in D,\forall_e\in E,\forall_t\in T \quad (12)$$

$$Z_{abt}=\{0,1\} \qquad for\ a\forall_a\in A,\forall_b\in B,\forall_t\in T \quad (13)$$

The weight of each uncertainty parameter represents the coordinate where the vector of the SVM model is perpendicular to the hyperplane (or decision surface). We utilized R (version 3.6.2), a programming language for statistical computing and graphics, to determine each uncertainty parameter's weight (Table 5.3). R codes can be found in Supplementary Materials, Appendix H. The failure rates were calculated by comparing the weight determined from the training data with the weight determined from the testing data, which is very low for all parameters. The manure and biochar quality rates (MQ_t and BQ_t) for each refinery site can be estimated, using the defined weight for each parameter. In this study, MQ_t and BQ_t are estimated at 60% and 70%, respectively. Additionally, the manure quality rate (higher rate indicating lower water content and higher carbon content) can help decision makers to select collection sites for better economic and environmental outcomes.

Table 5.3. Calculated weights for uncertainty parameters in training and testing datasets, using SVM technique.

	Carbon	**Moisture**	**Manure Quality Rate**	**pH**	**Carbon**	**Nutrient**	**Biochar Quality Rate**
Training Weight	0.81	3.73	2.18	43.30	3.22	0.05	2.14
Testing Weight	0.89	3.68	2.23	43.60	3.21	0.10	2.15

Due to the complexity of the proposed techno-economic optimization model, we utilized the metaheuristic approach, Genetic Algorithm implemented in MATLAB (version R2017a) to solve the model with 10 collection sites (MATLAB codes are provided in Supplementary Materials, Appendix

H). The applied computer system to solve the model has 32GB RAM, 64-bit OS, Intel Xeon CPU with Windows 10.

5.3.2 Environmental Assessment

An LCA method is applied using OpenLCA, along with information from previous studies to evaluate the environmental impacts of the manure-to-bioproducts life cycle [346–348]. LCA study includes four parts, which are the definition of goal and scope, life cycle inventory analysis, life cycle impact assessment, and interpretation.

Goal and Scope Definition. Environmental and economic impacts of bioenergy production from biomass conversion methods need to be assessed in comparison with the impacts of established fossil energy methods. LCA performed herein evaluates GWP for the manure to value-added products life cycle. GHG emission factors are used to calculate the GWP (in kg CO_2 equivalent) with the key factors being 28 kg CO_2 eq./kg CH_4 and 265 kg CO_2 eq./kg N_2O, which are acquired from the Intergovernmental Panel on Climate Change for a 100-year time horizon [349]. The scope of this study includes four distinct stages that can be categorized into two processes: (i) upstream processes, including raw material (cattle manure) collection, and (ii) midstream processes, involving on-site pretreatment (dewatering and size reduction), on-site converting manure to intermediate products (biochar, bio-oil, and syngas), on-site reusing intermediate products (e.g., bio-oil and syngas) for pretreatment purposes (i.e., heat and electricity), and biochar distribution. This scope considers a cradle-to-gate system boundary (Figure 5.4). The functional unit in this study is one kilogram of biochar, using the identified scope.

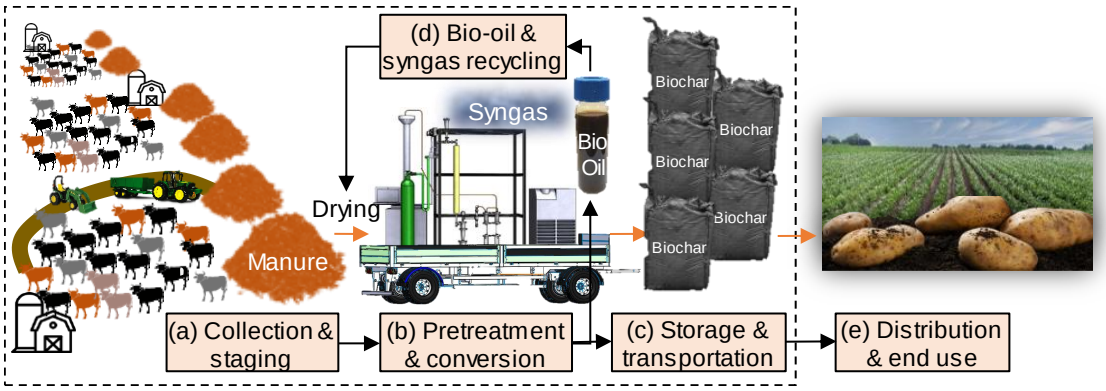

Figure 5.4. The dotted line shows the cradle-to-gate system boundary for the LCA of manure-to-biochar production in this study.

Life Cycle Inventory Analysis. In order to accurately evaluate the manure-based bioproducts production and distribution system, data was obtained from the AGRIBALYSE and OpenLCA databases for the input and output parameters [350]. Equipment used for the upstream collection of raw manure generally includes a forwarder and loader. Input into the dairy farm stage is cattle manure and fossil-based energy and lubricants required by the machinery, and outputs comprise of methane emitted from manure, as well as equipment operation emissions. GHG emission factor for the upstream includes collecting and hauling of manure.

After collection, the midstream processes start by loading manure into an on-site grinder and then into a rotary dryer for biomass pretreatment. Midstream pretreatment inputs are raw cattle manure and diesel fuel, and the outputs are pretreated biomass and GHG emissions, including fuel combustion and water vapor released during biomass drying. GWP is directly affected by manure moisture content and biomass quality. During pretreatment, dry biomass is run through a portable pyrolysis unit, utilizing nitrogen (as an inert gas) and a heat source, powered by electricity. Midstream pyrolysis inputs are pretreated biomass, nitrogen, fuel to produce electricity, and cooling water, while outputs consist of biochar (the focus of this study), bio-oil, and syngas as precursors to the final bioenergy products, as well as emissions. The emissions include biogenic GHGs produced in the conversion of biomass to biochar in addition to the syngas and emissions from fuel combustion. The produced biochar will be transported by a tanker, using diesel fuel to the distribution center. The fuel and its impact depend largely on truck trips and distance between the dairy farm and distribution centers.

Life Cycle Impact Assessment. Impact analysis is performed using data from a case study in the region surrounding Twin Falls, Idaho. The above-described process is converted into a production system using OpenLCA, focusing on biochar-based soil health improvement as the principal product of significance. Life cycle impact assessment was conducted using the CML-IA baseline method, created by the University of Leiden (version 1.5.5). Total upstream emission factors and GWP are calculated, using Eqs. (14) and (15):

$$\eta_{up} = R_{CO2} \times \eta_{up,CO2} + R_{CH4} \times \eta_{up,CH4} + R_{N2O} \times \eta_{up,N2O} \quad (14)$$

$$P_{up} = M_{manure} \times \eta_{up} \quad (15)$$

Midstream emission factors and GWP for biochar production are calculated, using Eqs. (16) and (17):

$$\Pi_{char} = R_{CO2} \times \Pi_{char,CO2} + R_{CH4} \times \Pi_{char,CH4} + R_{N2O} \times \Pi_{char,N2O} \quad (16)$$

$$P_{char} = M_{char} \times \Pi_{char} \quad (17)$$

Biochar transportation emission factors and GWP are calculated, using Eqs. (18) and (19):

$$\Pi_{trans} = R_{CO2} \times \Pi_{trans,CO2} + R_{CH4} \times \Pi_{trans,CH4} + R_{N2O} \times \Pi_{trans,N20} \quad (18)$$

$$P_{trans} = M_{char} \times \Pi_{trans} \times D \quad (19)$$

Interpretation. The major environmental impacts that are concluded in this study comprise of GWP (100 years), photochemical oxidation, and human toxicity. This information will be useful in grasping the environmental impacts of the inputs and outputs of the defined system and, thereby, help determine future efforts in enhancing the system's sustainability benefits. Emissions from the products of the system (e.g., bio-oil and biochar) are considered as biogenic and part of natural processes. The study also looks into each factor and its individual impact on the system as a whole. The largest contributor to GWP is methane emitted from cattle manure, which would decrease when manure is converted to other hydrocarbon compounds, such as high energy density bioproducts. Other GHGs are emitted from the dryer, grinder, pyrolysis unit, and trucks for transportation.

5.4 Case Study

To assess the proposed techno-economic and environmental assessment framework, we conducted a case study in Magic Valley, South of Idaho that has over 1,212,500 cows, and can produce approximately 16 million metric tons of manure per year (Figure 5.5) [351,352]. Idaho is the 3rd largest milk-producing state in the U.S., and dairy is Idaho's top agricultural industry [353,354]. From 2007 to 2017, the average farm size in Idaho has nearly doubled from 663 to 1,240 cows per farm [355].

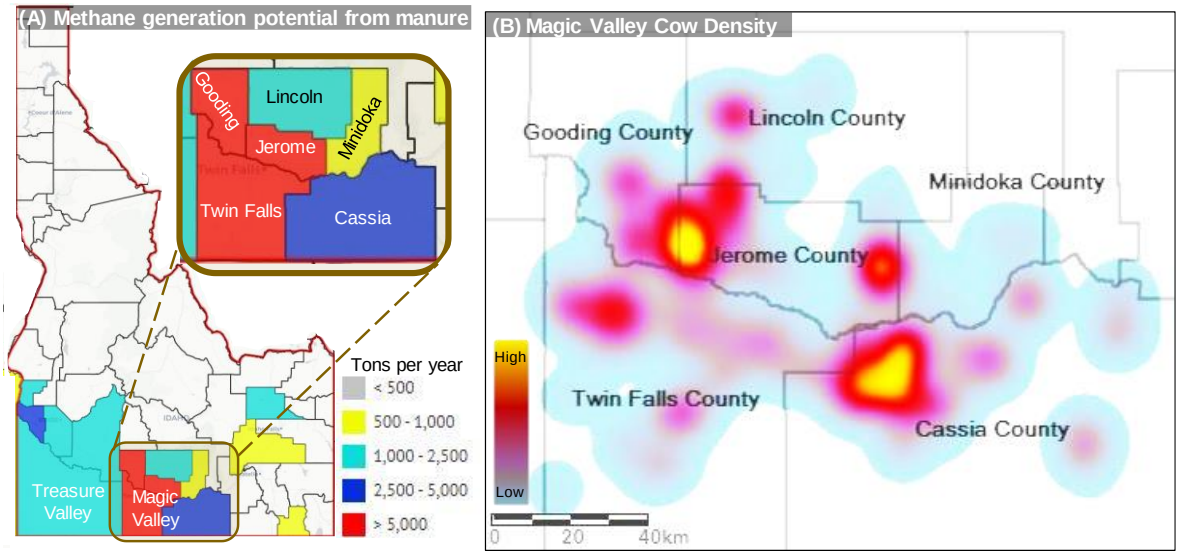

Figure 5.5. (A) Methane generation potential from animal manure (tons per year) in Southern Idaho; (B) six Idaho counties considered in our case study (ArcGIS 2019) – the map uses cool (blue) and warm (yellow and red) colors for low (3k-10k) and high (over 10k) cows, respectively.

The total number of collection sites in this region are over 30 dairies with over 3,000 cows per dairy farm. Actual dairy locations and cow counts data are obtained from ArcGIS and can be found in Supplementary Materials, Appendix G. The main case study considers ten large dairies, located in Lincoln, Gooding, and Cassia counties (Figure 5.5B) that have different cattle types (e.g., dairy and beef farming/ranching cows). The main case study requires different equipment for manure collection, drying, and size reduction, including compact tractor with loader and wagon, grinder, and rotary dryer. Two portable refinery units are used. The portable refinery unit travels to near the feedlots and dry lots to convert raw manure to biochar and bioenergy products, which reduces transportation fuel consumption and logistical costs associated with handling raw, high-moisture-content manure, and mitigates environmental emissions associated with manure storage and land application. Additionally, the following assumptions are made from earlier published studies or reports.

1. The short-term bio-oil storage tanker is considered as part of the refinery unit, and associated costs are included in the refinery operational costs.
2. The loader utilization rate is 60,000 tons per year [356].
3. The grinder utilization rate is 37,500 per year [357].
4. The dryer utilization rate is 37,500 per year [358].
5. The effective lifetime of the portable refinery is assumed for ten years.
6. The portable refinery capacity is 50 dry metric tons of biomass per day.

7. The annual scheduled portable refinery process is 328 for 12 hours per day.
8. Annual available cattle manure is at least 60,000 dry tons at ten large dairies in Magic Valley, Idaho [351,352].
9. The time horizon is one year.
10. Manure was received for free from the diaries in Twin Falls, ID.
11. The type of equipment and facilities are known.
12. The manure has between 70-80 wt% moisture content [337].
13. Conversion process yields for biochar, bio-oil, and syngas are 35%, 45%, and 20%, respectively, using the proposed portable refinery unit.
14. The roundtrip distance from the production site to the storage facility is assumed 100 miles (160 km) (ArcGIS 2019).
15. The manure pretreatment rate (PR) ranges from 5 to 10%, depending on manure moisture content (70-80%) [337].
16. The biochar quality rate (NR) ranges from 5 to 10%, depending on nutrient content (NPK) of biochar (0-2%).
17. The setup and breakdown of the portable refinery unit is a day, and the mileage charge is $1.6 per mile ($1 per km) [356].

The distance between large dairies is defined, using the shortest path, calculated using ArcGIS software. For the main case study, two portable refinery units are deployed for dairies 1-3 (with over 45,000 cows) and dairies 4-10 (with around 70,000 cows), as shown in Figure 5.6. The mean (μ) and variance (σ^2) for stochastic constraints (Eqs. (9) and (10)) in the techno-economic model are calculated for each dairy location, using the simulated datasets. The probability of manure and biochar quality rates (i.e., *PR* and *NR*) and average manure and biochar quality rates (i.e., MQ and BQ) are calculated, using datasets and SVM approach. *PR* and *NR* are probabilities, which are between 0 and 1. Dairy locations that have MQ and BQ below the defined average rate represent sites with low-quality manure or low-quality biochar that will be excluded from the final decision. Decision makers can simplify this setting by reducing the number of dairies and selecting qualified large dairies with a sufficient amount of low-moisture-content manure.

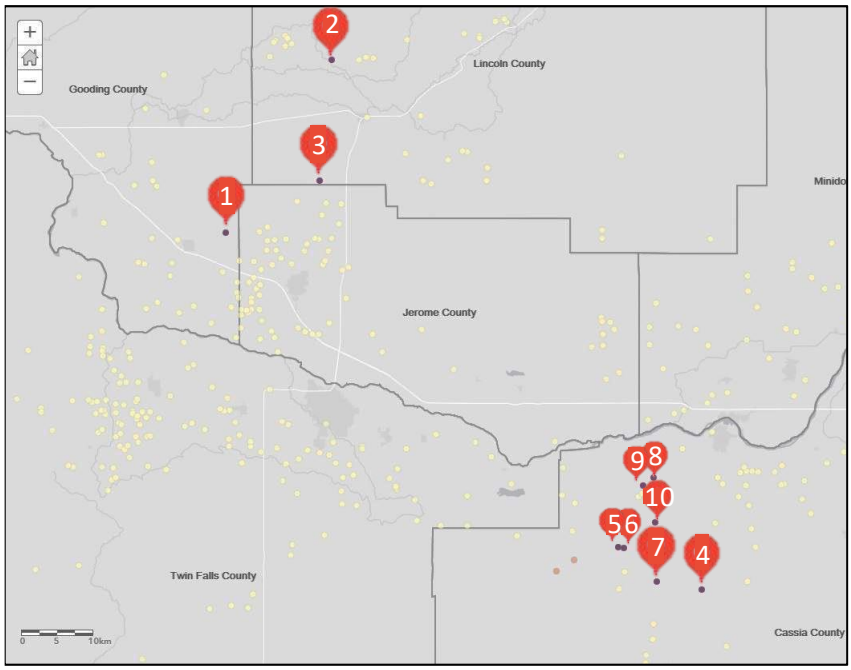

Figure 5.6. Large dairies involved in the main case study with over 10,000 cows in each dairy (ArcGIS 2019)

5.5 Results

According to the International Biochar Initiative (IBI) and European Biochar Certificate (EBC), biochar above 50% carbon content classifies as high quality, and below 50% carbon content classifies as pyrogenic carbonaceous material [359,360]. The elemental analyses performed by two analytical laboratories (i.e., BYU Environmental Analytical Lab and Huffman Hazen) indicate that the carbon content is around 25% and ash content is over 58%, along with nutrients, such as 1.5% nitrogen, 0.4 phosphates, and 1.5% potassium. The main chemical component of ash is carbon, which is produced during incomplete combustion. Based on the IBI and EBC classification, the produced manure-based biochar in this study could be classified as nutrient-rich carbonized biomass or high-quality biochar.

Several studies investigated various feedstocks (e.g., livestock manure, poultry litter, and agriculture residues) and production process parameters (e.g., operation temperature and reactor type) for producing nutrient-rich biochar [361–363]. Atienza-Martinez et al. (2019) assessed various production parameters for producing nutrient-rich biochar from dairy manure [364]. Their results indicate that the properties of biochar mainly depended on pyrolysis process temperature, but the reactor type (e.g., fast or slow pyrolysis) did not have a significant effect. Tsai et al. (2019) performed experiments to produce highly porous, nutrient-rich biochar from dairy manure [365]. They concluded that the produced biochar is a promising soil amendment because of the high porosity and the abundance of nutrients. Lehmann et al. (2015) reviewed biochar nutrient concentrations for

various feedstocks (e.g., agricultural residue, forest residue, and animal manure) and pyrolysis process parameters (e.g., reaction temperature) [361]. They concluded that manure-based biochars have noticeably higher nutrient content (e.g., nitrogen, phosphorous, and potassium) compared to biochar produced from other feedstock types, and pyrolysis process configurations can slightly affect the nutrient content of biochar.

Table 5.4 shows the results of proximate and ultimate analyses, including the properties of raw manure and produced biochar, and compares the empirical and Aspen HYSYS model results for validating the simulated model. Certain physicochemical properties (e.g., nutrient levels) were not able to be determined by the HYSYS simulation and have been left blank.

Table 5.4. Properties of raw manure and produced biochar

	Empirical studies		Aspen HYSYS model	
	Manure	Biochar	Manure	Biochar
Proximate Analysis				
Ash content (% w/w)	15.70	58.87	15.70	42.37
Volatile matter (% w/w)	56.4	26.8	-	-
pH	7.30	7.30	-	-
HHV (BTU/lb)	6455	3362	-	-
Ultimate Analysis				
Fixed carbon (% w/w)	17.30	12.40	17.30	-
Carbon (% w/w)	38.38	23.21	39.38	23.17
Hydrogen (% w/w)	5.17	1.79	5.79	3.70
Nitrogen (% w/w)	2.50	1.51	2.12	0.08
Sulfur (% w/w)	0.45	0.29	-	-
Phosphorous (% w/w)	0.29	0.45	-	-
Potassium (% w/w)	1.41	1.58	-	-
Oxygen (% w/w)	37.80	14.33	37.52	18.91

According to the HYSYS simulation, about 162 MW total energy was required to convert 50 metric tons of manure into biochar. Particularly, 26.57 MW was used for the preheater, 54.61 MW for the pyrolysis reactor, and 80.84 MW for the chiller. The required energy in the case study was provided by reusing intermediate products (e.g., bio-oil and syngas) for pretreatment purposes (i.e., heat and electricity), as well as the combustion of fossil fuels. Biochar nutrient levels for carbon, nitrogen, phosphorous, and potassium in the empirical studies are in line with those found in the literature [361–363].

5.5.1 Techno-economic results

The number of feasible and infeasible computational solution combinations are 2^{10} (1,024). The optimal solution after 500 iterations reports that 32,800 tons of cattle manure in the selected ten dairies would be converted to 11,480 tons of biochar and 14,760 tons of bio-oil (about 3.25 million gallons) over a one-year time horizon. The total cost and unit biochar cost for the main case with two portable refinery units are estimated at $2,722,746 per year and $237 per metric ton, respectively. The total cost and unit biochar cost for a single portable refinery unit are predicted to be $1,576,615 per year and $274 per metric ton, respectively. Table 5.5 presents the capital and operational costs of each point and process. Approximately 80% of the total cost is due to operational cost and 20% due to capital cost. The major operational cost is drying during the pretreatment phase. It is possible to reduce the drying cost if the manure is allowed to dry naturally in the field before mechanical drying or if the other pyrolysis products (e.g., syngas and bio-oil) are combusted to produce drying heat [366,367]. The cost of electricity used was the average retail price of $0.08/kWh as reported in the most recent U.S. Energy Information Administration for the Idaho state electricity profile (2018) [368].

Table 5.5. Detailed capital and operational costs, as well as the annual utilization rate of each process

Point to point[1]	**Process**	**Capital Cost ($/yr)**	**Variable Cost ($/yr)**	**Annual utilization rate (metric ton/yr)**	**Reference**
a to b	Collection	84,996	236,827	60,000	[369,370]
a to b	Grinding	164,044	582,656	37,500	[357]
a to b	Drying	81,337	862,686	37,500	[358]

Table 5.5. continued

a to b	Conversion	228,201	49,536	16,400	[371]
b to c	Char storage	80,798	167,034	11,480	[370]
b to d	Oil storage	182,653	-[2]	14,760	[370]
c to e	Transportation	71,455	285,846	50,000	[356]

[1] Points as shown in Fig. 4. a: Set of collection sites, b: Set of conversion sites, c: Set of biochar storage sites, d: Set of bio-oil storage sites, e: Set of biochar distribution centers; [2] Considered in portable refinery variable cost.

While the cost per metric ton of biochar estimated in this study is lower than in some other biochar economic studies, there is considerable uncertainty and volatility in biochar prices that make the future of the biochar market difficult to predict [33,372]. Until a biochar market price is well established, it is complicated to predict the exact profitability for any biochar production technology.

5.5.2 Environmental assessment results

LCA was performed for the conversion of raw manure into energy, using the portable pyrolysis refinery unit to delve into sustainable approaches across the manure life cycle. The majority of GHG emissions is CO_2 (68% of GHGs) generated from the pyrolysis unit, transportation, and machinery operation (Table 5.6). While the amount of CO_2 is significantly greater than CH_4 and N_2O, the latter two gases have much larger GWP and significant contribution to the overall climate change impact of the process. Looking strictly at the conversion process, the major contributing factors to environmental impact are the combustion of fuels for powering the machinery (e.g., grinder, dryer, and transportation), the water vapor generated while running the manure through the dryer, and syngas emission from the pyrolysis unit.

Table 5.6. Manure-to-bioproducts total pathway emissions for 50 metric tons of manure

Emissions	**Amount**	**Unit**
Water vapor	1.9E+4	kg
Nitrogen	2,950	kg
CO_2	1,333	kg

Table 5.6. continued

CO (biogenic)	1,174	kg
Hydrogen	630	kg
Methane	261	kg
Nitrogen oxides	2.17	kg
CO	0.35	kg
NMVOC	0.20	kg
Particulates < 2.5 um	0.10	kg
Particulates, > 2.5 um < 10um	5.4E-3	kg
N_2O	1.9E-3	kg

NMVOC: non-methane volatile organic compounds.

Table 5.7 shows the environmental impact of processing 50 metric tons of manure per day. Based on this analysis, C footprint, human toxicity, and photochemical oxidation would be the main environmental concerns, which could lead to adverse outcomes, such as climate change, detriment to respiratory health, and crop failure. Aguirre-Villegas et al. (2017) assessed dairy manure management practices in Wisconsin, USA, using LCA and survey data [373]. The results of the study showed GHG emissions per ton of manure range from 34-132 kg CO_2-eq for total manure management practices. GHG emissions from the manure-to-bioproducts pathway generate 172 kg CO_2-eq, having a similar level of impact on GWP as conventional manure management practices.

Table 5.7. Life cycle impact assessment data, using CML baseline

Impact Category	**Result**	**Reference Unit**
Acidification	1.08	kg SO_{-2} eq.
Eutrophication	0.28	kg PO_4 eq.
Freshwater Aquatic Ecotoxicity	0	kg 1,4-dichlorobenzene eq.
Climate Change (GWP 100)	8,642	kg CO_2 eq.

Table 5.7. continued

Human Toxicity	2.68	kg 1,4-dichlorobenzene eq.
Marine Aquatic Ecotoxicity	0	kg 1,4-dichlorobenzene eq.
Ozone Layer Depletion	0	kg CFC-11 eq.
Photochemical Oxidation	1.57	kg C_2H_4 eq.
Terrestrial Ecotoxicity	0	kg 1,4-dichlorobenzene eq.

Pareto analysis was also performed for assessing the environmental impacts of process emissions (Figure 5.7). This analysis presents a comparison of the impacts of each GHG emission on overall GWP. Each emission is converted into kg CO_2 eq. in order to accurately compare the impact. Pareto analysis follows the 80/20 rule, where 20% of the emissions cause 80% of the impact. While not always the case, this assumption and the corresponding analysis is extremely useful when determining potential processes requiring special attention.

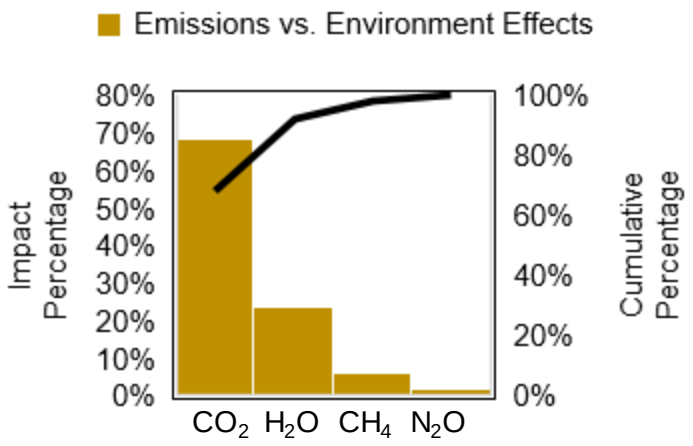

Figure 5.7. Pareto analysis of the impact of each emission on the environment

Analyzing the pretreatment stage shows that the emissions from fuel combustion had little impact compared to the other emissions. Rather, water vapor emitted at the pretreatment stage had the highest environmental impact for drying the raw manure from 50% to <5% moisture content that contributes approximately 80% of total emission-related GWP. While reducing this component is not easy due to the need for drying manure prior to pyrolysis, condensing and coupling water vapor with

other uses, such as on-site energy supply could be an option, although it may be commercially unfavorable. Emission from the pyrolysis stage mostly consists of incondensable gases. These byproducts are known collectively as syngas, which is composed of nitrogen gas with noticeable amounts of carbon monoxide, carbon dioxide, and methane, as well as exiting N_2 gas that serves as an inert gas in the pyrolysis process. Syngas has the potential to be captured and used as a heat or power source, as it is similar to natural gas in terms of composition but with a lower heating value [355].

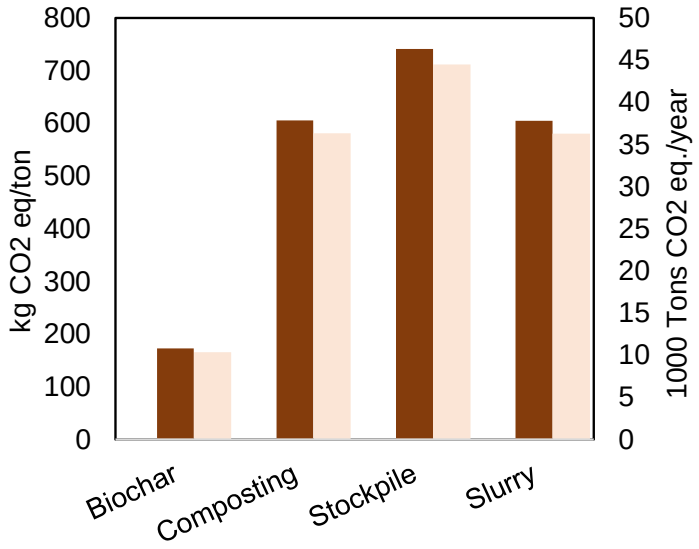

Figure 5.8. Emissions produced from processing one ton of dry manure and emissions per year for the case study area.

According to the case study, 172.8 kg CO_2 eq. is emitted to produce one metric ton of biochar. Figure 5.8 compares the GHG emissions (kg CO_2 eq. per ton and metric ton CO_2 eq. per year) from the proposed biochar production with traditional manure management practices [374]. It is shown that the proposed manure-to-bioproducts conversion produces significantly less emissions than other practices per ton of dry manure. This study does not consider GHG emissions from land application of manure, which has larger N_2O emissions than during manure storage [375]. Therefore, the overall environmental benefits of the proposed manure-to-bioproducts conversion could be even greater than the calculated results of this study. Besides carbon footprint, human toxicity impact of manure-to-bioproducts conversion is estimated as 0.18 kg 1,4-dichlorobenzene eq. for one metric ton of biochar. Methane is the sole contributor to photochemical oxidation impact. Manure can lead to environmental pollution when overapplied on cropland or when discharged to surface water with runoff [376]. Pathogens in manure affect soil and water quality with a consequent risk to human health through the food chain [377]. The manure-to-biochar conversion process is suggested to have minimal

acidification and eutrophication impacts, thus having advantages over conventional manure land application from the water quality perspective. Key contribution to these impacts was the combustion of diesel to run machinery and power transportation. Recycling gas and oil produced during operation to produce heat and power could help in alleviating the impact of GWP, as well as decreasing diesel consumption, subsequently lowering acidification and eutrophication impacts. In the future, more detailed post-processing data of pyrolysis products could be used to further refine environmental assessment results.

5.6 Sensitivity Analysis and Discussion

There are several major parameters that can affect the economic and environmental outcomes of the production process. Sensitivity analysis used herein explores the effect of the associated cost and GHG emission parameters as two major contributors to the economic and environmental performance. Key variables analyzed in this study include the number of portable refinery units and the refinery costs, as well as manure moisture content. Four scenarios are investigated and compared with the main case study, which provides insights into parameter tuning. Additionally, we conducted the cause and effect analysis to examine the key parameters that contribute to manure-to-biochar sustainability. The cause and effect (fishbone) diagram shows the facets of economic, environmental, and safety challenges, as well as the potential causes throughout the manure-to-biochar life cycle (Figure 5.9).

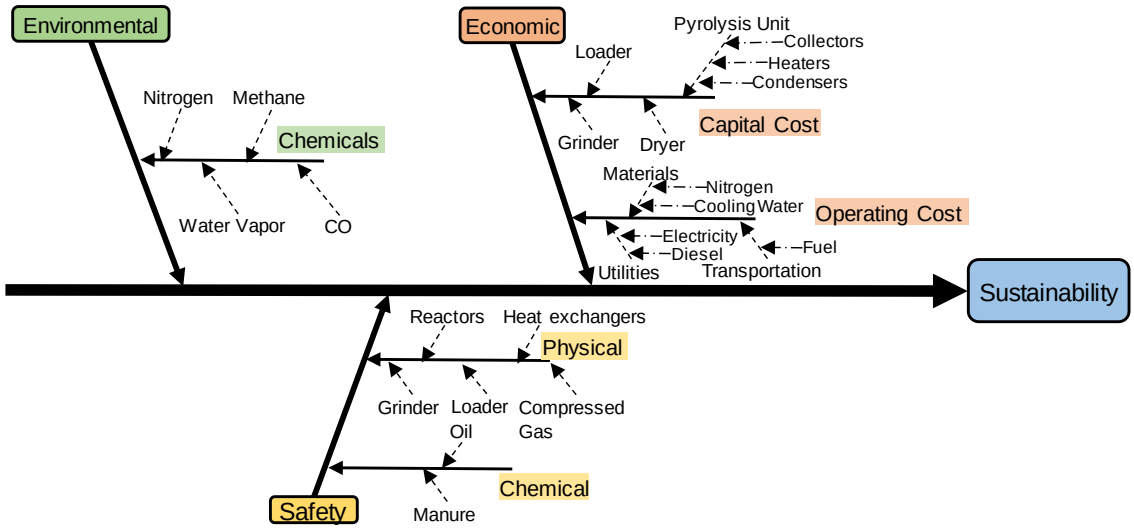

Figure 5.9. Fishbone diagram of process sustainability

5.6.1 Effect of raw manure moisture content

The pretreatment stage (i.e., size reduction and drying) is one of the main commercialization barriers for biochar production. Since the moisture content of raw manure can vary depending on conditions, we investigated the effect of this element on the commercial feasibility of biochar production. Two additional cases were considered, in Case 1, the manure moisture content is 15% less than in the main case study, and in Case 2, the manure moisture content is 15% more than in the main case study. GHG emissions and production costs are found to change monotonically with the moisture content of raw manure (Figure 5.10). Compared to the main case study, Case 1 could decrease GHG emissions by 10 kg CO_2 eq. per metric ton of biochar (1.1%) while Case 2 could increase GHG emissions by 3.3 kg CO_2 eq. per metric ton of biochar (0.3%). The change in the cost would also mirror this trend due to the change in energy (e.g., diesel) required for drying. Compared to the main case study, Case 1 would decrease the biochar production cost by 5%, and Case 2 would increase the cost by ~8% (Table 5.8).

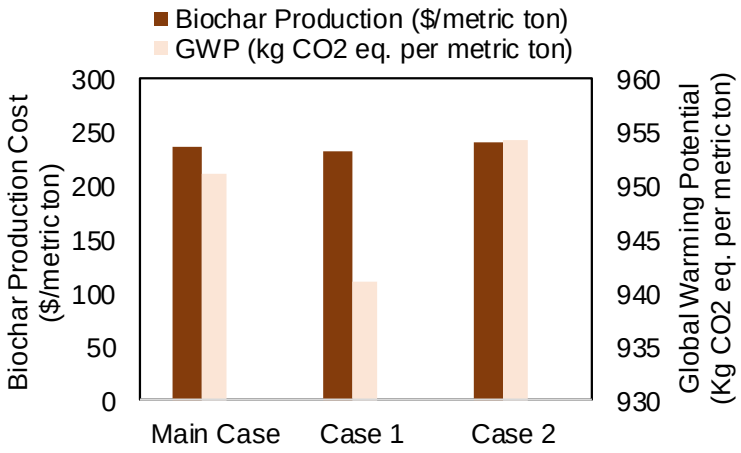

Figure 5.10. Effect of raw manure moisture content on economic and environmental aspects (moisture content of Main Case, Case 1, and Case 2 are 80%, 65%, and 95%, respectively).

Table 5.8. Effect of the moisture content of raw manure on cost and environmental impacts

Cases	Moisture Content (%)	Biochar Production ($/metric ton)	GWP (kg CO2 eq. per metric ton)
Main Case	80	237	951.1
Case 1 (-15%)	65	233	941.1
Case 2 (+15%)	95	242	954.4

5.6.2 Effect of portable refinery units

In the main case, the total amount of manure (1,404,000 metric tons per year or ~3,846 tons per day) is based on the amount available in 10 selected feedlots in the Twin Falls area. This annual manure amount requires the use of multiple refinery units, assuming a processing capacity of 50 metric tons per day for each unit. The number of portable refineries could affect the total annual cost of the collection-processing-distribution network flow and the total annual GHG emissions. This study considered two cases in addition to the main case that employs two refineries. In Case 3, the number of refineries is decreased to one, and in Case 4, the number of refineries is increased to four.

Total biochar production cost is found to change monotonically with the number of portable refineries utilized (Figure 5.11). Compared to the main case study, in Cases 3 and 4, biochar production cost per metric ton could increase by around 16% and decrease by about 8%, respectively (Table 5.9). Optimally, utilizing four portable refineries in Case 4 produces the largest amount of biochar for the lowest cost. While a higher number of refineries would increase environmental impacts of biomass collection, size reduction, and transport per day of operation, it would only slightly increase (0.1%) the environmental impacts per metric ton of biochar. Emissions released during upstream operations have a detrimental effect on environmental performance because these operations mostly rely on energy provided by fossil fuel. GWP 100 could increase by 42 kg CO_2 eq. per metric ton of biochar (4.4%) in Case 3 and decrease by 1.1 kg CO_2 eq. per metric ton of biochar (0.1%) in Case 4, with respect to the main case (Figure 5.11).

Table 5.9. Effect of the number of portable refineries on cost and environmental impact

Cases	**Portable Refineries**	**Biochar Production ($/metric ton)**	**GWP (kg CO_2 eq. per metric ton)**
Main Case	2	237	951.1
Case 3	1	274	993.3
Case 4	4	218	950.0

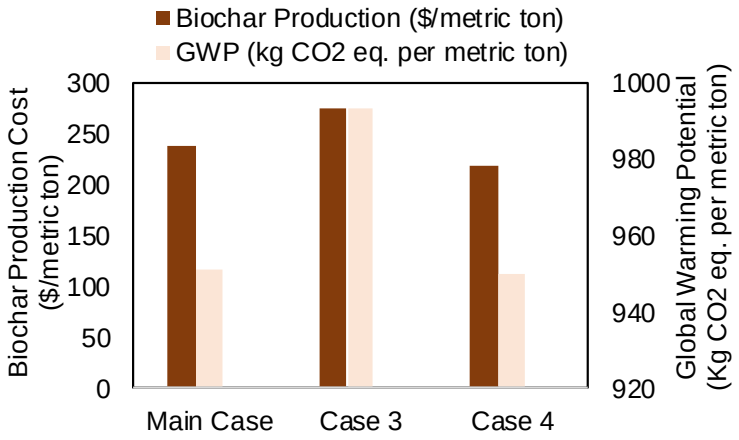

Figure 5.11. Effect of utilized portable refinery units on economic and environmental aspects (number of refineries in Main Case, Case 3, and Case 4 are 2, 1, and 4, respectively).

Due to the high level of uncertainty associated with future prices of biofuel and biochar, market prices of these bioproducts have been reported to have the largest impact on the net present value of main critical variables [33]. According to Laird (2009), the optimal amount of biochar for soil amendment is between 20-25 tons per acre. However, significant improvements to crop growth can be seen with as little as 0.9-2.2 tons per acre [378]. Assuming biochar price points between $231-$283, the soil application cost could be anywhere between $208-$623 per acre [321]. In this study, the resulting unit price for biochar production ($/ton) from cattle manure, using the developed Genetic Algorithm computational solution, indicates a reasonable comparison to the prices reported in recently published studies of operations with similar capacity (Table 5.10). Recycling agricultural organic materials has the potential to address several national priorities (e.g., food security, energy security, water security) and sustainability challenges (e.g., environmental pollution from petroleum-derived products). Besides, using nutrient-rich biomass for biochar production and subsequent soil application is one of the most promising approaches for biomass management and sustainable agriculture as this practice could simultaneously reduce the risk of agricultural runoff-introduced nutrient loading and improve crop growth and yields [312,379].

Table 5.10. Reported biochar production cost in recent studies

Reference	Technology	Capacity (ton/day)	Biomass type	Cost ($/ton)	Year
[322]	Slow Pyrolysis[1]	20,000	Pinewood	220-280	2014
[321]	Fast Pyrolysis/Gasifier	36	Poultry Litter	228-280	2015
[323]	Fast Pyrolysis	6.4	Biosolids	100-400	2019

Table 5.10. continued

[324]	Slow Pyrolysis	12	Forest Residue	1,044	2019
[330]	Fast pyrolysis[2]	2,000	Rice, Corn, Peanut	75-248, 87-250, 680-1,272	2019
[315]	Auger Pyrolysis	151	Wood	474-704	2019
This study	Mixed fast and slow pyrolysis	50	Cattle manure	218-274	2019

[1] Results generated by simulation software; [2] Case study performed in California, Iowa, and Florida, respectively.

It should be noted that biochar-based soil conditioner has many environmental benefits, which are not the focus of the current study (Fig. 4). Future research should extend environmental assessment for the cradle-to-grave system boundary to include biochar-based soil amendment that can facilitate the monetization of environmental benefits and avoided environmental costs, such as soil degradation and water pollution [380].

5.7 Conclusions

Producing biochar from animal manure is a potential approach to address several sustainability challenges, including manure management, inorganic fertilizer overuse, water-nutrient pollution due to agricultural runoff, and integrated crop-livestock farming. In addition, manure-based biochar can promote carbon management systems and GHG emission mitigation efforts. This study focuses on converting cattle manure to value-added products (e.g., biochar and bio-oil), using mixed pyrolysis reactors (i.e., fast and slow pyrolysis). The proposed evaluation procedure for multi-criteria decision making can overcome the existing deficiencies of earlier published studies, which are: (i) inconsistencies in addressing multiple aspects of sustainability (i.e., economic and environmental), (ii) incorporation of uncertainties in biomass supply and pretreatment requirements, and (iii) effective multi-criteria decision support system and computational solution that can facilitate decision making analysis. This study integrates technological aspects of manure-based biochar production with sustainability concepts in order to address commercialization challenges by exploring the economic and environmental feasibility, uncertainty parameters, mixed reactors, and portable conversion process. The results show that the proposed conversion pathway and method can reduce the bioproduct production cost and manure environmental impacts, and enhance sustainability benefits across manure-to-biochar supply chains. This study motivates the need for efficient pretreatment processes and distributed refineries to address the upstream and midstream challenges (e.g.,

collection, transportation, and dewatering) to convert manure-to-biochar near the collection sites. The developed multi-criteria decision making approach utilizes various methods to support and scale up sustainable biochar production. The results can be translated to other regions and countries to mitigate the negative impact of intensive livestock farming while promoting sustainable agriculture. Potential directions for future research include (i) exploration of smart production technology to increase the conversion process yield and reduce the energy used, (ii) exploration of social aspects to investigate the triple bottom line with associated uncertainties, and (iii) exploration of other technologies, system designs, and products to identify the viable commercial pathways and support bioenergy industry.

5.8 Nomenclature

Indices

a	Set of collection sites
b	Set of conversion sites
c	Set of biochar storage sites
co	Collection
cs	Biochar storage
d	Set of bio-oil storage sites
dr	Dryer
e	Set of biochar distribution centers
gr	Grinding
os	Bio-oil storage
py	Pyrolysis
tr	Truck
u	Utilization
t	Set of time

Parameters

AMN_t	Annual available cattle manure (metric ton/yr)
BQ_t	Average biochar quality rate (%)
CAP_b	Annual capacity of a conversion refinery unit (metric ton/yr)
C_{C-co}	Annual capital cost of collection ($/yr)
C_{C-cs}	Annual capital cost of biochar storage ($/yr)
C_{C-dr}	Annual capital cost of drying ($/yr)

C_{C-gr}	Annual capital cost of grinding ($/yr)
C_{C-os}	Annual capital cost of bio-oil storage ($/yr)
C_{C-py}	Annual capital cost of pyrolysis ($/yr)
C_{C-tr}	Annual capital cost of double-trailer truck ($/yr)
CO_u	Annual handling equipment (loader) utilization (metric ton/yr)
CS_u	Annual biochar storage equipment utilization (metric ton/yr)
C_{V-co}	Annual variable cost of collection ($/yr)
C_{V-cs}	Annual variable (labor and operational) cost of biochar storage ($/yr)
C_{V-dr}	Annual variable cost of drying ($/yr)
C_{V-gr}	Annual variable cost of grinding ($/yr)
C_{V-os}	Annual variable cost of bio-oil storage ($/yr)
C_{V-py}	Annual variable cost of pyrolysis ($/yr)
C_{V-tr}	Annual variable cost of double-trailer truck ($/yr)
CY_{char}	Conversion yield (%)
D	Distance (miles)
DR_u	Annual drying equipment utilization (metric ton/yr)
GR_u	Annual grinder utilization (metric ton/yr)
M	A large number
M_{char}	Mass of produced biochar (metric ton)
M_{manure}	Mass of raw manure (metric ton)
MQ_t	Average manure quality rate (%)
NCS_t	Number of selected collection sites
NR	Biochar nutrient content range (%)

OS_u	Annual bio-oil storage equipment utilization
P_{char}	Biochar production GWP (kg CO_2 eq.)
P_{trans}	Biochar transportation GWP (kg CO_2 eq.)
P_{up}	Upstream processes GWP (kg CO_2 eq.)
PR	Manure pre-treatment range, depends on moisture content (%)
PY_u	Annual pyrolysis utilization (metric ton/yr)
RCH4	Emissions rate of CH_4 (kg CO_2 eq./kg CH_4)
RCO2	Emissions rate of CO_2 (kg CO_2 eq./kg CO_2)
RN2O	Emissions rate of N_2O (kg CO_2 eq./kg N_2O)
TR_u	Annual truck utilization (metric ton/yr)
W	SVM weight
η_{char}	GHG emissions factor for biochar production process (kg CO_2 eq. per ton)
$\eta_{char,CH4}$	CH_4 emission factor of biochar production processes (kg CH_4 per ton)
$\eta_{char,CO2}$	CO_2 emission factor of biochar production processes (kg CO_2 per ton)
$\eta_{char,N2O}$	N_2O emission factor of biochar production processes (kg N_2O per ton)
η_{trans}	GHG emissions factor for biochar transportation (kg CO_2 eq. per ton-mile)
$\eta_{trans,CH4}$	CH_4 emission factor of biochar transportation (kg CH_4 per ton-mile)
$\eta_{trans,CO2}$	CO_2 emission factor of biochar transportation (kg CO_2 per ton-mile)
$\eta_{trans,N2O}$	N_2O emission factor of biochar transportation (kg N_2O per ton-mile)
η_{up}	GHG emissions factor for upstream processes (kg CO_2 eq. per ton)
$\eta_{up,CH4}$	CH_4 emission factor of upstream processes (kg CH_4 per ton)
$\eta_{up,CO2}$	CO_2 emission factor of upstream processes (kg CO_2 per ton)
$\eta_{up,N2O}$	N_2O emission factor of upstream processes (kg N_2O per ton)

φ	Phi
μ	Mean value
σ^2	Variance value

Decision Variables

$Char_{bct}$	Integer variable for biochar mass from conversion site *b* to storage site *c* during time period *t* (metric ton)
$Char_{cet}$	Integer variable for biochar mass from storage site *c* to distribution center *e* during time period *t* (metric ton)
MN_{abt}	Continuous variable for manure mass from collection site *a* to conversion site *b* during time period *t* (metric ton)
Oil_{bdt}	Integer variable for bio-oil mass from conversion site *b* to storage site *d* during time period *t* (metric ton)
Z_{abt}	Binary variable for manure from collection site *a* to conversion site *b* during time period *t*

Chapter 6: Conclusions

6.1 Summary

Global demand for energy is projected to increase 15% by 2050, and biomass-derived bioproducts play a crucial role in substituting fossil fuels and mitigating greenhouse gas emissions. Bioproducts from the pyrolysis of biomass feedstocks have shown great potential in addressing challenges across food-energy-water systems. However, due to the nascency of conversion technology, there is a demand for new inventions and cost-reducing approaches to meet market needs.

By performing systematic and critical reviews, the merits and critical challenges were identified relating to thermochemical conversion of lignocellulosic biomass and physicochemical upgrading technologies to produce bio-blendstocks. Bio-oil recovery and upgrading methods were analyzed and assessed for use in a single-step intensified process.

A custom mixed fast and slow pyrolysis process was designed and built to convert a variety of biomass feedstocks into bio-oil and biochar. The resulting bioproducts were characterized using several analytical techniques (e.g., proximate, ultimate, GC-MS, ESI-MS, FTIR, and thermal aging) for the selection of a feedstock that was best suited for further upgrading experiments. Bio-oil from pine displayed excellent thermal stability, process yield, and possessed high content of favorable platform molecules.

Catalytic pyrolysis on pine was then carried out using γ-alumina as the solid acid catalyst of interest. Both in-situ and ex-situ catalyst bed configurations were compared and assessed using the properties of the resulting bio-oil. Addition of γ-alumina successfully decreased acidic compounds while increasing esters in the bio-oil. While in-situ catalysis favored the production of ketones, bio-oil produced from ex-situ catalytic pyrolysis possessed high phenolic content and thermally stable properties. This makes the ex-situ catalytic bed configuration ideal for the next step of development of the pyrolysis reactor.

Effectiveness of methanol as liquid coolant for direct quenching of fast pyrolysis vapors in a custom impinger-type condenser was also assessed using fast pyrolysis. Methanol was able to condense a fraction of bio-oil that exhibited high phenolic content and a noticeable amount of fatty acid methyl ester content. Interactions with methanol also resulted in the most thermally stable bio-oil fractions with the lowest molecular weight. However, there was still a noticeable amount of acidic compounds.

Finally, a study focused on converting cattle manure to enhanced bioproducts using a portable pyrolysis unit was evaluated using multi-criteria decision making. Integration of techno-economic

and sustainability facets for manure-based biochar production attempted to address commercialization challenges by exploring general feasibility and uncertainty parameters.

6.2 Conclusions

The objective of this research was to identify and develop a thermochemical technology pathway for the conversion of biomass to enhanced bioproducts through examining pyrolysis unit configuration and product recovery techniques. Previous studies revealed the need for a single-step, intensified pathway for biomass-to-blendstocks production to compete with existing fossil fuel production. A combination γ-alumina with methanol impingers for fractionation could potentially produce an oil high in phenolics and small chain esters while low in acids. Decoration of γ-alumina with non-noble hdyrodeoxygenating metal catalyst could lead to an inexpensive route for biomass-to-hydrocarbon production. Also, the results of the techno-economic and life cycle assessments show that through the developed multi-criteria decision-making method, the proposed conversion pathway could reduce the bioproduct production cost and environmental impacts of traditional manure management. It was also shown to enhance sustainability benefits across manure-to-biochar supply chains. Ultimately, pyrolysis pathways were identified for cost-effective, environmentally safe bioproduct production.

6.3 Contributions

The novelties within this study contribute insight into advantages and deficiencies in the current pyrolysis unit design, paving the way for further optimization and upscaling. Portable refinery capability combined with a stable liquid product makes possible on-site biomass conversion followed by liquid product transportation to a stationary plant for further required upgrading without significant thermal or chemical degradation. This study:

- Identifies potential directions for future research through both critical and systematic literature reviews, and the proposed intensified process for lignocellulosic-based fuel blendstocks production.
- Incorporates a free-fall pyrolysis reactor design with catalyst bed integration to develop cost-effective ways to produce high-quality, thermally stable bio-oil.
- Promotes the progress of science and domestic bioeconomy through development and application of multi-criteria decision-making to assess bioproduct production costs and impacts.
- Examines pathways to advance national health through cutting carbon pollution from petroleum-based products and mitigate global warming via biomass-based products
- Evaluates ideas that support energy security via renewable energy solutions.

- Elucidates the basic principles that guide the production of stable bio-oil.

6.4 Future Work

This study has shown the stages of development of a mobile pyrolysis unit and the production and evaluation of bioproducts. Intensification through direct quenching and catalyst addition resulted in identification of a potential cost-effective biomass-to-biofuel pathway. On-site conversion was shown to help reduce costs associated with downstream and midstream challenges. In order to better understand and improve the free-fall catalytic fast pyrolysis conversion process, future studies should focus on the following directions:

- Exploration of multi-level chemical fractionation and characterization to simplify and reveal insights into physical, physicochemical, and chemical events caused by the complexity of the interplay among compounds and their root-causes.
- Examination of inexpensive hydrodeoxygenation catalysts in the ex-situ catalytic fast-pyrolysis configuration.
- Investigation on the effect of catalytic loading ratio and physical parameters on pyrolysis liquid product composition and yield.
- Further exploration of direct quenching with varying solvents and their physicochemical effects on the liquid product.
- Investigation of solvent promoting fractionation and reactive distillation integrated with catalytic fast pyrolysis.
- Exploration of social aspects in multi-criteria decision-making to investigate the triple bottom line with associated uncertainties.

References

[1] U.S. EIA, 2019, “Short-Term Energy Outlook - U.S. Energy Information Administration (EIA)” [Online]. Available: https://www.eia.gov/outlooks/steo/. [Accessed: 18-Oct-2018].

[2] “Total Energy Monthly Data - U.S. Energy Information Administration (EIA)” [Online]. Available: https://www.eia.gov/totalenergy/data/monthly/index.php. [Accessed: 11-May-2023].

[3] U.S. EIA, 2021, *Short-Term Energy Outlook*.

[4] Hansen, S., Mirkouei, A., and Diaz, L. A., 2020, “A Comprehensive State-of-Technology Review for Upgrading Bio-Oil to Renewable or Blended Hydrocarbon Fuels,” Renewable and Sustainable Energy Reviews, **118**.

[5] Alizadeh, R., Lund, P. D., and Soltanisehat, L., 2020, “Outlook on Biofuels in Future Studies: A Systematic Literature Review,” Renewable and Sustainable Energy Reviews, **134**, p. 110326.

[6] Hill, J., 2009, “Environmental Costs and Benefits of Transportation Biofuel Production from Food-and Lignocellulose-Based Energy Crops: A Review,” *Sustainable Agriculture*, E. Lichtfouse, M. Navarrete, P. Debaeke, S. Véronique, and C. Alberola, eds., Springer Netherlands, Dordrecht, pp. 125–139.

[7] McKendry, P., 2002, “Energy Production from Biomass (Part 2): Conversion Technologies,” Bioresource technology, **83**(1), pp. 47–54.

[8] U.S. EIA, 2014, *Annual Energy Outlook 2014 with Projections to 2040*, DOE/EIA-0383 (2014), Energy Information Administration, United States Department of Energy, Washington D.C., USA.

[9] Bartle, J. R., and Abadi, A., 2009, “Toward Sustainable Production of Second Generation Bioenergy Feedstocks†,” Energy & Fuels, **24**(1), pp. 2–9.

[10] Mirkouei, A., Haapala, K. R., Sessions, J., and Murthy, G. S., 2017, “A Mixed Biomass-Based Energy Supply Chain for Enhancing Economic and Environmental Sustainability Benefits: A Multi-Criteria Decision Making Framework,” Applied Energy, **206**, pp. 1088–1101.

[11] Mirkouei, A., Mirzaie, P., Haapala, K. R., Sessions, J., and Murthy, G. S., 2016, "Reducing the Cost and Environmental Impact of Integrated Fixed and Mobile Bio-Oil Refinery Supply Chains," Journal of cleaner production, **113**, pp. 495–507.

[12] Iliopoulou, E. F., Triantafyllidis, K. S., and Lappas, A. A., 2019, "Overview of Catalytic Upgrading of Biomass Pyrolysis Vapors toward the Production of Fuels and High-Value Chemicals," WIREs Energy and Environment, **8**(1), p. e322.

[13] Uddin, M. N., Techato, K., Taweekun, J., Rahman, M. M., Rasul, M. G., Mahlia, T. M. I., and Ashrafur, S. M., 2018, "An Overview of Recent Developments in Biomass Pyrolysis Technologies," Energies, **11**(11), p. 3115.

[14] Venderbosch, R. H., 2019, "Fast Pyrolysis," *Thermochemical Processing of Biomass*, John Wiley & Sons, Ltd, pp. 175–206.

[15] OASMAA, A., and Elliott, D. C., 2012, "Process for Stabilizing Fast Pyrolysis Oil, and Stabilized Fast Pyrolysis Oil."

[16] Bridgwater, A. V., 2012, "Review of Fast Pyrolysis of Biomass and Product Upgrading," Biomass and Bioenergy, **38**(Supplement C), pp. 68–94.

[17] Zhang, Q., Chang, J., Wang, T., and Xu, Y., 2007, "Review of Biomass Pyrolysis Oil Properties and Upgrading Research," Energy Conversion and Management, **48**(1), pp. 87–92.

[18] Murugappan, K., Mukarakate, C., Budhi, S., Shetty, M., R. Nimlos, M., and Román-Leshkov, Y., 2016, "Supported Molybdenum Oxides as Effective Catalysts for the Catalytic Fast Pyrolysis of Lignocellulosic Biomass," Green Chemistry, **18**(20), pp. 5548–5557.

[19] Nishu, Liu, R., Rahman, Md. M., Sarker, M., Chai, M., Li, C., and Cai, J., 2020, "A Review on the Catalytic Pyrolysis of Biomass for the Bio-Oil Production with ZSM-5: Focus on Structure," Fuel Processing Technology, **199**, p. 106301.

[20] Dickerson, T., and Soria, J., 2013, "Catalytic Fast Pyrolysis: A Review," Energies, **6**(1), pp. 514–538.

[21] Palla, V. S. K. K., Papadikis, K., and Gu, S., 2015, "Computational Modelling of the Condensation of Fast Pyrolysis Vapours in a Quenching Column. Part A: Hydrodynamics, Heat Transfer and Design Optimisation," Fuel Processing Technology, **131**, pp. 59–68.

[22] Bridgwater, A. V., 2012, “Review of Fast Pyrolysis of Biomass and Product Upgrading,” Biomass and Bioenergy, **38**, pp. 68–94.

[23] Papari, S., and Hawboldt, K., 2018, “A Review on Condensing System for Biomass Pyrolysis Process,” Fuel Processing Technology, **180**, pp. 1–13.

[24] Dufour, A., Girods, P., Masson, E., Normand, S., Rogaume, Y., and Zoulalian, A., 2007, “Comparison of Two Methods of Measuring Wood Pyrolysis Tar,” Journal of Chromatography A, **1164**(1), pp. 240–247.

[25] Oasmaa, A., Kuoppala, E., Selin, J.-F., Gust, S., and Solantausta, Y., 2004, “Fast Pyrolysis of Forestry Residue and Pine. 4. Improvement of the Product Quality by Solvent Addition,” Energy Fuels, **18**(5), pp. 1578–1583.

[26] Wenting, F., Ronghou, L., Weiqi, Z., Yuanfei, M., and Renzhan, Y., 2014, “Influence of Methanol Additive on Bio-Oil Stability,” International Journal of Agricultural and Biological Engineering, **7**(3), pp. 83–92.

[27] Van de Velden, M., Baeyens, J., and Boukis, I., 2008, “Modeling CFB Biomass Pyrolysis Reactors,” Biomass and Bioenergy, **32**(2), pp. 128–139.

[28] Bare, R., Struhs, E., Mirkouei, A., Overturf, K., and Small, B., 2023, “Engineered Biomaterials for Reducing Phosphorus and Nitrogen Levels from Downstream Water of Aquaculture Facilities,” Processes.

[29] Lawrinenko, M., Laird, D. A., and van Leeuwen, J. H., 2017, “Sustainable Pyrolytic Production of Zerovalent Iron,” ACS Sustainable Chem. Eng., **5**(1), pp. 767–773.

[30] Gupta, S., and Kua, H. W., 2017, “Factors Determining the Potential of Biochar As a Carbon Capturing and Sequestering Construction Material: Critical Review,” Journal of Materials in Civil Engineering, **29**(9), p. 04017086.

[31] Mirkouei, A., and Kardel, K., 2017, “Enhance Sustainability Benefits Through Scaling-up Bioenergy Production from Terrestrial and Algae Feedstocks,” *Proceedings of the 2017 ASME IDETC/CIE: 22nd Design for Manufacturing and the Life Cycle Conference*.

[32] Mirkouei, A., 2016, “Techno-Economic Optimization and Environmental Impact Analysis for a Mixed-Mode Upstream and Midstream Forest Biomass to Bio-Products Supply Chain,” Oregon State University.

[33] Campbell, R. M., Anderson, N. M., Daugaard, D. E., and Naughton, H. T., 2018, "Financial Viability of Biofuel and Biochar Production from Forest Biomass in the Face of Market Price Volatility and Uncertainty," Applied Energy, **230**, pp. 330–343.

[34] BP, 2020, *Statistical Review of World Energy*, London, UK.

[35] Azar, C., and Lindgren, K., 2003, "Global Energy Scenarios Meeting Stringent CO_2 Constraints— Cost-Effective Fuel Choices in the Transportation Sector," Energy Policy, p. 16.

[36] Castillo-Villar, K. K., 2014, "Metaheuristic Algorithms Applied to Bioenergy Supply Chain Problems: Theory, Review, Challenges, and Future," Energies, **7**(11), pp. 7640–7672.

[37] U.S. DOE, 2012, *Advanced Biofuels Cost of Production*.

[38] Brown, T. R., and Brown, R. C., 2013, "A Review of Cellulosic Biofuel Commercial-Scale Projects in the United States," Biofuels, Bioproducts and Biorefining, **7**(3), pp. 235–245.

[39] Xiu, S., and Shahbazi, A., 2012, "Bio-Oil Production and Upgrading Research: A Review," Renewable and Sustainable Energy Reviews, **16**(7), pp. 4406–4414.

[40] Czernik, S., and Bridgwater, A. V., 2004, "Overview of Applications of Biomass Fast Pyrolysis Oil," Energy Fuels, **18**(2), pp. 590–598.

[41] Carpenter, D., Westover, T. L., Czernik, S., and Jablonski, W., 2014, "Biomass Feedstocks for Renewable Fuel Production: A Review of the Impacts of Feedstock and Pretreatment on the Yield and Product Distribution of Fast Pyrolysis Bio-Oils and Vapors," Green Chemistry, **16**(2), pp. 384–406.

[42] Chen, W.-H., Lin, B.-J., Huang, M.-Y., and Chang, J.-S., 2015, "Thermochemical Conversion of Microalgal Biomass into Biofuels: A Review," Bioresource technology, **184**, pp. 314–327.

[43] Lehto, J., Oasmaa, A., Solantausta, Y., Kytö, M., and Chiaramonti, D., 2014, "Review of Fuel Oil Quality and Combustion of Fast Pyrolysis Bio-Oils from Lignocellulosic Biomass," Applied Energy, **116**, pp. 178–190.

[44] Zhang, L., Liu, R., Yin, R., and Mei, Y., 2013, "Upgrading of Bio-Oil from Biomass Fast Pyrolysis in China: A Review," Renewable and Sustainable Energy Reviews, **24**, pp. 66–72.

[45] Gilkey, M. J., and Xu, B., 2016, "Heterogeneous Catalytic Transfer Hydrogenation as an Effective Pathway in Biomass Upgrading," ACS Catal., **6**(3), pp. 1420–1436.

[46] Luo, J., Fang, Z., and Smith, R. L., 2014, "Ultrasound-Enhanced Conversion of Biomass to Biofuels," Progress in Energy and Combustion Science, **41**, pp. 56–93.

[47] Bussemaker, M. J., and Zhang, D., 2013, "Effect of Ultrasound on Lignocellulosic Biomass as a Pretreatment for Biorefinery and Biofuel Applications," Ind. Eng. Chem. Res., **52**(10), pp. 3563–3580.

[48] Hu, L., Lin, L., and Liu, S., 2014, "Chemoselective Hydrogenation of Biomass-Derived 5-Hydroxymethylfurfural into the Liquid Biofuel 2,5-Dimethylfuran," Ind. Eng. Chem. Res., **53**(24), pp. 9969–9978.

[49] Gallezot, P., 2008, "Catalytic Conversion of Biomass: Challenges and Issues," ChemSusChem, **1**(8–9), pp. 734–737.

[50] Xiao, X., Chen, B., Chen, Z., Zhu, L., and Schnoor, J. L., 2018, "Insight into Multiple and Multilevel Structures of Biochars and Their Potential Environmental Applications: A Critical Review," Environ. Sci. Technol., **52**(9), pp. 5027–5047.

[51] Venderbosch, R. H., Prins, W., and others, 2010, "Fast Pyrolysis Technology Development," Biofuels, bioproducts & biorefining, **4**(2), p. 178.

[52] Fan, L., Zhang, Y., Liu, S., Zhou, N., Chen, P., Cheng, Y., Addy, M., Lu, Q., Omar, M. M., Liu, Y., Wang, Y., Dai, L., Anderson, E., Peng, P., Lei, H., and Ruan, R., 2017, "Bio-Oil from Fast Pyrolysis of Lignin: Effects of Process and Upgrading Parameters," Bioresource Technology, **241**, pp. 1118–1126.

[53] Ramirez-Corredores, M. M., 2013, "Chapter 6 - Pathways and Mechanisms of Fast Pyrolysis: Impact on Catalyst Research," *The Role of Catalysis for the Sustainable Production of Bio-Fuels and Bio-Chemicals*, K.S. Triantafyllidis, A.A. Lappas, and M. Stöcker, eds., Elsevier, Amsterdam, pp. 161–216.

[54] Zhou, X., Li, W., Mabon, R., and Broadbelt, L. J., 2018, "A Mechanistic Model of Fast Pyrolysis of Hemicellulose," Energy & Environmental Science, **11**(5), pp. 1240–1260.

[55] Suriapparao, D. V., and Vinu, R., 2018, "Effects of Biomass Particle Size on Slow Pyrolysis Kinetics and Fast Pyrolysis Product Distribution," Waste Biomass Valor, **9**(3), pp. 465–477.

[56] Struhs, E., Mirkouei, A., You, Y., and Mohajeri, A., 2020, "Techno-Economic and Environmental Assessments for Nutrient-Rich Biochar Production from Cattle Manure: A Case Study in Idaho, USA," Applied Energy, **279**, p. 115782.

[57] Khosravanipour Mostafazadeh, A., Solomatnikova, O., Drogui, P., and Tyagi, R. D., 2018, "A Review of Recent Research and Developments in Fast Pyrolysis and Bio-Oil Upgrading," Biomass Conv. Bioref., **8**(3), pp. 739–773.

[58] Sharifzadeh, M., Sadeqzadeh, M., Guo, M., Borhani, T. N., Murthy Konda, N. V. S. N., Garcia, M. C., Wang, L., Hallett, J., and Shah, N., 2019, "The Multi-Scale Challenges of Biomass Fast Pyrolysis and Bio-Oil Upgrading: Review of the State of Art and Future Research Directions," Progress in Energy and Combustion Science, **71**, pp. 1–80.

[59] Imran, A., Bramer, E. A., Seshan, K., and Brem, G., 2018, "An Overview of Catalysts in Biomass Pyrolysis for Production of Biofuels."

[60] Brown, T. R., Thilakaratne, R., Brown, R. C., and Hu, G., 2013, "Techno-Economic Analysis of Biomass to Transportation Fuels and Electricity via Fast Pyrolysis and Hydroprocessing," Fuel, **106**, pp. 463–469.

[61] Zhang, H., Xiao, R., Huang, H., and Xiao, G., 2009, "Comparison of Non-Catalytic and Catalytic Fast Pyrolysis of Corncob in a Fluidized Bed Reactor," Bioresource Technology, **100**(3), pp. 1428–1434.

[62] Ciesielski, P. N., Pecha, M. B., Bharadwaj, V. S., Mukarakate, C., Leong, G. J., Kappes, B., Crowley, M. F., Kim, S., Foust, T. D., and Nimlos, M. R., 2018, "Advancing Catalytic Fast Pyrolysis through Integrated Multiscale Modeling and Experimentation: Challenges, Progress, and Perspectives," WIREs Energy and Environment, **7**(4), p. e297.

[63] Chen, X., Chen, Y., Yang, H., Wang, X., Che, Q., Chen, W., and Chen, H., 2019, "Catalytic Fast Pyrolysis of Biomass: Selective Deoxygenation to Balance the Quality and Yield of Bio-Oil," Bioresource technology, **273**, pp. 153–158.

[64] Dutta, A., Schaidle, J. A., Humbird, D., Baddour, F. G., and Sahir, A., 2016, "Conceptual Process Design and Techno-Economic Assessment of Ex Situ Catalytic Fast Pyrolysis of Biomass: A Fixed Bed Reactor Implementation Scenario for Future Feasibility," Top Catal, **59**(1), pp. 2–18.

[65] Ray, A. E., Williams, C. L., Hoover, A. N., Li, C., Sale, K. L., Emerson, R. M., Klinger, J., Oksen, E., Narani, A., Yan, J., Beavers, C. M., Tanjore, D., Yunes, M., Bose, E., Leal, J. H., Bowen, J. L., Wolfrum, E. J., Resch, M. G., Semelsberger, T. A., and Donohoe, B. S., 2020,

"Multiscale Characterization of Lignocellulosic Biomass Variability and Its Implications to Preprocessing and Conversion: A Case Study for Corn Stover," ACS Sustainable Chem. Eng., **8**(8), pp. 3218–3230.

[66] Elliott, D. C., Biller, P., Ross, A. B., Schmidt, A. J., and Jones, S. B., 2015, "Hydrothermal Liquefaction of Biomass: Developments from Batch to Continuous Process," Bioresource Technology, **178**, pp. 147–156.

[67] Özdenkçi, K., De Blasio, C., Muddassar, H. R., Melin, K., Oinas, P., Koskinen, J., Sarwar, G., and Järvinen, M., "A Novel Biorefinery Integration Concept for Lignocellulosic Biomass," Energy Conversion and Management.

[68] Xu, D., Lin, G., Guo, S., Wang, S., Guo, Y., and Jing, Z., 2018, "Catalytic Hydrothermal Liquefaction of Algae and Upgrading of Biocrude: A Critical Review," Renewable and Sustainable Energy Reviews, **97**, pp. 103–118.

[69] Shuping, Z., Yulong, W., Mingde, Y., Kaleem, I., Chun, L., and Tong, J., 2010, "Production and Characterization of Bio-Oil from Hydrothermal Liquefaction of Microalgae Dunaliella Tertiolecta Cake," Energy, **35**(12), pp. 5406–5411.

[70] Biller, P., and Ross, A. B., 2011, "Potential Yields and Properties of Oil from the Hydrothermal Liquefaction of Microalgae with Different Biochemical Content," Bioresource Technology, **102**(1), pp. 215–225.

[71] Valdez, P. J., Nelson, M. C., Wang, H. Y., Lin, X. N., and Savage, P. E., 2012, "Hydrothermal Liquefaction of Nannochloropsis Sp.: Systematic Study of Process Variables and Analysis of the Product Fractions," Biomass and Bioenergy, **46**, pp. 317–331.

[72] Duan, P., and Savage, P. E., 2011, "Hydrothermal Liquefaction of a Microalga with Heterogeneous Catalysts," Ind. Eng. Chem. Res., **50**(1), pp. 52–61.

[73] Toor, S. S., Rosendahl, L., and Rudolf, A., 2011, "Hydrothermal Liquefaction of Biomass: A Review of Subcritical Water Technologies," Energy, **36**(5), pp. 2328–2342.

[74] Gollakota, A. R. K., Kishore, N., and Gu, S., 2018, "A Review on Hydrothermal Liquefaction of Biomass," Renewable and Sustainable Energy Reviews, **81**, pp. 1378–1392.

[75] Ponnusamy, V. K., Nagappan, S., Bhosale, R. R., Lay, C.-H., Duc Nguyen, D., Pugazhendhi, A., Chang, S. W., and Kumar, G., 2020, "Review on Sustainable Production of Biochar

through Hydrothermal Liquefaction: Physico-Chemical Properties and Applications," Bioresource Technology, **310**, p. 123414.

[76] Pandey, A., Larroche, C., Gnansounou, E., Khanal, S. K., Dussap, C.-G., and Ricke, S., 2019, *Biomass, Biofuels, Biochemicals: Biofuels: Alternative Feedstocks and Conversion Processes for the Production of Liquid and Gaseous Biofuels*, Academic Press.

[77] Rajvanshi, A. K., 1986, "Biomass Gasification," Alternative energy in agriculture, **2**(4), pp. 82–102.

[78] Tijmensen, M. J. A., Faaij, A. P. C., Hamelinck, C. N., and van Hardeveld, M. R. M., 2002, "Exploration of the Possibilities for Production of Fischer Tropsch Liquids and Power via Biomass Gasification," Biomass and Bioenergy, **23**(2), pp. 129–152.

[79] Xu, C., Chen, S., Soomro, A., Sun, Z., and Xiang, W., 2018, "Hydrogen Rich Syngas Production from Biomass Gasification Using Synthesized Fe/CaO Active Catalysts," Journal of the Energy Institute, **91**(6), pp. 805–816.

[80] Chiodini, A., Bua, L., Carnelli, L., Zwart, R., Vreugdenhil, B., and Vocciante, M., 2017, "Enhancements in Biomass-to-Liquid Processes: Gasification Aiming at High Hydrogen/Carbon Monoxide Ratios for Direct Fischer-Tropsch Synthesis Applications," Biomass and Bioenergy, **106**, pp. 104–114.

[81] Rafati, M., Wang, L., Dayton, D. C., Schimmel, K., Kabadi, V., and Shahbazi, A., 2017, "Techno-Economic Analysis of Production of Fischer-Tropsch Liquids via Biomass Gasification: The Effects of Fischer-Tropsch Catalysts and Natural Gas Co-Feeding," Energy Conversion and Management, **133**, pp. 153–166.

[82] Santos, R. G. dos, and Alencar, A. C., 2020, "Biomass-Derived Syngas Production via Gasification Process and Its Catalytic Conversion into Fuels by Fischer Tropsch Synthesis: A Review," International Journal of Hydrogen Energy, **45**(36), pp. 18114–18132.

[83] Molino, A., Larocca, V., Chianese, S., and Musmarra, D., 2018, "Biofuels Production by Biomass Gasification: A Review," Energies, **11**(4), p. 811.

[84] Asadullah, M., Ab Rasid, N. S., Kadir, S. A. S. A., and Azdarpour, A., 2013, "Production and Detailed Characterization of Bio-Oil from Fast Pyrolysis of Palm Kernel Shell," Biomass and Bioenergy, **59**, pp. 316–324.

[85] Shemfe, M. B., Gu, S., and Ranganathan, P., 2015, "Techno-Economic Performance Analysis of Biofuel Production and Miniature Electric Power Generation from Biomass Fast Pyrolysis and Bio-Oil Upgrading," Fuel, **143**, pp. 361–372.

[86] Wilkomirsky, I., Moreno, E., and Berg, A., 2014, "Bio-Oil Production from Biomass by Flash Pyrolysis in a Three-Stage Fluidized Bed Reactors System," Journal of Materials Science and Chemical Engineering, **02**(02), pp. 6–10.

[87] Daugaard, D. E., Jones, S. T., Dalluge, D. L., and Brown, R. C., 2015, "Selective Temperature Quench and Electrostatic Recovery of Bio-Oil Fractions."

[88] Abdullah, N., and Gerhauser, H., 2008, "Bio-Oil Derived from Empty Fruit Bunches," Fuel, **87**(12), pp. 2606–2613.

[89] Kulprathipanja, S., Palmas, P., and Myers, D. N., 2016, "Heat Removal and Recovery in Biomass Pyrolysis."

[90] Robinson, N. M., 2000, "Design, Modeling and Construction of a Novel Ablative Fast Pyrolysis Reactor and Product Collection System," PhD Thesis, Aston University.

[91] Park, H. C., Choi, H. S., and Lee, J. E., 2016, "Heat Transfer of Bio-Oil in a Direct Contact Heat Exchanger during Condensation," Korean J. Chem. Eng., **33**(4), pp. 1159–1169.

[92] Dalluge, D. L., Whitmer, L. E., Polin, J. P., Choi, Y. S., Shanks, B. H., and Brown, R. C., 2019, "Comparison of Direct and Indirect Contact Heat Exchange to Improve Recovery of Bio-Oil," Applied Energy, **251**, p. 113346.

[93] Brothier, M., Turchet, J.-P., and Estubier, P., 2009, "Device for Purification of a Gas Flow Containing Condensable Vapours."

[94] Berruti, F. M., Lenkiewicz, K., Xu, R., Bedmutha, R. J., Nova, S., Berruti, F., and Briens, C., 2007, "Novel Fluid Bed Pilot Plant for the Production of Bio-Oil from Biomass through Fast Pyrolysis," Récents Progrès en Génie des Procédés, **94**, pp. 1–8.

[95] Teixeira, A. R., Mooney, K. G., Kruger, J. S., Williams, C. L., Suszynski, W. J., Schmidt, L. D., Schmidt, D. P., and Dauenhauer, P. J., 2011, "Aerosol Generation by Reactive Boiling Ejection of Molten Cellulose," Energy Environ. Sci., **4**(10), pp. 4306–4321.

[96] Licht, W., 1988, *Air Pollution Control Engineering: Basic Calculations for Particulate Collection, Second Edition*, CRC Press.

[97] Bologa, A. M., Paur, H.-, Seifert, H., and Wascher, T., 2005, "Pilot-Plant Testing of a Novel Electrostatic Collector for Submicrometer Particles," IEEE Transactions on Industry Applications, **41**(4), pp. 882–890.

[98] Huang, S.-H., and Chen, C.-C., 2001, "Filtration Characteristics of a Miniature Electrostatic Precipitator," Aerosol Science and Technology, **35**(4), pp. 792–804.

[99] Bedmutha, R. J., Ferrante, L., Briens, C., Berruti, F., and Inculet, I., 2009, "Single and Two-Stage Electrostatic Demisters for Biomass Pyrolysis Application," Chemical Engineering and Processing: Process Intensification, **48**(6), pp. 1112–1120.

[100] Tumbalam Gooty, A., Li, D., Briens, C., and Berruti, F., 2014, "Fractional Condensation of Bio-Oil Vapors Produced from Birch Bark Pyrolysis," Separation and Purification Technology, **124**, pp. 81–88.

[101] Awad, M. B., and Castle, G. S. P., 1975, "Ozone Generation in an Electrostatic Precipitator With a Heated Corona Wire," Journal of the Air Pollution Control Association, **25**(4), pp. 369–374.

[102] Mizuno, A., 2000, "Electrostatic Precipitation," IEEE Transactions on Dielectrics and Electrical Insulation, **7**(5), pp. 615–624.

[103] Jaworek, A., Krupa, A., and Czech, T., 2007, "Modern Electrostatic Devices and Methods for Exhaust Gas Cleaning: A Brief Review," Journal of Electrostatics, **65**(3), pp. 133–155.

[104] Weitkamp, J., and Puppe, L., 2013, *Catalysis and Zeolites: Fundamentals and Applications*, Springer Science & Business Media.

[105] Vasalos, I. A., Lappas, A., Iatridis, D., and Voutetakis, S., 1996, "Design Construction and Experimental Results of a Circulating Fluid Bed FCC Pilot Plant," *IV CFB Congress*.

[106] David, E., 2020, "Evaluation of Hydrogen Yield Evolution in Gaseous Fraction and Biochar Structure Resulting from Walnut Shells Pyrolysis," Energies, **13**(23), p. 6359.

[107] Antonakou, E. V., Dimitropoulos, V. S., and Lappas, A. A., 2006, "Production and Characterization of Bio-Oil from Catalytic Biomass Pyrolysis," Thermal Science, **10**(3), pp. 151–160.

[108] Guo, X., Wang, S., Guo, Z., Liu, Q., Luo, Z., and Cen, K., 2010, "Pyrolysis Characteristics of Bio-Oil Fractions Separated by Molecular Distillation," Applied Energy, **87**(9), pp. 2892–2898.

[109] Pinheiro Pires, A. P., Arauzo, J., Fonts, I., Domine, M. E., Fernández Arroyo, A., Garcia-Perez, M. E., Montoya, J., Chejne, F., Pfromm, P., and Garcia-Perez, M., 2019, "Challenges and Opportunities for Bio-Oil Refining: A Review," Energy & Fuels, **33**(6), pp. 4683–4720.

[110] Wu, Z., Rodgers, R. P., and Marshall, A. G., 2004, "Two- and Three-Dimensional van Krevelen Diagrams: A Graphical Analysis Complementary to the Kendrick Mass Plot for Sorting Elemental Compositions of Complex Organic Mixtures Based on Ultrahigh-Resolution Broadband Fourier Transform Ion Cyclotron Resonance Mass Measurements," Anal. Chem., **76**(9), pp. 2511–2516.

[111] Buss, W., Hertzog, J., Pietrzyk, J., Carré, V., Mackay, C. L., Aubriet, F., and Mašek, O., 2021, "Comparison of Pyrolysis Liquids from Continuous and Batch Biochar Production—Influence of Feedstock Evidenced by FTICR MS," Energies, **14**(1), p. 9.

[112] Pollard, A. S., Rover, M. R., and Brown, R. C., 2012, "Characterization of Bio-Oil Recovered as Stage Fractions with Unique Chemical and Physical Properties," Journal of Analytical and Applied Pyrolysis, **93**, pp. 129–138.

[113] Schulzke, T., Conrad, S., and Westermeyer, J., 2016, "Fractionation of Flash Pyrolysis Condensates by Staged Condensation," Biomass and Bioenergy, **95**, pp. 287–295.

[114] Persson, H., Han, T., Sandström, L., Xia, W., Evangelopoulos, P., and Yang, W., 2018, "Fractionation of Liquid Products from Pyrolysis of Lignocellulosic Biomass by Stepwise Thermal Treatment," Energy, **154**, pp. 346–351.

[115] Lindfors, C., Kuoppala, E., Oasmaa, A., Solantausta, Y., and Arpiainen, V., 2014, "Fractionation of Bio-Oil," Energy Fuels, **28**(9), pp. 5785–5791.

[116] Hu, H.-S., Wu, Y.-L., and Yang, M.-D., 2018, "Fractionation of Bio-Oil Produced from Hydrothermal Liquefaction of Microalgae by Liquid-Liquid Extraction," Biomass and Bioenergy, **108**, pp. 487–500.

[117] Ware, R. L., Rodgers, R. P., Marshall, A. G., Mante, O. D., Dayton, D. C., Verdier, S., Gabrielsen, J., and Rowland, S. M., 2020, "Tracking Elemental Composition through

Hydrotreatment of an Upgraded Pyrolysis Oil Blended with a Light Gas Oil," Energy Fuels, **34**(12), pp. 16181–16186.

[118] Stefanidis, S. D., Kalogiannis, K. G., and Lappas, A. A., 2018, "Co-Processing Bio-Oil in the Refinery for Drop-in Biofuels via Fluid Catalytic Cracking," WIREs Energy and Environment, **7**(3), p. e281.

[119] Fogassy, G., Thegarid, N., Schuurman, Y., and Mirodatos, C., 2012, "The Fate of Bio-Carbon in FCC Co-Processing Products," Green Chemistry, **14**(5), pp. 1367–1371.

[120] Hita, I., Arandes, J. M., and Bilbao, J., 2020, "Upgrading of Bio-Oil via Fluid Catalytic Cracking," *Chemical Catalysts for Biomass Upgrading*, John Wiley & Sons, Ltd, pp. 61–96.

[121] Lappas, A. A., Samolada, M. C., Iatridis, D. K., Voutetakis, S. S., and Vasalos, I. A., 2002, "Biomass Pyrolysis in a Circulating Fluid Bed Reactor for the Production of Fuels and Chemicals," Fuel, **81**(16), pp. 2087–2095.

[122] Ma, W., Liu, B., Zhang, R., Gu, T., Ji, X., Zhong, L., Chen, G., Ma, L., Cheng, Z., and Li, X., 2018, "Co-Upgrading of Raw Bio-Oil with Kitchen Waste Oil through Fluid Catalytic Cracking (FCC)," Applied Energy, **217**, pp. 233–240.

[123] Elliott, D. C., Hart, T. R., Neuenschwander, G. G., Rotness, L. J., and Zacher, A. H., 2009, "Catalytic Hydroprocessing of Biomass Fast Pyrolysis Bio-Oil to Produce Hydrocarbon Products," Environmental Progress & Sustainable Energy, **28**(3), pp. 441–449.

[124] Wildschut, J., Mahfud, F. H., Venderbosch, R. H., and Heeres, H. J., 2009, "Hydrotreatment of Fast Pyrolysis Oil Using Heterogeneous Noble-Metal Catalysts," Ind. Eng. Chem. Res., **48**(23), pp. 10324–10334.

[125] Elliott, D. C., Hart, T. R., Neuenschwander, G. G., Rotness, L. J., and Zacher, A. H., 2012, "Catalytic Hydroprocessing of Biomass Fast Pyrolysis Bio-Oil to Produce Hydrocarbon Products," Environmental Progress & Sustainable Energy, **28**(3), pp. 441–449.

[126] Wang, H., Male, J., and Wang, Y., 2013, "Recent Advances in Hydrotreating of Pyrolysis Bio-Oil and Its Oxygen-Containing Model Compounds," Acs Catalysis, **3**(5), pp. 1047–1070.

[127] Botella, L., Stankovikj, F., Sánchez, J. L., Gonzalo, A., Arauzo, J., and Garcia-Pérez, M., 2018, "Bio-Oil Hydrotreatment for Enhancing Solubility in Biodiesel and the Oxydation Stability of Resulting Blends," Front. Chem., **6**.

[128] Han, Y., McIlroy, D. N., and McDonald, A. G., 2016, “Hydrodeoxygenation of Pyrolysis Oil for Hydrocarbon Production Using Nanospring Based Catalysts,” Journal of Analytical and Applied Pyrolysis, **117**(Supplement C), pp. 94–105.

[129] Wang, H., and Wang, Y., 2016, “Characterization of Deactivated Bio-Oil Hydrotreating Catalysts,” Topics in Catalysis, **59**(1), pp. 65–72.

[130] Gholizadeh, M., Gunawan, R., Hu, X., de Miguel Mercader, F., Westerhof, R., Chaitwat, W., Hasan, M. M., Mourant, D., and Li, C.-Z., 2016, “Effects of Temperature on the Hydrotreatment Behaviour of Pyrolysis Bio-Oil and Coke Formation in a Continuous Hydrotreatment Reactor,” Fuel Processing Technology, **148**, pp. 175–183.

[131] Zacher, A. H., Olarte, M. V., Santosa, D. M., Elliott, D. C., and Jones, S. B., 2014, “A Review and Perspective of Recent Bio-Oil Hydrotreating Research,” Green Chemistry, **16**(2), pp. 491–515.

[132] Han, Y., Gholizadeh, M., Tran, C.-C., Kaliaguine, S., Li, C.-Z., Olarte, M., and Garcia-Perez, M., 2019, “Hydrotreatment of Pyrolysis Bio-Oil: A Review,” Fuel Processing Technology, **195**, p. 106140.

[133] Chadderdon, X. H., Chadderdon, D. J., Matthiesen, J. E., Qiu, Y., Carraher, J. M., Tessonnier, J.-P., and Li, W., 2017, “Mechanisms of Furfural Reduction on Metal Electrodes: Distinguishing Pathways for Selective Hydrogenation of Bioderived Oxygenates,” J. Am. Chem. Soc., **139**(40), pp. 14120–14128.

[134] Deng, W., Xu, K., Xiong, Z., Chaiwat, W., Wang, X., Su, S., Hu, S., Qiu, J., Wang, Y., and Xiang, J., 2019, “Evolution of Aromatic Structures during the Low-Temperature Electrochemical Upgrading of Bio-Oil,” Energy Fuels, **33**(11), pp. 11292–11301.

[135] Elangovan, S., Larsen, D., Hartvigsen, J. J., Mosby, J. M., Staley, J., Elwell, J., and Karanjikar, M., 2015, “(Invited) Electrochemical Upgrading of Bio-Oil,” ECS Trans., **66**(3), p. 1.

[136] Lister, T. E., Diaz, L. A., Lilga, M. A., Padmaperuma, A. B., Lin, Y., Palakkal, V. M., and Arges, C. G., 2018, “Low-Temperature Electrochemical Upgrading of Bio-Oils Using Polymer Electrolyte Membranes,” Energy Fuels, **32**(5), pp. 5944–5950.

[137] Carneiro, J., and Nikolla, E., 2019, “Electrochemical Conversion of Biomass-Based Oxygenated Compounds,” Annual Review of Chemical and Biomolecular Engineering, **10**(1), pp. 85–104.

[138] Hanh, H. D., Dong, N. T., Okitsu, K., Nishimura, R., and Maeda, Y., 2009, “Biodiesel Production through Transesterification of Triolein with Various Alcohols in an Ultrasonic Field,” Renewable Energy, **34**(3), pp. 766–768.

[139] Wu, P., Yang, Y., Colucci, J. A., and Grulke, E. A., 2007, “Effect of Ultrasonication on Droplet Size in Biodiesel Mixtures,” Journal of the American Oil Chemists’ Society, **84**(9), pp. 877–884.

[140] Peshkovsky, S. L., and Peshkovsky, A. S., 2008, “Shock-Wave Model of Acoustic Cavitation,” Ultrasonics Sonochemistry, **15**(4), pp. 618–628.

[141] Qin, L., Shao, Y., Hou, Z., Jia, Y., and Jiang, E., 2019, “Ultrasonic-Assisted Upgrading of the Heavy Bio-Oil Obtained from Pyrolysis of Pine Nut Shells with Methanol and Octanol Solvents,” Energy & Fuels, **33**(9), pp. 8640–8648.

[142] Xu, X., Li, Z., Sun, Y., Jiang, E., and Huang, L., 2018, “High-Quality Fuel from the Upgrading of Heavy Bio-Oil by the Combination of Ultrasonic Treatment and Mutual Solvent,” Energy Fuels.

[143] Alsbou, E., and Helleur, B., 2014, “Accelerated Aging of Bio-Oil from Fast Pyrolysis of Hardwood,” Energy Fuels, **28**(5), pp. 3224–3235.

[144] Yang, S.-K., and Duan, P.-G., 2017, “Effect of Ultrasonic Pretreatment on the Properties of Bio-Oil,” Energy Sources, Part A: Recovery, Utilization, and Environmental Effects, **39**(9), pp. 941–945.

[145] Kumar, G., 2017, “Ultrasonic-Assisted Reactive-Extraction Is a Fast and Easy Method for Biodiesel Production from Jatropha Curcas Oilseeds,” Ultrasonics Sonochemistry, **37**, pp. 634–639.

[146] Xie, W., Li, R., and Lu, X., 2015, “Pulsed Ultrasound Assisted Dehydration of Waste Oil,” Ultrasonics Sonochemistry, **26**, pp. 136–141.

[147] Rogers, J. G., and Brammer, J. G., 2012, “Estimation of the Production Cost of Fast Pyrolysis Bio-Oil,” Biomass and Bioenergy, **36**, pp. 208–217.

[148] Jones, S. B., and Male, J. L., 2012, *Production of Gasoline and Diesel from Biomass via Fast Pyrolysis, Hydrotreating and Hydrocracking: 2011 State of Technology and Projections to 2017*, Pacific Northwest National Laboratory.

[149] Brown, D., Rowe, A., and Wild, P., 2013, "A Techno-Economic Analysis of Using Mobile Distributed Pyrolysis Facilities to Deliver a Forest Residue Resource," Bioresource technology, **150**, pp. 367–376.

[150] Wang, W.-C., and Jan, J.-J., 2018, "From Laboratory to Pilot: Design Concept and Techno-Economic Analyses of the Fluidized Bed Fast Pyrolysis of Biomass," Energy, **155**, pp. 139–151.

[151] van Schalkwyk, D. L., Mandegari, M., Farzad, S., and Görgens, J. F., 2020, "Techno-Economic and Environmental Analysis of Bio-Oil Production from Forest Residues via Non-Catalytic and Catalytic Pyrolysis Processes," Energy Conversion and Management, **213**, p. 112815.

[152] Lane, J., 2016, "KIOR: The inside True Story of a Company Gone Wrong," Biofuels Digest, Miami, USA, 17th May.

[153] Gollakota, A. R. K., Reddy, M., Subramanyam, M. D., and Kishore, N., 2016, "A Review on the Upgradation Techniques of Pyrolysis Oil," Renewable and Sustainable Energy Reviews, **58**, pp. 1543–1568.

[154] Saidi, M., Samimi, F., Karimipourfard, D., Nimmanwudipong, T., C. Gates, B., and Reza Rahimpour, M., 2014, "Upgrading of Lignin-Derived Bio-Oils by Catalytic Hydrodeoxygenation," Energy & Environmental Science, **7**(1), pp. 103–129.

[155] Li, Z., Kelkar, S., Raycraft, L., Garedew, M., Jackson, J. E., Miller, D. J., and Saffron, C. M., 2014, "A Mild Approach for Bio-Oil Stabilization and Upgrading: Electrocatalytic Hydrogenation Using Ruthenium Supported on Activated Carbon Cloth," Green Chemistry, **16**(2), pp. 844–852.

[156] Reddy Kannapu, H. P., Mullen, C. A., Elkasabi, Y., and Boateng, A. A., 2015, "Catalytic Transfer Hydrogenation for Stabilization of Bio-Oil Oxygenates: Reduction of p-Cresol and Furfural over Bimetallic Ni–Cu Catalysts Using Isopropanol," Fuel Processing Technology, **137**, pp. 220–228.

[157] Elliott, D. C., 2016, “Transportation Fuels from Biomass via Fast Pyrolysis and Hydroprocessing,” Advances in bioenergy. The sustainability challenge. Lund P. D., Byrne J., Berndes G., Vasalos IA (eds), Wiley, West Sussex, United Kingdom.

[158] Patel, M., and Kumar, A., 2016, “Production of Renewable Diesel through the Hydroprocessing of Lignocellulosic Biomass-Derived Bio-Oil: A Review,” Renewable and Sustainable Energy Reviews, **58**, pp. 1293–1307.

[159] Rover, M. R., Hall, P. H., Johnston, P. A., Smith, R. G., and Brown, R. C., 2015, “Stabilization of Bio-Oils Using Low Temperature, Low Pressure Hydrogenation,” Fuel, **153**, pp. 224–230.

[160] Wang, W., Yang, Y., Bao, J., and Zhuo, C., 2009, “Influence of Ultrasonic on the Preparation of Ni–Mo–B Amorphous Catalyst and Its Performance in Phenol Hydrodeoxygenation,” Journal of Fuel Chemistry and Technology, **37**(6), pp. 701–706.

[161] Wu, Z., Cherkasov, N., Cravotto, G., Borretto, E., Ibhadon, A. O., Medlock, J., and Bonrath, W., 2015, “Ultrasound- and Microwave-Assisted Preparation of Lead-Free Palladium Catalysts: Effects on the Kinetics of Diphenylacetylene Semi-Hydrogenation,” ChemCatChem, **7**(6), pp. 952–959.

[162] Struhs, E., Hansen, S., Mirkouei, A., Ramirez-Corredores, M. M., Sharma, K., Spiers, R., and Kalivas, J. H., 2021, “Ultrasonic-Assisted Catalytic Transfer Hydrogenation for Upgrading Pyrolysis-Oil,” Ultrasonics Sonochemistry, **73**, p. 105502.

[163] Vasalos, I. A., Lappas, A. A., Kopalidou, E. P., and Kalogiannis, K. G., 2016, “Biomass Catalytic Pyrolysis: Process Design and Economic Analysis,” WIREs Energy Environ, **5**(3), pp. 370–383.

[164] Mu, W., Ben, H., Ragauskas, A., and Deng, Y., 2013, “Lignin Pyrolysis Components and Upgrading—Technology Review,” Bioenerg. Res., **6**(4), pp. 1183–1204.

[165] Yang, H., Yan, R., Chen, H., Lee, D. H., and Zheng, C., 2007, “Characteristics of Hemicellulose, Cellulose and Lignin Pyrolysis,” Fuel, **86**(12), pp. 1781–1788.

[166] Schutyser, W., Renders, T., Van den Bosch, S., Koelewijn, S.-F., Beckham, G. T., and Sels, B. F., 2018, “Chemicals from Lignin: An Interplay of Lignocellulose Fractionation, Depolymerisation, and Upgrading,” Chemical Society Reviews, **47**(3), pp. 852–908.

[167] U.S. EIA, 2021, *Oil and Petroleum Products Explained*.

[168] Myllyviita, T., Holma, A., Antikainen, R., Lähtinen, K., and Leskinen, P., 2012, "Assessing Environmental Impacts of Biomass Production Chains – Application of Life Cycle Assessment (LCA) and Multi-Criteria Decision Analysis (MCDA)," Journal of Cleaner Production, **29–30**, pp. 238–245.

[169] Mohan, D., Pittman, Charles U., and Steele, P. H., 2006, "Pyrolysis of Wood/Biomass for Bio-Oil: A Critical Review," Energy Fuels, **20**(3), pp. 848–889.

[170] Lehto, J., 2007, "Determination of Kinetic Parameters for Finnish Milled Peat Using Drop Tube Reactor and Optical Measurement Techniques," Fuel, **86**(12), pp. 1656–1663.

[171] Ellens, C. J., and Brown, R. C., 2012, "Optimization of a Free-Fall Reactor for the Production of Fast Pyrolysis Bio-Oil," Bioresource Technology, **103**(1), pp. 374–380.

[172] Punsuwan, N., and Tangsathitkulchai, C., 2014, "Product Characterization and Kinetics of Biomass Pyrolysis in a Three-Zone Free-Fall Reactor," International Journal of Chemical Engineering, **2014**, p. e986719.

[173] Boucher, M. E., Chaala, A., Pakdel, H., and Roy, C., 2000, "Bio-Oils Obtained by Vacuum Pyrolysis of Softwood Bark as a Liquid Fuel for Gas Turbines. Part II: Stability and Ageing of Bio-Oil and Its Blends with Methanol and a Pyrolytic Aqueous Phase," Biomass and Bioenergy, **19**(5), pp. 351–361.

[174] Czernik, S., Johnson, D. K., and Black, S., 1994, "Stability of Wood Fast Pyrolysis Oil," Biomass and Bioenergy, **7**(1–6), pp. 187–192.

[175] Oasmaa, A., Leppaemaeki, E., Koponen, P., Levander, J., and Tapola, E., 1997, "Physical Characterization of Biomass-Based Pyrolysis Liquids. Application of Standard Fuel Oil Analyses."

[176] Zanzi, R., Sjöström, K., and Björnbom, E., 1996, "Rapid High-Temperature Pyrolysis of Biomass in a Free-Fall Reactor," Fuel, **75**(5), pp. 545–550.

[177] Yu, Q., Brage, C., Chen, G., and Sjöström, K., 1997, "Temperature Impact on the Formation of Tar from Biomass Pyrolysis in a Free-Fall Reactor," Journal of Analytical and Applied Pyrolysis, **40–41**, pp. 481–489.

[178] Li, S., Xu, S., Liu, S., Yang, C., and Lu, Q., 2004, "Fast Pyrolysis of Biomass in Free-Fall Reactor for Hydrogen-Rich Gas," Fuel Processing Technology, **85**(8–10), pp. 1201–1211.

[179] Wei, L., Xu, S., Zhang, L., Zhang, H., Liu, C., Zhu, H., and Liu, S., 2006, "Characteristics of Fast Pyrolysis of Biomass in a Free Fall Reactor," Fuel Processing Technology, **87**(10), pp. 863–871.

[180] Onay, O., and Koçkar, O. M., 2006, "Pyrolysis of Rapeseed in a Free Fall Reactor for Production of Bio-Oil," Fuel, **85**(12), pp. 1921–1928.

[181] Zhang, L., Xu, S., Zhao, W., and Liu, S., 2007, "Co-Pyrolysis of Biomass and Coal in a Free Fall Reactor," Fuel, **86**(3), pp. 353–359.

[182] Pattiya, A., Sukkasi, S., and Goodwin, V., 2012, "Fast Pyrolysis of Sugarcane and Cassava Residues in a Free-Fall Reactor," Energy, **44**(1), pp. 1067–1077.

[183] Pidtasang, B., Udomsap, P., Sukkasi, S., Chollacoop, N., and Pattiya, A., 2013, "Influence of Alcohol Addition on Properties of Bio-Oil Produced from Fast Pyrolysis of Eucalyptus Bark in a Free-Fall Reactor," Journal of Industrial and Engineering Chemistry, **19**(6), pp. 1851–1857.

[184] Chen, L., Dupont, C., Salvador, S., Grateau, M., Boissonnet, G., and Schweich, D., 2013, "Experimental Study on Fast Pyrolysis of Free-Falling Millimetric Biomass Particles between 800°C and 1000°C," Fuel, **106**, pp. 61–66.

[185] Zhao, H., Yan, H.-X., Liu, M., Sun, B.-B., Zhang, Y., Dong, S.-S., Qi, L.-B., and Qin, S., 2013, "Production of Bio-Oil from Fast Pyrolysis of Macroalgae Enteromorpha Prolifera Powder in a Free-Fall Reactor," Energy Sources, Part A: Recovery, Utilization, and Environmental Effects, **35**(9), pp. 859–867.

[186] Hu, Z., Zhang, L., Liu, Z., Xiao, B., and Liu, S., 2013, "Experimental Study on Bio-Oil Production from Pyrolysis of Biomass Micron Fuel (BMF) in a Free-Fall Reactor," Fuel, **106**, pp. 552–557.

[187] Quan, C., Xu, S., An, Y., and Liu, X., 2014, "Co-Pyrolysis of Biomass and Coal Blend by TG and in a Free Fall Reactor," J Therm Anal Calorim, **117**(2), pp. 817–823.

[188] Ngo, T.-A., and Kim, J., 2014, "Fast Pyrolysis of Pine Wood Chip in a Free Fall Reactor: The Effect of Pyrolysis Temperature and Sweep Gas Flow Rate," Energy Sources, Part A: Recovery, Utilization, and Environmental Effects, **36**(11), pp. 1158–1165.

[189] Zhang, J., Quan, C., Qiu, Y., and Xu, S., 2015, "Effect of Char on Co-Pyrolysis of Biomass and Coal in a Free Fall Reactor," Fuel Processing Technology, **135**, pp. 73–79.

[190] Gable, P., and Brown, R. C., 2016, “Effect of Biomass Heating Time on Bio-Oil Yields in a Free Fall Fast Pyrolysis Reactor,” Fuel, **166**, pp. 361–366.

[191] Rueangsan, K., Trisupakitti, S., Senajuk, W., and Morris, J., 2022, “Fast Pyrolysis of Dipterocarpus Alatus Roxb and Rubber Wood in a Free-Fall Reactor,” Energy Sources, Part A: Recovery, Utilization, and Environmental Effects, **44**(1), pp. 2489–2496.

[192] Rueangsan, K., Kraisoda, P., Heman, A., Tasarod, H., Wangkulangkool, M., Trisupakitti, S., and Morris, J., 2021, “Bio-Oil and Char Obtained from Cassava Rhizomes with Soil Conditioners by Fast Pyrolysis,” Heliyon, **7**(11), p. e08291.

[193] U.S. Department of Energy, Idaho National Laboratory, 2016, “Bioenergy Feedstock Library” [Online]. Available: https://bioenergylibrary.inl.gov/Home/Home.aspx. [Accessed: 25-Jan-2022].

[194] Ozawa, T., 2000, “Thermal Analysis — Review and Prospect,” Thermochimica Acta, **355**(1), pp. 35–42.

[195] Flynn, J. H., and Wall, L. A., 1966, “General Treatment of the Thermogravimetry of Polymers,” J Res Natl Bur Stand A Phys Chem, **70A**(6), pp. 487–523.

[196] Flynn, J. H., 1983, “The Isoconversional Method for Determination of Energy of Activation at Constant Heating Rates,” Journal of Thermal Analysis, **27**(1), pp. 95–102.

[197] Sotoudehniakarani, F., Alayat, A., and McDonald, A. G., 2019, “Characterization and Comparison of Pyrolysis Products from Fast Pyrolysis of Commercial Chlorella Vulgaris and Cultivated Microalgae,” Journal of Analytical and Applied Pyrolysis, **139**, pp. 258–273.

[198] Faix, O., Meier, D., and Fortmann, I., 1990, “Gas Chromatographic Separation and Mass Spectrometric Characterization of Monomeric Lignin Derived Products,” Holz als roh-und werkstoff, **48**(7/8), pp. 281–285.

[199] Faix, O., Meier, D., and Fortmann, I., 1990, “Thermal Degradation Products of Wood. A Collection of Electron-Impact (EI) Mass Spectra of Monomeric Lignin Derived Products.,” Holz als Roh- und Werkstoff, **48**(9), pp. 351–354.

[200] Faix, O., Fortmann, I., Bremer, J., and Meier, D., 1991, “Thermal Degradation Products of Wood. A Collection of Electron-Impact (EI) Mass Spectra of Polysaccharide Derived Products,” Holz als Roh- und Werkstoff (Germany, F.R.).

[201] Sotoudehnia, F., Baba Rabiu, A., Alayat, A., and McDonald, A. G., 2020, "Characterization of Bio-Oil and Biochar from Pyrolysis of Waste Corrugated Cardboard," Journal of Analytical and Applied Pyrolysis, **145**, p. 104722.

[202] Grønli, M. G., Várhegyi, G., and Di Blasi, C., 2002, "Thermogravimetric Analysis and Devolatilization Kinetics of Wood," Ind. Eng. Chem. Res., **41**(17), pp. 4201–4208.

[203] Alvarenga, L. M., Xavier, T. P., Barrozo, M. A. S., Bacelos, M. S., and Lira, T. S., 2016, "Determination of Activation Energy of Pyrolysis of Carton Packaging Wastes and Its Pure Components Using Thermogravimetry," Waste Management, **53**, pp. 68–75.

[204] Cheng, K., Winter, W. T., and Stipanovic, A. J., 2012, "A Modulated-TGA Approach to the Kinetics of Lignocellulosic Biomass Pyrolysis/Combustion," Polymer Degradation and Stability, **97**(9), pp. 1606–1615.

[205] Carrier, M., Loppinet-Serani, A., Denux, D., Lasnier, J.-M., Ham-Pichavant, F., Cansell, F., and Aymonier, C., 2011, "Thermogravimetric Analysis as a New Method to Determine the Lignocellulosic Composition of Biomass," Biomass and Bioenergy, **35**(1), pp. 298–307.

[206] Raveendran, K., Ganesh, A., and Khilar, K. C., 1996, "Pyrolysis Characteristics of Biomass and Biomass Components," Fuel, **75**(8), pp. 987–998.

[207] Hu, M., Chen, Z., Wang, S., Guo, D., Ma, C., Zhou, Y., Chen, J., Laghari, M., Fazal, S., Xiao, B., Zhang, B., and Ma, S., 2016, "Thermogravimetric Kinetics of Lignocellulosic Biomass Slow Pyrolysis Using Distributed Activation Energy Model, Fraser–Suzuki Deconvolution, and Iso-Conversional Method," Energy Conversion and Management, **118**, pp. 1–11.

[208] Sanchez-Silva, L., López-González, D., Villaseñor, J., Sánchez, P., and Valverde, J. L., 2012, "Thermogravimetric–Mass Spectrometric Analysis of Lignocellulosic and Marine Biomass Pyrolysis," Bioresource Technology, **109**, pp. 163–172.

[209] Wang, S., Liu, Q., Luo, Z., Wen, L., and Cen, K., 2007, "Mechanism Study on Cellulose Pyrolysis Using Thermogravimetric Analysis Coupled with Infrared Spectroscopy," Front. Energy Power Eng. China, **1**(4), pp. 413–419.

[210] Grammelis, P., Basinas, P., Malliopoulou, A., and Sakellaropoulos, G., 2009, "Pyrolysis Kinetics and Combustion Characteristics of Waste Recovered Fuels," Fuel, **88**(1), pp. 195–205.

[211] Santos, K. G., Lobato, F. S., Lira, T. S., Murata, V. V., and Barrozo, M. A. S., 2012, "Sensitivity Analysis Applied to Independent Parallel Reaction Model for Pyrolysis of Bagasse," Chemical Engineering Research and Design, **90**(11), pp. 1989–1996.

[212] Brebu, M., and Vasile, C., 2010, "Thermal Degradation of Lignin—a Review," Cellulose Chemistry & Technology, **44**(9), p. 353.

[213] Mitchell, P. J., Dalley, T. S. L., and Helleur, R. J., 2013, "Preliminary Laboratory Production and Characterization of Biochars from Lignocellulosic Municipal Waste," Journal of Analytical and Applied Pyrolysis, **99**, pp. 71–78.

[214] Ding, Y., Ezekoye, O. A., Lu, S., Wang, C., and Zhou, R., 2017, "Comparative Pyrolysis Behaviors and Reaction Mechanisms of Hardwood and Softwood," Energy Conversion and Management, **132**, pp. 102–109.

[215] Zanatta, E. R., Reinehr, T. O., Awadallak, J. A., Kleinübing, S. J., dos Santos, J. B. O., Bariccatti, R. A., Arroyo, P. A., and da Silva, E. A., 2016, "Kinetic Studies of Thermal Decomposition of Sugarcane Bagasse and Cassava Bagasse," J Therm Anal Calorim, **125**(1), pp. 437–445.

[216] Bridgwater, A. V., Meier, D., and Radlein, D., 1999, "An Overview of Fast Pyrolysis of Biomass," Organic Geochemistry, **30**(12), pp. 1479–1493.

[217] Mahadevan, R., Adhikari, S., Shakya, R., Wang, K., Dayton, D., Lehrich, M., and Taylor, S. E., 2016, "Effect of Alkali and Alkaline Earth Metals on In-Situ Catalytic Fast Pyrolysis of Lignocellulosic Biomass: A Microreactor Study," Energy Fuels, **30**(4), pp. 3045–3056.

[218] Bradbury, A. G. W., Sakai, Y., and Shafizadeh, F., 1979, "A Kinetic Model for Pyrolysis of Cellulose," Journal of Applied Polymer Science, **23**(11), pp. 3271–3280.

[219] Sadaka, S., Boateng, A. A., and others, 2009, *Pyrolysis and Bio-Oil*, [Cooperative Extension Service], University of Arkansas, US Department of ….

[220] Tsai, W. T., Lee, M. K., and Chang, Y. M., 2006, "Fast Pyrolysis of Rice Straw, Sugarcane Bagasse and Coconut Shell in an Induction-Heating Reactor," Journal of Analytical and Applied Pyrolysis, **76**(1), pp. 230–237.

[221] Kim, K. H., Eom, I. Y., Lee, S. M., Choi, D., Yeo, H., Choi, I.-G., and Choi, J. W., 2011, "Investigation of Physicochemical Properties of Biooils Produced from Yellow Poplar Wood

(Liriodendron Tulipifera) at Various Temperatures and Residence Times," Journal of Analytical and Applied Pyrolysis, **92**(1), pp. 2–9.

[222] Kim, K. H., Kim, T.-S., Lee, S.-M., Choi, D., Yeo, H., Choi, I.-G., and Choi, J. W., 2013, "Comparison of Physicochemical Features of Biooils and Biochars Produced from Various Woody Biomasses by Fast Pyrolysis," Renewable Energy, **50**, pp. 188–195.

[223] Ippolito, J. A., Cui, L., Kammann, C., Wrage-Mönnig, N., Estavillo, J. M., Fuertes-Mendizabal, T., Cayuela, M. L., Sigua, G., Novak, J., Spokas, K., and Borchard, N., 2020, "Feedstock Choice, Pyrolysis Temperature and Type Influence Biochar Characteristics: A Comprehensive Meta-Data Analysis Review," Biochar, **2**(4), pp. 421–438.

[224] Oasmaa, A., and Czernik, S., 1999, "Fuel Oil Quality of Biomass Pyrolysis Oils-State of the Art for the End Users," Energy Fuels, **13**(4), pp. 914–921.

[225] Igalavithana, A. D., Mandal, S., Niazi, N. K., Vithanage, M., Parikh, S. J., Mukome, F. N. D., Rizwan, M., Oleszczuk, P., Al-Wabel, M., Bolan, N., Tsang, D. C. W., Kim, K.-H., and Ok, Y. S., 2017, "Advances and Future Directions of Biochar Characterization Methods and Applications," Critical Reviews in Environmental Science and Technology, **47**(23), pp. 2275–2330.

[226] Oasmaa, A., and Kuoppala, E., 2003, "Fast Pyrolysis of Forestry Residue. 3. Storage Stability of Liquid Fuel," Energy Fuels, **17**(4), pp. 1075–1084.

[227] Elliott, D. C., Oasmaa, A., Preto, F., Meier, D., and Bridgwater, A. V., 2012, "Results of the IEA Round Robin on Viscosity and Stability of Fast Pyrolysis Bio-Oils," Energy Fuels, **26**(6), pp. 3769–3776.

[228] Zhang, J., Jiang, Y., F. Easterling, L., Anstner, A., Li, W., Z. Alzarieni, K., Dong, X., Bozell, J., and I. Kenttämaa, H., 2021, "Compositional Analysis of Organosolv Poplar Lignin by Using High-Performance Liquid Chromatography/High-Resolution Multi-Stage Tandem Mass Spectrometry," Green Chemistry, **23**(2), pp. 983–1000.

[229] Khuenkaeo, N., and Tippayawong, N., 2020, "Production and Characterization of Bio-Oil and Biochar from Ablative Pyrolysis of Lignocellulosic Biomass Residues," Chemical Engineering Communications, **207**(2), pp. 153–160.

[230] Poletto, M., 2018, *Lignin: Trends and Applications*, BoD – Books on Demand.

[231] S. Mettler, M., H. Mushrif, S., D. Paulsen, A., D. Javadekar, A., G. Vlachos, D., and J. Dauenhauer, P., 2012, "Revealing Pyrolysis Chemistry for Biofuels Production: Conversion of Cellulose to Furans and Small Oxygenates," Energy & Environmental Science, **5**(1), pp. 5414–5424.

[232] Milne, T., Agblevor, F., Davis, M., Deutch, S., and Johnson, D., 1997, "A Review of the Chemical Composition of Fast-Pyrolysis Oils from Biomass," *Developments in Thermochemical Biomass Conversion: Volume 1 / Volume 2*, A.V. Bridgwater, and D.G.B. Boocock, eds., Springer Netherlands, Dordrecht, pp. 409–424.

[233] Bharath, G., Hai, A., Rambabu, K., Banat, F., Jayaraman, R., Taher, H., Bastidas-Oyanedel, J.-R., Ashraf, M. T., and Schmidt, J. E., 2020, "Systematic Production and Characterization of Pyrolysis-Oil from Date Tree Wastes for Bio-Fuel Applications," Biomass and Bioenergy, **135**, p. 105523.

[234] Lyu, G., Wu, S., and Zhang, H., 2015, "Estimation and Comparison of Bio-Oil Components from Different Pyrolysis Conditions," Frontiers in Energy Research, **3**.

[235] Agblevor, Foster. A., Beis, S., Mante, O., and Abdoulmoumine, N., 2010, "Fractional Catalytic Pyrolysis of Hybrid Poplar Wood," Ind. Eng. Chem. Res., **49**(8), pp. 3533–3538.

[236] Isahak, W. N. R. W., Hisham, M. W., Yarmo, M. A., and Hin, T. Y., 2012, "A Review on Bio-Oil Production from Biomass by Using Pyrolysis Method," Renewable and sustainable energy reviews, **16**(8), pp. 5910–5923.

[237] Miettinen, I., Mäkinen, M., Vilppo, T., and Jänis, J., 2015, "Compositional Characterization of Phase-Separated Pine Wood Slow Pyrolysis Oil by Negative-Ion Electrospray Ionization Fourier Transform Ion Cyclotron Resonance Mass Spectrometry," Energy Fuels, **29**(3), pp. 1758–1765.

[238] Jarvis, J. M., McKenna, A. M., Hilten, R. N., Das, K. C., Rodgers, R. P., and Marshall, A. G., 2012, "Characterization of Pine Pellet and Peanut Hull Pyrolysis Bio-Oils by Negative-Ion Electrospray Ionization Fourier Transform Ion Cyclotron Resonance Mass Spectrometry," Energy Fuels, **26**(6), pp. 3810–3815.

[239] Miettinen, I., Kuittinen, S., Paasikallio, V., Mäkinen, M., Pappinen, A., and Jänis, J., 2017, "Characterization of Fast Pyrolysis Oil from Short-Rotation Willow by High-Resolution Fourier Transform Ion Cyclotron Resonance Mass Spectrometry," Fuel, **207**, pp. 189–197.

[240] Liu, Y., Shi, Q., Zhang, Y., He, Y., Chung, K. H., Zhao, S., and Xu, C., 2012, "Characterization of Red Pine Pyrolysis Bio-Oil by Gas Chromatography–Mass Spectrometry and Negative-Ion Electrospray Ionization Fourier Transform Ion Cyclotron Resonance Mass Spectrometry," Energy Fuels, **26**(7), pp. 4532–4539.

[241] E. Harman-Ware, A., Orton, K., Deng, C., Kenrick, S., Carpenter, D., and R. Ferrell, J., 2020, "Molecular Weight Distribution of Raw and Catalytic Fast Pyrolysis Oils: Comparison of Analytical Methodologies," RSC Advances, **10**(7), pp. 3789–3795.

[242] McKinley, J., 1989, "Biomass Liquefaction: Centralized Analysis," Final report. Vancouver: BC Research. Project, (403837).

[243] Pandey, K. K., 1999, "A Study of Chemical Structure of Soft and Hardwood and Wood Polymers by FTIR Spectroscopy," Journal of Applied Polymer Science, **71**(12), pp. 1969–1975.

[244] Faix, O., 1992, "Fourier Transform Infrared Spectroscopy," *Methods in Lignin Chemistry*, S.Y. Lin, and C.W. Dence, eds., Springer, Berlin, Heidelberg, pp. 83–109.

[245] Le, D. M., Nielsen, A. D., Sørensen, H. R., and Meyer, A. S., 2017, "Characterisation of Authentic Lignin Biorefinery Samples by Fourier Transform Infrared Spectroscopy and Determination of the Chemical Formula for Lignin," Bioenerg. Res., **10**(4), pp. 1025–1035.

[246] Wang, L., Zhang, R., Li, J., Guo, L., Yang, H., Ma, F., and Yu, H., 2018, "Comparative Study of the Fast Pyrolysis Behavior of Ginkgo, Poplar, and Wheat Straw Lignin at Different Temperatures," Industrial Crops and Products, **122**, pp. 465–472.

[247] Zhang, J., Sekyere, D. T., Niwamanya, N., Huang, Y., Barigye, A., and Tian, Y., 2022, "Study on the Staged and Direct Fast Pyrolysis Behavior of Waste Pine Sawdust Using High Heating Rate TG-FTIR and Py-GC/MS," ACS Omega, **7**(5), pp. 4245–4256.

[248] Zhao, J., Xiuwen, W., Hu, J., Liu, Q., Shen, D., and Xiao, R., 2014, "Thermal Degradation of Softwood Lignin and Hardwood Lignin by TG-FTIR and Py-GC/MS," Polymer Degradation and Stability, **108**, pp. 133–138.

[249] Cai, W., Liu, Q., Shen, D., and Wang, J., 2019, "Py-GC/MS Analysis on Product Distribution of Two-Staged Biomass Pyrolysis," Journal of Analytical and Applied Pyrolysis, **138**, pp. 62–69.

[250] Xu, F., Wang, B., Yang, D., Ming, X., Jiang, Y., Hao, J., Qiao, Y., and Tian, Y., 2018, "TG-FTIR and Py-GC/MS Study on Pyrolysis Mechanism and Products Distribution of Waste Bicycle Tire," Energy Conversion and Management, **175**, pp. 288–297.

[251] U.S. DOE Energy Information Administration, 2023, *Monthly Energy Review - August 2023*.

[252] Venderbosch, R. H., 2015, "A Critical View on Catalytic Pyrolysis of Biomass," ChemSusChem, **8**(8), pp. 1306–1316.

[253] Easterly, J. L., 2002, "Assessment of Bio-Oil as a Replacement for Heating Oil," Northeast Regional Biomass Program, **1**, pp. 1–15.

[254] Jacobson, K., Maheria, K. C., and Kumar Dalai, A., 2013, "Bio-Oil Valorization: A Review," Renewable and Sustainable Energy Reviews, **23**, pp. 91–106.

[255] Ramirez-Corredores, M. M., and Sanchez, V., 2012, "Challenges on the Quality of Biomass Derived Products for Bringing Them into the Fuels Market," Journal of Energy and Power Engineering, **6**(3).

[256] Li, B., Ou, L., Dang, Q., Meyer, P., Jones, S., Brown, R., and Wright, M., 2015, "Techno-Economic and Uncertainty Analysis of in Situ and Ex Situ Fast Pyrolysis for Biofuel Production," Bioresource Technology, **196**, pp. 49–56.

[257] Brady, M. P., Keiser, J. R., Leonard, D. N., Whitmer, L., and Thomson, J. K., 2014, "Corrosion Considerations for Thermochemical Biomass Liquefaction Process Systems in Biofuel Production," JOM, **66**(12), pp. 2583–2592.

[258] Yang, Z., Kumar, A., and Huhnke, R. L., 2015, "Review of Recent Developments to Improve Storage and Transportation Stability of Bio-Oil," Renewable and Sustainable Energy Reviews, **50**, pp. 859–870.

[259] Trueba, M., and Trasatti, S. P., 2005, "γ-Alumina as a Support for Catalysts: A Review of Fundamental Aspects," European Journal of Inorganic Chemistry, **2005**(17), pp. 3393–3403.

[260] Mosallanejad, S., Dlugogorski, B. Z., Kennedy, E. M., and Stockenhuber, M., 2018, "On the Chemistry of Iron Oxide Supported on γ-Alumina and Silica Catalysts," ACS Omega, **3**(5), pp. 5362–5374.

[261] Zhang, L., Bao, Z., Xia, S., Lu, Q., and Walters, K., 2018, "Catalytic Pyrolysis of Biomass and Polymer Wastes," Catalysts, **8**(12), p. 659.

[262] Gupta, S., and Mondal, P., 2021, “Catalytic Pyrolysis of Pine Needles with Nickel Doped Gamma-Alumina: Reaction Kinetics, Mechanism, Thermodynamics and Products Analysis,” Journal of Cleaner Production, **286**, p. 124930.

[263] Junming, X., Jianchun, J., Yunjuan, S., and Yanju, L., 2008, “Bio-Oil Upgrading by Means of Ethyl Ester Production in Reactive Distillation to Remove Water and to Improve Storage and Fuel Characteristics,” Biomass and Bioenergy, **32**(11), pp. 1056–1061.

[264] Mahfud, F. H., Melián-Cabrera, I., Manurung, R., and Heeres, H. J., 2007, “Biomass to Fuels: Upgrading of Flash Pyrolysis Oil by Reactive Distillation Using a High Boiling Alcohol and Acid Catalysts,” Process Safety and Environmental Protection, **85**(5), pp. 466–472.

[265] Cai, W., and Liu, R., 2016, “Performance of a Commercial-Scale Biomass Fast Pyrolysis Plant for Bio-Oil Production,” Fuel, **182**, pp. 677–686.

[266] Sotoudehnia, F., Orji, B., Mengistie, E., Alayat, A. M., and McDonald, A. G., 2021, “Catalytic Upgrading of Pyrolysis Wax Oil Obtained from Waxed Corrugated Cardboard Using Zeolite Y Catalyst,” Energy Fuels, **35**(11), pp. 9450–9461.

[267] Diebold, J. P., and Czernik, S., 1997, “Additives To Lower and Stabilize the Viscosity of Pyrolysis Oils during Storage,” Energy Fuels, **11**(5), pp. 1081–1091.

[268] Ellens, C. J., and Brown, R. C., 2012, “Optimization of a Free-Fall Reactor for the Production of Fast Pyrolysis Bio-Oil,” Bioresource Technology, **103**(1), pp. 374–380.

[269] Struhs, E., Sotoudehnia, F., Mirkouei, A., McDonald, A. G., and Ramirez-Corredores, M. M., 2022, “Effect of Feedstocks and Free-Fall Pyrolysis on Bio-Oil and Biochar Attributes,” Journal of Analytical and Applied Pyrolysis, **166**, p. 105616.

[270] Matsuoka, K., Shinbori, T., Kuramoto, K., Nanba, T., Morita, A., Hatano, H., and Suzuki, Y., 2006, “Mechanism of Woody Biomass Pyrolysis and Gasification in a Fluidized Bed of Porous Alumina Particles,” Energy Fuels, **20**(3), pp. 1315–1320.

[271] Quirino, R. L., Tavares, A. P., Peres, A. C., Rubim, J. C., and Suarez, P. A. Z., 2009, “Studying the Influence of Alumina Catalysts Doped with Tin and Zinc Oxides in the Soybean Oil Pyrolysis Reaction,” J Am Oil Chem Soc, **86**(2), pp. 167–172.

[272] Ateş, F., and Işıkdağ, M. A., 2009, “Influence of Temperature and Alumina Catalyst on Pyrolysis of Corncob,” Fuel, **88**(10), pp. 1991–1997.

[273] Du, S., Sun, Y., Gamliel, D. P., Valla, J. A., and Bollas, G. M., 2014, "Catalytic Pyrolysis of Miscanthus×giganteus in a Spouted Bed Reactor," Bioresource Technology, **169**, pp. 188–197.

[274] Chen, G.-B., Li, Y.-H., Chen, G.-L., and Wu, W.-T., 2017, "Effects of Catalysts on Pyrolysis of Castor Meal," Energy, **119**, pp. 1–9.

[275] Y. Jia, L., Raad, M., Hamieh, S., Toufaily, J., Hamieh, T., M. Bettahar, M., Mauviel, G., Tarrighi, M., Pinard, L., and Dufour, A., 2017, "Catalytic Fast Pyrolysis of Biomass: Superior Selectivity of Hierarchical Zeolites to Aromatics," Green Chemistry, **19**(22), pp. 5442–5459.

[276] Ghorbannezhad, P., Park, S., and Onwudili, J. A., 2020, "Co-Pyrolysis of Biomass and Plastic Waste over Zeolite- and Sodium-Based Catalysts for Enhanced Yields of Hydrocarbon Products," Waste Management, **102**, pp. 909–918.

[277] Wang, K., Johnston, P. A., and Brown, R. C., 2014, "Comparison of In-Situ and Ex-Situ Catalytic Pyrolysis in a Micro-Reactor System," Bioresource Technology, **173**, pp. 124–131.

[278] Luo, G., and Resende, F. L. P., 2016, "In-Situ and Ex-Situ Upgrading of Pyrolysis Vapors from Beetle-Killed Trees," Fuel, **166**, pp. 367–375.

[279] Rafiq, M. K., Bachmann, R. T., Rafiq, M. T., Shang, Z., Joseph, S., and Long, R., 2016, "Influence of Pyrolysis Temperature on Physico-Chemical Properties of Corn Stover (Zea Mays L.) Biochar and Feasibility for Carbon Capture and Energy Balance," PLOS ONE, **11**(6), p. e0156894.

[280] Crombie, K., Mašek, O., Sohi, S. P., Brownsort, P., and Cross, A., 2013, "The Effect of Pyrolysis Conditions on Biochar Stability as Determined by Three Methods," GCB Bioenergy, **5**(2), pp. 122–131.

[281] Qian, C., Li, Q., Zhang, Z., Wang, X., Hu, J., and Cao, W., 2020, "Prediction of Higher Heating Values of Biochar from Proximate and Ultimate Analysis," Fuel, **265**, p. 116925.

[282] Hassan, E. M., Steele, P. H., and Ingram, L., 2009, "Characterization of Fast Pyrolysis Bio-Oils Produced from Pretreated Pine Wood," Appl Biochem Biotechnol, **154**(1–3), pp. 3–13.

[283] Kang, B.-S., Lee, K. H., Park, H. J., Park, Y.-K., and Kim, J.-S., 2006, "Fast Pyrolysis of Radiata Pine in a Bench Scale Plant with a Fluidized Bed: Influence of a Char Separation System and Reaction Conditions on the Production of Bio-Oil," Journal of Analytical and Applied Pyrolysis, **76**(1–2), pp. 32–37.

[284] Hu, B., Lu, Q., Jiang, X., Liu, J., Cui, M., Dong, C., and Yang, Y., 2019, "Formation Mechanism of Hydroxyacetone in Glucose Pyrolysis: A Combined Experimental and Theoretical Study," Proceedings of the Combustion Institute, **37**(3), pp. 2741–2748.

[285] Pham, T. N., Sooknoi, T., Crossley, S. P., and Resasco, D. E., 2013, "Ketonization of Carboxylic Acids: Mechanisms, Catalysts, and Implications for Biomass Conversion," ACS Catal., **3**(11), pp. 2456–2473.

[286] Hu, B., Zhang, Z., Xie, W., Liu, J., Li, Y., Zhang, W., Fu, H., and Lu, Q., 2022, "Advances on the Fast Pyrolysis of Biomass for the Selective Preparation of Phenolic Compounds," Fuel Processing Technology, **237**, p. 107465.

[287] Horne, P. A., Nugranad, N., and Williams, P. T., 1995, "Catalytic Coprocessing of Biomass-Derived Pyrolysis Vapours and Methanol," Journal of Analytical and Applied Pyrolysis, **34**(1), pp. 87–108.

[288] Kim, J.-S., and Park, K.-B., 2020, "Production of Phenols by Lignocellulosic Biomass Pyrolysis," *Production of Biofuels and Chemicals with Pyrolysis*, Z. Fang, R.L. Smith Jr, and L. Xu, eds., Springer, Singapore, pp. 289–319.

[289] Kim, J.-S., 2015, "Production, Separation and Applications of Phenolic-Rich Bio-Oil – A Review," Bioresource Technology, **178**, pp. 90–98.

[290] Grioui, N., Halouani, K., and Agblevor, F. A., 2014, "Bio-Oil from Pyrolysis of Tunisian Almond Shell: Comparative Study and Investigation of Aging Effect during Long Storage," Energy for Sustainable Development, **21**, pp. 100–112.

[291] Zhang, Q., Chang, J., Wang, and Xu, Y., 2006, "Upgrading Bio-Oil over Different Solid Catalysts," Energy Fuels, **20**(6), pp. 2717–2720.

[292] Liu, Y., Lotero, E., and Goodwin, J. G., 2006, "A Comparison of the Esterification of Acetic Acid with Methanol Using Heterogeneous versus Homogeneous Acid Catalysis," Journal of Catalysis, **242**(2), pp. 278–286.

[293] Xu, F., Xu, Y., Lu, R., Sheng, G.-P., and Yu, H.-Q., 2011, "Elucidation of the Thermal Deterioration Mechanism of Bio-Oil Pyrolyzed from Rice Husk Using Fourier Transform Infrared Spectroscopy," J. Agric. Food Chem., **59**(17), pp. 9243–9249.

[294] Chen, H., Ferrari, C., Angiuli, M., Yao, J., Raspi, C., and Bramanti, E., 2010, "Qualitative and Quantitative Analysis of Wood Samples by Fourier Transform Infrared Spectroscopy and Multivariate Analysis," Carbohydrate Polymers, **82**(3), pp. 772–778.

[295] NOAA, 2019, "Carbon Dioxide Levels in Atmosphere Hit Record High in May" [Online]. Available: https://www.noaa.gov/news/carbon-dioxide-levels-in-atmosphere-hit-record-high-in-may.

[296] Belmonte, B. A., Benjamin, M. F. D., and Tan, R. R., 2018, "Bi-Objective Optimization of Biochar-Based Carbon Management Networks," Journal of Cleaner Production, **188**, pp. 911–920.

[297] Kleiner, K., 2009, "The Bright Prospect of Biochar," Nature Clim Change, **1**(906), pp. 72–74.

[298] Lee, J., Yang, X., Cho, S.-H., Kim, J.-K., Lee, S. S., Tsang, D. C., Ok, Y. S., and Kwon, E. E., 2017, "Pyrolysis Process of Agricultural Waste Using CO2 for Waste Management, Energy Recovery, and Biochar Fabrication," Applied energy, **185**, pp. 214–222.

[299] Uchimiya, M., Lima, I. M., Klasson, K. T., and Wartelle, L. H., 2010, "Contaminant Immobilization and Nutrient Release by Biochar Soil Amendment: Roles of Natural Organic Matter," Chemosphere, **80**(8), pp. 935–940.

[300] Lian, F., and Xing, B., 2017, "Black Carbon (Biochar) In Water/Soil Environments: Molecular Structure, Sorption, Stability, and Potential Risk," Environ. Sci. Technol., **51**(23), pp. 13517–13532.

[301] Leng, L., and Huang, H., 2018, "An Overview of the Effect of Pyrolysis Process Parameters on Biochar Stability," Bioresource Technology, **270**, pp. 627–642.

[302] Biederman, L. A., and Harpole, W. S., 2012, "Biochar and Its Effects on Plant Productivity and Nutrient Cycling: A Meta-Analysis," GCB Bioenergy, **5**(2), pp. 202–214.

[303] Yao, Y., Gao, B., Chen, J., and Yang, L., 2013, "Engineered Biochar Reclaiming Phosphate from Aqueous Solutions: Mechanisms and Potential Application as a Slow-Release Fertilizer," Environmental science & technology, **47**(15), pp. 8700–8708.

[304] Agegnehu, G., Nelson, P. N., and Bird, M. I., 2016, "Crop Yield, Plant Nutrient Uptake and Soil Physicochemical Properties under Organic Soil Amendments and Nitrogen Fertilization on Nitisols," Soil and Tillage Research, **160**, pp. 1–13.

[305] Hayyat, A., Javed, M., Rasheed, I., Ali, S., Shahid, M. J., Rizwan, M., Javed, M. T., and Ali, Q., 2016, "Role of Biochar in Remediating Heavy Metals in Soil," *Phytoremediation,* Springer, pp. 421–437.

[306] Santos, F. M., and Pires, J. C., 2018, "Nutrient Recovery from Wastewaters by Microalgae and Its Potential Application as Bio-Char," Bioresource technology, **267**, pp. 725–731.

[307] Achim Gerlach and Hans-Peter Schmidt, 2012, "The Use of Biochar in Cattle Farming."

[308] Tan, X., Liu, S., Liu, Y., Gu, Y., Zeng, G., Hu, X., Wang, X., Liu, S., and Jiang, L., 2017, "Biochar as Potential Sustainable Precursors for Activated Carbon Production: Multiple Applications in Environmental Protection and Energy Storage," Bioresource Technology, **227**, pp. 359–372.

[309] Cha, J. S., Park, S. H., Jung, S.-C., Ryu, C., Jeon, J.-K., Shin, M.-C., and Park, Y.-K., 2016, "Production and Utilization of Biochar: A Review," Journal of Industrial and Engineering Chemistry, **40**, pp. 1–15.

[310] Ali, I., 2014, "Water Treatment by Adsorption Columns: Evaluation at Ground Level," Separation & Purification Reviews, **43**(3), pp. 175–205.

[311] Jeffery, S., Verheijen, F. G. A., van der Velde, M., and Bastos, A. C., 2011, "A Quantitative Review of the Effects of Biochar Application to Soils on Crop Productivity Using Meta-Analysis," Agriculture, Ecosystems & Environment, **144**(1), pp. 175–187.

[312] Hersh, B., Mirkouei, A., Sessions, J., Rezaie, B., and You, Y., 2019, "A Review and Future Directions on Enhancing Sustainability Benefits across Food-Energy-Water Systems: The Potential Role of Biochar-Derived Products," AIMS Environmental Science, **6**(5), p. 379.

[313] Hansen, S., and Mirkouei, A., 2018, "Past Infrastructures and Future Machine Intelligence (MI) for Biofuel Production: A Review and MI-Based Framework," American Society of Mechanical Engineers. DOI: 10.1115/DETC2018-86150.

[314] Delaney, M., 2015, *Northwest Biochar Commercialization Strategy Paper*, U.S. Forest Service and the Oregon Department of Forestry.

[315] Sessions, J., Smith, D., Trippe, K. M., Fried, J. S., Bailey, J. D., Petitmermet, J. H., Hollamon, W., Phillips, C. L., and Campbell, J. D., 2019, "Can Biochar Link Forest Restoration with Commercial Agriculture?," Biomass and Bioenergy, **123**, pp. 175–185.

[316] Wrobel-Tobiszewska, A., Boersma, M., Sargison, J., Adams, P., and Jarick, S., 2015, "An Economic Analysis of Biochar Production Using Residues from Eucalypt Plantations," Biomass and Bioenergy, **81**, pp. 177–182.

[317] Mohammadi, A., Cowie, A. L., Cacho, O., Kristiansen, P., Anh Mai, T. L., and Joseph, S., 2017, "Biochar Addition in Rice Farming Systems: Economic and Energy Benefits," Energy, **140**, pp. 415–425.

[318] GVR, 2017, "Biochar Market Size" [Online]. Available: https://www.marketwatch.com/press-release/biochar-market-size-worth-31461-million-by-2025-cagr-132-grand-view-research-inc-2018-05-30.

[319] Rosas, J. G., Gómez, N., Cara, J., Ubalde, J., Sort, X., and Sánchez, M. E., 2015, "Assessment of Sustainable Biochar Production for Carbon Abatement from Vineyard Residues," Journal of Analytical and Applied Pyrolysis, **113**, pp. 239–247.

[320] Panwar, N. L., Pawar, A., and Salvi, B. L., 2019, "Comprehensive Review on Production and Utilization of Biochar," SN Appl. Sci., **1**(2), p. 168.

[321] Huang, Y., Anderson, M., McIlveen-Wright, D., Lyons, G. A., McRoberts, W. C., Wang, Y. D., Roskilly, A. P., and Hewitt, N. J., 2015, "Biochar and Renewable Energy Generation from Poultry Litter Waste: A Technical and Economic Analysis Based on Computational Simulations," Applied Energy, **160**, pp. 656–663.

[322] Shabangu, S., Woolf, D., Fisher, E. M., Angenent, L. T., and Lehmann, J., 2014, "Techno-Economic Assessment of Biomass Slow Pyrolysis into Different Biochar and Methanol Concepts," Fuel, **117**, pp. 742–748.

[323] Patel, S., Kundu, S., Paz-Ferreiro, J., Surapaneni, A., Fouche, L., Halder, P., Setiawan, A., and Shah, K., 2019, "Transformation of Biosolids to Biochar: A Case Study," Environmental Progress & Sustainable Energy, **38**(4), p. 13113.

[324] Sahoo, K., Bilek, E., Bergman, R., and Mani, S., 2019, "Techno-Economic Analysis of Producing Solid Biofuels and Biochar from Forest Residues Using Portable Systems," Applied Energy, **235**, pp. 578–590.

[325] Mirkouei, A., Haapala, K. R., Sessions, J., and Murthy, G. S., 2017, "A Review and Future Directions in Techno-Economic Modeling and Optimization of Upstream Forest Biomass to Bio-Oil Supply Chains," Renewable and Sustainable Energy Reviews, **67**, pp. 15–35.

[326] Oldfield, T. L., Sikirica, N., Mondini, C., López, G., Kuikman, P. J., and Holden, N. M., 2018, "Biochar, Compost and Biochar-Compost Blend as Options to Recover Nutrients and Sequester Carbon," Journal of environmental management, **218**, pp. 465–476.

[327] Mirkouei, A., Haapala, K. R., Sessions, J., and Murthy, G. S., 2016, "Reducing Greenhouse Gas Emissions for Sustainable Bio-Oil Production Using a Mixed Supply Chain," *ASME 2016 International Design Engineering Technical Conferences and Computers and Information in Engineering Conference*, American Society of Mechanical Engineers, p. V004T05A031.

[328] Azzi, E. S., Karltun, E., and Sundberg, C., 2019, "Prospective Life Cycle Assessment of Large-Scale Biochar Production and Use for Negative Emissions in Stockholm," Environ. Sci. Technol., **53**(14), pp. 8466–8476.

[329] Thers, H., Djomo, S. N., Elsgaard, L., and Knudsen, M. T., 2019, "Biochar Potentially Mitigates Greenhouse Gas Emissions from Cultivation of Oilseed Rape for Biodiesel," Science of The Total Environment, **671**, pp. 180–188.

[330] Li, W., Dumortier, J., Dokoohaki, H., Miguez, F. E., Brown, R. C., Laird, D., and Wright, M. M., 2019, "Regional Techno-Economic and Life-Cycle Analysis of the Pyrolysis-Bioenergy-Biochar Platform for Carbon-Negative Energy," Biofuels, Bioproducts and Biorefining.

[331] Rajabi Hamedani, S., Kuppens, T., Malina, R., Bocci, E., Colantoni, A., and Villarini, M., 2019, "Life Cycle Assessment and Environmental Valuation of Biochar Production: Two Case Studies in Belgium," Energies, **12**(11), p. 2166.

[332] El Hanandeh, A., 2013, "Carbon Abatement via Treating the Solid Waste from the Australian Olive Industry in Mobile Pyrolysis Units: LCA with Uncertainty Analysis," Waste Management & Research, **31**(4), pp. 341–352.

[333] Bushell, A., 2018, "A Pricing Model And Environmental Impact Analysis For Manure-Based Biochar As A Soil Amendment," PhD Thesis, Duke University.

[334] Mau, V., and Gross, A., 2018, "Energy Conversion and Gas Emissions from Production and Combustion of Poultry-Litter-Derived Hydrochar and Biochar," Applied Energy, **213**, pp. 510–519.

[335] Dodds, W. K., Bouska, W. W., Eitzmann, J. L., Pilger, T. J., Pitts, K. L., Riley, A. J., Schloesser, J. T., and Thornbrugh, D. J., 2009, "Eutrophication of U.S. Freshwaters: Analysis of Potential Economic Damages," Environ. Sci. Technol., **43**(1), pp. 12–19.

[336] Lysyk, T. J., Easton, E. R., and Evenson, P. D., 1985, “Seasonal Changes in Nitrogen and Moisture Content of Cattle Manure in Cool-Season Pastures,” Journal of Range Management, **38**(3), p. 251.

[337] Augustin, C., and Rahman, S., 2010, “Composting Animal Manures: A Guide to the Process and Management of Animal Manure Compost.”

[338] Choudhury, H. A., Chakma, S., and Moholkar, V. S., 2015, “Biomass Gasification Integrated Fischer-Tropsch Synthesis,” *Recent Advances in Thermo-Chemical Conversion of Biomass*, Elsevier, pp. 383–435.

[339] Brinker, R. W., Miller, D., Stokes, B. J., and Lanford, B. L., 2002, “Machine Rates for Selected Forest Harvesting Machines,” Circular 296 (revised). Alabama Agric. Exp. Station, Auburn University.

[340] U.S. Bureau of Labor Statistics, 1985, “Producer Price Index by Commodity for Machinery and Equipment: Engineering and Scientific Instruments,” FRED, Federal Reserve Bank of St. Louis [Online]. Available: https://fred.stlouisfed.org/series/WPU1185. [Accessed: 07-Nov-2019].

[341] Manyà, J. J., 2012, “Pyrolysis for Biochar Purposes: A Review to Establish Current Knowledge Gaps and Research Needs,” Environ. Sci. Technol., **46**(15), pp. 7939–7954.

[342] Jeff Lorimor, Wendy Powers, and Al Sutton, 2004, “Manure Characterisitics.”

[343] Brewer, C. E., Schmidt-Rohr, K., Satrio, J. A., and Brown, R. C., 2009, “Characterization of Biochar from Fast Pyrolysis and Gasification Systems,” Environmental Progress & Sustainable Energy, **28**(3), pp. 386–396.

[344] Enders, A., Hanley, K., Whitman, T., Joseph, S., and Lehmann, J., 2012, “Characterization of Biochars to Evaluate Recalcitrance and Agronomic Performance,” Bioresource Technology, **114**, pp. 644–653.

[345] Eghball, B., Power, J. F., Gilley, J. E., and Doran, J. W., 1997, “Nutrient, Carbon, and Mass Loss during Composting of Beef Cattle Feedlot Manure,” Journal of Environment Quality, **26**(1), p. 189.

[346] Sandars, D. L., Audsley, E., Cañete, C., Cumby, T. R., Scotford, I. M., and Williams, A. G., 2003, “Environmental Benefits of Livestock Manure Management Practices and Technology by Life Cycle Assessment,” Biosystems Engineering, **84**(3), pp. 267–281.

[347] Aguirre-Villegas, H., Larson, R. A., and Ruark, M. D., 2016, “Methane Emissions from Dairy Cattle: An Overview,” p. 5.

[348] Cantrell, K. B., Hunt, P. G., Uchimiya, M., Novak, J. M., and Ro, K. S., 2012, “Impact of Pyrolysis Temperature and Manure Source on Physicochemical Characteristics of Biochar,” Bioresource Technology, **107**, pp. 419–428.

[349] IPCC, 2007, *2.10.2 Direct Global Warming Potentials - AR4 WGI Chapter 2: Changes in Atmospheric Constituents and in Radiative Forcing*.

[350] OpenLCA, 2019, “The Source for LCA Datasets” [Online]. Available: https://nexus.openlca.org/database/Agribalyse. [Accessed: 25-Nov-2019].

[351] USDA, 2019, “National Agricultural Statistics Service” [Online]. Available: https://www.nass.usda.gov/Statistics_by_State/Idaho/Publications/Livestock_Press_Releases/2019/CE_CAT.pdf.

[352] USDA, 2019, “Animal Manure Management” [Online]. Available: https://www.nrcs.usda.gov/wps/portal/nrcs/detail/null/?cid=nrcs143_014211.

[353] USDA, 2019, “Milk Production” [Online]. Available: https://www.nass.usda.gov/Publications/Todays_Reports/reports/mkpr0419.pdf. [Accessed: 04-Feb-2020].

[354] Idaho State Department of Agriculture, 2017, “Idaho Livestock” [Online]. Available: https://agri.idaho.gov/main/idaho-livestock/. [Accessed: 04-Feb-2020].

[355] Lauer, M., Hansen, J. K., Lamers, P., and Thrän, D., 2018, “Making Money from Waste: The Economic Viability of Producing Biogas and Biomethane in the Idaho Dairy Industry,” Applied Energy, **222**, pp. 621–636.

[356] Zamora-Cristales, R., Sessions, J., Murphy, G., and Boston, K., 2013, “Economic Impact of Truck–Machine Interference in Forest Biomass Recovery Operations on Steep Terrain,” Forest Products Journal, **63**(5–6), pp. 162–173.

[357] Anderson, N., Chung, W., Loeffler, D., and Jones, J. G., 2012, “A Productivity and Cost Comparison of Two Systems for Producing Biomass Fuel from Roadside Forest Treatment Residues,” Forest Products Journal, **62**(3), pp. 222–233.

[358] J. Zhou, 2011, “Case Study: Thermal Design of a Biomass Drying Process Using Low Grade Heat from Steel Industry.”

[359] IBI, 2015, “Standardized Product Definition and Product Testing Guidelines for Biochar That Is Used in Soil.”

[360] Hans-Peter Schmidt, 2015, “European Biochar Certificate (EBC) - Guidelines Version 6.1.”

[361] Joseph, S., Lehmann, J., and Earthscan from Routledge, 2015, *Biochar for Environmental Management : Science, Technology and Implementation*, Routledge, London.

[362] Uzoma, K. C., Inoue, M., Andry, H., Fujimaki, H., Zahoor, A., and Nishihara, E., 2011, “Effect of Cow Manure Biochar on Maize Productivity under Sandy Soil Condition,” Soil Use and Management, **27**(2), pp. 205–212.

[363] Cao, X., and Harris, W., 2010, “Properties of Dairy-Manure-Derived Biochar Pertinent to Its Potential Use in Remediation,” Bioresource Technology, **101**(14), pp. 5222–5228.

[364] Atienza-Martínez, M., Ábrego, J., Gea, G., and Marías, F., 2020, “Pyrolysis of Dairy Cattle Manure: Evolution of Char Characteristics,” Journal of Analytical and Applied Pyrolysis, **145**, p. 104724.

[365] Tsai, W.-T., Hsu, C.-H., and Lin, Y.-Q., 2019, “Highly Porous and Nutrients-Rich Biochar Derived from Dairy Cattle Manure and Its Potential for Removal of Cationic Compound from Water,” Agriculture, **9**(6), p. 114.

[366] Sokhansanj, S., and Webb, E., 2016, “Evaluating Industrial Drying of Cellulosic Feedstock for Bioenergy: A Systems Approach,” Biofuels, Bioproducts and Biorefining, **10**(1), pp. 47–55.

[367] Solarte-Toro, J. C., Chacón-Pérez, Y., and Cardona-Alzate, C. A., 2018, “Evaluation of Biogas and Syngas as Energy Vectors for Heat and Power Generation Using Lignocellulosic Biomass as Raw Material,” Electronic Journal of Biotechnology, **33**, pp. 52–62.

[368] U.S. EIA, 2020, “State Electricity Profiles” [Online]. Available: https://www.eia.gov/electricity/state/idaho/.

[369] Flint, B. R., 2013, “Analysis and Operational Considerations of Biomass Extraction on Steep Terrain in Western Oregon.”

[370] Zamora-Cristales, R., and Sessions, J., 2016, “Modeling Harvest Forest Residue Collection for Bioenergy Production,” Journal of Forest Engineering.

[371] Sorenson, C. B., 2010, "A Comparative Financial Analysis of Fast Pyrolysis Plants in Southwest Oregon," The University of Montana Missoula, MT.

[372] Brown, T. R., Wright, M. M., and Brown, R. C., 2011, "Estimating Profitability of Two Biochar Production Scenarios: Slow Pyrolysis vs Fast Pyrolysis," Biofuels, Bioproducts and Biorefining, **5**(1), pp. 54–68.

[373] Aguirre-Villegas, H. A., and Larson, R. A., 2017, "Evaluating Greenhouse Gas Emissions from Dairy Manure Management Practices Using Survey Data and Lifecycle Tools," Journal of Cleaner Production, **143**, pp. 169–179.

[374] Pattey, E., Trzcinski, M. K., and Desjardins, R. L., 2005, "Quantifying the Reduction of Greenhouse Gas Emissions as a Resultof Composting Dairy and Beef Cattle Manure," Nutrient Cycling in Agroecosystems, **72**(2), pp. 173–187.

[375] Ebner, J. H., Labatut, R. A., Rankin, M. J., Pronto, J. L., Gooch, C. A., Williamson, A. A., and Trabold, T. A., 2015, "Lifecycle Greenhouse Gas Analysis of an Anaerobic Codigestion Facility Processing Dairy Manure and Industrial Food Waste," Environ. Sci. Technol., **49**(18), pp. 11199–11208.

[376] He, Z., Pagliari, P. H., and Waldrip, H. M., 2016, "Applied and Environmental Chemistry of Animal Manure: A Review," Pedosphere, **26**(6), pp. 779–816.

[377] Girotto, F., and Cossu, R., 2017, "Animal Waste: Opportunities and Challenges," *Sustainable Agriculture Reviews*, E. Lichtfouse, ed., Springer International Publishing, Cham, pp. 1–13.

[378] Laird, D., 2009, "Farm," Biochar Farms.

[379] Xu, M., Gao, P., Yang, Z., Su, L., Wu, J., Yang, G., Zhang, X., Ma, J., Peng, H., and Xiao, Y., 2019, "Biochar Impacts on Phosphorus Cycling in Rice Ecosystem," Chemosphere, **225**, pp. 311–319.

[380] Pourhashem, G., Hung, S. Y., Medlock, K. B., and Masiello, C. A., 2019, "Policy Support for Biochar: Review and Recommendations," GCB Bioenergy, **11**(2), pp. 364–380.

Appendices

Appendix A. Compounds identified by GC-MS in bio-oil samples from hybrid poplar, pine, maple, and Sugarcane bagasse produced at 550°C

Compound Name	M^+	Formula	Apex RT (min)	Hybrid Poplar	Pine	Maple	Sugarcane Bagasse
				(µg/mg)			
Propanoic acid	74	$C_3H_6O_2$	3.09	0.81	-	0.49	-
Propanal, 2,3-dihydroxy-, (S)-	90	$C_3H_6O_3$	3.13	0.31	0.35	0.29	0.29
Ethyl-1-propenyl ether	86	$C_5H_{10}O$	3.32	-	-	0.21	0.12
Diethylene glycol	106	$C_4H_{10}O_3$	3.36	0.60	0.38	0.23	0.24
Acetic acid	60	$C_2H_4O_2$	3.67	6.26	4.44	4.92	5.57
3-Penten-2-one, (E)-	84	C_5H_8O	3.84	-	0.24	0.11	0.25
2,2'-Bioxirane	86	$C_4H_6O_2$	4.06	-	-	0.45	0.29
2,2-Dimethoxybutane	118	$C_6H_{14}O_2$	4.17	-	-	0.08	-
1-Hydroxy-2-butanone	88	$C_4H_8O_2$	4.35	0.95	0.67	0.92	0.83
Propanal-2-one	72	$C_3H_4O_2$	4.41	2.10	0.88	2.55	0.34
Succindialdehyde	86	$C_4H_6O_2$	4.66	2.15	0.76	0.35	-
Butanal, 3-methyl-	86	$C_5H_{10}O$	4.83	6.28	1.06	5.18	1.42
3-Furaldehyde	96	$C_5H_4O_2$	5.34	0.33	0.28	0.26	0.23
Isocrotonic acid	86	$C_4H_6O_2$	5.62	-	-	-	0.31
Hydroxyacetaldehyde	60	$C_2H_4O_2$	5.75	1.32	0.91	1.06	1.18
Furfural	96	$C_5H_4O_2$	5.82	3.57	3.62	3.77	3.22
2-Furfuryl alcohol	98	$C_5H_6O_2$	6.38	0.33	0.47	0.24	0.42

Appendix A. continued

2-Butanone	72	C_4H_8O	6.46	0.97	0.92	0.39	0.64
2,3-Butanedione	86	$C_4H_6O_2$	6.74	1.04	1.00	0.98	1.30
Furan,tetrahydro-2,5 dimethoxy-	132	$C_6H_{12}O_3$	7.03	0.33	0.30	0.16	0.16
Styrene	104	C_8H_8	7.28	-	0.28	-	-
Tetrahydro-4-methyl-3-furanone	100	$C_5H_8O_2$	7.61	0.42	0.21	0.13	-
3-Hexanol	102	$C_6H_{14}O$	7.45	-	-	0.23	0.44
2-Cyclopenten-1-one, 2-methyl-	96	C_6H_8O	7.74	0.41	0.50	0.25	0.30
2-Acetylfuran	110	$C_6H_6O_2$	7.88	0.48	0.33	0.26	0.34
2(5H)-Furanone	84	$C_4H_4O_2$	8.03	2.83	2.43	1.98	2.38
Methoxy-dihydrofuran	100	$C_5H_8O_2$	8.11	0.80	0.58	0.75	0.64
2-Cyclopenten-1-one, 2-hydroxy-	98	$C_5H_6O_2$	8.25	0.54	1.81	0.55	0.71
2(5H)-Furanone, 5-methyl-	98	$C_5H_6O_2$	8.73	0.48	0.43	0.24	0.20
Benzaldehyde	106	C_7H_6O	9.2	0.32	0.17	0.19	0.12
Phenylglyoxal	105	$C_8H_6O_2$	9.32	-	0.45	0.28	0.10
2-Furancarboxaldehyde, 5-methyl-	110	$C_6H_6O_2$	9.4	0.81	0.64	1.05	0.67
5-Methylfurfural	110	$C_6H_6O_2$	9.45	0.72	0.43	0.37	0.41
1-Hexanol	102	$C_6H_{14}O$	9.61	-	-	0.10	0.11
Hexanoic acid	116	$C_6H_{12}O_2$	9.82	-	0.35	0.22	0.12
Phenol	94	C_6H_6O	9.94	11.52	1.36	0.12	1.88

Appendix A. continued

2H-Pyran-2,6(3H)-dione	112	$C_5H_4O_3$	10.33	-	-	0.20	0.14
Cyclohexanone, 4-methylidene-	110	$C_7H_{10}O$	10.45	0.39	0.52	0.67	0.97
Ethanone, 1-cyclopentyl-	112	$C_7H_{12}O$	10.55	0.17	0.29	0.10	-
Methyl-dihydro-(2H)-pyran-2-one	112	$C_6H_8O_2$	10.89	0.16	0.35	0.24	0.22
1,2-Cyclopentanedione, 3-methyl-	112	$C_6H_8O_2$	11.28	1.85	1.30	0.91	1.15
2-Cyclopenten-1-one, 2,3-dimethyl-	110	$C_7H_{10}O$	11.65	0.14	0.17	0.15	0.14
1,3-Dioxolane, 2-ethyl-	102	$C_5H_{10}O_2$	11.82	0.84	0.85	0.13	0.36
4-Methyl-5H-furan-2-one	98	$C_5H_6O_2$	11.88	0.25	0.45	0.28	0.41
Phenol, 2-methyl-	108	C_7H_8O	12.11	0.73	0.86	0.23	0.45
2(3H)-Furanone, 5-acetyldihydro-	128	$C_6H_8O_3$	12.26	0.46	0.37	0.32	0.48
Methyl phenyl ketone	120	C_8H_8O	12.48	-	0.26	0.21	-
Phenol, 3-methyl-	108	C_7H_8O	12.75	0.59	1.01	0.28	0.83
Phenol, 2-methoxy-	124	$C_7H_8O_2$	13.17	2.31	2.78	1.44	1.74
Tetrahydro-3-furanmethanol	102	$C_5H_{10}O_2$	13.38	0.72	-	0.25	0.46
Octanal	128	$C_8H_{16}O$	13.41	-	-	0.41	-
1.5-Anhydro-arabinofuranose	132	$C_5H_8O_4$	13.55	-	0.29	-	-
Maltol	126	$C_6H_6O_3$	13.88	0.57	0.45	0.27	0.27
2-Cyclopenten-1-one,3-ethyl-2 hydroxy-	126	$C_7H_{10}O_2$	14.02	0.40	0.20	0.13	0.22

Appendix A. continued

Furan, tetrahydro-2,5-dimethoxy-	132	$C_6H_{12}O_3$	14.3	0.32	0.32	0.13	0.11
2,3-Dimethylphenol	122	$C_8H_{10}O$	14.87	-	0.69	0.11	0.10
2-Hydroxy-3-methylbenzaldehyde	136	$C_8H_8O_2$	15.14	-	0.28	-	-
Benzoic acid	122	$C_7H_6O_2$	15.28	0.61	-	-	-
2,3-Dihydroxybenzaldehyde	138	$C_7H_6O_3$	15.41	0.59	0.67	0.48	1.51
3-Ethylphenol	122	$C_8H_{10}O$	15.47	-	0.37	-	-
Benzene, 1,2,3-trichloro-	180	$C_6H_3C_{l3}$	15.74	7.56	5.84	5.89	4.97
Creosol	138	$C_8H_{10}O_2$	16.19	1.23	2.60	0.98	0.88
Catechol	110	$C_6H_6O_2$	16.37	1.46	1.94	0.94	0.80
1,4:3,6-Dianhydro-α-d glucopyranose	144	$C_6H_8O_4$	16.71	0.39	-	0.18	0.28
2(3H)-Furanone,dihydro-4,4-dimethyl-	114	$C_6H_{10}O_2$	17.04	0.19	-	-	2.60
2,3-Anhydro-d-mannosan	144	$C_6H_8O_4$	17.2	0.22	-	0.42	0.09
5-Hydroxymethylfurfural	126	$C_6H_6O_3$	17.3	0.21	0.53	0.34	0.08
6-Hydroxy-9-oxa-bicyclo[3.3.1]nonan-3-one	156	$C_8H_{12}O_3$	17.82	0.16	0.40	0.14	0.13
1,2-Benzenediol, 3-methoxy-	140	$C_7H_8O_3$	18.15	1.61	0.58	0.83	1.24
2-Methyl-5-hydroxybenzofuran	148	$C_9H_8O_2$	18.29	-	0.23	-	-
Phenol, 4-ethyl-2-methoxy-	152	$C_9H_{12}O_2$	18.62	1.37	0.90	0.65	0.64

Appendix A. continued

1,2-Benzenediol, 4-methyl-	124	$C_7H_8O_2$	18.92	0.38	1.62	0.34	0.12
Benzaldehyde, 4-hydroxy-	122	$C_7H_6O_2$	19.43	0.44	0.33	0.37	0.35
2-Methoxy-4-vinylphenol	150	$C_9H_{10}O_2$	19.59	0.21	0.34	-	0.75
2-Ethylbenzaldehyde	134	$C_9H_{10}O$	20.28	-	0.16	-	-
Phenol, 2,6-dimethoxy-	154	$C_8H_{10}O_3$	20.6	3.90	0.67	2.18	2.22
Eugenol	164	$C_{10}H_{12}O_2$	20.74	0.96	1.05	0.80	0.65
Phenol, 2-methoxy-4-propyl-	166	$C_{10}H_{14}O_2$	20.99	0.38	0.36	0.20	-
1,3-Benzenediol, 4-ethyl-	138	$C_8H_{10}O_2$	21.41	0.38	1.05	-	0.70
Vanillin	152	$C_8H_8O_3$	21.88	1.71	2.43	1.86	2.01
Isoeugenol	164	$C_{10}H_{12}O_2$	22.07	0.50	0.72	0.43	0.37
3,5-Dimethoxy-4-hydroxytoluene	168	$C_9H_{12}O_3$	23.06	1.42	2.80	1.28	0.85
trans-Isoeugenol	164	$C_{10}H_{12}O_2$	23.12	0.79	4.48	0.73	1.23
Phenol, 2-methoxy-4-propyl-	166	$C_{10}H_{14}O_2$	23.4	0.47	1.20	0.47	0.22
Levoglucosan	162	$C_6H_{10}O_5$	24.07	6.42	13.20	6.61	7.17
Benzoic acid, 4-hydroxy-	138	$C_7H_6O_3$	24.58	1.40	-	-	-
5-tert-Butylpyrogallol	182	$C_{10}H_{14}O_3$	25.01	0.34	0.27	0.40	0.17
2-Propanone,1-(4-hydroxy-3-methoxyphenyl)-	180	$C_{10}H_{12}O_3$	25.16	0.43	0.53	0.34	0.30
4-(2,5-Dimethylphenyl)butanoic acid	192	$C_{12}H_{16}O_2$	25.8	-	0.22	-	-

Appendix A. continued

Phenol, 4-ethenyl-2,6-dimethoxy-	180	$C_{10}H_{12}O_3$	25.94	0.69	0.61	0.50	0.43
4-(1-Hydroxyallyl)-2methoxyphenol	180	$C_{10}H_{12}O_3$	26.19	-	0.41	0.36	-
1-(4-Hydroxy-3-methoxyphenyl)propan-1-one	180	$C_{10}H_{12}O_3$	26.37	-	0.43	-	-
Phenol,2,6-dimethoxy-4-(2-propenyl)-	194	$C_{11}H_{14}O_3$	26.81	1.26	0.20	1.20	0.77
Homovanillic acid	182	$C_9H_{10}O_4$	27.47	-	1.03	1.44	0.74
Dihydroconiferyl alcohol	182	$C_{10}H_{14}O_3$	27.87	-	0.67	-	-
Syringol,4-propenyl(cis)	194	$C_{11}H_{14}O_3$	27.93	0.65	-	0.80	0.39
Syringaldehyde	182	$C_9H_{10}O_4$	28.17	2.15	1.15	2.99	0.97
Coniferyl alcohol	180	$C_{10}H_{12}O_3$	28.38	0.40	0.68	0.30	0.20
1,7-di-iso-propylnaphthalene	212	C16H20	28.65	-	-	-	0.10
Syringol-4-Propenyl(trans)	194	$C_{11}H_{14}O_3$	29.02	1.22	0.28	1.09	1.17
Homosyringaldehyde	196	$C_{10}H_{12}O_4$	29.15	0.71	0.16	1.07	0.19
Acetosyringone	196	$C_{10}H_{12}O_4$	29.77	2.30	2.93	3.08	0.08
Syringylacetone	210	$C_{11}H_{14}O_4$	30.58	0.78	0.24	0.97	-
trans-Sinapyl alcohol	210	$C_{11}H_{14}O_4$	31.56	0.41	0.46	0.55	0.12
1-Propanone, 1-(4-hydroxy-3,5-dimethoxyphenyl)-	210	$C_{11}H_{14}O_4$	31.69	0.29	-	0.31	0.20
5-(3-Hydroxypropyl)-2,3-dimethoxyphenol	212	$C_{11}H_{16}O_4$	33.04	0.22	-	-	-

Appendix A. continued

Pentadecanoic acid	242	$C_{15}H_{30}O_2$	33.51	0.36	-	0.61	0.27
Palmitic acid	256	$C_{16}H_{32}O_2$	34.15	0.67	0.34	0.33	0.96
trans-Sinapaldehyde	208	$C_{11}H_{12}O_4$	34.81	1.62	0.23	2.59	0.62
cis-Sinapyl alcohol	210	$C_{11}H_{14}O_4$	35	0.30	-	0.37	0.20
Oleic Acid	282	$C_{18}H_{34}O_2$	37.46	-	0.95	0.21	0.56
Normetadrenaline	183	$C_9H_{13}NO_3$	39.51	0.18	-	-	-
4'-Methoxy-2-hydroxystilbene	226	$C_{15}H_{14}O_2$	40.52	-	1.03	0.17	-
5-Hydroxy-7-methoxyflavanone	270	$C_{16}H_{14}O_4$	42.11	-	1.17	-	-
5,7-Dimethoxyflavanone	284	$C_{17}H_{16}O_4$	43.74	-	0.58	-	-
Pentadecanal-	226	$C_{15}H_{30}O$	43.99	-		-	0.33
Flavokawain b	284	$C_{17}H_{16}O_4$	44.89	-	0.57	-	-
Tectochrysin	268	$C_{16}H_{12}O_4$	45.39	-	0.88	-	-
(E)-3,3'-Dimethoxy-4,4'-dihydroxystilbene	272	$C_{16}H_{16}O_4$	46.6	0.39	0.59	0.37	0.17

Appendix B. Compounds identified by GC-MS in bio-oil samples produced during in-situ catalytic fast pyrolysis at 550°C

Compound Name	**M^+**	**Formula**	**Apex RT**	**ug/mg**
L-Glyceraldehyde	90	$C_3H_6O_3$	3.54	0.48
Isopropenyl methyl ketone	84	C_5H_8O	3.80	0.04
2-sec-butyl-Cyclopentanone	140	$C_9H_{16}O$	3.98	0.09
Hydroxyacetone	74	$C_3H_6O_2$	4.31	14.52
Succindialdehyde	86	$C_4H_6O_2$	4.54	4.34
Furfural	96	$C_5H_4O_2$	5.63	1.86
2-Furanmethanol	98	$C_5H_6O_2$	6.14	0.15
Butyraldehyde	100	$C_6H_{12}O$	6.24	0.54
Acetol acetate	116	$C_5H_8O_3$	6.52	0.53
Dimethoxytetrahydrofuran	132	$C_6H_{12}O_3$	7.17	1.54
Hexanedial	114	$C_6H_{10}O_2$	7.46	0.14
2(5H)-Furanone	84	$C_4H_4O_2$	7.78	2.69
2-Hydroxycyclopent-2-en-1-one	98	$C_5H_6O_2$	7.95	2.64
6-Hydroxy-hexan-2-one	116	$C_6H_{12}O_2$	8.46	0.07
1,3-Octanediol	146	$C_8H_{18}O_2$	9.07	0.27
(E)-3-Decenol	156	$C_{10}H_{20}O$	9.16	0.55
Phenol	94	C_6H_6O	9.62	0.93
6,8-Dioxabicyclo[3.2.1]octane	114	$C_6H_{10}O_2$	10.12	0.2
3-Methyl-1,2-cyclopentanedione	112	$C_6H_8O_2$	10.95	1.39
3(2H)-Furanone, dihydro-5-isopropyl-	128	$C_7H_{12}O_2$	11.48	0.26
1,6-Anhydro-2,4-dideoxy-β-D-arabo-hexopyranose	130	$C_6H_{10}O_3$	11.59	0.22

Appendix B. continued

o-Cresol	108	C_7H_8O	11.78	0.34
m-Cresol	108	C_7H_8O	12.41	0.41
Guaiacol	124	$C_7H_8O_2$	12.79	2.69
trans-1,2-Cyclopentanediol	102	$C_5H_{10}O_2$	13.03	1.52
4-Methylhexanoic acid	130	$C_7H_{14}O_2$	13.51	0.24
3-Hexanone, 6-methoxy-2-methyl-	144	$C_8H_{16}O_2$	13.92	0.24
p-Xylenol	122	$C_8H_{10}O$	14.54	0.01
α,β-Gluco-octonic acid lactone	238	$C_8H_{14}O_8$	14.62	0.08
3-Ethyl-3-heptanol	144	$C_9H_{20}O$	15.18	0.29
Dodecanal	184	$C_{12}H_{24}O$	15.68	0.6
Creosol	138	$C_8H_{10}O_2$	15.82	2.09
Tetrahydrofuran, 2-methyl-5-pentyl-	156	$C_{10}H_{20}O$	15.94	0.1
Catechol	110	$C_6H_6O_2$	16.09	2.01
1,4:3,6-Dianhydro-α-d-glucopyranose	144	$C_6H_8O_4$	16.37	0.94
3,4-Anhydro-d-galactosan	144	$C_6H_8O_4$	16.83	0.22
5-Hydroxymethylfurfural	126	$C_6H_6O_3$	17.09	0.49
6-Acetyl-β-d-mannose	222	$C_8H_{14}O_7$	17.24	0.13
2-Dodecenoic acid	198	$C_{12}H_{22}O_2$	17.37	0.13
l-Gala-l-ido-octose	240	$C_8H_{16}O_8$	17.92	0.18
p-Ethylguaiacol	152	$C_9H_{12}O_2$	18.23	0.4
4-Methylcatechol	124	$C_7H_8O_2$	18.64	0.79
Vinyl guaiacol	150	$C_9H_{10}O_2$	19.20	0.72
2,3-Bis(acetyloxy)propyl dodecanoate	358	$C_{19}H_{34}O_6$	19.41	0.35

Appendix B. continued

Eugenol	164	$C_{10}H_{12}O_2$	20.34	0.62
Geraniol	154	$C_{10}H_{18}O$	21.18	1.03
Vanillin	152	$C_8H_8O_3$	21.53	1.51
Isoeugenol	164	$C_{10}H_{12}O_2$	21.67	0.21
Erythorbic acid	176	$C_6H_8O_6$	22.04	0.03
trans-Isoeugenol	164	$C_{10}H_{12}O_2$	22.71	2.94
Cerulignol	166	$C_{10}H_{14}O_2$	23.04	0.42
3(2H)-Benzofuranone, 2,6-dimethyl-	162	$C_{10}H_{10}O_2$	23.44	0.26
Levoglucosan	162	$C_6H_{10}O_5$	23.93	6.02
Guaiacylacetone	180	$C_{10}H_{12}O_3$	24.79	0.2
L-Glucose	180	$C_6H_{12}O_6$	24.99	0.28
Coniferyl alcohol	180	$C_{10}H_{12}O_3$	25.84	0.14
2,7-Anhydro-l-galacto-heptulofuranose	192	$C_7H_{12}O_6$	27.06	0.67
Homovanillic acid	182	$C_9H_{10}O_4$	27.51	0.25
Cyclopropanetetradecanoic acid, 2-octyl-, methyl ester	394	$C_{26}H_{50}O_2$	27.71	0.15
Coniferyl aldehyde	178	$C_{10}H_{10}O_3$	29.45	0.7
n-Hexadecanoic acid	256	$C_{16}H_{32}O_2$	33.75	0.35
d-Mannose	180	$C_6H_{12}O_6$	34.15	0.1
Ethyl palmitate	284	$C_{18}H_{36}O_2$	34.38	0.07
Spirost-8-en-11-one, 3-hydroxy-, (3β,5α,14β,20β,22β,25R)-	428	$C_{27}H_{40}O_4$	36.94	0.09
Octadecanoic acid	284	$C_{18}H_{36}O_2$	37.45	0.03
Ethyl stearate	312	$C_{20}H_{40}O_2$	38.01	0.04
Hexanedioic acid, bis(2-ethylhexyl) ester	370	$C_{22}H_{42}O_4$	41.44	1.56

Appendix C. Compounds identified by GC-MS in bio-oil samples produced during ex-situ catalytic fast pyrolysis at 550°C

Compound Name	**M^+**	**Formula**	**Apex RT**	**ug/mg**
Isobutanol	74	$C_4H_{10}O$	3.18	0.07
L-Glyceraldehyde	90	$C_3H_6O_3$	3.55	0.41
Isopropenyl methyl ketone	84	C_5H_8O	3.82	0.07
Acetate, 4-hydroxy-3-methyl-2-butenyl-	144	$C_7H_{12}O_3$	3.99	0.17
Hydroxyacetone	74	$C_4H_8O_3$	4.33	4.65
Succindialdehyde	86	$C_4H_6O_2$	4.56	2.60
Dihydro-4-hydroxy-2-(3H)-furanone	102	$C_4H_6O_3$	4.71	4.15
Furfural	96	$C_5H_4O_2$	5.65	3.17
2-Furanmethanol	98	$C_5H_6O_2$	6.15	0.31
Methallyl acetate	114	$C_6H_{10}O_2$	6.26	0.56
Acetol acetate	116	$C_5H_8O_3$	6.54	0.92
Dimethoxytetrahydrofuran	132	$C_6H_{12}O_3$	7.19	2.40
2-Methyl-2-cyclopentenone	96	C_6H_8O	7.49	0.29
2,4-Dimethylcyclohexanol	128	$C_8H_{16}O$	7.63	0.01
2(5H)-Furanone	84	$C_4H_4O_2$	7.81	3.11
2-Hydroxycyclopent-2-en-1-one	98	$C_5H_6O_2$	8.00	4.39
2(5H)-Furanone, 5-methyl-	98	$C_5H_6O_2$	8.46	0.16
2-Furancarboxaldehyde, 5-methyl-	110	$C_6H_6O_2$	9.11	1.56
2H-Pyran-2-methanol, tetrahydro-	116	$C_6H_{12}O_2$	9.30	0.07
Phenol	94	C_6H_6O	9.63	2.26
6,8-Dioxabicyclo[3.2.1]octane	114	$C_6H_{10}O_2$	10.13	1.55

Appendix C. continued

2-(3-Hydroxy-propyl)-cyclohexane-1,3-dione	170	$C_9H_{14}O_3$	10.63	0.01
6-(1-Hydroxy-1-methylethyl)-3-methylcyclohex-3-enone	168	$C_{10}H_{16}O_2$	10.79	0.04
3-Methyl-1,2-cyclopentanedione	112	$C_6H_8O_2$	10.99	2.03
5-Methyl-5-octen-1-ol	142	$C_9H_{18}O$	11.31	0.07
Oxirane, (1,1-dimethylbutyl)-	128	$C_8H_{16}O$	11.57	1.20
o-Cresol	108	C_7H_8O	11.79	1.05
1,2,6-Hexanetriol	134	$C_6H_{14}O_3$	12.13	0.94
p-Cresol	108	C_7H_8O	12.42	1.57
11-Oxa-dispiro[4.0.4.1]undecan-1-ol	168	$C_{10}H_{16}O_2$	12.61	0.22
Guaiacol	124	$C_7H_8O_2$	12.81	4.45
1,6-Anhydro-2,4-dideoxy-β-D-arabo-hexopyranose	130	$C_6H_{10}O_3$	13.04	0.63
2,6-Xylenol	122	$C_8H_{10}O$	13.29	0.05
1-Octene, 3-(methoxymethoxy)-	172	$C_{10}H_{20}O_2$	13.52	0.28
3-Ethyl-2-hydroxy-2-cyclopenten-1-one	126	$C_7H_{10}O_2$	13.68	0.11
4-Hydroxy-3-methylpent-2-enoic acid, methyl ester	144	$C_7H_{12}O_3$	13.93	0.29
p-Xylenol	122	$C_8H_{10}O$	14.52	0.64
5-Hydroxy-4,4,6-trimethyl-7-oxabicyclo[4.1.0]heptan-2-one	170	$C_9H_{14}O_3$	14.76	0.11
3-Ethyl-3-heptanol	144	$C_9H_{20}O$	15.14	1.22
Creosol	138	$C_8H_{10}O_2$	15.82	4.20
Catechol	110	$C_6H_6O_2$	16.07	4.59

Appendix C. continued

1,4:3,6-Dianhydro-α-d-glucopyranose	144	$C_6H_8O_4$	16.42	0.42
6-Methylenebicyclo[3.2.0]hept-3-en-2-one	120	C_8H_8O	16.58	0.11
2-Dodecenoic acid	198	$C_{12}H_{22}O_2$	16.71	0.11
d-Mannose	180	$C_6H_{12}O_6$	16.87	0.97
5-Hydroxymethylfurfural	126	$C_6H_6O_3$	17.04	1.74
Dodecanoic acid, 3-hydroxy-	216	$C_{12}H_{24}O_3$	17.53	0.41
Octan-2-one, 3,6-dimethyl-	156	$C_{10}H_{20}O$	18.01	0.31
p-Ethylguaiacol	152	$C_9H_{12}O_2$	18.22	1.00
2-Butyl-3-methylcyclopent-2-en-1-one	152	$C_{10}H_{16}O$	18.38	0.02
4-Methylcatechol	124	$C_7H_8O_2$	18.60	3.04
Methyl 8-oxooctanoate	172	$C_9H_{16}O_3$	19.05	0.71
Vinyl guaiacol	150	$C_9H_{10}O_2$	19.20	2.88
3-Cyclopropylcarbonyloxydodecane	254	$C_{16}H_{30}O_2$	19.32	0.33
Chavicol	134	$C_9H_{10}O$	19.93	0.19
Eugenol	164	$C_{10}H_{12}O_2$	20.34	1.89
4-Ethylcatechol	138	$C_8H_{10}O_2$	21.08	0.73
Vanillin	152	$C_8H_8O_3$	21.53	2.90
1,1-Diethoxyacetone	146	$C_7H_{14}O_3$	22.06	0.13
5,8-Epoxy-3H-2-benzopyran, 4,4a,5,8-tetrahydro-5,8-dimethyl-, (4aα,5α,8α)-	178	$C_{11}H_{14}O_2$	22.42	0.02
Isoeugenol	164	$C_{10}H_{12}O_2$	22.73	6.07
D-Allose	180	$C_6H_{12}O_6$	22.85	1.89
Cerulignol	166	$C_{10}H_{14}O_2$	23.03	1.44

Appendix C. continued

Hydroxychavicol	150	$C_9H_{10}O_2$	23.39	0.39
Apocynin	166	$C_9H_{10}O_3$	23.72	1.49
Levoglucosan	162	$C_6H_{10}O_5$	24.31	6.19
Guaiacylacetone	180	$C_{10}H_{12}O_3$	24.78	0.64
d-Glycero-d-ido-heptose	210	$C_7H_{14}O_7$	25.05	0.71
Vanillic acid	168	$C_8H_8O_4$	25.65	0.83
1'-Hydroxyeugenol	180	$C_{10}H_{12}O_3$	25.81	0.57
2(3H)-Naphthalenone, 4,4a,5,6,7,8-hexahydro-1-methoxy-	180	$C_{11}H_{16}O_2$	25.99	0.21
1-(4-Ethoxyphenyl)propan-1-ol	180	$C_{11}H_{16}O_2$	26.11	0.04
2,7-Anhydro-l-galacto-heptulofuranose	192	$C_7H_{12}O_6$	27.16	1.20
Dihydroconiferyl alcohol	182	$C_{10}H_{14}O_3$	27.49	0.90
4,6-Dimethoxysalicylaldehyde	182	$C_9H_{10}O_4$	27.82	0.08
Coniferyl alcohol	180	$C_{10}H_{12}O_3$	28.03	0.30
(E)-2,6-Dimethoxy-4-(prop-1-en-1-yl)phenol	194	$C_{11}H_{14}O_3$	28.62	0.10
Ethanone, 1-(1-hydroxy-2,6,6-trimethyl-2,4-cyclohexadien-1-yl)-	180	$C_{11}H_{16}O_2$	29.24	0.01
Coniferyl aldehyde	178	$C_{10}H_{10}O_3$	29.41	2.73
n-Hexadecanoic acid	256	$C_{16}H_{32}O_2$	33.74	0.16
2-Cyclopropene-1-carboxylic acid, 2-(1,1-dimethyl-5-oxohexyl)-, methyl ester	224	$C_{13}H_{20}O_3$	34.96	0.24
9-Hexadecenoic acid	254	$C_{16}H_{30}O_2$	37.03	0.05
4'-Methoxy-2-hydroxystilbene	226	$C_{15}H_{14}O_2$	40.52	0.05
Hexa-hydro-farnesol	228	$C_{15}H3_2O$	41.45	0.15

Appendix C. continued

Dehydroabietic acid	300	$C_{20}H_{28}O_2$	42.25	0.15
Ethyl 9,9-diformylnona-2,4,6,8-tetraenoate	234	$C_{13}H_{14}O_4$	42.90	0.04
(E)-3,3'-Dimethoxy-4,4'-dihydroxystilbene	272	$C_{16}H_{16}O_4$	45.98	0.40

Appendix D. Compounds identified by GC-MS in bio-oil samples collected during fast pyrolysis from methanol impinger.

Compound Name	**M^+**	**Formula**	**Apex RT**	**ug/mg**
L-Glyceraldehyde	90	$C_3H_6O_3$	3.56	0.36
Dihydropyran	82	C5H8O	3.99	0.01
Acetic acid, methyl ester	74	C3H6O2	4.33	3.50
Succindialdehyde	86	C4H6O2	4.56	1.13
Acetol	74	C3H6O2	4.72	2.25
Furfural	96	C5H4O2	5.65	0.74
3-Hydroxydecanoic acid	188	C10H20O3	5.97	0.70
2-Furanmethanol	98	C5H6O2	6.17	0.26
4-Penten-2-one, 3-methyl-	98	C6H10O	6.55	0.49
Dimethoxytetrahydrofuran	132	C6H12O3	6.79	0.64
2(5H)-Furanone	84	C4H4O2	7.81	2.06
2-Hydroxycyclopent-2-en-1-one	98	C5H6O2	7.99	3.80
6-Hydroxy-hexan-2-one	116	C6H12O2	8.48	0.03
3,5-Octadien-2-ol	126	C8H14O	8.90	0.86
1,2-Hexanediol, 2-methyl-	132	C7H16O2	9.08	1.56
Phenol	94	C6H6O	9.64	0.89
6,8-Dioxabicyclo[3.2.1]octane	114	C6H10O2	10.13	1.97
3-Methyl-1,2-cyclopentanedione	112	C6H8O2	10.97	1.56
Hexanal dimethyl acetal	146	C8H18O2	11.43	0.64
1-Octyn-4-ol	126	C8H14O	11.61	0.41

Appendix D. continued

o-Cresol	108	C7H8O	11.80	0.29
Oxirane, 2-butyl-3-methyl-, cis-	114	C7H14O	12.07	0.11
p-Cresol	108	C7H8O	12.43	0.51
Guaiacol	124	C7H8O2	12.82	3.55
trans-1,2-Cyclopentanediol	102	C5H10O2	13.06	0.46
6-Hydroxy-9-oxa-bicyclo[3.3.1]nonan-3-one	156	C8H12O3	13.61	0.92
Butanedioic acid, 3-hydroxy-2,2-dimethyl-, dimethyl ester, (R)-	190	C8H14O5	14.15	0.84
p-Xylenol	122	C8H10O	14.53	0.37
4H,5H-Pyrano[4,3-d]-1,3-dioxin, tetrahydro-8a-methyl	158	C8H14O3	14.80	0.34
3-Ethyl-3-heptanol	144	C9H20O	15.14	3.56
Dodecanal	184	C12H24O	15.72	1.27
Creosol	138	C8H10O2	15.83	3.45
Catechol	110	C6H6O2	16.11	4.76
2,4-Dimethylcyclohexanol	128	C8H16O	16.30	0.84
1,4:3,6-Dianhydro-α-d-glucopyranose	144	C6H8O4	16.42	0.40
Coumaran	120	C8H8O	16.60	0.16
Octan-2-one, 3,6-dimethyl-	156	C10H20O	16.87	0.21
5-Hydroxymethylfurfural	126	C6H6O3	17.06	0.73
6-Acetyl-β-d-mannose	222	C8H14O7	17.27	0.09
l-Gala-l-ido-octose	240	C8H16O8	18.02	0.21
p-Ethylguaiacol	152	C9H12O2	18.23	0.83

Appendix D. continued

4-Methylcatechol	124	C7H8O2	18.62	1.53
Vinyl guaiacol	150	C9H10O2	19.21	5.03
Octanoic acid, 6-ethyl-3-octyl ester	284	C18H36O2	19.31	1.02
Chavicol	134	C9H10O	19.95	0.17
Syringol	154	C8H10O3	20.24	0.33
Eugenol	164	C10H12O2	20.35	1.76
d-Mannose	180	C6H12O6	20.91	1.39
4-Ethylcatechol	138	C8H10O2	21.10	0.86
Vanillin	152	C8H8O3	21.54	2.76
Isoeugenol	164	C10H12O2	21.68	0.90
trans-Isoeugenol	164	C10H12O2	22.73	6.91
Cerulignol	166	C10H14O2	23.04	6.06
Hydroxychavicol	150	C9H10O2	23.45	0.37
10-Heptadecen-8-ynoic acid, methyl ester, (E)-	278	C18H30O2	23.61	0.17
Apocynin	166	Apocynin	23.72	1.42
Levoglucosan	162	C6H10O5	24.46	16.36
Guaiacylacetone	180	C10H12O3	24.79	0.57
3-tert-Butyl-4-hydroxyanisole	180	C11H16O2	25.57	1.46
Coniferyl alcohol	180	C10H12O3	25.82	0.73
2(3H)-Naphthalenone, 4,4a,5,6,7,8-hexahydro-1-methoxy-	180	C11H16O2	26.00	0.21
2,4,7,9-Tetramethyl-5-decyn-4,7-diol	226	C14H26O2	26.13	0.03
2,7-Anhydro-l-galacto-heptulofuranose	192	C7H12O6	27.20	0.93

Appendix D. continued

Homovanillic acid	182	C9H10O4	27.51	1.27
Syringylaldehyde	182	C9H10O4	27.82	0.20
(E)-2,6-Dimethoxy-4-(prop-1-en-1-yl)phenol	194	C11H14O3	28.63	0.37
Coniferyl aldehyde	178	C10H10O3	29.42	3.80
4-((1E)-3-Hydroxy-1-propenyl)-2-methoxyphenol	180	C10H12O3	29.51	5.51
6,9-Octadecadiynoic acid, methyl ester	290	C19H30O2	33.39	0.06
n-Hexadecanoic acid	256	C16H32O2	33.75	0.37
5-Benzofuranacetic acid, 6-ethenyl-2,4,5,6,7,7a-hexahydro-3,6-dimethyl-α-methylene-2-oxo-, methyl ester	276	C16H20O4	34.47	0.11
1-Cyclohexene-1-carboxylic acid, 4-(1,5-dimethyl-3-oxohexyl)-, methyl ester, [R-(R*,R*)]-	266	C16H26O3	34.97	0.39
9-Hexadecenoic acid	254	C16H30O2	37.04	0.34
Ethyl iso-allocholate	436	C26H44O5	40.13	0.11
Gibberellic acid	346	C19H22O6	40.54	0.04
Cyclopropanetetradecanoic acid, 2-octyl-, methyl ester	394	C26H50O2	41.46	0.11
2-[4-methyl-6-(2,6,6-trimethylcyclohex-1-enyl)hexa-1,3,5-trienyl]cyclohex-1-en-1-carboxaldehyde	324	C23H32O	41.58	0.14
Dehydroabietic acid	300	C20H28O2	42.28	0.77
Pregan-20-one, 2-hydroxy-5,6-epoxy-15-methyl-	346	C22H34O3	42.91	0.14

Appendix D. continued

(E)-3,3'-Dimethoxy-4,4'-dihydroxystilbene	272	C16H16O4	45.98	0.90
1,4-Benzenedicarboxylic acid, bis(2-ethylhexyl) ester	390	C24H38O4	47.87	0.47

Appendix E. Aspen HYSYS simulation process flow diagram parameters.

Material Streams												
Variables	**Unit**	**Inert Gas**	**1**	**Biomass**	**2**	**Reactor Inlet**	**Vapor Phase**	**Gas/Liquid Mix**	**Syngas**	**Bio-oil**	**HQ Biochar**	**LQ Biochar**
Vapor Fraction		1.0	1.0	0.0	1.0	1.0	1.0	1.0	1.0	0.0	0.0	0.15
Temperature	C	21.1	200.0	21.1	196.7	550.0	549.4	22.0	22.0	22.0	183.9	183.9
Pressure	kPa	101.3	101.3	101.3	101.3	99.3	99.3	97.3	97.3	97.3	99.3	99.3
Mass Flow	tonne/d	12,278	12,278	50.0	12,328	12,328	12,321	12,321	12,291	29.9	7.1	7.0
Heat Flow	MW	-0.6	25.9	-3.2	22.7	77.7	77.7	-3.4	-1.7	-1.6	0.1	0.0

1: Heated gas; 2: Inert gas/biomass mixture

Appendix F. SVM training and testing datasets

Training dataset

Sample #	Carbon Content (%)	Moisture Content (%)	Manure Quality Rate (%)	pH (10^{-1})	Carbon Content (%)	Nutrient Content (%)	Biochar Quality Rate (%)
1	15	77	41.4	95	70	2	46.7
2	14	71	46.0	86	64	1	42.7
3	14	73	44.4	90	68	1	45.5
4	16	77	41.6	89	66	1	44
5	16	72	45.6	92	74	3	50.3
6	19	75	43.8	90	64	1	42.3
7	12	76	41.6	85	74	3	51
8	15	80	39.0	88	73	1	49.7
9	16	72	45.6	83	65	1	43.8
10	16	78	40.8	85	62	1	41.2
11	15	75	43.0	83	63	2	42.3
12	19	80	39.8	84	74	2	51
13	16	77	41.6	83	67	1	45.4
14	18	72	46.0	86	64	2	42.8
15	17	79	40.2	83	68	2	46.3
16	15	77	41.4	85	69	3	47
17	17	75	43.4	93	68	1	45.2
18	12	77	40.8	93	64	2	42.1
19	17	70	47.4	90	66	3	44.1
20	18	79	40.4	94	75	2	50.8
21	15	80	39.0	83	66	3	44.8
22	16	73	44.8	93	72	3	48.6
23	17	71	46.6	92	62	1	40.5
24	18	80	39.6	84	73	2	50.2
25	15	71	46.2	95	75	1	50.6
26	17	78	41.0	90	70	2	47.2
27	18	80	39.6	91	71	2	47.9
28	19	70	47.8	92	67	3	44.7
29	17	80	39.4	92	71	1	47.7
30	15	75	43.0	90	64	1	42.3

Testing dataset

Sample #	Carbon Content (%)	Moisture Content (%)	Manure Quality Rate (%)	pH (10^{-1})	Carbon Content (%)	Nutrient Content (%)	Biochar Quality Rate (%)
1	18	75	43.6	90	64	1	42.3
2	16	72	45.6	85	64	3	43
3	17	70	47.4	95	67	1	44.2
4	17	77	41.8	88	63	2	41.8
5	16	79	40	93	73	1	49.2
6	19	72	46.2	85	68	2	46.1
7	12	80	38.4	86	75	3	51.7
8	12	70	46.4	90	68	2	45.6
9	15	73	44.6	83	74	2	51.1
10	19	72	46.2	88	63	2	41.8

Appendix G. Magic Valley dairy locations, cow counts (ArcGIS 2019)

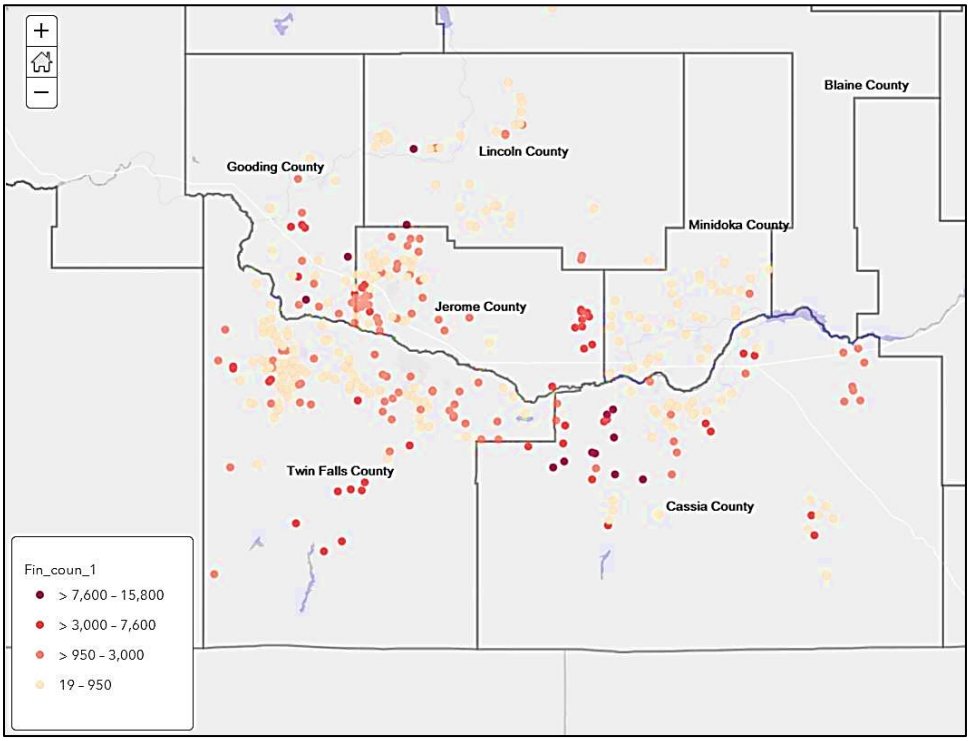

Selected large dairy locations for manure collection, with over 10,000 cows in each dairy (ArcGIS 2019)

Dairy #	County	Cow Type	Size	Counts	Location
1	Gooding	Dairy	Large	15,800	2901 S 2300 E, Wendell, ID 83355
2	Lincoln	Dairy	Large	15,800	425 3 Mile Rd W, Shoshone, ID 83352
3	Lincoln	-	Large	15,400	350 E 900 N, Jerome, ID 83338
4	Cassia	Feedlot	Large	10,000	1300 S, Oakley, ID 83346
5	Cassia	-	Large	10,000	900 W 1000 S Burley, ID 83318
6	Cassia	-	Large	10,000	920 S 800 W Burley, ID 83318
7	Cassia	Ranch	Large	10,000	Oakley, ID 83346
8	Cassia	-	Large	10,000	500 W 400 S, Burley, ID 83318
9	Cassia	-	Large	10,000	657 W 500 S, Burley, ID 83318
10	Cassia	Calf	Large	10,000	605 S 600 W, Burley, ID 83318

Appendix H. Computational solution (RStudio and MATLAB) codes

RStudio codes for calculating weights, using SVM method:

```
install.packages("e1071")

library("e1071")

str(training)

summary(training)

ss <- svm(training, data=training, kernel="linear", scale=F)

weight <- t(ss$coefs) %*% ss$SV

weight


str(testing)

summary(testing)

ss <- svm(testing, data=testing, kernel="linear", scale=F)

weight <- t(ss$coefs) %*% ss$SV

weight


str(accesstrain)

summary(accesstrain)

ss <- svm(accesstrain, data=accesstrain, kernel="linear", scale=F)

weight <- t(ss$coefs) %*% ss$SV

weight


str(accesstest)
```

```
summary(accesstest)

ss <- svm(accesstest, data=accesstest, kernel="linear", scale=F)

weight <- t(ss$coefs) %*% ss$SV

weight
```

MATLAB codes for solving the mathematical model, using the genetic algorithm:

```
global NFE Penalty nSite nQuarter T;


%% Assign Problem Parameters

Assigndata;


%% Problem Definition

CostFunction=@Fitness;   % Cost Function

nVar=nSite;     % Number of Decision Variables


%% GA Parameter

MaxIt=500;         % Maximum Number of Iterations

nPop=100;           % Population Size

pCrossover=0.7;     % Parents (Offsprings) Population Size Ratio

nCrossover=round(pCrossover*nPop/2)*2;

pMutation=0.05;      % Mutants Population Size Ratio

nMutation=round(pMutation*nPop);

TournamentSelectionSize=3;

Penalty=1000;
```

```
%% Initialization *generate an initial random population of bit strings*
NFE=0;
individual.Position1=[];
individual.Position2=[];
individual.Sol=[];
individual.Cost=[];
pop=repmat(individual,nPop,1);

for i=1:nPop
   for j=1:nQuarter
      pop(i).Position1{j}=randi([0 1],1,nSite(j));
      if sum(pop(i).Position1{j})>T(j)
         t=sum(pop(i).Position1{j})-T;
         a=find(pop(i).Position1{j}==1);
         a=a(randperm(numel(a)));
         a=a(1:t);
         pop(i).Position1{j}(a)=0;
      end
      pop(i).Position2{j}=rand(1,nSite(j));
   end
   [pop(i).Cost, pop(i).Sol]=CostFunction(pop(i).Position1,pop(i).Position2);
end
```

```
% Sort Population
Costs=[pop.Cost];
[Costs, SortOrder]=sort(Costs);
pop=pop(SortOrder);
WorstCost=Costs(end);

BestSol=[];
BestCost=zeros(MaxIt,1);
MeanCost=zeros(MaxIt,1);

nfe=zeros(MaxIt,1);

%% GA Main Loop

for it=1:MaxIt

   % Crossover
   pop2=repmat(individual,nCrossover/2,2);
   for k=1:nCrossover/2

      i1=TournamentSelection(pop,TournamentSelectionSize);
      i2=TournamentSelection(pop,TournamentSelectionSize);

      [pop2(k,1).Position1, pop2(k,2).Position1]=Crossover1(pop(i1).Position1,pop(i2).Position1);
```

```
    [pop2(k,1).Position2, pop2(k,2).Position2]=Crossover2(pop(i1).Position2,pop(i2).Position2);

    [pop2(k,1).Cost, pop2(k,1).Sol]=CostFunction(pop2(k,1).Position1,pop2(k,1).Position2);

    [pop2(k,2).Cost, pop2(k,2).Sol]=CostFunction(pop2(k,2).Position1,pop2(k,2).Position2);


end

pop2=pop2(:);



% Mutation

pop3=repmat(individual,nMutation,1);

for k=1:nMutation


    i1=TournamentSelection(pop,TournamentSelectionSize);


    pop3(k).Position1=Mutate1(pop(i1).Position1);

    pop3(k).Position2=Mutate2(pop(i1).Position2);


    [pop3(k).Cost, pop3(k).Sol]=CostFunction(pop3(k).Position1,pop3(k).Position2);


end


% Merge Populations

pop=[pop

     pop2
```

```
        pop3];  %#ok

    % Sort Population
    Costs=[pop.Cost];
    [Costs, SortOrder]=sort(Costs);
    pop=pop(SortOrder);
    WorstCost=max(WorstCost,Costs(end));

    % Delete Extra Individuals
    pop=pop(1:nPop);
    Costs=Costs(1:nPop);

    % Save Results
    BestSol=pop(1);
    BestCost(it)=Costs(1);
    MeanCost(it)=mean(Costs);
    nfe(it)=NFE;

    % Show Information
    disp(['Iteration ' num2str(it) ':   ' ...
        'Best Cost = ' num2str(BestCost(it)) '  , ' ...
        'Mean Cost = ' num2str(MeanCost(it))]);
end
```

```
%% Results

figure;

subplot(2,1,1);

semilogy(BestCost,'r','LineWidth',2);

hold on;

semilogy(MeanCost,'b:','LineWidth',2);

xlabel('Generation (Iteration)');

legend('Best Costs','Mean Costs');

subplot(2,1,2);

semilogy(nfe,BestCost,'r','LineWidth',2);

hold on;

semilogy(nfe,MeanCost,'b:','LineWidth',2);

xlabel('Function Evaluations');  % fitness func. uses func. eval. to calcul. a value of worth for individual and compare with each other

legend('Best Costs','Mean Costs');

xlim([0 nfe(end)]);
```